ACYCLIC CHELATES FOR IMAGING WITH RADIOMETALS

by

Eszter Boros

B.Sc., Universität Zürich, 2006
M. Sc., Universität Zürich, 2007

A THESIS SUBMITTED IN PARTIAL FULFILLMENT OF
THE REQUIREMENTS FOR THE DEGREE OF

DOCTOR OF PHILOSOPHY

in

THE FACULTY OF GRADUATE STUDIES

(Chemistry)

THE UNIVERSITY OF BRITISH COLUMBIA

(Vancouver)

July 2011

Abstract

This thesis investigates acyclic chelates containing pyridine, carboxylate and amino groups and their fast and efficient and stable coordination of the (radio-)metals ^{99m}Tc, Re, Cu, ^{64}Cu, Ga, $^{67/68}$Ga. The radiometals mentioned are all of significant interest for SPECT (single photon emission computed tomography) and PET (positron emission tomography) imaging, two of the most important non-invasive diagnostic tools in the clinic. The design, synthesis, radiolabelling, evaluation of stability, and *in vivo* investigation are presented for three variably charged, novel, short C_8 chain derivatized chelates for the $[M(CO)_3]^+$ core (M = ^{99m}Tc or Re). Distinct localization of these small amphiphilic molecules *in vivo* was studied via biodistribution and imaging and was found to be dependent on the charge of the polar moiety. In an attempt to identify a universal chelate applicable to the $[M(CO)_3]^+$ core and ^{64}Cu, the synthesis of the dipin bifunctional chelate system, capable of fast coordination of Cu, its radionuclide ^{64}Cu, as well as the $[M(CO)_3]^+$ core (M = ^{99m}Tc, Re) is described. The versatility of the dipin ligand system is based on its ability to adopt a variety of binding modes, tridentate when protected, tetradentate when deprotected. Based on this small, tetradentate scaffold, a series of acyclic chelates with varying bite angle and denticity were synthesized and screened for their ability to coordinate radioisotopes of Ga and Cu under mild conditions within a short period of time. It was found that the linear N_4O_2 chelate H_2dedpa coordinates $^{67/68}$Ga quantitatively to form $[^{67}Ga(dedpa)]^+$ after 10 min at room temperature with exceptional kinetic inertness towards human *apo*-transferrin. The corresponding ^{64}Cu complex maintains inertness against serum proteins within 2 h, but shows 23 % transchelation to serum proteins after 24 h. Both potential small molecule perfusion agents, as well as peptide conjugated versions as applications of the H_2dedpa scaffold are reported. Both types of derivatives maintained the labelling and radiolabelled complex ($^{67/68}$Ga and ^{64}Cu) stability properties found with the non-derivatized versions, further indicating the H_2dedpa scaffold is a useful platform for the development of clinically applicable radiopharmaceuticals.

Preface

Chapter 2 is based on work conducted at UBC, TRIUMF, the McMaster Institute of Applied Radiation Sciences (McIARS) and the McMaster Centre for Preclinical and Translational Imaging (MCPTI). Radiochemical synthesis and HPLC purification were done in the laboratory of Prof. John Valliant, under the instruction of Dr. Andrea Armstrong. Imaging of the animals on their SPECT/CT scanner was done by Troy Farncombe, Chantal Saab, and Rod Rhem. Biodistribution and subsequent evaluation of the imaging and biodistribution data was done by Prof. Urs O. Häfeli. This work has also been published and reproduced in part with permission from: Boros, Eszter; Häfeli, Urs O.; Patrick, Brian O.; Adam, Michael J.; Orvig, Chris. *Design, Synthesis, and Imaging of Small Amphiphilic Rhenium and ^{99m}Technetium Tricarbonyl Complexes.* Bioconjugate Chem. (2009), 20(5), 1002-1009. Copyright 2009 American Chemical Society. http://pubs.acs.org/doi/pdf/10.1021/bc900022c. I conducted all synthetic experiments, radiochemistry and wrote most of the manuscript with the editorial help of Chris Orvig. Urs O. Häfeli generated the bar graphs of the biodistribution, curves of all ^{99m}Tc-compounds' levels in selected organs taken from the SPECT/CT images and sagittal and coronal plane SPECT/CT images. The solid state structure determination was done by Dr. Brian O. Patrick.

The work in Chapter 3 has been published: Boros, Eszter; Lin, Yi-Heng S.; Ferreira, Cara L.; Patrick, Brian O.; Häfeli, Urs O.; Adam, Michael J.; Orvig, Chris. *One to chelate them all: investigation of a versatile, bifunctional chelate for ^{64}Cu, ^{99m}Tc, Re and Co.* Dalton Trans., 2011 (23), 6253-6259. Reproduced by permission of The Royal Society of Chemistry (RSC). http://pubs.rsc.org/en/content/articlepdf/2011/dt/c0dt01458c. Model chelates H_2dipin, Me_2dipin, Cu complexes thereof and precursors for the functionalization were synthesized first by Yi-Heng Scott Lin under my instruction and supervision and were included in his Bachelor Honours thesis. Remaining synthetic work on conjugation with biotin, radiochemistry and all of the $[Re(CO)_3]^+$ work was done by myself. I was responsible for writing the manuscript with the editorial help of Cara L. Ferreira and Chris Orvig. The solid state structure determination was done by Dr. Brian O. Patrick.

Parts of Chapter 4 have been published and are reproduced in part with permission from: Boros, Eszter; Ferreira, Cara L.; Cawthray, Jacqueline F.; Price, Eric W.; Patrick, Brian O.; Wester, Dennis W.; Adam, Michael J.; Orvig, Chris. *Acyclic Chelate with Ideal Properties for ^{68}Ga PET Imaging Agent Elaboration.* J. Am. Chem. Soc. (2010), 132(44), 15726-15733. Copyright 2010 American Chemical Society. http://pubs.acs.org/doi/pdf/10.1021/ja106399h. I conducted all synthetic experiments, radiochemistry, generated the bar graphs of the biodistribution and wrote most of the manuscript with the editorial help of Cara L. Ferreira and Chris Orvig. The diamino precursor of H_2dp-bb-NO_2 was synthesized by Eric W. Price. Biodistribution data were collected by Dr. Dawn Waterhouse of the BC Cancer Agency. Potentiometric measurements were conducted by Dr. Jacqueline F. Cawthray. The solid state structure determination was done by Dr. Brian O. Patrick.

The solid state structure determination in Chapter 5 was done by Dr. Brian O. Patrick. Glenn Bremner (Wolf group) assisted with Cyclic Voltammetry measurements.

Work presented in Chapter 7 has been accepted for publication: "New Ga Derivatives of the H_2dedpa Scaffold with Improved Clearance and Persistent Heart Uptake", Boros, E.; Ferreira, Cara L.; Patrick Brian O.; Adam, Michael J.; Orvig ,Chris. *Nucl. Med. Biol.* (2011) in press. Copyright 2011 Elsevier. Biodistribution on the ^{67}Ga complexes reported in Chapter 7 were carried out by Dr. Dawn Waterhouse of the BC Cancer Agency. The solid state structure determination was done by Dr. Brian O. Patrick.

Table of Contents

List of Tables

List of Figures

List of Schemes

List of Symbols and Abbreviations

~	approximate
2D	two dimensional
3D	three dimensional
6SS	N,N'-bis(2,2-dimethyl-2-mercaptoethyl)ethylenediamine-N,N'-diacetic acid
α	alpha or alpha particle
Å	angstrom, $10 \cdot 10^{-10}$ metre
A	ampère
β	beta
β^-	beta particle
β^+	positron
γ	gamma ray
δ	delta or chemical shift in parts per million (NMR)
ε	epsilon
μ	micro (10^{-6})
Ac	acetyl
AcOH	acetic acid
Anal.	analytical
atm	atmosphere
Bn	benzyl
t-Boc	N-*tert*-butoxycarbonyl
Boc_2O	di-*tert*-butyl-dicarbonate
°C	degrees celsius
calcd.	calculated
CB-DO2A	4,10-bis(carboxymethyl)-1,4,7,10-tetraazabicyclo[5.5.2]tetradecane
CB-TE2A	4,11-bis(carboxymethyl)-1,4,8,11-tetraazabicyclo[6.6.2]hexadecane
Ci	Curie
cm^{-1}	wavenumber

CT	computed tomography
CV	cyclic voltammetry
d	day(s) or doublet (NMR)
DIAMSAR	1,8-diamino-3,6,10,13,16,19- hexaazabicyclo(6,6,6)eicosane
DMF	dimethylformamide
DMSO	dimethylsulfoxide
DOTA	1,4,7,10-tetraazacyclododecane -N,N',N'',N'''-tetraacetic acid
EA	elemental analysis
EC	N,N'-ethylene-di-L-cysteine
EDMA	ethyldimethylamine
ESI-MS	electrospray ionization mass spectrometry
EtOAc	ethyl acetate
EtOH	ethanol
eV	electron volt
eq	equivalent(s)
f	fission
fac	facial
FDA	Food and Drug Administration (USA)
FDG	^{18}F-2-deoxy-2-fluoro-D-glucose
FMISO	^{18}F-fluoromisonidazole
g	gram
h	hour(s)
HMBC	heteronuclear multiple bond coherence
HSQC	heteronuclear single bond coherence
HPLC	high performance liquid chromatography
HYNIC	hydrazinopyridine-3-carboxylic acid
Hz	hertz (s^{-1})
IR	infrared
ID	injection dose
J	coupling constant (NMR)
k	kilo

K_{ML}	thermodynamic complex stability constant
L	litre or ligand
m	milli- or medium or multiplet
M	molar (moles/ litre) or mega
MeOH	methanol
min	minute(s)
mol	mole
MAG_3	mercaptoacetyltriglycine
MRI	magnetic resonance imaging
MS	mass spectrometry
m/z	mass per unit charge
n	nano (10^{-9}) or number of unit
NHE	normal hydrogen electrode
NMR	nuclear magnetic resonance
n. o.	not observed
n. d.	not determined
NOTA	1,4,7-triazacyclononane-1,4,7-triacetic acid
NRU	National Research Universal (reactor)
ORTEP	Oak Ridge Thermal Ellipsoid Plot Program
PBS	phosphate buffered saline
PCTA	3,6,9,15-tetraazabicyclo[9.3.1]-pentadeca-1(15),11,13-triene-3,6,9-triacetic acid
Pd/C	palladium on carbon (10% by weight)
PET	positron emission tomography
pH	$-\log[H_3O]^+$
pM	-log[free metal]
ppm	parts per million
q	quartet (NMR)
®	trademark
R_f	retention factor
R_t	retention time

s	singlet (NMR) or strong (IR)
SD	standard deviation
SPECT	single photon emission computed tomography
t	triplet (NMR) or time
$t_{1/2}$	half-life
TAME-Hex	tris(aminomethyl)- ethane-*N*,*N*,*N*',*N*',*N*'',*N*''-hexaacetic acid
THF	tetrahydrofuran
TFA	trifluoroacetic acid
TLC	thin layer chromatography
UV	ultraviolet
V	volt
w	weak (IR)

Acknowledgements

What a crazy ride this has been. First and foremost, I must thank my dear husband and best friend, Labros. You are always there for me, make me laugh, listen to my complaints and encourage me to keep pushing for my dreams. My parents, for supporting their beloved, only child in moving across the world to pursue a career as a scientist instead of becoming a globetrotting WTA tennis player.

The Bosses Chris and Mike are greatly acknowledged. Your persistence and belief in the Ga project for almost one decade prior to my arrival was the great basis for what followed. I was lucky to be at the right place at the right time. Thank you for all the support and the freedom to pursue all the other scientific interests I had, even if sometimes they were far off my "main" main group metal... It's all a young, aspiring scientist could wish for. Cara, without you, this would not all have been possible. Thank you for your scientific help and your friendship. The girls: Ashlee, Danielle, Jen, Meryn, Tulin, it was so good to have you around, more girls nights out, please. Eric, balling! Scott, thank you for all your hard work night and day (literally) on the Cu/Tc project. "Little" Mike, for all your good work during the summer of 2010 and the introduction to Canadian rock music from the last century. The rest of the Orvig group for being around, always busy and hard working, making fabulous group meeting treats.

All collaborators, essential to my work: Dr. Urs O. Häfeli (both of my Tc projects), Dr. Dawn Waterhouse and Dr. Brent Sutherland (animal studies), Dr. Janet McIntosh (for eluting the ^{68}Ga generator on oddest dates and times) Dr. Jacqueline Cawthray (Potentiometry) and Dr. Dennis Wester (for supporting our collaborative work with NORDION). Dr. Brian O. Patrick for all the solid state structure elucidation, even when some of the crystals I brought down to the X-ray lab were incredibly minuscule. The MS Staff (Marshall, Derek, David, Yun) and the NMR staff, especially Maria, Jason and Paul for all their help. UBC is acknowledged for awarding me a Four Year Fellowship, NSERC and NORDION for the generous support of my research. I also want to thank some stellar scientists for motivating me. Roger: I will never forget how you told me "you are good, but slow". I am working on that… I am grateful for everything you taught me. Peter, Thomas, Suzy, Tom, your enthusiasm and devotion to the science and to our field has and will continue to truly inspire me.

To my grandfather,
who never ceases to ask about my science,
supports and encourages me.

Chapter 1: Introduction

1.1 Medicinal Inorganic Chemistry

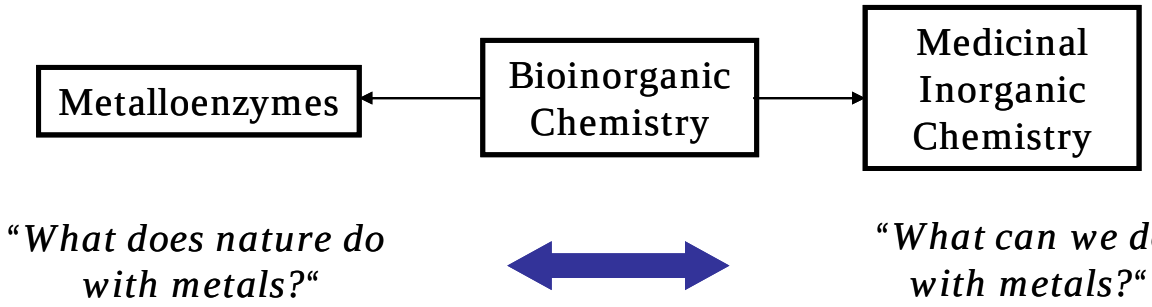

Figure 1.1 The author's view of the field of bioinorganic chemistry.

Bioinorganic chemistry is a broad field, and can be generally split into two subfields: metalloenzyme research and medicinal inorganic chemistry (Figure 1.1).[1] Metalloenzyme research tries to understand how metals are transported, stored and used in catalysis of essential biological processes.

The area of interest of the Orvig group is medicinal inorganic chemistry. Paul Ehrlich, who succeeded in finding a treatment for syphilis by screening a library of organoarsenates in 1909, is regarded as one of the pioneers of the field.[2] Since then, a myriad of coordination compounds has been investigated for therapeutic and diagnostic applications. Anticancer agents based on Pt such as Cisplatin,[3] antirheumatic agents based on Au such as Auranofin,[4] or perfusion imaging agents based on ^{99m}Tc such as Cardiolite[5] are some of the most widely applied metal-based drugs worldwide (Figure 1.2).

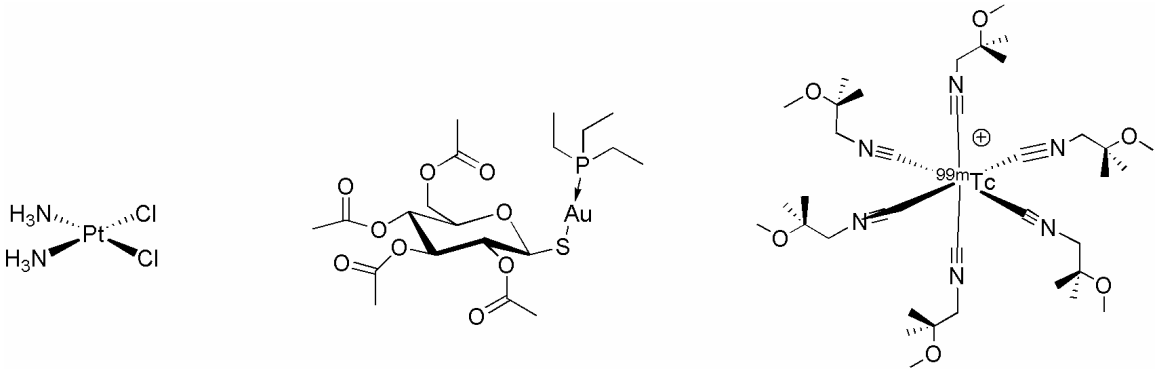

Figure 1.2 Cisplatin, Auranofin and Cardiolite (left to right).

The vast difference in structure and composition of these complexes, and the metals they contain, exemplifies the great variety of metals in medicine.

1.2 Medicinal Imaging

Non-invasive imaging serves as one of the most important diagnostic tools in the clinic. Besides X-ray images, which can only show the contrast between the heavier elements found for example in bone (Ca, P) versus the lighter elements found in soft tissues (C, H, O, N), other more sophisticated imaging techniques have been developed and are in use in the clinic.[6]

Magnetic resonance imaging (MRI) has become an increasingly important technique in the armamentarium of the modern clinician. This fairly young technology, originally introduced by Lauterbur in 1973,[7] is a powerful tool to visualize the most abundant molecule in biological tissue, water. Compared to single photon emission computed tomography (SPECT) and positron emission tomography (PET), MRI has the advantages of no ionizing radiation and enhanced spatial resolution increasing the attractiveness of this technology.[8] The ability of the magnetic moments of water protons to interact with an applied magnetic field, depending on the local environment of the water molecule, can be used to identify different tissues due to their characteristic consistency and water content.[9] This effect can be greatly enhanced in the presence of paramagnetic contrast agents containing Gd(III).[10]

On its own, Gd(III) is highly toxic due to its similar size to Ca(II); therefore, Gd(III) is chelated to form thermodynamically stable complexes in order to decrease toxicity and improve clearance. Most contrast agents in current clinical applications are non-target specific agents[11] and require high concentrations ($\geq$ 0.1 mM) to achieve a detectable change in MRI signal.[12] In the case of non-target specific, extracellular, commercial contrast agents with a relaxivity of about 4 mM^{-1} s^{-1}, a concentration of approximately 125 μM is necessary to achieve robust tissue contrast.

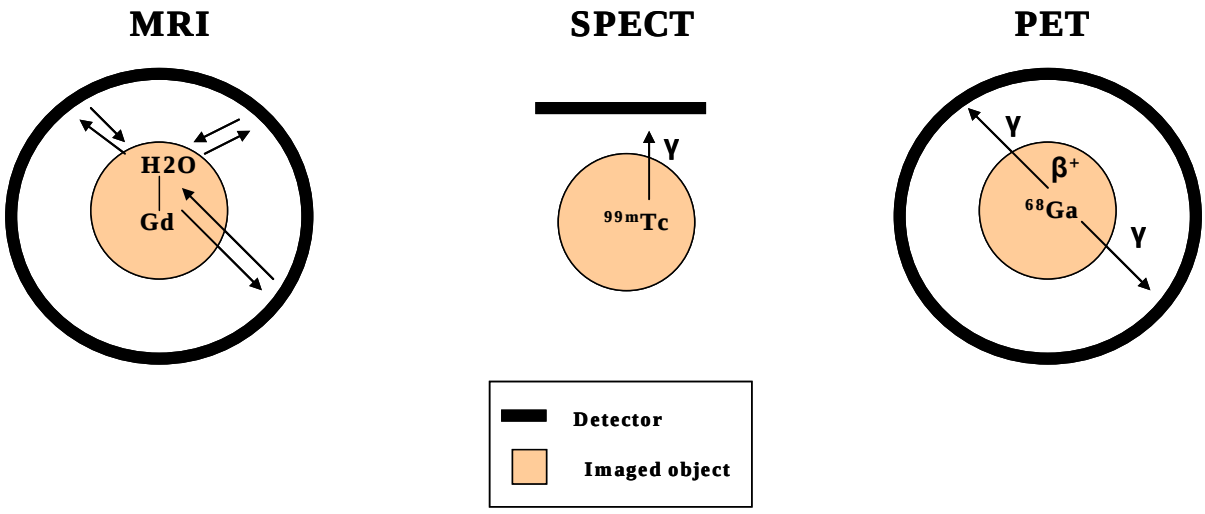

Figure 1.3 Schematic description of imaging techniques mentioned in Chapter 1.2.

These criteria currently render MRI a somewhat limited technique and, for many applications inferior to techniques, based on radioactive elements, such as SPECT and PET (schemes provided in Figure 1.3).

Radioactive elements have unstable nuclei, which decay by emitting one or more types of ionizing radiation: alpha particles (equivalent to a helium nucleus, α), positrons (β^+), high energy electrons (β^-) or gamma radiation (γ). α and β^- are found to have less kinetic energy due to their increased mass; therefore, they have only a short range. The smaller the space over which the energy is transferred, the more damaging the interaction will be to its surroundings.[13] This renders them useful for therapeutic applications, where large amounts of dose are delivered specifically to a certain area in order to damage that area of interest. The emission relevant for SPECT is a single photon, also denoted as γ. These light particles have great kinetic energy and will interact only weakly with tissue. The γ rays can be detected by a γ camera, consisting of a multihole lead collimator, a scintillating medium and an array of photomultipliers. After collection of an array of such 2D images, a tomographic algorithm is used to reconstruct the corresponding 3D image. As an added complication, the energy of the γ can greatly vary depending on the radionuclide used.[14] This can represent a problem with radionuclides other than ^{99m}Tc, since most SPECT cameras are tuned for the emission properties of this specific nuclide.

PET provides immediate, higher resolution 3D information on the location of the

radiation source. PET is based on positron emission, denoted as β^+. Being antimatter, any β^+, regardless of its emission energy, always annihilates with an electron in the immediate vicinity of the area of decay and produces two 511 keV γ rays oriented at 180° to one another. Simultaneous detection of both γ rays allows for precise localization of the β^+ source. This makes PET a desireable imaging technique.

Both SPECT and PET have the great advantage of being highly sensitive techniques; the presence of a radionuclide at concentrations of 100 pM and lower eliminates any possible inherent pharmacological side effects of these compounds. This also reduces the "toxicity" of this type of imaging as the radiation exposure is about the same dose as a chest X-ray. In Table 1.1, the most widely used and investigated radionuclides for imaging purposes are summarized, together with their emission properties.[15]

Table 1.1 Widely used and investigated radionuclides for imaging.

radionuclide	$t_{1/2}$	decays to	used in clinic?	imaging modality (relevant particle)
^{11}C	20.4 min	^{11}B	clinical trials[16]	PET (β^+)
^{18}F	109.7 min	^{18}O	yes	PET (β^+)
^{64}Cu	12.8 h	^{64}Ni	clinical trials[16]	PET (β^+)
^{67}Ga	78 h	^{67}Zn	yes	SPECT (γ, 184 keV)
^{68}Ga	68 min	^{68}Zn	clinical trials[16]	PET (β^+)
^{99m}Tc	6.01 h	^{99}Tc	yes	SPECT (γ, 140.5 keV)
^{111}In	67.4 h	^{111}Cd	yes	SPECT (γ, 171 keV)
^{123}I	13.22 h	^{123}Te	yes	SPECT (γ, 157 keV)

Covalent incorporation of ^{11}C or ^{18}F requires sequential synthetic techniques, often even after the labelling step, while radiometals can be incorporated using simple coordination chemistry without additional chemical modifications post-labelling. This makes radiometals especially attractive for kit-formulations, where the nuclear medicine technician can synthesize the ready-to-use radiopharmaceutical by simple addition and

mixing of the radionuclide with the non-radioactive components of the radiopharmaceutical. Scheme 1.1 shows the preparations of routinely used radiopharmaceuticals FDG (^{18}F-2-deoxy-2-fluoro-D-glucose) and ^{99m}Tc-Sestamibi. This thesis focuses on fast and facile incorporation of a variety of radiometals into potential radiopharmaceuticals.

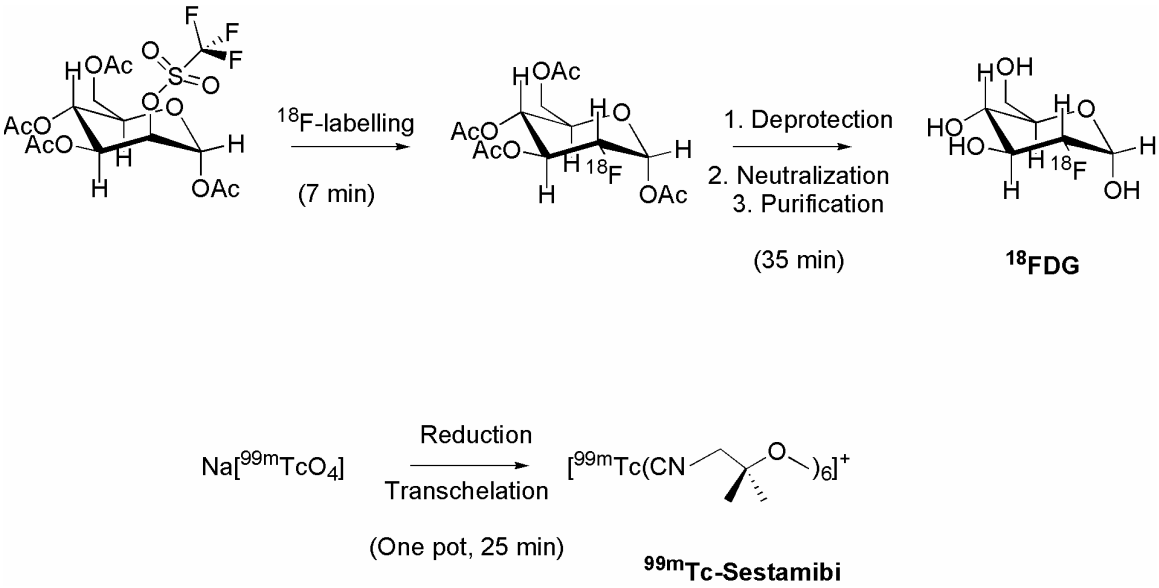

Scheme 1.1 Preparation of ^{18}FDG and ^{99m}Tc-Sestamibi.

1.3 Therapy in Nuclear Medicine

Another advantage of the use of radionuclides in the clinic includes the therapy aspect. Some radionuclides emit α or β^- particles upon decay, rendering them suitable for therapeutic applications. The mode of action of therapeutic radionuclides is the specific killing of cells by emitting a particle with a characteristic energy within a small area.[15] A long half-life is preferred for a prolonged treatment time, as well as localization at the target site before most of the dose is decayed in order to keep the exposure to non-target tissue as low as possible. β^- emitters deliver particles with average ranges of 0.2 to 4 mm. α emitters are found to have a one order of magnitude shorter range, which could facilitate more target specific agent delivery without harming the surrounding non-target tissue; however, no α emitting radiopharmaceuticals are yet in use in the clinic.[17]

By conjugation of a targeting molecule such as an antibody, peptide or small

molecule that targets a specific type of tissue or tumor, to a radionuclide with imaging properties one can image the area of interest. By subsequent use of the same targeting molecule incorporating a radionuclide with therapeutic emissions, one can provide therapeutic value simply by switching the radionuclide. Radionuclides fullfilling these criteria are referred to as "imaging and therapy pairs". An overview of radionuclides of current interest for therapeutic applications, as well as corresponding pairs is summarized in Table 1.2.[15]

Table 1.2 Widely used and investigated radionuclides for therapy.

radionuclide	$t_{1/2}$	decays to	use in clinic?	emitted particle	avg. energy emitted	range* [mm]	imaging pair?
^{64}Cu	12.8 h	^{64}Zn	clinical trials[16]	β^-	573 keV	~2.1	^{64}Cu (β^+)
^{67}Cu	61.9 h	^{67}Zn	no	β^-	141 keV	0.26	^{64}Cu (β^+)
^{90}Y	64.1 h	^{90}Zr	yes	β^-	932 keV	4.0	^{86} Y (β^+) (^{111}In)[18]
^{186}Re	3.8 d	^{186}Os	yes	β^-	349 keV	1.1	^{99m}Tc[19] (γ)
^{188}Re	17 h	^{188}Os	yes	β^-	764 keV	3.1	^{99m}Tc (γ)
^{177}Lu	6.7 d	^{177}Hf	clinical trials[16]	β^-	133 keV	0.23	^{177}Lu (γ)
^{211}At	7.2 h	^{207}Bi	clinical trials[16]	α	6.79 MeV	0.06	

** mean range in H_2O*

^{64}Cu is an intrinsic imaging and therapy pair and therefore of great interest to the radiopharmaceutical community. Chapters 3, 5 and 6 evaluate new chelate systems for this radionuclide, as well as a multifunctional chelate for use with ^{64}Cu, Re and ^{99m}Tc.

1.4 Radioisotope Production and Generators

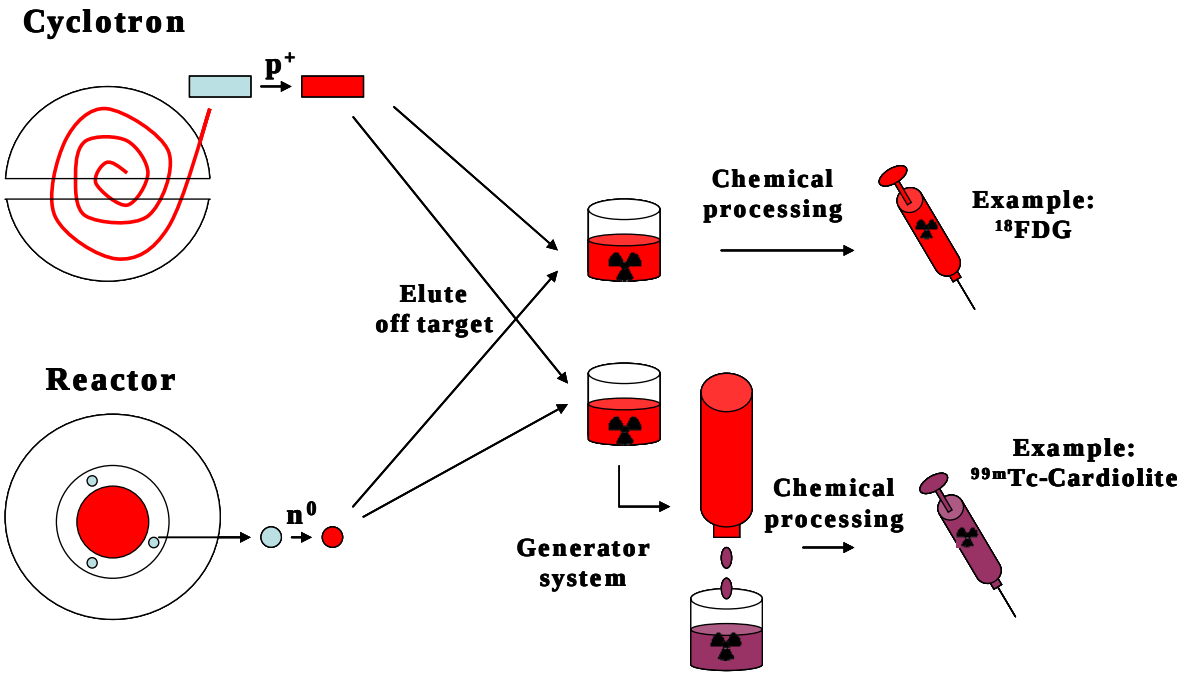

Figure 1.4 Schematic production pathway for radiopharmaceuticals.

While many radionuclides have favourable properties for imaging and therapy, the ease of production can be a greatly limiting factor for both clinical applications and research. Radioisotopes can be produced in two main facilities: cyclotrons or reactors.

Briefly, reactor-produced isotopes are furnished by irradiation of a non-radioactive target with a neutron flux in a specific energy range. Subsequently, the radioactive product is extracted from the target, processed and ready for incorporation into the actual radiopharmaceutical. Cyclotron-produced isotopes are synthesized by irradiation of a non-radioactive target with a beam consisting of protons, deuterions or alpha nuclei. The subsequent processing is analogous to reactor-produced isotopes (Figure 1.4).

These types of immediate radiopharmaceutical production after generation of the radionuclide are dependent on the presence of a production facility (reactor or cyclotron) in the immediate vicinity. This is especially true for isotopes with relatively short half-lives such as ^{18}F and ^{11}C. Despite the current commercial availability of cyclotrons that

are virtually 1/10 of the size of the cyclotrons manufactured in the 1980s, the need for isotope production in close proximity to the patient remains a greatly limiting factor for the application of radionuclides, which depends on this production pathway, such as ^{18}F and ^{11}C.

Generator systems alleviate this spatial problem because they serve as portable radionuclide dispensaries. In order to furnish a generator system, the parent nuclide must have a reasonably long half-life, must be produced at a reactor or cyclotron facility, and should be immobilized on a sorbent. The parent nuclide then decays to produce the daughter nuclide, which can be conveniently eluted off the sorbent material and subsequently chemically processed to afford the radiopharmaceutical. Due to their small size, generators can be shipped and used at clinics far removed from cyclotron or reactor facilities. Cyclotron produced radionuclides and generator systems relevant to work presented in this thesis, together with production method and decay properties, are summarized in Table 1.3.

Table 1.3 Widely used and investigated radionuclides and their production.[15]

daughter nuclide	parent nuclide	$t_{1/2}$ parent nuclide	production of parent	clinically used generator?
^{99m}Tc	^{99}Mo	66 h	^{235}U [n, f] (reactor) ^{98}Mo [n, γ] (reactor)	yes
^{188}Re	^{188}W	69.4 d	^{186}W [n, γ] (reactor)	no
^{186}Re	-	-	^{185}Re [n, γ] (reactor)	-
^{68}Ga	^{68}Ge	271 d	^{69}Ga[p, 2n] (cyclotron)	clinical trials[16]
^{67}Ga	-	-	^{68}Zn[p, 2n] (cyclotron)	-
^{64}Cu	-	-	^{64}Ni[p, n] (cyclotron)	-

The relative ease of production of ^{99}Mo for the past four decades, and the favourable decay properties of both parent and daughter nuclide has led to domination of

the imaging field by the SPECT nuclide ^{99m}Tc. Hence, the majority of radiopharmaceuticals are ^{99m}Tc-based agents, used in 85% of the millions of scans performed annually in nuclear medicine.[20]

1.5 Isotope Supply Problems

Due to aging reactor facilities that produce the global supply of ^{99}Mo such as the NRU in Chalk River, Ontario, the supply of ^{99}Mo to all of North America, parts of South America and Asia has been impacted by reactor shut-downs. This looming problem became a full-blown isotope crisis when the only operating reactor, NRU, was shut down unexpectedly in 2007, and the failure of the replacement reactors MAPLE 1 and 2 tore a large hole in the global isotope supply.

Solutions to this isotope supply problem include two different, strongly contrasting approaches. One is to find a convenient route to produce ^{99m}Tc and/or its parent nuclide ^{99}Mo via the increasingly available cyclotron facilities,[21] and the other is to investigate other radionuclides with favourable properties to replace ^{99m}Tc-based radiopharmaceuticals. Due to the multiple decade "reign" of the market by ^{99m}Tc, the development of other radionuclides with suitable properties for imaging has not been vigorously pursued.

Now, in light of this recent crisis, alternatives are being seriously re-evaluated. The criteria for selection include: cyclotron production, optimal decay properties for PET or SPECT and suitably long half-life, with generator availability being strongly preferred. The radioisotopes ^{64}Cu and ^{68}Ga are amongst the most suitable candidates. ^{64}Cu is of interest because of its dual β^-/ β^+ emission and reasonably long half-life which could allow shipping and applications for antibodies and other slowly localizing targeting vectors. ^{68}Ga is attractive because it can be eluted from a ^{68}Ge-based generator. Compared to the ^{99m}Tc-based system, the ^{68}Ga-generator would also have a much longer lifetime in the clinic. The positron emission would allow for higher resolution scans and the short half-life of ^{68}Ga would limit the exposure for patients. In addition, while ^{99m}Tc is eluted as $^{99m}TcO_4^-$ (oxidation state VII) from the generator and must be reduced in most cases in order to have the capability to form coordination compounds, ^{68}Ga is eluted

as its only stable and ready to chelate oxidation state III.

While the original concept for the ^{68}Ga-generator was developed over half a century ago,[22] the problem of ^{68}Ge bleed-through upon column elution remained an issue for several decades.[23] Only recently, due to rekindled interest in alternative generator technologies, attempts have been made to solve this problem, but the current commercially available generators are designated "for research purposes only".[24] The generator system is not FDA approved, hence the number of current routinely used ^{68}Ga based imaging agents in the clinic is zero. A clinical phase IV study on ^{68}Ga-DOTA-NOC is recruiting patients currently,[16] which is promising; however, the sophisticated labelling and purification procedure necessary adds an additional hurdle for the simple translation of this technology into the clinic.

1.6 Chelates for the Purpose of Radiometal Coordination

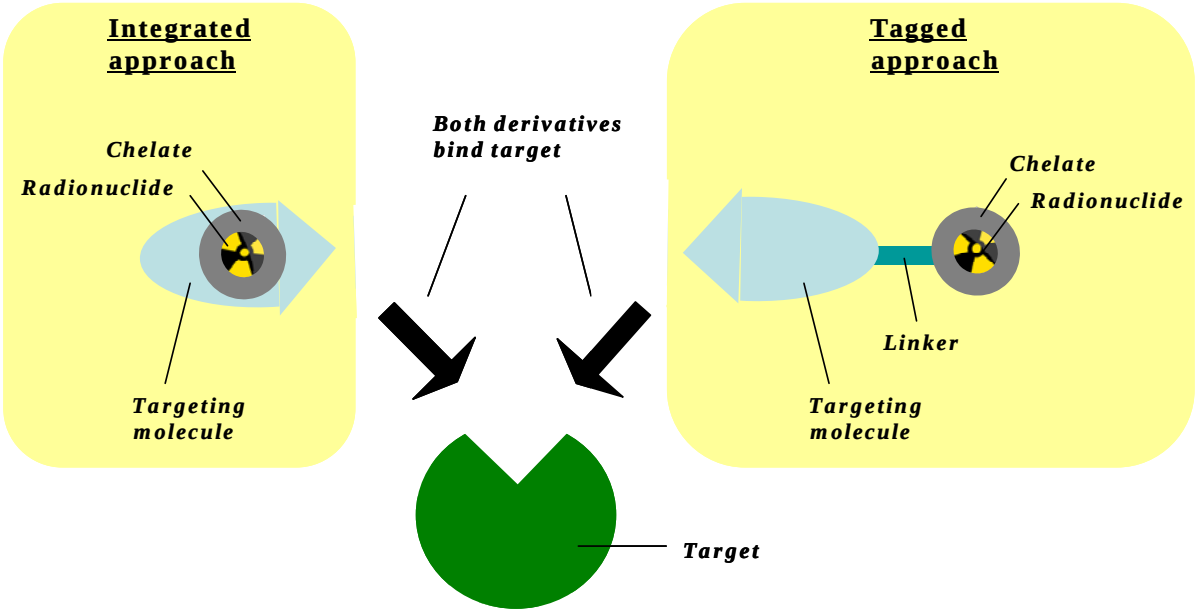

Figure 1.5 Scheme of two complexes following two different methodologies for radiometal incorporation while targeting the same receptor.

Radiometals by themselves generally have no targeting ability. Specific targeting of tissues or organs can be achieved by coordination of the radiometal to specific scaffolds. This can be done by using two distinct methodologies: integration or tagging

(Figure 1.5). In the case of the integrated approach, the metal complex is part of the moiety relevant for target binding. For the tagged approach, the metal complex is not essential for binding of the target and is usually attached to the targeting moiety by a linker. Both methodologies require a chelate system to be present which binds the metal strongly in order to avoid metal loss by decomplexation *in vivo*. The chelate itself can strongly influence clearance or localization of the radiopharmaceutical.

1.7 Coordination Chemistry of ^{99m}Tc

As the only naturally radioactive second row transition metal, Tc has no stable isotope. ^{99}Tc is the most readily available isotope with a half-life of 2.13 x 10^5 years.[25] While most Tc chemists were accustomed to working with this long lived radioisotope several decades ago, nowadays, strict regulations for work with extremely long lived isotopes has limited this practice. Now, the heavier, group 7 congener Re is frequently used to study the corresponding coordination complexes on a macroscopic level. Despite small differences in redox chemistry ($[ReO_4]^-$ is somewhat harder to reduce then $[TcO_4]^-$) and ligand preference (Re is softer than Tc), the similarity between the two metals and their main, stable oxidation states is great enough for the validation of Re complexes as macroscopic placeholders for the corresponding microscopic ^{99m}Tc complexes.

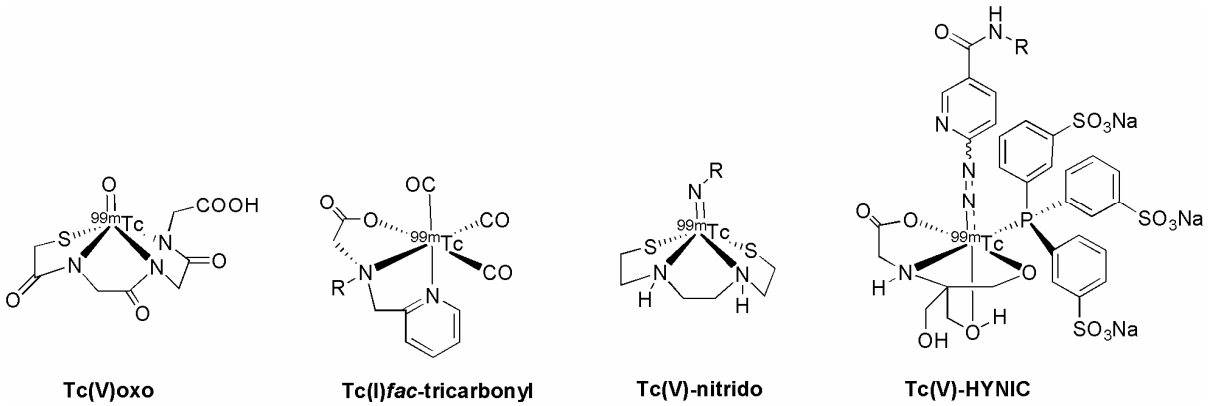

Figure 1.6 Four of the most commonly used ^{99m}Tc synthons; Tc(oxo) with a MAG_3-type coordination environment, $[Tc(CO)_3]^+$ coordinated by a typical tridentate ligand, Tc(nitrido) with an $N_{4-x}S_x$ type chelate and Tc(HYNIC) with a typical coordination environment. All chelates can be derivatized through the variable R functionality.

Because of the extremely small quantity of the radiochemical complexes (~10^{-10} M), the most frequently used characterization tool is measurement of retention time on radio-HPLC or radio-TLC; the retention time of the fully characterized Re complex can be found on the corresponding UV-HPLC trace for comparison.

Due to the extensive investigation of ^{99m}Tc over multiple decades and the variety of oxidation states available, a great number of successfully used coordination environments have been developed. The different cores are preferentially coordinated by multidentate ligand systems, which can be modulated for their pharmacokinetic behaviour. The oxo core is among the earlier developments of ^{99m}Tc chemistry. Some of the most frequently used coordinating ligands are of the $N_{4-x}S_x$ type, first developed by Davison, Orvig and coworkers.[26] Mercaptoacetyltriglycine (MAG_3) remains one of the predominant ligand systems used in the clinic as a small molecule imaging agent,[27] but it has also been widely explored as a bifunctional chelate.[28-30] Drawbacks of this core are the harsh reduction conditions required using $SnCl_2$. The reduction must be done in the presence of either the MAG_3 ligand or with an intermediate easily exchangable ligand system such as glucoheptonate or gluconate, in order to avoid rapid re-oxidation or the formation of *syn* and *anti* isomers,[31] which can exhibit different *in vivo* behaviour.[32] Subsequently, the field of Tc chemistry endeavoured to find a new ^{99m}Tc core which would obviate the need for harsh reducing agents and solve the isomer problem.

Among two earlier solutions are the nitrido $[TcN]^{2+}$-core[33] and the Tc(HYNIC)-core.[34] While both systems exhibit interesting coordination chemistry and can produce stable complexes, the multi-step labelling procedure and difficulties in characterizing the chemical structure of the complexes formed render these systems incompatible with kit formulations. Abandoning the high oxidation state Tc(V)oxo-core however constituted a different approach; Alberto and coworkers first published a kit formulation, which produces the *fac*-$[^{99m}Tc(CO)_3]^+$ core[35] with three labile aquo ligands. The compound $[^{99m}Tc(CO)_3(H_2O)_3]^+$ is stable and soluble in aqueous solution and the water ligands can be readily exchanged using bi- and tri-dentate ligand systems (Figure 1.6).[36] The low-spin, d^6 system exhibits increased inertness compared to the Tc(V)oxo-core (d^2), slowing ligand exchange rates and providing a highly versatile, stable coordination environment, even with ligand systems such as the cyclopentadienyl moiety[37] and truncated, nido-

carboranes.[38] This facilitates simple modification of the pharmacokinetic behaviour by adaptation of the coordinating ligand system and has led to a wide variety of applications for small molecule imaging agents[39-41] including bioconjugates of small molecules[42,43] and a plethora of peptide conjugates.[44-47] One aspect of the broad ligand tolerance of the $[^{99m}Tc(CO)_3]^+$ core is showcased in this thesis in Chapter 2.

1.8 Coordination Chemistry of ^{64}Cu

^{64}Cu ($t_{1/2}$ = 12.7 h, β^+ 17.4 %, E_{max} = 0.656 MeV, β^- 39 %, E_{max} = 0.573 MeV) is a cyclotron-produced radionuclide of interest for both positron emission tomography (PET) and radiotherapy.[48] Unlike Tc, Cu has naturally occurring stable isotopes, which serve as a convenient tool for the investigation and characterization of the coordination complexes formed, both micro- and macroscopically. The most relevant oxidation states present in aqueous solution are Cu(I) and Cu(II). As Cu(I), the metal ion has a d^{10} configuration with a preference for rather soft ligands, forming a variety of fairly labile complexes.[49] Under normal, oxidative conditions the predominant oxidation state is Cu(II), where the metal ion has a d^9 configuration with preference for borderline hard ligand systems. Predominant complex geometries with tetra- to hexadentate environments are square planar, trigonal bipyramidal, square pyramidal and distorted octahedral.

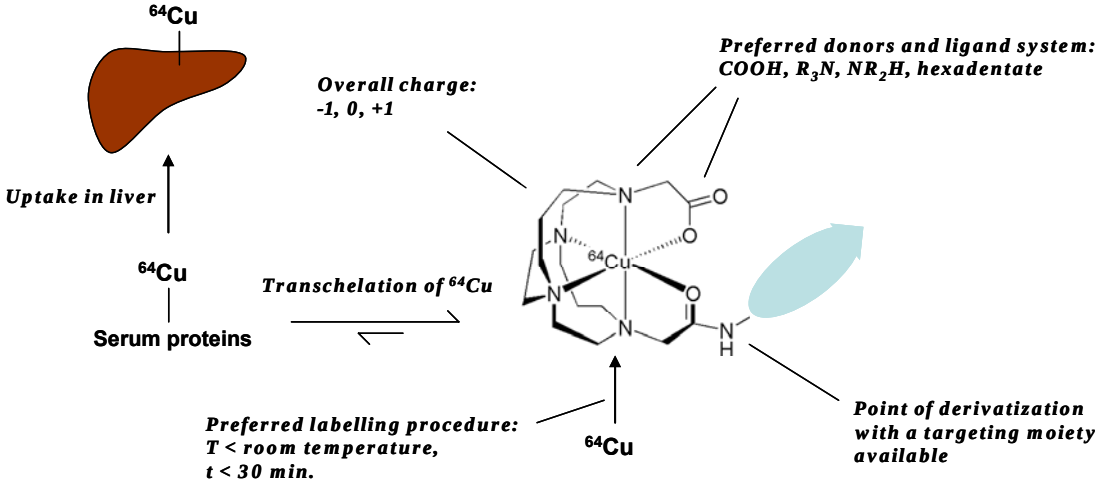

Figure 1.7 Summary of desired properties for the optimal chelate for ^{64}Cu, shown on the example of the ^{64}Cu complex with a derivatized version of the cross-bridged macrocycle CB-TE2A.

The latter is prone to Jahn-Teller distortion, manifested in axial elongation or

equatorial compression of bonds in the corresponding complexes. Due to rapid ligand exchange kinetics, the stable coordination of Cu(II) is a difficult task, but important in radiochemical applications. Rapid coordination of the radiometal under mild conditions is an advantage (especially if sensitive biomolecules are present) but not essential. If dissociated from the coordinating ligand *in vivo*, ^{64}Cu rapidly associates with serum proteins and subsequently accumulates in the liver, impacting clearance and possibly imaging.[50] The overall charge of the complex must be -1, 0 or +1 in order to facilitate clearance of the complex *in vivo*. Cross-bridged macrocyclic and cage-like hexadentate ligand systems such as 4,11-bis(carboxymethyl)-1,4,8,11-tetraazabicyclo[6.6.2]-hexadecane (CB-TE2A) are among the current front runners for stable coordination with minimal metal ion loss even after multiple days of incubation under physiologically relevant conditions (Figure 1.7).

Acyclic chelates often fall victim to rapid decomplexation kinetics, resulting in the loss of the radiometal. Chapter 5 gives a more elaborate review of current literature on Cu(II) chelates for the purpose of radiolabelling and investigates an unusual acyclic chelate for the purpose of stable Cu(II) chelation. Work described in Chapter 3 attempts to bridge the vastly different ^{99m}Tc and ^{64}Cu technologies.

1.9 Coordination Chemistry of $^{67/68}$Ga

Although Ga is a main group metal, it has many similarities to transition metals with respect to its coordination chemistry. Because of its low redox potential, Ga(III) is the only relevant oxidation state in aqueous media, with its valence electrons in a d^{10} configuration. While tetradentate to hexadentate coordination is observed with geometries ranging over tetrahedral,[51] square pyramidal[52] and distorted octahedral,[53-56] many Ga coordination complexes tend to be rather labile. In order to be suitable for applications as a radiopharmaceutical, the Ga(III) ion must be coordinated in a stable fashion; preventing the radiochemical complex from *in vivo* hydrolysis to water soluble $[Ga(OH)_4]^-$ (the predominant species at physiological conditions) or transchelation by the iron scavenging protein transferrin leading to subsequent bone uptake (Figure 1.8).[57]

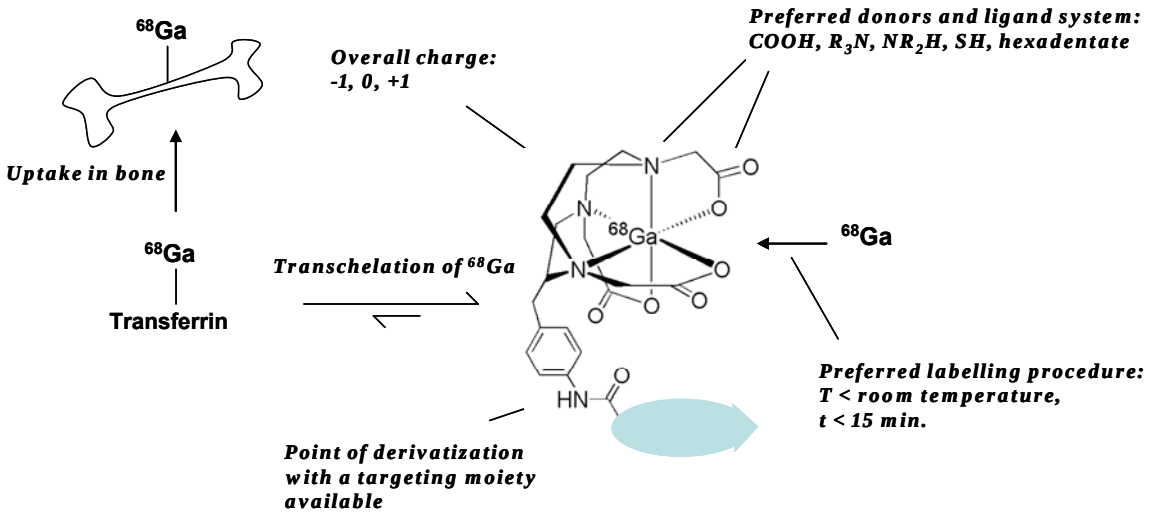

Figure 1.8 Summary of desired properties for the optimal chelate for ^{68}Ga, shown on the example of the ^{68}Ga complex with a derivatized version of the macrocycle NOTA.

Ga(III) is present as the hydrated cation at pH < 3, so coordination must happen under acidic conditions. Paired with the short half-life of ^{68}Ga (68 minutes), these limitations make the coordination of this radiometal non-trivial. The Ga(III) cation prefers hexadentate chelation using hard ligand systems much like a redox innocent Fe(III). The similarity to Fe(III) in charge and ionic radius explains the high affinity of Ga(III) for *apo*-transferrin. Few ligand systems have established themselves as reliable bifunctional chelates for radiopharmaceutical applications. These ligands are predominantly macrocylic, and form complexes with Ga(III) with an overall charge of -1, 0 or +1 in order to facilitate clearance of the complex *in vivo*. Due to the slow kinetics of most macrocycles compared to acyclic chelates,[58] only one routinely used functionalized chelate, 1,4,7-triazacyclononane-1,4,7-triacetic acid (NOTA), is capable of coordinating ^{68}Ga at room temperature within less then 15 minutes and holding on to the metal in a stable fashion *in vivo*.[58]

The only ^{68}Ga-based radiopharmaceutical in clinical studies, ^{68}Ga-DOTANOC (Figure 1.9)[59] relies on a complex pre- and post-labelling purification system, because the macrocyclic chelate used for this conjugate is 1,4,7,10-tetraazacyclododecane -N,N',N",N'"-tetraacetic acid (DOTA), a chelate with less than favourable labelling properties.[60] A kit formulation, where the generator is directly eluted into a vial containing the ligand system, forming a ready-to-inject radiopharmaceutical and

obviating the need for lengthy purification procedures could be a major advantage for a compound with potential for clinical applications. Rapid coordination is an attractive property for kit formulations, thus acyclic chelates may have great and so far underestimated potential if fast decomplexation can be impeded.

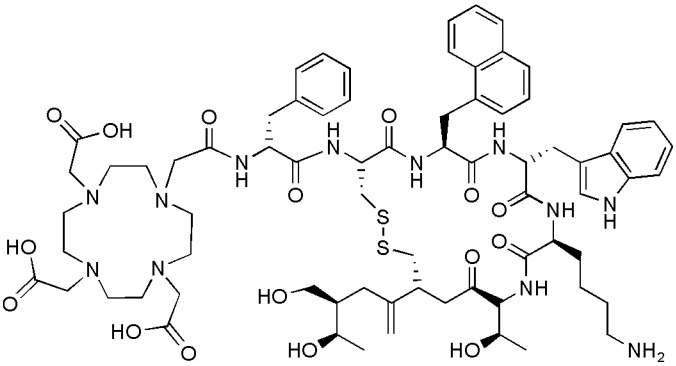

Figure 1.9 DOTANOC, a somatostatin analogue currently used with ^{68}Ga in clinical trials.

The introduction to Chapter 4 completes this small overview given above, while the experimental part elaborates on the screening of acyclic chelates containing amino, pyridine and carboxylate ligands for the fast and efficient coordination of ^{68}Ga at room temperature. This represents both a continuation of, but also a somewhat new spin on, the Orvig group's two decade long investigation of group 13 metal complexes.

1.10 Thesis Overview

This thesis focuses on exploring the synthesis of ligand systems and their corresponding coordination chemistry with metals of great relevance for nuclear medicine applications. The ultimate goal in each chapter is the investigation of the radioactive complex and the corresponding non-radioactive coordination complex, but great detail of the actual organic syntheses of ligand systems is included, as the ligand systems are integral to the development of potential imaging agents. All systems investigated are acyclic ligands containing pyridine and/or carboxylate donor groups.

Chapter 2 focuses on the synthesis, chemistry and biological behaviour of three amphiphilic complexes of Re and ^{99m}Tc(CO)$_3$ with different coordination spheres while carrying the same lipophilic aliphatic "tail". The multi-step synthesis is a key focus of

this chapter, which also includes the coordination compounds, radiochemistry and contrasting biodistributions of the three radiolabelled complexes.

Chapter 3 attempts to bridge the contrasting coordination chemistry of the $[M(CO)_3]^+$ core (M = Re, ^{99m}Tc) with ^{64}Cu by designing and synthesizing both a model compound and a biotin conjugate of a flexible, acyclic ligand scaffold capable of fast coordination of both radiometals. While the basic ligand structure had been reported previously,[61] the functionalization has not been previously attempted.

The tetradentate ligand system investigated in Chapter 3 provides the basis for the small library of acyclic ligands with various bite sizes and denticities investigated for Ga(III) radionuclide coordination in Chapter 4. The various acyclic ligand systems were compared with respect to radiolabelling efficiency and the stability of the resulting complex. The most suitable ligand system (termed H_2dedpa, Figure 1.10) was found to be surprisingly stable against *apo*-transferrin. Subsequently, two model compounds for possible functionalization and conjugation to targeting molecules were also synthesized and investigated for coordination properties with radioactive and non-radioactive Ga.

Chapter 5 investigates the viability of the H_2dedpa ligand system for the coordination of radioactive and non-radioactive isotopes of Cu. Redox properties were also investigated; these are relevant for comparison to other frequently used ligand systems for ^{64}Cu.

Chapter 6 describes the functionalization of the H_2dedpa ligand system with targeting moieties, following the tagged approach (Figure 1.5). This chapter has a significant synthetic focus and culminates in the successful syntheses of two conjugates of the small, cyclic peptide RGD that targets angiogenesis.[62] Subsequently, both conjugates were tested for their ability to coordinate the radionuclides $^{67/68}$Ga and ^{64}Cu, and yield results similar to those obtained for the corresponding, non-functionalized model compounds investigated in Chapters 4 and 5.

Chapter 7 investigates functionalization of the ligand system following the integrated approach (Figure 1.5). Because H_2dedpa forms a cationic complex upon coordinating Ga(III), attempts were made to mimic the routinely used SPECT agents for myocardial perfusion imaging, which are cationic, lipophilic structures. These extensive synthetic efforts culminated in seven different H_2dedpa derivatives exhibiting a range of

lipophilicity. The biodistribution of these compounds was also investigated to evaluate their potential for cardiac imaging.

Finally, Chapter 8 summarizes and concludes the work showcased in this thesis and gives some perspectives for future work with the H_2dedpa scaffold.

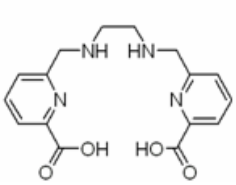

Figure 1.10 H_2dedpa.

Chapter 2: Small Amphiphilic Rhenium and ^{99m}Technetium Tricarbonyl Complexes*

2.1 Introduction

Because of its availability and low cost, ^{99m}Tc has been a radionuclide of interest in radiopharmaceutical chemistry and nuclear medicine for the past four decades.[63] Tc also has ideal physical properties ($t_{1/2}$ = 6 h, γ = 141 keV) for imaging with single photon emission computed tomography (SPECT).[64] As a result, its chemistry has been extensively researched and the vast majority of nuclear medicine scans utilize this isotope. While many compounds in the clinic still rely on high oxidation state ^{99m}Tc cores[65] demanding harsh labelling conditions, more recent research has focused on the versatile and highly stable *fac*-$[^{99m}Tc(CO)_3(H_2O)_3]^+$ complex developed by Alberto *et al*.[35] The *fac*-$[^{99m}Tc(CO)_3(H_2O)_3]^+$ complex has a ^{99m}Tc(I) metal center in a d^6 low-spin electron configuration, rendering it inert toward a broad range of experimental conditions. It can be prepared in high yields via a commercially available kit (Isolink, Covidien, Mansfield, MA) under aqueous conditions using the boranocarbonate anion as the reducing agent and *in situ* CO source.[35] Simple exchange of the three water molecules can be achieved with suitable chelates in a *fac* coordination mode,[66,67] shown previously in examples of small molecule constructs as potential perfusion agents, or in targeted agent bioconjugates such as derivatized amino acids, carbohydrates, peptides, and nucleosides.[36,68,69] These mild labelling conditions are more applicable for use with potential highly sensitive biomolecules.

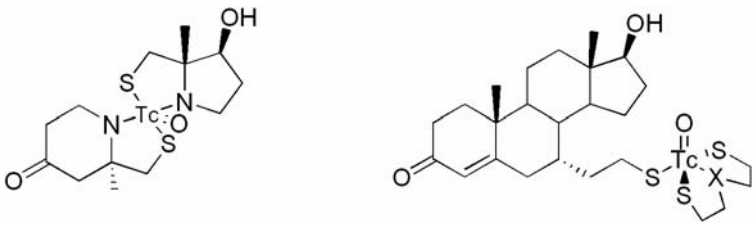

Figure 2.1 Examples of the integrated (left) and tagged (right) approach on steroid scaffolds.

* Work presented in this chapter has been published: "Design, Synthesis, and Imaging of Small Amphiphilic Rhenium and ^{99m}Technetium Tricarbonyl Complexes", E. Boros, U. O. Häfeli, B. O. Patrick, M. J. Adam, C. Orvig , *Bioconjugate Chem* **20** , 1002-1009 (2009).

Two distinct methodologies can be followed to incorporate ^{99m}Tc into novel imaging agents: the so-called "tagged" approach.[70] and the "integrated" or "technetium-based" approach.[71] Examples are represented in Figure 2.1 from the work of Katzenellenbogen and coworkers, who have found ways of using both methodologies on the same targeting moiety. The work in this chapter describes efforts towards obtaining a simple, small, and non-target specific complex following the "integrated" approach. It was the aim to explore the *in vivo* properties of novel, amphiphilic metal complexes of the $[^{99m}Tc(CO)_3]^+$ core. In an attempt to achieve this, the synthesis incorporated a mimic of the charge distribution of molecules highly abundant and essential to cell membranes, aiming for an *in vivo* distribution of the resulting complexes comparable to other small amphiphilic molecules such as cocamidopropyl betaine (CAPB, zwitterionic), sodium dodecylsulfate (SDS, anionic),[72] and glyceryl laurate (neutral) (Figure 2.2). These compounds, also known as surfactants, are known to integrate into the lipid bilayer before their concentration (much larger than the concentration range imaging agents usually operate at) exceeds the saturation concentration and solubilizes the membrane.[73] By utilizing significantly shorter lipophilic chains, it is proposed that a large fraction of liver uptake can be obviated, opposed to complexes bearing longer aliphatic carbon chains.[74]

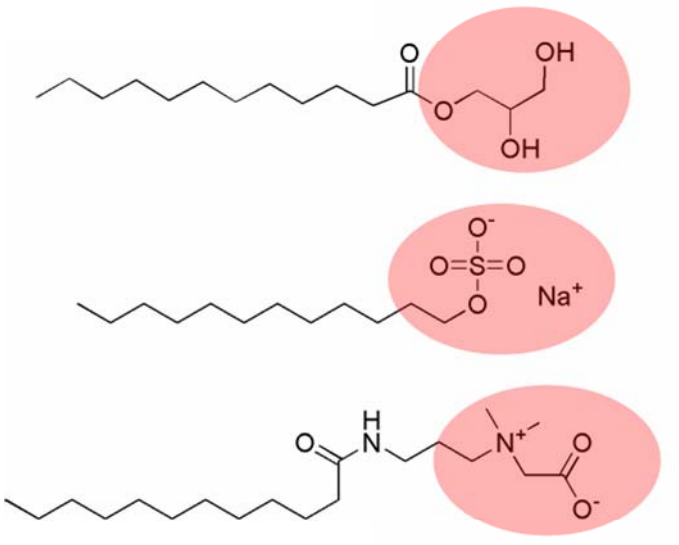

Figure 2.2 Examples of commercial surfactants with different polar head groups (denoted in red): neutral, anionic and zwitterionic (from top to bottom).

Various entities were examined, including a neutral, anionic and amphiphilic complex. Bidentate attachment onto the $[^{99m}Tc(CO)_3]^+$ core has been widely explored by previous members of the Orvig group and has been found to have decreased *in vitro* stability, hence tridentate chelates were chosen.[40] Two ligand systems investigated in this work have been explored previously and their stability and coordination mode have been found to have excellent properties.[36]

Each lipophilic residue was incorporated by attachment of a short, saturated C_8-chain in a consistent fashion via a simple ester bond joined with an ethanolamine linker piece. By forming the coordination complex, compounds with an overall structure analogous to commercially available surfactants (Figure 2.2) are furnished. This differs strongly from the previously used tagged approach with long-chain fatty acids used as lipiodol surrogates for liver targeting,[74] as well as from conventional fatty acid type labelling for the purpose of cardiac imaging,[75,76] where carboxylic acids are not used for coordination but for potential oxidation by the fast metabolizing heart muscle (Figure 2.3). [77]

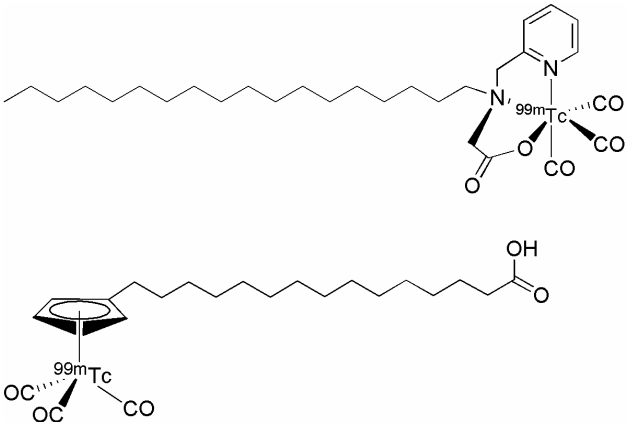

Figure 2.3 Previously reported $[Tc(CO)_3]^+$ complexes bearing long aliphatic chains.[74,76]

2.2 Experimental

2.2.1 Materials and Methods

$Re(CO)_5Br$ is commercially available (Strem). The analytical thin-layer chromatography (TLC) plates were aluminum-backed ultrapure silica gel 250 μm; the flash column silica gel (standard grade, 60 Å, 32-63 mm) was acquired from Silicycle. ^1H and ^{13}C NMR spectra were recorded on Bruker AV300 or AV400 instruments at ambient temperature; the NMR spectra are expressed on the δ scale and referenced to residual solvent peaks or internal tetramethylsilane. Electrospray ionization mass spectrometry (ESI-MS) spectra were recorded on a Micromass LCT instrument at the Department of Chemistry, University of British Columbia. High-performance liquid chromatography (HPLC) analysis of cold compounds was done on a Phenomenex Synergi 4 μm Hydro-RP 80A column (250 mm × 4.6 mm) on a Waters WE 600 HPLC system equipped with a 2478 dual-wavelength absorbance UV detector run using the Empower software package. IR spectra were collected neat in the solid or liquid state on a Thermo Nicolet 6700 FT-IR spectrometer. TLC analysis of radiolabeled compounds was performed on a Bioscan-System 200 Imaging scanner equipped with a Bioscan-Autochanger 100. Radio-TLCs were prepared with acetonitrile as the mobile phase. HPLC analyses of radiolabeled complexes were performed on a Knauer Wellchrom K-1001 HPLC equipped with a K-2501 absorption detector and a Capintec radiometric well counter. A Phenomenex Hydro- Synergi 4 μm C18 RP analytical column with dimensions 250 × 4.6 mm was used for both analysis and purification. HPLC solvents consisted of 0.1% trifluoroacetic acid in water (solvent A) and methanol (solvent B). Samples were analyzed and purified with a linear gradient method (100% solvent A to 100% solvent B over 30 min). For biodistributions, organ samples were counted in a Packard Cobra II autogamma counter one to two days after administration. μSPECT and CT images were recorded on an XSPECT instrument from Gamma Medica (Northridge, CA).

2.2.2 Ligand Synthesis

(2-Hydroxyethyl)carbamic acid tert-butyl ester (1).

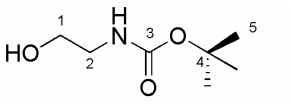

Boc_2O (2.18 g, 10 mmol) was added to ethanolamine (610 mg, 10 mmol) at 0 °C and allowed to stir for 1 h. A colorless precipitate formed immediately with the evolution of heat. Column chromatography (hexanes/ethyl acetate, silica, 6:1) with subsequent evaporation of the solvent yields 1.45 g (9.9 mmol, yield 90 %, R_f 0.1) of the desired product as a colourless oil. ^{1}H NMR (300 MHz, $CDCl_3$, δ): 3.55 (t, $^3J_{1,2}$ = 5.8 Hz, *H1*, 2H), 3.14 (t, $^3J_{1,2}$ =5.8 Hz, *H2*, 2H), 1.33 (t, *H5*, 9H). ^{13}C NMR (75 MHz, $CDCl_3$, δ): 155.6 (*C3*), 79.3 (*C4*), 61.6 (*C1*), 42.9 (*C2*), 28.1(*C5*). IR (cm^{-1}): 1682 (m), 1517 (m), 1164 (m). HR-ESI-MS calcd. for $C_7H_{15}NNaO_3$: 184.1887, found: 184.1874 $[M + Na]^+$.

Octanoic acid 2-*tert*-butoxycarbonylaminoethyl ester (2).

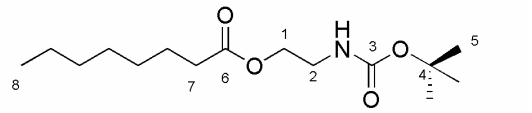

(2-Hydroxyethyl)carbamic acid *tert*-butyl ester (**1**, 1.45 g, 9.9 mmol) was dissolved in toluene (50 mL) to afford a clear solution. EDMA (ethyldimethylamine, 20 mL) and octanoyl chloride (1.908 g,11.78 mmol, 1.3 eq) were added dropwise simultaneously. A cloudy precipitate formed immediately, and the reaction solution was stirred at room temperature for another 1.5 h, after which time the solvent and a large fraction of the added EDMA were evaporated under reduced pressure. The residue was redissolved in H_2O (30 mL) and extracted into ether (30 mL) twice. The organic phase was collected and the solvent evaporated under reduced pressure to afford the crude product as a yellow oil which was purified by column chromatography (silica, hexanes/ethyl acetate, 1:1, R_f = 0.6) to yield octanoic acid 2-*tert*-butoxycarbonylaminoethyl ester (1.505 g, 5.45 mmol, yield 53 %) after solvent evaporation. ^{1}H NMR (400 MHz, $CDCl_3$, δ): 4.07 (t, *H7*, 2H), 3.33 (t, $^3J_{1,2}$ = 7.6 Hz, *H2*, 2H), 2.27 (t, $^3J_{1,2}$ =7.6 Hz, *H1*, 2H), 1.57 (m, CH_2, 2H), 1.40 (s, *H5*, 9H), 1.24 (m, CH_2, 8H), 0.83 (t, *H8*, 3H). ^{13}C NMR (100 MHz, $CDCl_3$, δ): 173.5 (*C6*), 155.7 (*C3*), 79.6 (*C4*), 63.2 (*C1*), 39.55 (*C2*), 33.9, (*C7*), 31.5, (*C*H$_2$), 28.7 (*C*H$_2$), 28.2 (*C5*), 24.7 (*C*H$_2$), 22.4

(CH_2), 13.9 ($C8$). IR (cm^{-1}): 1684 (m), 1631 (m), 1482 (w). HR-ESI-MS calcd. for $C_{15}H_{29}KNO_4$: 326.1734, found: 326.1731 $[M + K]^+$.

Octanoic acid 2-aminoethyl ester (3).

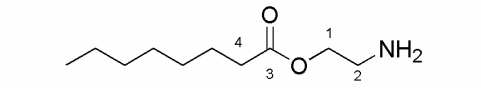

2-*tert*-Butoxycarbonylaminoethyl ester (**2**, 1.505 g, 5.45 mmol) was dissolved in dichloromethane (4 mL). Trifluoroacetic acid (4 mL) was added, and the reaction solution was stirred for 20 min after which time a slow change of colour to light yellow was observed. TFA and CH_2Cl_2 were removed *in vacuo*, and the oily residue was purified by column chromatography (CH_2Cl_2/ CH_3OH, 4:1, R_f = 0.15) yielding 2-aminoethyl ester octanoic acid (444 mg, 2.37 mmol, yield 43 %) after rotary evaporation as a colourless oil which solidifies upon standing. ^{1}H NMR (300 MHz, CD_3OD, δ): 3.55 (t, $^3J_{1,2}$ = 5.8 Hz, *H1*,2H), 3.25 (t, $^3J_{1,2}$ = 5.8 Hz, *H2*, 2H), 2.18 (t, $^3J_{4,CH_2}$ = 6.01 Hz, *H4,* 2H), 1.57 (m, CH_2, 2H), 1.28 (m, CH_2, 8H), 0.86 (t, CH_3, 3H). ^{13}C NMR (75 MHz, CD_3OD, δ): 173.7 (*C3*), 62.3 (*C1*), 43.4 (*C2*), 37.6-23.9 (six signals, CH_2), 14.7 (CH_3). IR (cm^{-1}): 3312 (w), 2954 (s), 2924 (s), 2855 (s), 1637 (s),1552 (m), 1464 (m). HR-ESI-MS calcd. for $C_{10}H_{21}NNaO_2$: 210.1470, found: 210.1481 $[M + Na]^+$.

Octanoic acid 2-[(pyridin-2-ylmethyl)amino]ethyl ester (4).

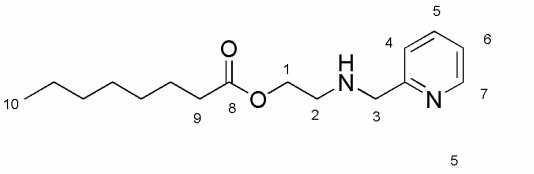

Octanoic acid 2-aminoethyl ester (**3**, 0.51 g, 2.7 mmol) was dissolved in dry ethanol (15 mL). Na_2CO_3 (10 equiv, 2.86 g) was added to afford a turbid solution. Pyridine-2-aldehyde (0.27 g, 237 μL, 0.95 eq) was added, and the reaction mixture was stirred overnight at room temperature. After formation of the intermediate imine was confirmed by TLC, $NaBH_4$ (95 mg, 2.51 mmol, 0.98 eq) was added and the reaction mixture was subsequently stirred for another 1 h. CH_2Cl_2 (20 mL) was then added and extracted twice with a saturated solution of $NaHCO_3$ (20 mL). The organic fractions were collected, and the solvent was evaporated. The crude product was purified by column chromatography (silica, CH_2Cl_2/ CH_3OH, 85:15, R_f = 0.55) yielding octanoic acid 2-[(pyridin-2-ylmethyl)amino]ethyl ester (361 mg, 1.3 mmol, yield 48 %) as a colourless oil with low viscosity, after evaporation of the solvent. ^{1}H NMR (300

MHz, $CDCl_3$, δ): 8.48 (m, $^3J_{6,7}$ = 5.6 Hz, *H7*, 1H), 7.66 (m, $^3J_{4,5}$ = 7.7 Hz , *H5*, 1H), 7.32 (d, $^3J_{4,5}$ = 7.7 Hz, *H4*, 1H), 7.17 (t, $^3J_{6,7}$ = 5.6 Hz, *H6*, 1H), 3.91 (s, *H3*, 2H), 3.63 (m, *H2,* 2H), 2.14 (t, $^3J_{9,\ CH_2}$ = 6.01 Hz, *H9*, 2H), 1.56 (m, CH_2, 2H), 1.22 (m, CH_2, 8H), 0.82 (t, $^3J_{10,\ CH_2}$ = 6.3 Hz, *H10*, 3H). ^{13}C NMR (75 MHz, $CDCl_3$, δ): 174.5 (*C8*), 149.0 (*C7*), 148.3 (*C5*), 136.8 (*C4*), 122.3 (*C6*), 120.7 (*C7*), 64.3 (*C3*), 61.6 (*C2*), 54.1 (*C1*), 42.1-22.5 (six signals, CH_2), 13.9 (*C10*). IR (cm^{-1}): 3294 (br), 2925 (s), 2855 (s), 1632 (s), 1595 (s), 1549 (m). HR-ESI-MS calcd. for $C_{17}H_{30}N_2NaO_2$: 317.2205, found: 317.2188 $[M + Na]^+$.

Octanoic acid 2-(*tert*-butoxycarbonylmethylpyridin-2-ylmethylamino)ethyl ester (5).

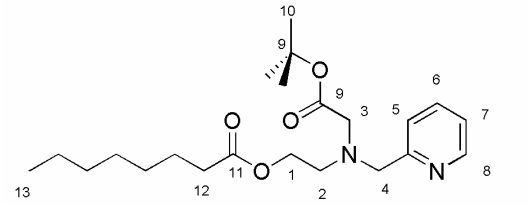

Octanoic acid 2-[(pyridin-2-ylmethyl)amino]ethyl ester (**4**, 361 mg, 1.3 mmol) was dissolved in dry CH_2Cl_2 (20 mL). Na_2CO_3 (about 10 eq, 2.86 g) was added to afford a turbid solution. *tert*-Butyl bromoacetate (1.4 eq, 354 mg, 1.8 mmol) was added and the mixture was stirred for 2 days. The solvent was evaporated after confirmation of product presence by ESI-MS. The crude product was purified by column chromatography (silica, CH_2Cl_2/ CH_3OH, 95:5, R_f = 0.8) and yielded the final product (109 mg, 0.27 mmol, yield 21%) after rotary evaporation of all solvents as a light yellow oil. ^{1}H NMR (300 MHz, $CDCl_3$, δ): 8.52 (d, $^3J_{7,8}$ = 4.1 Hz, *H8*, 1H), 7.68 (m, $^3J_{5,6}$ = 5.2 Hz, *H6*, 1H), 7.56 (d, $^3J_{5,6}$ = 5.2 Hz, *H5*, 1H), 7.17 (m, $^3J_{7,8}$ = 4.1 Hz, *H7*, 1H), 4.16 (t, $^3J_{1,2}$ = 5.7 Hz, *H1*, 2H), 4.03 (s, *H4*, 2H), 3.40 (s, *H3*, 2H), 3.00 (t, $^3J_{1,2}$ = 5.7 Hz, *H2*, 2H), 2.26 (t, $^3J_{12,\ CH_2}$ = 7.6 Hz, *H12*, 2H), 1.56 (m, CH_2, 2H), 1.46 (s, *H10*, 9 H), 1.26 (m, CH_2, 8H), 0.87 (t, $^3J_{13,\ CH_2}$ = 6.0 Hz, *H13*, 3H). ^{13}C NMR (75 MHz, $CDCl_3$, δ): 184.6 (*C9*), 173.7 (*C11*), 148.6 (*C8*), 136.8 (*C6*), 122.9 (*C5*), 122.1 (*C7*), 62.5 (*C1*), 60.3 (*C4*), 56.2 (*C3*), 52.5 (*C2*), 34.2-22.5 (six signals, CH_2) 28.2 (*C10*), 14.0 (*C13*). HR-ESI-MS calcd. for $C_{22}H_{36}N_2NaO_4$: 415.2573, found: 415.2584 $[M + Na]^+$.

Octanoic acid 2-(bis-*tert*-butoxycarbonylmethylamino)ethyl ester (6).

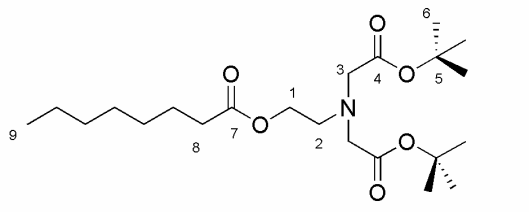

2-*tert*-butoxycarbonylaminoethyl ester (**3**, 0.1 g, 0.53 mmol) was dissolved in dry CH_2Cl_2 (10 mL). Na_2CO_3 (1 g) was added to afford a turbid solution. *tert*-Butyl bromoacetate (209 mg, 179 μL, 1.06 mmol, 2 eq) was added, and the mixture was stirred for 2 days. After the presence of the product was confirmed by ESI-MS, the solvent was evaporated and the crude mixture was purified by column chromatography (silica, hexanes/ethyl acetate, 1:1, R_f = 0.8) to yield the desired product (60 mg, 0.144 mmol, yield 27 %) after rotary evaporation of all solvents. ^{1}H NMR (75 MHz, $CDCl_3$, δ): 4.13 (t, $^3J_{1,\ 2}$ = 4.6 Hz, *H1*, 2H), 3.69 (s, *H3*, 4H), 3.45 (t, $^3J_{1,\ 2}$ = 4.6, Hz, *H2*, 2H), 2.95 (t, $^3J_{8,\ CH2}$ = 5.4 Hz, *H8*, 2H), 1.55 (m, CH_2, 2H), 1.41 (s, *H6*, 18 H), 1.21 (m, CH_2, 8H), 0.84 (t, *H9*, 3H). ^{13}C NMR (75 MHz, $CDCl_3$, δ): 170.2 (*C7*), 166.0 (*C4*), 62.7 (*C1*), 58.2 (*C3*), 52.4 (*C2*), 34.1-22.4 (six signals, *C*H_2), 27.6 (*C6*), 13.9 (*C9*). HR-ESI-MS calcd. for $C_{22}H_{41}NNaO_6$: 317.2832, found: 317.2844 $[M + Na]^+$.

Bis-*tert*-butoxycarbonylmethyl(2-octanoyloxyethyl)pyridin-2-ylmethylammonium bromide (7).

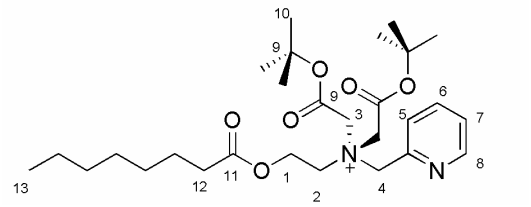

This compound is afforded as a side product of the synthesis of *N*-*N*-(*tert*-butylcarboxyethyl)-pyridinemethyl-2-aminoethyl ester octanoic acid and separated from the main product **5** by column chromatography (silica, CH_2Cl_2/ CH_3OH, 95:5, R_f = 0.35) yielding the product (37 mg, 0.072 mmol, yield 5.6 %) after solvent evaporation as a light orange oil. ^{1}H NMR (300 MHz, $CDCl_3$, δ): 9.59 (d, $^3J_{7,\ 8}$ = 4.8 Hz, *H8*, 1H), 8.48 (t, $^3J_{5,\ 6}$ = 7.7 Hz, *H6*, 1H), 8.21 (d, $^3J_{5,\ 6}$ = 7.7 Hz, *H5*, 1H), 8.05 (t, $^3J_{7,\ 8}$ = 4.8 Hz, *H7*, 1H), 4.38 (t, *H1*, 2H), 4.10 (s, $^3J_{1,\ 2}$ = 5.4 Hz, *H4*, 2H), 3.71 (s, *H3,* 2H), 2.92 (t, $^3J_{1,\ 2}$ = 5.4 Hz, *H2*, 2H), 2.26 (t, $^3J_{12,\ CH2}$ = 7.5 Hz, *H12*, 2H), 1.56 (m, CH_2, 2H), 1.47 (s, *H10*, 18 H), 1.23 (m, CH_2, 8H), 0.83 (t, $^3J_{13,\ CH2}$ = 5.9 Hz, *H13*, 3H). ^{13}C NMR (75 MHz, $CDCl_3$, δ): 187.2 (*C9*), 173.7 (*C11*), 169.5 (*C8*), 164.7 (*C6*), 155.4 (*C5*), 128.8 (*C7*), 64.7 (*C2*), 61.7, (*C4*) 55.3 (*C3*), 52.65

(*C12*), 34.04-22.42 (six signals, *C*H_2) 27.25 (*C10*), 13.91 (*C13*). HR-ESI-MS calcd. for $C_{28}H_{47}N_2O_6^+$: 507.3429, found: 507.3411 $[M]^+$.

Octanoic acid 2-(carboxymethylpyridin-2-ylmethylamino)ethyl ester (HL1).

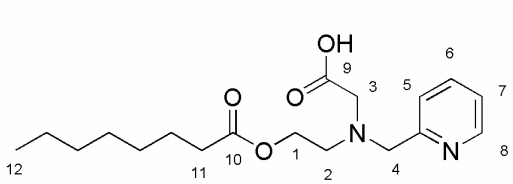

Octanoic acid 2-(*tert*-butoxycarbonylmethyl pyridin-2-ylmethylamino)ethyl ester (**5**, 109 mg, 0.27 mmol) was dissolved in dry CH_2Cl_2 (1 mL). TFA (1 mL) was added, and the reaction mixture was stirred for 30 min at room temperature. Xylene (1 mL) was added, and all the solvents were evaporated under reduced pressure to yield the product H**L1** (45 mg, 0.133 mmol, yield 49 %) after solvent evaporation. ^{1}H NMR (400 MHz, CD_3OD, δ): 8.76 (d, $^3J_{7,8}$ = 5.4 Hz, *H8*, 1H), 8.41 (t, $^3J_{5,6}$ = 7.6 Hz, *H6*, 1H), 7.93 (d, $^3J_{5,6}$ = 7.6 Hz, *H5*, 1H), 7.86 (t, $^3J_{7,8}$ = 5.4 Hz, *H7*, 1H), 4.48 (s, *H3*, 2H), 4.22 (t, $^3J_{1,2}$ = 5.1 Hz, *H2*, 2H), 3.78 (s, *H4*, 2H), 3.23 (t, $^3J_{1,2}$ = 5.1 Hz, *H1*, 2H), 2.28 (t, $^3J_{11,CH2}$ = 7.6 Hz, *H11*, 2H), 1.56 (m, C*H*$_2$, 2H), 1.29 (m, C*H*$_2$, 8H), 0.9 (t, $^3J_{12,CH2}$ = 6.8 Hz, *H12*, 3H). ^{13}C NMR (100 MHz, CD_3OD, δ): 184.2 (*C9*), 171.4 (*C10*), 156.1 (*C8*), 146.1 (*C6*), 144.4 (*C5*), 127.0 (*C7*), 84.2 (*C3*), 63.1 (*C4*), 57.8 (*C2*), 55.3 (*C11*), 35.2-23.9 (six signals, *C*H_2), 13.9 (*C12*). IR (cm^{-1}): 2929 (w), 2858 (w), 1727 (m), 1668 (m). HR-ESI-MS calcd. for $C_{18}H_{29}N_2O_4$: 337.2127, found: 337.2120 $[M + H]^+$.

Octanoic acid 2-(bis-carboxymethylamino)ethyl ester (H_2L2).

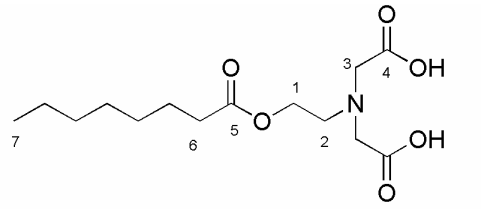

The exact same procedure as for H**L1** was followed with octanoic acid 2-(bis-*tert*-butoxycarbonylmethyl-amino)ethyl ester (**6**, 120 mg, 0.288 mmol) to yield H_2**L2** (56 mg, 0.184 mmol, yield 64 %). ^{1}H NMR (400 MHz, CD_3OD, δ): 4.36 (t, $^3J_{1,2}$ = 5.2 Hz, *H1*, 2H), 3.85 (s, *H3*, 4H), 3.33 (t, $^3J_{1,2}$ = 5.2 Hz, *H2*, 2H), 2.35 (t, $^3J_{6,CH2}$ = 7.5 Hz, *H6*, 2H), 1.61 (m, C*H*$_2$, 2H), 1.32 (m, C*H*$_2$, 8H), 0.89 (t, $^3J_{7,CH2}$ = 6.0 Hz, *H7*, 3H). ^{13}C NMR (100 MHz, CD_3OD, δ): 183.61 (*C4*), 177.18 (*C5*), 62.45 (*C3*), 57.55 (*C2*), 55.64 (*C1*), 38.33 - 24.10 (six signals, *C*H_2), 16.22 (*C7*). IR (cm^{-1}): 2928 (w), 2857 (w), 1737 (m), 1682 (m). HR-ESI-MS calcd. for $C_{14}H_{26}N_2O_6$: 304.1760, found: 304.1739 $[M + H]^+$.

Bis-carboxymethyl-(2-octanoyloxy-ethyl)-pyridin-2-ylmethylammonium trifluoroacetate (H_2L3)(TFA).

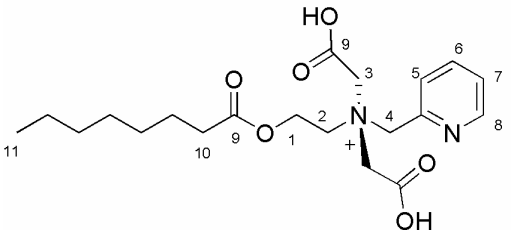

The exact same procedure as for H**L1** was followed with bis-*tert*-butoxycarbonylmethyl(2-octanoyloxy -ethyl)pyridin-2-ylmethylammonium chloride (**7**, 37 mg, 0.072 mmol) to afford H_2**L3** (12 mg, 0.0303 mmol, yield 42 %). ^{1}H NMR (400 MHz, CD_3OD, *δ*): 8.95 (d, $^3J_{7,\,8}$ = 5.2 Hz, *H8*, 1H), 8.65 (t, $^3J_{5,\,6}$ = 8.8 Hz, *H6*, 1H), 8.30 (t, $^3J_{5,\,6}$ = 8.8 Hz, *H5*, 1H), 8.11 (t, $^3J_{7,\,8}$ = 5.2 Hz, *H7*, 1H), 4.14 (t, $^3J_{1,\,2}$ = 5.2 Hz, *H1*, 2H), 4.07 (s, *H4*, 2H), 3.91 (s, *H3*, 4H), 3.91 (t, $^3J_{1,\,2}$ = 5.2 Hz, *H2*, 2H), 2.19 (t, $^3J_{11,\,CH_2}$ = 7.5 Hz, *H10*, 2H), 1.60 (m, CH_2, 2H), 1.31 (m, CH_2, 8H), 0.90 (t, $^3J_{12,\,CH_2}$ = 6.7 Hz, *H11*, 3H). ^{13}C NMR (100 MHz, CD_3OD, *δ*): 186.22 (*C9*), 172.1 (*C10*), 169.48 (*C8*), 163.94 (*C6*), 128.20 (*C5*), 65.31 (*C4)*, 61.79 (*C2*) 56.65 (*C3*), 52.65 (*C11*), 37.26-23.81 (six signals, *C*H_2), 14.54 (*C12*). IR (cm^{-1}): 2927 (w), 2857 (w), 1731 (m), 1630 (m). HR-ESI-MS calcd. for $C_{20}H_{31}N_2O_6^+$: 395.2177, found: 395.2197 $[M]^+$.

2.2.3 Synthesis of $Re(CO)_3^+$ Complexes

Octanoic acid 2-(carboxymethylpyridin-2-ylmethylamino)ethyl ester tricarbonyl rhenium(I) [Re(L1)(CO) $_3$].

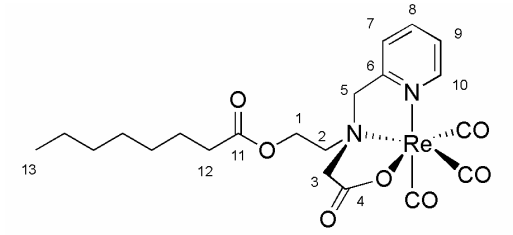

A solution of $[NEt_4]_2[ReBr_3(CO)_3]$ (40 mg, 0.052 mmol) and H**L1** (17 mg, 0.052 mmol) in CH_3OH (5 mL) was refluxed overnight. The solution flask was placed in the freezer for 2 h to afford the product as a white solid (21 mg, 0.034 mmol, yield 66 %) after filtration. Small, colourless crystals were obtained by slow diffusion of the product dissolved in CH_2Cl_2 into diethyl ether. HPLC-R_t= 21.3 minutes. ^{1}H NMR (300 MHz, $CDCl_3$, *δ*): 8.84 (d, $^3J_{9,\,10}$ = 5.1 Hz, *H10*, 1H), 7.79 (m, $^3J_{9,\,10}$ = 5.1 Hz, *H9*, 1H), 7.56 (d, $^3J_{7,\,8}$ = 7.6 Hz, *H7*, 1H), 7.46 (t, $^3J_{7,\,8}$ = 7.6 Hz, *H8*, 1H), 4.55 (dd, $^2J_{3,\,3'}$ = 14.4 Hz, *H3*, 2H), 4.48 (m, $^3J_{1,\,2}$ = 7.2 Hz , *H2*, 2H), 3.89 (s, *H5*, $^2J_{5,\,5'}$ = 16.8 Hz, 2H), 3.78 (q, $^3J_{1,}$

$_2$ = 7.2 Hz, *H1*, 2H), 2.40 (t, $^3J_{12,\ CH_2}$ = 7.7 Hz, *H12*, 2H), 1.54 (m, CH_2, 2H), 1.30 (m, CH_2, 8H), 0.89 (t, $^3J_{13,\ CH_2}$ = 6.9 Hz, *H13*, 3H). ^{13}C NMR (125 MHz, $CDCl_3$, δ): 196.8 (*CO*), 196.1 (*CO*), 195.1 (*CO*), 178.1 (*C10*), 172.8 (*C9*), 157.5 (*C10*), 152.5 (*C9*), 139.6 (*C7*), 125.7 (*C8*), 122.8 (*C6*), 84.2 (*C3*), 68.3 (*C5*), 67.4 (*C1*), 61.5 (*C2*), 69.6 (*C12*) 35.2-23.9 (six signals, *C*H_2), 8.5 (*C13*). IR (cm^{-1}): 2020 (m) (ν_{CO}), 1905 (w) (ν_{CO}), 1870 (m) (ν_{CO}). HR-ESI-MS calcd. for $C_{21}H_{28}N_2O_7{}^{185}Re$: 605.1426, found: 605.1410 $[M + H]^+$.

Sodium octanoic acid 2-(bis-carboxymethylamino)ethyl ester tricarbonylrhenate Na[Re(L2)(CO)$_3$].

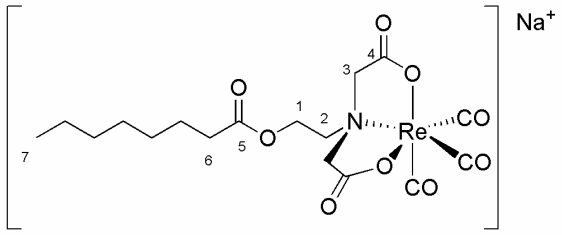

A solution of $[NEt_4]_2[ReBr_3(CO)_3]$ (40 mg, 0.052 mmol) and H_2**L2** (16 mg, 0.052 mmol) in CH_3OH (5 mL) was allowed to reflux overnight. The solvent was evaporated, and the oily residue was purified by preparative HPLC to afford the product as a white solid (5 mg, 0.0087 mmol, yield 15 %) after rotary evaporation of all solvents. HPLC-R_t= 14.01 minutes. ^{1}H NMR (300 MHz, CD_3OD, δ): 4.38 (s, $^2J_{3,\ 3'}$ = 16.2 Hz, *H3*, 4H) 3.67 (t, $^3J_{1,\ 2}$ = 6.0 Hz *, H2,* 2H), 3.78 (t, $^3J_{1,\ 2}$ = 6.0 Hz, *H1,* 2H), 2.39 (t, *H6*, 2H), 1.62 (m, CH_2, 2H), 1.31 (m, CH_2, 8H), 0.90 (t, $^3J_{7,\ CH_2}$ = 6.7 Hz, *H7*, 3H). ^{13}C NMR (125 MHz, CD_3OD, δ): 196.8 (*CO*), 195.7 (*CO*), 177.5 (*C4*), 172.9 (*C5*), 66.5 (*C3*), 62.5 (*C1*), 62.1 (*C2*), 60.16 (*C6*) 33.0 - 21.8 (six signals, *C*H_2), 12.5 (*C7*). IR (cm^{-1}): 2017 (m) (ν_{CO}), 1881 (m, br) (ν_{CO}), 1606 (w). HR-ESI-MS calcd. for $C_{17}H_{24}N_2O_9{}^{185}Re$: 570.0902, found: 570.0914 $[M]^-$.

Bis-carboxymethyl-(2-octanoyloxyethyl)pyridin-2-ylmethylammonium tricarbonylrhenium [Re(L3)(CO)$_3$].

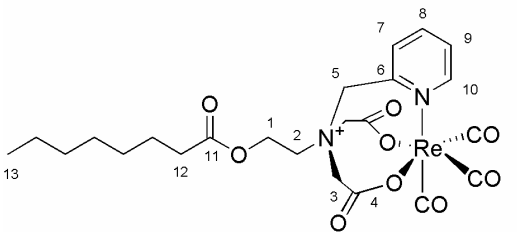

A solution of $[NEt_4]_2[ReBr_3(CO)_3]$ (4 mg, 0.0052 mmol) and H_2**L3** (1.6 mg, 0.0052 mmol) in CH_3OH (5 mL) was allowed to reflux overnight. The solvent was evaporated, and the oily residue was purified by preparative HPLC to afford the product as a

yellow solid (3 mg, 0.0045 mmol, yield 86 %). HPLC-R_t= 18.7 minutes. ^{1}H NMR (400 MHz, CD_3OD, δ): 8.96 (d, *H10*, 1H), 8.66 (t, *H8*, 1H), 8.30 (d, *H7*, 1H), 8.08 (t, *H9*, 1H), 5.71 (s, *H3*, 4H), 4.36 (t, *H5*, 2H), 4.14 (s, *H2*, 2H), 3.97 (t, *H1*, 2H), 2.32 (*H12*, 2H), 1.54 (m, CH_2, 2H), 1.30 (m, CH_2, 8H), 0.90 (t, *H13*, 3H). ^{13}C NMR (125 MHz, CD_3OD, δ): 197.2 (*CO*), 195.5 (*CO*), 176.5 (*C4*), 173.1 (*C11*), 151.1 (*C9*), 137.9 (*C7*), 127.1 (*C8*), 121.6 (*C6*), 72.5 (*C3*), 68.1 (*C2*), 64.5 (*C1*), 62.1 (*C12*) 38.0 - 22.2 (six signals, *C*H_2), 11.7 (*C13*). IR (cm-1): 2018 (s) (ν_{CO}), 1894 (m) (ν_{CO}), 1874 (m), 1661 (w). HR-ESI-MS calcd. for $C_{23}H_{30}N_2O_9{}^{185}Re$: 663.1481, found: 663.1483.

2.2.4 X-ray Diffraction Analysis of [Re(CO)$_3$L1]

Colourless crystals of [Re(CO)$_3$**L1**] were obtained by slow diffusion of the product dissolved in CH_2Cl_2 into diethyl ether. The sample was mounted on a glass fiber and cooled to 173 K. X-ray data were collected and processed using a Bruker X8 APEX II diffractometer using graphite-monochromated Mo Kα radiation (λ = 0.71073 Å) to a maximum 2θ value of 48.0°. Data were collected and integrated using the Bruker SAINT software package[78] and corrected for Lorentz and polarization effects, as well as for absorption effects, using the multiscan technique (SADABS).[79] The X-ray structure was solved using direct methods (SIR92)[80] and expanded using Fourier techniques.[81] All calculations were performed using the SHELXTL crystallographic software package.[82] The collection and analysis of the data was done by Dr. Brian O. Patrick.

2.2.5 Synthesis of ^{99m}Tc(CO)$_3$ Complexes

The organometallic precursor [^{99m}Tc(H$_2$O)$_3$(CO)$_3$]$^+$ was prepared from a saline solution of Na[^{99m}TcO$_4$] (1 mL, 5.4 mCi) using the Isolink kit. A solution of Na[^{99m}TcO$_4$] (1 mL) was added to the Isolink kit, and the vial was heated to reflux for 25 min. Upon cooling, 0.1 M HCl solution (1 mL) was added to adjust the pH to 7-8. Labelling was achieved by mixing an aliquot (0.2 mL) of the [^{99m}Tc(H$_2$O)$_3$(CO)$_3$]$^+$ precursor with a 0.1 mM aqueous solution of **L1-L3** (pH 7-7.5, 0.1 M $NaHCO_3$ solution, 1 mL) at 90 °C for 25 (**L1**), 35 (**L2**), or 45 (**L3**) min. Analysis was performed by HPLC and TLC. HPLC solvents consisted of

0.1% trifluoroacetic acid in water (solvent A) and neat methanol (solvent B). Samples were analyzed with a linear gradient method (100% solvent A to 100% solvent B over 30 min). TLC's were developed with acetonitrile as the mobile phase.

2.2.6 Cysteine and Histidine Stability Challenges

To a solution of either cysteine (0.1 M, 0.9 mL) or histidine (0.1 M, 0.9 mL) in PBS (1 mM, pH 7.4) was added a solution of the ^{99m}Tc complex (0.1 mL, final ligand concentration 10^{-5} M). The samples were incubated at 37 °C and aliquots analyzed after 24 h by analytical TLC and HPLC.

2.2.7 Octanol-Water-Distribution Coefficients

The log $P_{o/w}$ values of complexes [^{99m}Tc(CO)$_3$**L1**], Na[^{99m}Tc(CO)$_3$**L2**], and [^{99m}Tc(CO)$_3$**L3**] were determined by extraction with equivalent amounts of octanol and aqueous solutions of the ^{99m}Tc complex.[83] Octanol (1 mL) was mixed with an equivalent amount of the aqueous reaction mixture and stirred for 1 min. Subsequently, the two phases were partitioned, and the activity of both was determined by the measurement of activity of 5 μL droplets of each solution on a radio-TLC-plate.

2.2.8 Imaging and Biodistribution

Animals were used in accordance with the regulations on the protection of animals in Canada. Female C57Bl/6 mice were obtained from Sarah Reid, McMaster University. Each mouse had a 4 mm tumor in its neck, grown from a primary cell line at passage six derived from mammary tumors of a PyVMT transgenic mouse. ^{99m}Tc complexes were prepared as described above. While two complexes [^{99m}Tc(CO)$_3$**L1**] and Na[^{99m}Tc(CO)$_3$**L2**], were injected without any further purification because of their high radiochemical yield, [^{99m}Tc(CO)$_3$**L3**] was purified by preparative HPLC before injection. The solvent was removed from the collected fraction *in vacuo*, and [^{99m}Tc(CO)$_3$**L3**] was redissolved in 0.9 % NaCl saline solution. Aliquots (100 μL) of complex solutions of [^{99m}Tc(CO)$_3$**L1**], Na[^{99m}Tc(CO)$_3$**L2**], and [^{99m}Tc(CO)$_3$**L3**] were injected into groups of four mice via their tail

vein. After injection of [^{99m}Tc(CO)$_3$**L1**] and Na[^{99m}Tc(CO)$_3$**L2**], dynamic imaging was carried out during the first 15 min. All animals were imaged under isoflurane anesthesia in the supine position during the first 15 min, and then 1, 2, and 4 h after injection for 15 min each. After the last time point, animals were sacrificed by pentobarbital administration, and samples of blood, liver, kidney, muscle, spleen, heart, brain, lung, gallbladder, intestine, stomach, bladder and tumor were removed, weighed, and counted in a gamma counter. Results are expressed as the percentage of the injected dose per gram of tissue (% ID/g). Imaging of the animals on their SPECT/CT scanner was done by Troy Farncombe, Chantal Saab, and Rod Rhem. Biodistribution and subsequent evaluation of the imaging and biodistribution data was done by Prof. Urs O. Häfeli.

2.3 Results and Discussion

2.3.1 Ligand Preparation

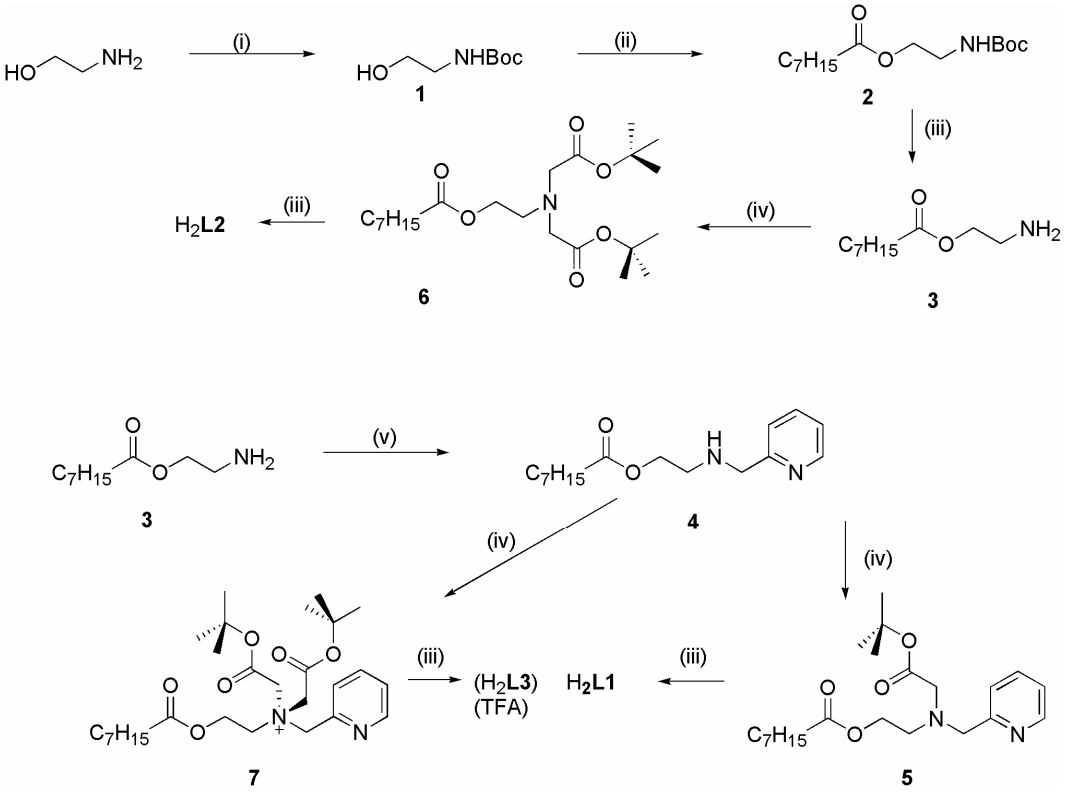

Scheme 2.1 Synthetic methods to furnish ligand systems H**L1**, H_2**L2**, and H_2**L3.** (i) Boc_2O, neat (ii) Octanoyl 1-chloride, EDMA, toluene, (iii) TFA/ CH_2Cl_2 (1:1) (iv) ***tert***-Butyl bromoacetate, Na_2CO_3, CH_2Cl_2 (v) Pyridine-2-aldehyde, EtOH.

The tridentate chelate moieties of H**L1** and H_2**L2** were selected for this study because they have been previously shown to form highly stable complexes with the metals of interest.[36] The chelation entity of H_2**L3** is novel, arising from the synthesis of H**L1** where its *tert*-butyl-protected form appears as a byproduct in the synthesis of *tert*-butyl protected H**L1**. All three ligand systems were synthesized from ethanolamine. Intermediate **1** (Scheme 2.1) was synthesized through protection of the free amine of ethanolamine as the tert-butyl carbamate or Boc, in order to prevent reaction of the acid chloride with the much more reactive amine in the subsequent reaction step. Compound **1** was then esterified using the acid chloride of octanoic acid, forming **2**. Subsequent deprotection of the amine yields **3**, which served as a synthon to furnish all three ligand systems.

For ligand systems H**L1** and H_2**L3, 3** was reacted with one equivalent pyridine-2-aldehyde to form an imino intermediate, which was then reduced to afford **4** in a one pot reaction (Scheme 2.1). Subsequent alkylation of **4** yields both protected ligand systems **5** and **7**. Due to the added ionicity of the quaternary amine on **7**, separation of the two products is easily achieved with column chromatography, as both compounds had easily distinguishable R_f values. Deprotection to yield H**L1** and H_2**L3** proceeds through acid catalyzed saponification, cleaving exclusively the *tert*-butyl protection group.[84] In order to synthesize the H_2**L2** system, intermediate **4** was alkylated with two equivalents of *tert*-butyl bromoacetate. Double alkylation and subsequent purification with column chromatography yields the protected ligand **6**. Analogous to deprotection of **5** and **7**, the *tert*-butyl protection groups are removed using acid catalysis, leaving the aliphatic ester unaltered.[84]

The identity of all ligands was confirmed by characterization through ^{1}H and ^{13}C NMR spectroscopy, as well as mass spectrometry and IR spectroscopy. All compounds synthesized have the appearance of thick oils, characteristic of compounds bearing aliphatic chains of significant length.

2.3.2 Preparation of Re Complexes

$[Re(CO)_3]^+$ complexes were synthesized as macroscopic models for the $^{99m}Tc(CO)_3$ complexes by mixing a methanolic solution of ligand with $[NEt_4]_2[ReBr_3(CO)_3]$ previously dissolved in H_2O, and stirring the mixture at elevated temperatures overnight.[85] While the

neutral complex [Re(CO)$_3$**L1**] precipitates from the reaction solution, solutions of the complexes Na[Re(CO)$_3$**L2**] or [Re(CO)$_3$**L3**] turn slightly yellow in color without precipitation of the product. Na[Re(CO)$_3$**L2**] and [Re(CO)$_3$**L3**] were isolated and purified via preparative HPLC.

A sample of characteristic ^{1}H spectra, documenting the change of environment of specific protons upon coordination is shown (Figure 2.4) for H**L1** and [Re(CO)$_3$**L1**].

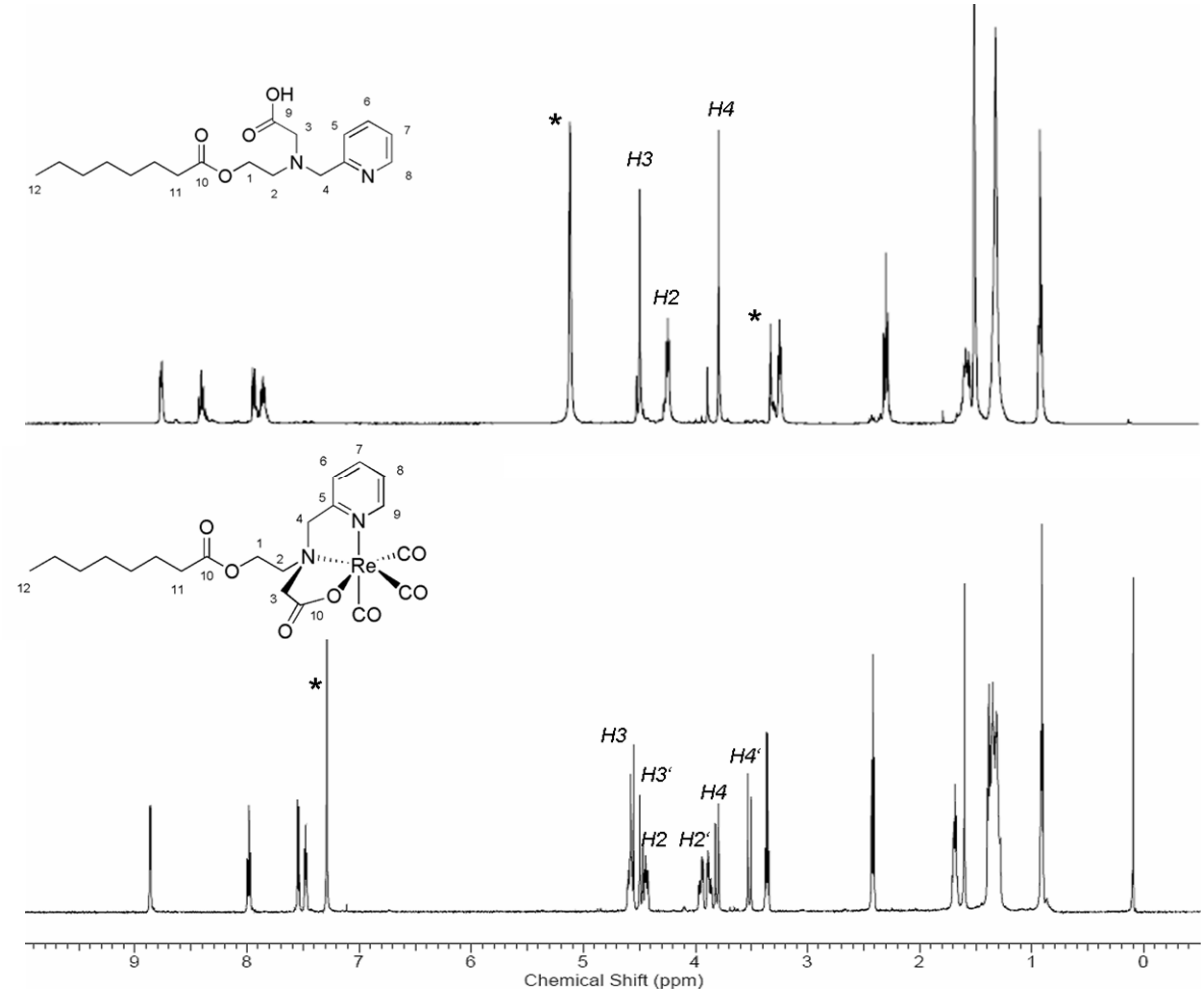

Figure 2.4 ^{1}H NMR spectra (300 MHz, 298 K) of H**L1** (a) and [Re(CO)$_3$**L1**] (b), * denotes residual reference solvent peak, while characteristic diastereotopic protons are highlighted with their assignments (water and silicone grease, at 1.56 and 0.07 are also observed in both spectra as minor impurities).

The CH_2 groups bearing *H3* and *H4* appear as singlet peaks in H**L1** and *H2* appears as a triplet, coupling to *H1*. In [Re(CO)$_3$**L1**], the same protons, formerly homotopic protons, now appear as two diastereotopic protons with different chemical shifts showing strong ^{2}J coupling to each other. Both *H3* and *H4* within [Re(CO)$_3$**L1**] appear as a doublet of doublets,

while the highly structured conformation of the complex causes *H2* to appear as two distinct multiplet signals due to coordination of the neighbouring amine, which constitutes one of the donor atoms within the coordination complex (Figure 2.4).[69] The ^{13}C NMR spectra of the complexes show other characteristic features such as the diagnostic peaks for the non-equivalent carbonyls. In the case of [$Re(CO)_3$**L1**], three non-equivalent peaks are observed between 195.1 and 196.8 ppm, mirroring the different chemical environment of each carbonyl of this complex.[86] In both Na[$Re(CO)_3$**L2**] and [$Re(CO)_3$**L3**], however, only two peaks are observed for the carbonyls on the *fac*-$[Re(CO)_3]^+$ core, since both these complexes are found to have a mirror plane. Observation of all carbonyl peaks in the region of 194 – 197 ppm is characteristic for these types of complexes.[87]

Another useful characterization tool is IR spectroscopy, where intense, diagnostic CO bands between 2020 and 1875 cm^{-1} can be assigned to the *fac*- [$Re(CO)_3$**L**]-products. While in $[Re(H_2O)(CO)_3]^+$ the characteristic stretching frequencies can be found at 2000 and 1868 cm^{-1}, a shift to higher wave numbers is observed upon coordination.[87] These carbonyl stretching frequencies can be easily distinguished from the other carbonyl stretching frequencies present, which originate from the two types of carbonyls present in the ligand systems. The carbonyl linking chelate and aliphatic residue are only mildly affected by the event of metal coordination, while the coordinating carbonyl is affected in all cases. Due to interaction with the metal center, the IR frequency is slightly decreased.

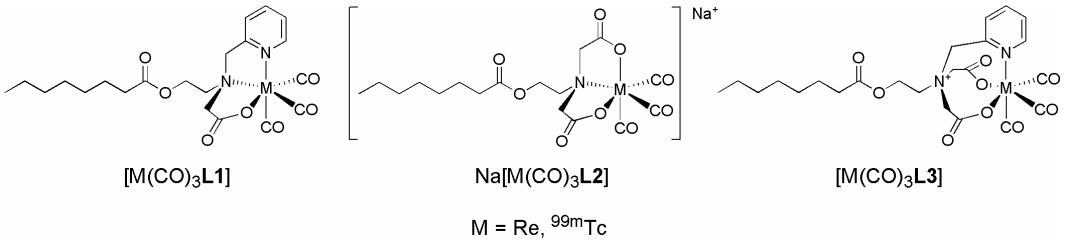

Figure 2.5 Complexes described within this chapter.

Mass spectrometry also gave conclusive results on identifying the desired complexes (Figure 2.5). Due to two stable Re isotopes present (^{187}Re 62.6 %, ^{185}Re 37.4 %) the corresponding ([$Re(CO)_3$**L1**] + H)$^+$, [$Re(CO)_3$**L2**]$^-$ and ([$Re(CO)_3$**L3**] + H)$^+$ appear with the diagnostic isotope distributions of Re. It is interesting to note that due its zwitterionic nature, the overall charge of [$Re(CO)_3$**L3**] is indeed neutral. This is also confirmed by the $[M + H]^+$ observed.

2.3.3 X-Ray Diffraction Structural Characterization of [Re(CO)$_3$L1]

The [Re(CO)$_3$**L1**] complex (Figure 2.6, Table 2.1) displays a nearly perfect octahedral coordination sphere, with the three carbonyl ligands facially coordinated at approximately 90° to one another. The bond lengths between the individual CO ligands are in accordance with other Re(CO)$_3$ complexes reported.[88] The Re-CO bond lengths are all close to 1.9 Å and therefore shorter than the Re-O bond length (2.142 Å) and the Re-N bond lengths (2.184 Å, 2.227 Å). The Re-N2 bond proves to be the longest because of the nondirected lone pair on the tertiary amine nature of the nitrogen atom N2.

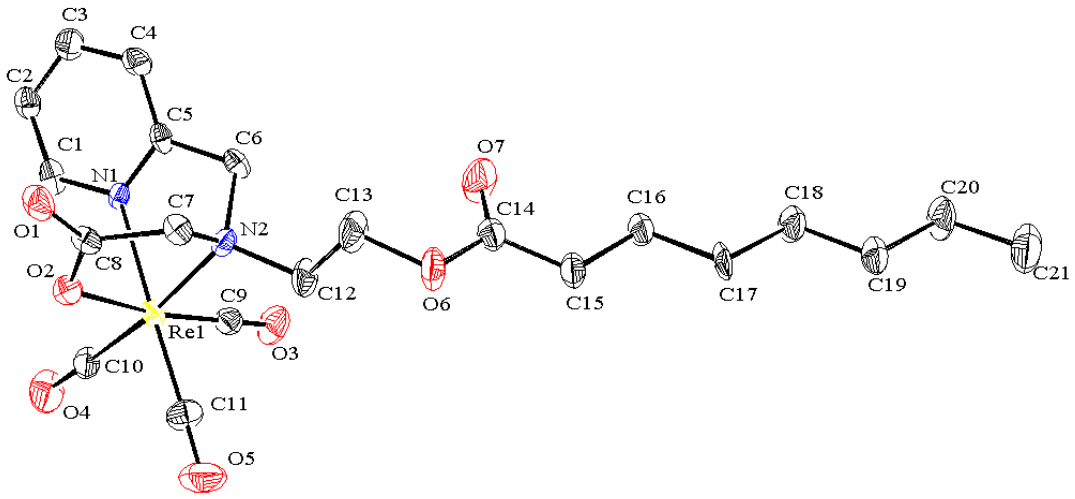

Figure 2.6 ORTEP view of [Re(CO)$_3$**L1**], showing the atom numbering scheme (50% thermal ellipsoids).

Table 2.1 Selected bond lengths in [Re(CO)$_3$**L1**] ([Å]) and angles ([°]).

bond	length [Å]	angle	degree[°]
C(9)-Re(1)	1.928(12)	O(2)-Re(1)- N(1)	78.2(3)
C(10)-Re(1)	1.909(12)	N(1)-Re(1)- N(2)	77.2(3)
C(11)-Re(1)	1.918(11)	N(2)-Re(1)- C(11)	97.0(4)
N(1)-Re(1)	2.184(8)	C(9)-Re(1)- C(11)	88.6(5)
N(2)-Re(1)	2.227(8)	C(10)-Re(1)- C(11)	88.8(5)
O(2)-Re(1)	2.142(6)	C(10)-Re(1)- C(9)	87.1(5)
C(10)-O(4)	1.158(13)	C(10)-Re(1)- O(2)	97.5(4)
C(11)-O(5)	1.168(14)	C(10)-Re(1)- N(1)	96.8(4)

2.3.4 Radiolabelling

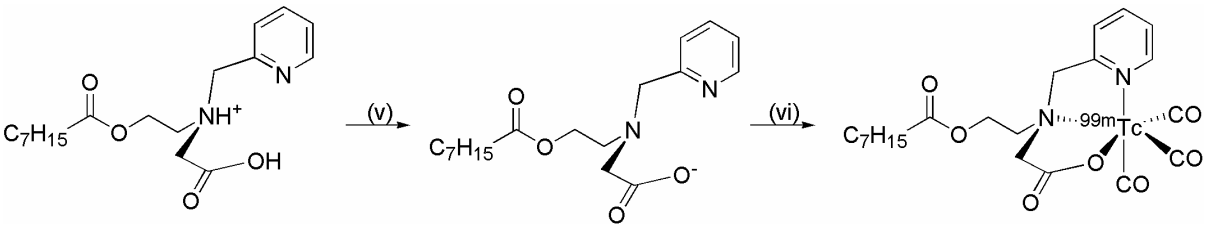

Scheme 2.2 Sample synthesis scheme for $^{99m}Tc(CO)_3$ complexes, here shown on [$^{99m}Tc(CO)_3$**L1**]. (v) $NaHCO_3$ (0.1 M) (vi) $[^{99m}Tc(H_2O)_3(CO)_3]^+$, 90°C, 25-45 min.

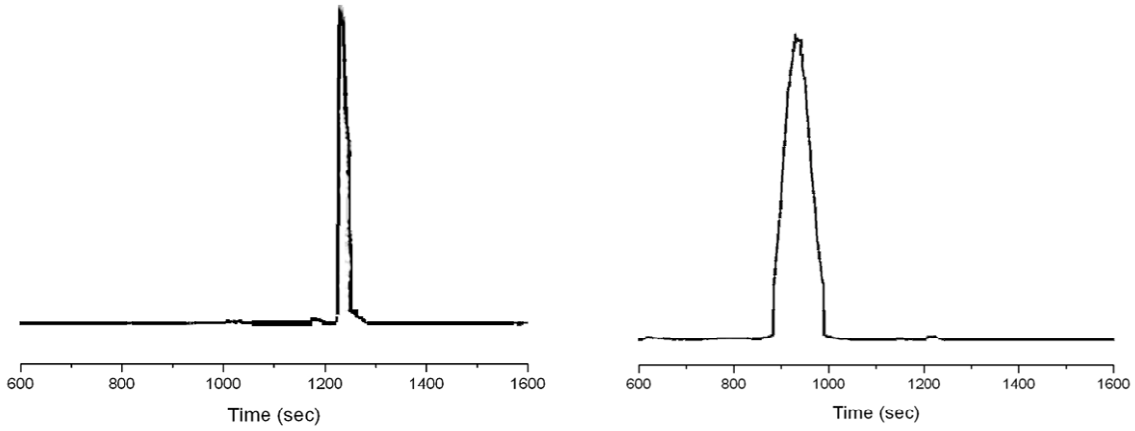

Figure 2.7 γ-HPLC traces of the crude reaction mixtures of [$^{99m}Tc(CO)_3$**L1**] (left) and [^{99m} Tc(CO)$_3$**L2**]$^-$ (right).

The complexes [$^{99m}Tc(CO)_3$**L1**] and [$^{99m}Tc(CO)_3$**L2**]$^-$ were prepared in high radiochemical yield through reaction of *fac*-[$^{99m}Tc(CO)_3(H_2O)_3]^+$ with the ligands H**L1** and H_2**L2**. Due to residual acidity after HPLC purification of the ligands using an acidic aqueous mobile phase, the ligands were initially deprotonated with 0.1 $NaHCO_3$ (2 molar eq) and added to the technetium tricarbonyl solution with final concentrations of approximately 3×10^{-4} M. After a reaction time of 25-35 min at 90 °C, the chelation reaction was 95% complete as verified by HPLC and radio-TLC analysis. No major by-products were detected by HPLC. A sample reaction scheme is shown (Scheme 2.2) as well as γ-HPLC traces of the crude reaction mixtures (Figure 2.7). The retention times mirror the difference between charged and neutral complexes well.

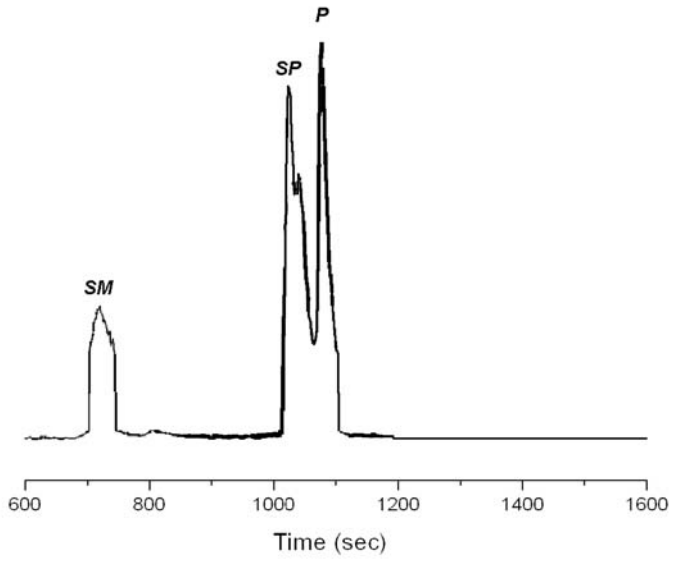

Figure 2.8 γ-HPLC traces of the crude reaction mixtures of [^{99m}Tc(CO)$_3$**L3**], SM denotes starting material, P denotes product and SP stands for side products.

[^{99m}Tc(CO)$_3$**L3**] was produced in only 32 % yield after a 45 min reaction time. Several by-products were visible in the γ-trace of the crude HPLC spectrum from coordination with decomposition fragments of H_2**L3**, resulting from the high-temperature reaction conditions (Figure 2.8). Cleavage of one of the chelate arms to afford one of the other ligand systems is unlikely, since the retention time of the decomposition product does not match any of the other retention times observed. Since the reaction proceeds in the presence of considerable amounts of base, a reaction mechanism similar to a Hofmann type E2 elimination, which typically proceeds in the presence of heat and base, seems plausible. The observed, shorter retention time of the side product would be in accordance with such a process; however, synthetic investigations on the corresponding cold complexes were not undertaken. The peak of the desired product was assigned by comparison of the retention time of the fully characterized Re complex isolated by HPLC purification. The investigated properties described in this subchapter are outlined in Table 2.2.

Table 2.2 Summarized experimental properties of the three $^{99m}Tc(CO)_3$ complexes.

Complex	Radiochemical yield [%]	t [min]	T [°C]	Ligand conc. (M)	t_R [min] ^{99m}Tc (Re)	Log $P_{o/w}$	R_f
$[^{99m}Tc(CO)_3\mathbf{L1}]$	> 95%	25	90	$3x10^{-4}$	20.5 (21.3)	-0.034	0.49
$[^{99m}Tc(CO)_3\mathbf{L2}]^-$	> 95%	35	90	$3.3x10^{-4}$	15.6 (14.01)	-1.014	0.39
$[^{99m}Tc(CO)_3\mathbf{L3}]$	32%	45	90	$1x10^{-3}$	18.1 (18.7)	-0.38	0.46

2.3.5 *In Vitro* Stability and log $P_{o/w}$

To investigate the complex stability toward the naturally occurring amino acids cysteine and histidine (both can act as potential tridentate ligands),[88] the ^{99m}Tc-complexes were incubated in 10^{-3} M cysteine/histidine solutions in PBS (pH 7.4, 37 °C) for 24 h. In the subsequent HPLC analyses of the solutions, no noticeable decomposition could be detected for any of the three complexes, rendering them stable *in vitro*.

The lipophilicity of the complexes was determined by evaluation of water/octanol partition coefficients. $[^{99m}Tc(CO)_3\mathbf{L2}]^-$ should be the most ionic compound by virtue of its full -1 charge, followed by the zwitterionic $[^{99m}Tc(CO)_3\mathbf{L3}]$ and then the neutral $[^{99m}Tc(CO)_3\mathbf{L1}]$; this was confirmed by the order of lipophilicity log $P_{o/w}$ values ranging from $[^{99m}Tc(CO)_3\mathbf{L1}] > [^{99m}Tc(CO)_3\mathbf{L3}] > [^{99m}Tc(CO)_3\mathbf{L2}]^-$ (listed in the order from highest to lowest lipophilicity, Table 2.2). This was also confirmed by order of HPLC retention times, where the most lipophilic complex will be retained for the longest time on the column. Radio-TLC measurements match in a similar manner, since the most lipophilic compound will have the greatest retention factor, whereas the most polar will have the smallest. It is important to note however that these compounds, especially the charged complex, are considerably lipophilic despite the presence of a fairly large polar fraction. The $[^{99m}Tc(CO)_3]^+$ core contributes strongly to this lipophilicity.

2.3.6 *In Vivo* Evaluations

Imaging of all three compounds was performed at 15 min, 1 h, 2 h, and 4 h after injection. Biodistribution studies were performed at the 4 h time point after injection (Table 2.3). This tumor-bearing model was used to evaluate the imaging potential of [^{99m}Tc(CO)$_3$**L1**], [^{99m}Tc(CO)$_3$**L2**]$^-$, and [^{99m}Tc(CO)$_3$**L3**]. Data from the imaging is displayed

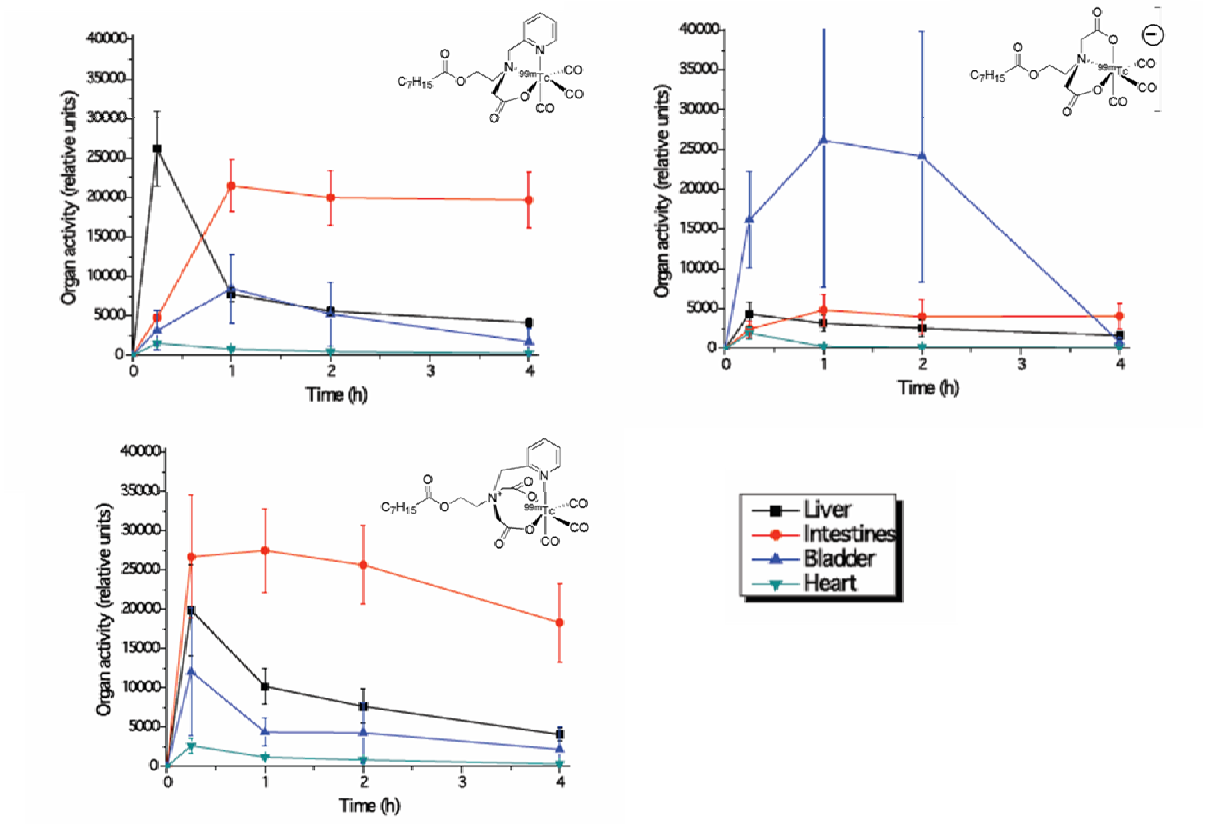

in Figure 2.9.

Figure 2.9 Activity (counts/pixel) levels vs. time curves for each of the evaluated compounds in select organs taken from the planar scintigraphy images.

Imaging screenshots of mice 15 min postinjection are shown in Figure 2.10. All compounds show very distinct biodistribution behaviour. The *in vivo* distribution of [^{99m}Tc(CO)$_3$**L1**] was followed from the onset of injection for the first 15 minutes. Very fast localization of the complex in the liver was observed, with clearance through the intestines, which is confirmed through the biodistribution data at the 4 h time point. The compound

showed large uptake of activity in liver, intestines, and feces. This behaviour is not surprising considering that this complex has no overall charge and a barely negative log $P_{o/w}$ value. Compound [^{99m}Tc(CO)$_3$**L2**]$^-$ was also followed after injection with dynamic imaging. Here, fast processing of the compound through the kidneys, within the first 5 - 10 min after injection, and consequent localization in the bladder, followed by excretion, was observed. The excretion of large portions of the dose is confirmed by the small fraction of the originally injected dose in the biodistribution measurements at the 4 h time point. The negative log $P_{o/w}$ value of this compound, due to its localized negative charge, determines its fate to be excreted through the renal tract.[89] Finally, for [^{99m}Tc(CO)$_3$**L3**] after 1 h after injection, high localization in the gall bladder was observed, paired with slow clearance through the intestines. The biodistribution profile shows some similarity to the profile of [^{99m}Tc(CO)$_3$**L1**], but with faster excretion through the intestines and the renal system (high percentage of dose in the feces, elevated organ/blood ratio in kidneys), which may be a consequence of the increased polarity of the complex (compared to [^{99m}Tc(CO)$_3$**L1**]). No significant heart, brain, or tumor uptake was observed for any of the investigated compounds.

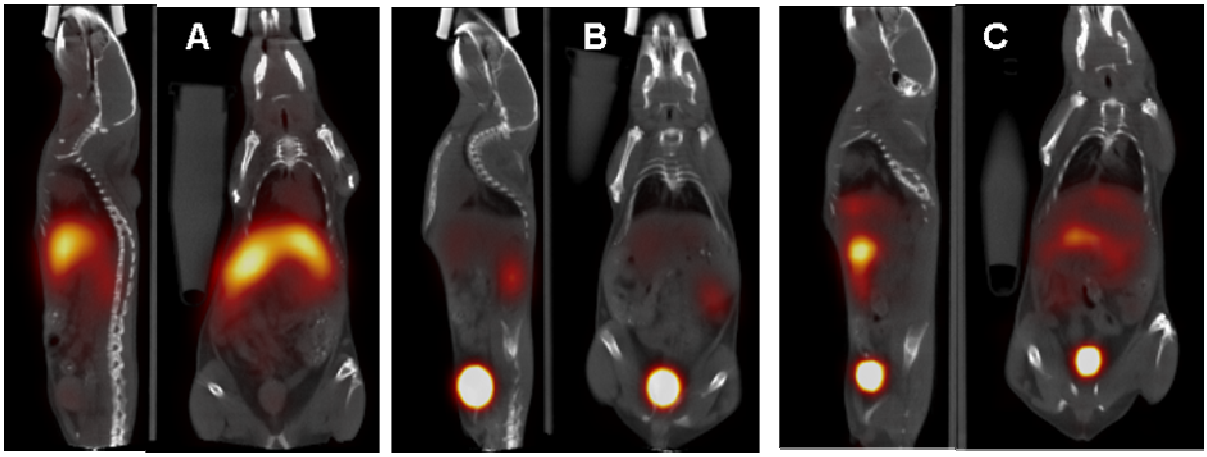

Figure 2.10 Representative μSPECT/CT pictures taken 15 min after injection of A) [^{99m}Tc(CO)$_3$L1], B) [^{99m}Tc(CO)$_3$L2]$^-$ and C) [^{99m}Tc(CO)$_3$L3]. Transverse (left) and coronal (right) planes shown in each case. Hot spots within the images are the liver in A, bladder and some residual activity in the kidneys in B and the gall bladder with liver uptake and bladder in C.

Table 2.3 Biodistribution, % ID/g ± SD (n = 4) of all complexes at the 4 h time point.

Organ	[^{99m}Tc(CO)$_3$**L1**]	[^{99m}Tc(CO)$_3$**L2**]$^-$	[^{99m}Tc(CO)$_3$**L3**]
Blood	0.73 ± 0.17	0.42 ± 0.12	0.68 ± 0.24
Heart	0.42 ± 0.05	0.20 ± 0.04	0.48 ± 0.14
Tumor	0.27 ± 0.03	0.16 ± 0.06	0.18 ± 0.02
Liver	7.37 ± 1.35	2.34 ± 0.49	6.20 ± 1.46
Kidney	3.43 ± 0.37	1.75 ± 0.18	4.14 ± 1.34
Lung	0.68 ± 0.12	0.45 ± 0.08	0.65 ± 0.18
Intestines	1.50 ± 0.49	0.37 ± 0.20	1.69 ± 0.75
Brain	0.02 ± 0.01	0.02 ± 0.01	0.02 ± 0.01
Bladder	1.57 ± 1.57	0.74 ± 0.66	3.07 ± 2.59
Muscle	0.20 ± 0.07	0.03 ± 0.02	0.26 ± 0.26
Spleen	0.36 ± 0.04	0.38 ± 0.12	0.38 ± 0.18
Feces	65.34 ± 43.03	9.14 ± 4.49	132.37 ± 86.29
Gallbladder	52.52 ± 40.40	24.83 ± 18.58	13.28 ± 14.74

2.4 Conclusions

For the first time, small amphiphilic ^{99m}Tc(CO)$_3$ complexes, one with a localized negative charge, one zwitterionic complex, and one neutral molecule, have been synthesized, fully characterized, and investigated for their lipophilicity and behavior *in vivo*. For the zwitterionic complex, a new type of chelation entity was incorporated, forming eight-membered rings between the metal center and the ligand sphere. Growing crystals of this complex in order to determine the coordination environment was attempted for an extended period of time but failed due to the "sticky" nature of this complex, arising from its zwitterionic, amphiphilic molecular structure. This novel chelate proved to be slower coordinating than the other two systems investigated, but still have high stability toward cysteine and histidine challenges. Lower reaction yields arose from the instability of the ligand toward prolonged heating at 90 °C, and the formation of by-products which could be separated by HPLC. The products afforded by this decomposition were capable of coordinating to the metal center making an additional purification step inevitable.

For a more efficient mimic of phospholipid-type molecules, a technetium-tagged approach may be more suitable, such as for example attachment of a small neutral ^{99m}Tc complex to the aliphatic residue of the corresponding amphiphilic molecule. In order to increase the impact of the lipophilic tail on the biodistribution of the entire molecule, the aliphatic chain could be further elongated.

Changing the charge of a small amphiphilic molecule resulted in highly contrasting biodistribution behaviour *in vivo*. This is somewhat surprising considering the negligible impact of the lipophilic residue. This may have importance in the future design of small molecule imaging agents using the $[^{99m}Tc(CO)_3]^+$ core.

Chapter 3: Investigation of the H_2dipin Scaffold as Chelate with Adjustable Denticity for ^{64}Cu, Re and ^{99m}Tc[†]

3.1 Introduction: Multifunctional Chelate Systems

The development of new radiopharmaceuticals for imaging and therapy of disease is a constantly burgeoning field.[60,90] Due to the availability and properties of the ^{99m}Tc generator over the past 3 decades, the development of novel imaging agents has centred around this particular isotope[20] and has been strongly affected by the recent shortage of its parent ^{99}Mo. The Orvig group, like many other research groups, has recognized a need for closer investigation of potential imaging agents based on alternative isotopes[60,91] and has long-standing experience with stable and radioactive transition and main group metals.[92]

Of specific importance is the ability to choose isotopes according to their properties such as $t_{1/2}$, mode and energy of decay, range of emitted particle, or even availablity.[93,94] The need for different chelates specific to each radiometal, or particular leaving groups for the incorporation of radiohalogens or ^{11}C, imposes a non-negligible additional difficulty and often obviates the fast and simple synthesis of analogous targeting vectors for labelling with a different radionuclide.

In this chapter, the design and synthesis of a versatile, universal chelate system, able to label a variety of metals of different oxidation states and varying coordination environment preferences, is described. All metals investigated in this chapter have radioisotopes that are of considerable interest for either imaging or therapy.

^{64}Cu ($t_{1/2}$=12.7 h, β^+ 17.4%, E_{max}=0.656 MeV, β^- 39%, E_{max}= 0.573 MeV) is of strong current interest for both positron emission tomography (PET) and radiotherapy.[48] The longer half-life is more applicable to developing PET agents with larger biomolecules, such as affibodies, that may require longer circulation times before imaging to achieve optimal target uptake.[95]

[†] Work presented in this chapter has been published: "One to Chelate Them All: Investigation of a Versatile, Bifunctional Chelate for ^{64}Cu, ^{99m}Tc, Re and Co", E. Boros, Y.-H. S. Lin, C. L. Ferreira, B. O. Patrick, U. O. Häfeli, M. J. Adam, C. Orvig , *Dalton Trans.* **40** , 6253-6259 (2011).

^{99m}Tc is the most commonly used isotope in nuclear medicine, partly due to its near ideal physical properties ($t_{1/2}$ = 6 h, γ = 140 keV).[64] The $[^{99m}Tc(CO)_3]^+$ core can be conveniently prepared by the Isolink kit developed by Alberto and coworkers[96] and serves as a scaffold that can be easily chelated through exchange of the three labile H_2O molecules to form highly stable complexes with tridentate ligands.[36] The stable isotopes of Re serve as cold congeners for radioactive Tc and are used to optimize non-radioactive chemistry and perform standard characterization techniques, while $^{186/188}$Re is attractive for therapeutic β^- applications. ^{186}Re ($t_{1/2}$ = 90 h, β = 1.07 MeV, max. range in tissue = 5 mm, γ = 137 keV) is suitable for treating smaller tumours, whereas ^{188}Re ($t_{1/2}$ = 17 h, β = 2.1 MeV, max. range in tissue = 11 mm, γ = 155 keV) is suitable for treating larger tumours. ^{186}Re is reactor produced (neutron irradiation of ^{185}Re), while ^{188}Re can be furnished with high specific activity from a ^{188}W/^{188}Re generator system in the form of $[^{188}ReO_4]^-$.[97,98] Due to great similarities with the group 7 congener Tc, ligand systems used with the latter are usually adequate for stable and radioactive Re isotopes.

All (radio-)metals described have a preference for being coordinated by polyamino-carboxylate ligands of a variety of denticities.[90]

3.1.1 Prior Art on H_2dipin Type Chelates

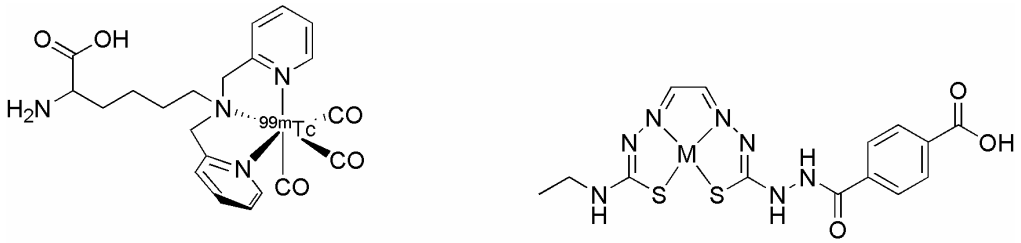

$[^{99m}Tc(CO)_3(DpK)]^+$ M = ^{99m}Tc, ^{64}Cu

Figure 3.1 Examples of the previously reported ligand systems DpK (SAAC approach[46]) and bifunctional, multi-purpose ATSE.[94]

Despite the fact that most acyclic ligands have low stability with Cu(II),[99] select examples such as the thiosemicarbazone H_2ATSM (diacetyl-bis(N-4-

methylthiosemicarbazone)) still are a viable option for the stable chelation of this metal (Figure 3.1).[100] This chelate has been used to synthesize potential small molecule imaging agents for hypoxia, as well as the bifunctional chelate ATSE/A (Diacetyl-2-(4-*N*-ethyl-3-thiosemicarbazone)-3-(4-*N*-amino-3-thiosemicarbazone),[94] which was shown to chelate both ^{64}Cu and ^{99m}Tc. However, the identity of the Tc complex could never be fully assigned and both radiochemical complexes exhibited only moderate serum stability.[94]

The versatile SAAC (single amino acid chelate) approach of Valliant, Babich, Zubieta and coworkers[42] has been used to successfully introduce a chelate for the $[^{99m}Tc(CO)_3]^+$ core into peptide sequences, however the tridenticity of this approach limits applications for other metals. There is a limited set of examples of multifunctional chelation systems seen in the literature that incorporate both the group 7 metals, as well as other commonly used trivalent radiometals.[55,101]

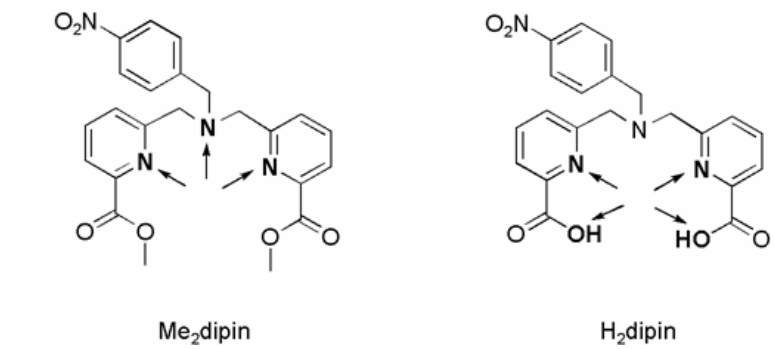

Figure 3.2 Multifunctional ligand system dip described in this chapter; the variable denticity is indicated by the arrows.

By introduction of two additional carboxylate arms, the dipicolyl amine chelation entity can be enhanced in denticity to form the "dip" (di-picolyl-carboxylate) ligand system which contains two pyridine carboxylate moieties joined by a benzyl amine functionality for derivatization. The chelate system itself was previously investigated for Pb^{2+} and found to bind this particular metal ion in a pentagonal, planar fashion.[61]

In this chapter, different chelation modes of dip are investigated, namely tetradentate, square planar coordination of the the divalent metal Cu^{2+} and *fac*-tridentate for the $[M(CO)_3]^+$ cores (M = Re, ^{99m}Tc) (Figure 3.2). A model bifunctional chelate system was developed and the viability of the system for simple functionalization was illustrated through synthesis and coordination of biotin conjugates.

Biotin is a water soluble molecule also known as vitamin H (Figure 3.3).[102] *In vivo*, biotin acts as a coenzyme involved in metabolism and in the production of important biomolecules such as fatty acids and antibodies. At the same time, it has a very high affinity towards avidin and streptavidin ($K_d \sim 10^{-15}$M),[103] which has led to many biochemical applications that are dependent on this strong affinity.[104] The biotin-avidin interaction has also been investigated in the area of targeted cancer radiotherapy.[105] Conjugation of the bifunctional chelate described in this chapter to biotin is therefore highly relevant, and serves as a convenient proof of principle for the feasibility of the ligand design.

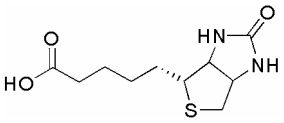

Figure 3.3 Biotin.

3.2 Experimental

3.2.1 Materials and Methods

Refer to Chapter 2.2 for general information. A Phenomenex Jupiter 5 μm C18 RP analytical column with dimensions 100 × 4.6 mm was used to purify [$Re(CO)_3(Me_2$dipin-biotin)]Br. HPLC solvents consisted of 0.1% trifluoroacetic acid in water (solvent A) and acetonitrile (solvent B). Samples were analyzed and purified with a linear gradient method (100% solvent A to 100% solvent B over 30 min). ^{64}Cu was obtained as a dilute HCl solution (MDS Nordion); it was commercially available from Nordion at the time of the ^{64}Cu experiments. Product specification reports specific activity of the ^{64}Cu to be > 5000Ci/g with < 0.2 micrograms of Cu per mCi. The HPLC system used for analysis of the ^{64}Cu labelled compounds consisted of a Waters Alliance HT 2795 separation module equipped with a Raytest Gabbistar NaI detector and a Waters 996 photodiode array (PDA) detector. The analyses of ^{64}Cu labelled compounds and their serum stabilities were analyzed on a Waters XBridge BEH130 4.6 mm × 150 mm column. [$^{99m}TcO_4$]$^-$ was provided by Vancouver Coastal Health UBC hospital. Reaction monitoring of ^{99m}Tc

experiments was performed by TLC (see above), using a mobile phase mixture of methanol and dichloromethane (1:4). Radioactive TLCs were measured using a phosphor imager (Cyclone storage phosphor imager with (20 × 25) cm^2 phosphor screen, Perkin-Elmer, Waltham, MA, USA) and analyzed using OptiQuest software. The $[^{99m}Tc(H_2O)_3(CO)_3]^+$ precursor was synthesized using the Isolink kit (Covidien, St. Louis, MO). 4-(Aminomethyl)-N-(9-fluorenylmethoxycarbonyl) phenylamine hydrochloride and biotin-TFP were prepared according to literature steps.[104,106] 4-(Aminomethyl)-N-(9-fluorenylmethoxycarbonyl)phenylamine hydrochloride and 4-(aminomethyl)-N-(9-fluorenylmethoxycarbonyl)phenylamino-di-pyridine-2-carboxylic acid methyl ester was synthesized by Scott Lin as part of his bachelor thesis.[107]

3.2.2 Synthesis of Ligands

6-Formylpyridine-2-carboxylic acid methyl ester (1).

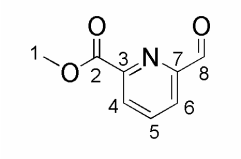

6-Hydroxymethylpyridine-2-carboxylic acid methyl ester (2.333 g, 13.95 mmol) and SeO_2 (1.421 g, 12.80 mmol) were refluxed in 1, 4-dioxane (80 mL) for 2.5 hours. The reaction mixture was cooled to room temperature, and the black solid was filtered off. Dioxane was removed from the filtrate by rotary evaporation. A mixture of white and red solids remained. The crude product was purified by column chromatography (silica, chloroform) as an off-white solid (1.107 g, 6.70 mmol, yield 48 %). ^{1}H NMR (300 MHz, $CDCl_3$, δ): 10.20 (s, *H8*, 1H), 8.35 (dd, $^3J_{4,5}$ = 7.5 Hz, $^4J_{4,6}$ = 1.1 Hz, *H4*, 1H), 8.15 (d, $^3J_{5,6}$ = 7.8 Hz, $^4J_{4,6}$ = 1.1 Hz, *H6*, 1H), 8.04 (t, $^3J_{4,5}$ = 7.5 Hz, $^3J_{5,6}$ = 7.8 Hz, *H5*, 1H), 4.08 (s, *H1*, 3H). ^{13}C NMR (75 MHz, $CDCl_3$, δ): 192.8 (*C8*), 165.0 (*C2*), 152.9 (*C7*), 148.7 (*C3*), 138.6 (*C5*), 129.2 (*C4*), 124.5 (*C6*), 53.5 (*C1*). HR-ESI-MS calcd. for $C_8H_8NO_3$: 166.0504, found: 166.0501 $[M + H]^+$.

6-[(4-Nitrobenzylamino)methyl]-di-pyridine-2-carboxylic acid methyl ester (2, Me_2dipin-NO_2).

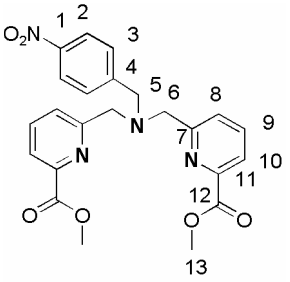

4-Nitrobenzylamine·HCl (0.457 g, 2.42 mmol) was stirred in dichloromethane (7 mL). NaOH (1 M, 3.5 mL) and H_2O (2 mL) were added to the suspension, and the mixture was stirred for 30 minutes until all solids dissolved. The organic layer was separated from the aqueous layer, which was extracted with dichloromethane (5 x 5 mL). The combined organic layer was reduced by rotary evaporation to afford an orange oil. To this orange oil was added **1** (0.800 g, 4.84 mmol, 2 eq) and $NaBH(OAc)_3$ (2.567 g, 12.11 mmol, 5 eq), and the mixture was refluxed for 25 hours in 1,2-dichloroethane (80 mL). The reaction was quenched with saturated aqueous Na_2CO_3 (40 mL) and extracted with dichloromethane (5 x 15 mL). The combined organic layers were dried over anhydrous $MgSO_4$. The solvent was removed to give a brown oil, which was recrystallized with 4:1 CH_3OH / CH_2Cl_2. Brown crystals were collected (0.580 g, 1.29 mmol, yield 53 %). ^{1}H NMR (300 MHz, $CDCl_3$, δ): 8.17 (d, $^3J_{9,\,10}$ = 8.7 Hz, *H10,* 2H), 8.02 (d, $^3J_{8,\,9}$ = 7.5 Hz, *H8,* 2H), 7.85 (t, $^3J_{8,\,9}$ = 7.5 Hz, $^3J_{9,\,10}$ = 8.7 Hz, *H9,* 2H), 7.78 (d, $^3J_{2,\,3}$ = 8.4 Hz, *H2,* 2H), 7.61 (d, $^3J_{2,\,3}$ = 8.4 Hz, *H3,* 2H), 4.01 (s, *H13,* 6H), 3.96 (s, *H6,* 4H), 3.83 (s, *H5,* 2H). ^{13}C NMR (75 MHz, $CDCl_3$, δ): 165.9 (*C12*), 159.6 (*C7*), 147.7 (*C11*), 147.4 (*C1*), 146.8 (*C4*), 137.7 (*C9*), 129.7 (*C3*), 126.3 (*C8*) , 124.0 (*C10*), 123.8 (*C2*), 60.0 (*C6*), 57.9 (*C5*), 53.1 (*C13*). IR (neat, cm^{-1}): 1717 (s), 1516 (w), 1337 (m). HR-ESI-MS calcd. for $C_{23}H_{22}NaN_4O_6$: 473.1437, found: 473.1433 $[M + H]^+$.

6-[(4-Nitrobenzylamino)methyl]-di-pyridine-2-carboxylic acid (3, H_2dipin-NO_2).

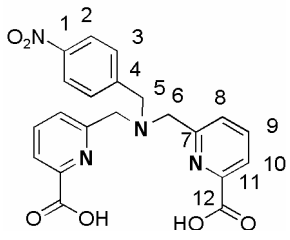

6-[(4-Nitrobenzylamino)methyl]-di-pyridine-2-carboxylic acid methyl ester (**2**, 102 mg, 0.227 mmol) was dissolved and stirred in THF (16 mL). LiOH (22 mg, 0.908 mmol, 4 eq) was added and the solution turned light yellow. The mixture was stirred for 2 hours, after which time the solvent was removed by rotary evaporation. The crude mixture was then washed with dichloromethane to yield a yellow solid. This was then redissolved in H_2O and acidified with conc. HCl to afford the corresponding HCl salt. ^{1}H

NMR (300 MHz, D_2O, δ): 8.03 (d, $^3J_{9,10}$ = 9.2 Hz, *H10,* 2H), 7.68 (d, $^3J_{8,9}$ = 8.7 Hz, *H8,* 2H), 7.61 (t, $^3J_{8,9}$ = 8.7 Hz, $^3J_{9,10}$ = 9.2 Hz, *H9,* 2H), 7.53 (d, $^3J_{2,3}$ = 6.9 Hz, *H2,* 2H), 7.44 (d, $^3J_{2,3}$ = 6.9 Hz, *H3,* 2H), 3.83 (s, *H6,* 4H), 3.79 (s, *H5,* 2H). ^{13}C NMR (75 MHz, D_2O, δ): 172.6 (*C12*), 157.2 (*C7*), 152.2 (*C11*), 146.2 (*C1*), 146.0 (*C4*), 137.6 (*C9*), 129.6 (*C3*), 125.2 (*C8*) , 122.8 (*C10*), 121.6 (*C2*), 60.0 (*C6*), 58.2 (*C5*). IR (neat, cm^{-1}, of acidified species): 1739 (s), 1523 (m), 1340 (s, br). HR-ESI-MS calcd. for $C_{21}H_{17}N_4O_6$: 421.1148, found: 421.1145 [M – H] $^-$. Elemental Analysis calcd. (found) for $C_{21}H_{18}N_4O_6 \cdot HCl \cdot H_2O$: C, 52.70 (52.13); H, 4.44 (4.16); N, 11.75 (11.43).

6-[(4-Aminobenzylamino)methyl]-di-pyridine-2-carboxylic acid methyl ester (4, Me_2dipin-NH_2).

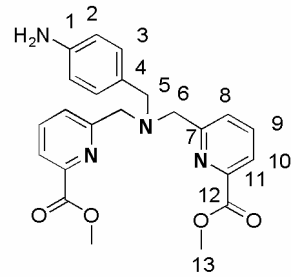

4-(aminomethyl)-N-(9-fluorenylmethoxycarbonyl)phenylamino-di-pyridine-2-carboxylic acid methyl ester (40 mg, 0.0623 mmol) was stirred in 20% piperidine/DMF (4 mL) for 30 minutes at room temperature. A small volume of CH_2Cl_2 was added, and the mixture was extracted three times with aqueous saturated $NaHCO_3$ solution (15 mL). Basic extraction with $NaHCO_3$ was repeated (3 x 5 mL). The organic layer was evaporated and then triturated with hexane. Rotary evaporation to remove hexane afforded the product as a yellow solid (24 mg, yield 92 %). ^{1}H NMR (300 MHz, $CDCl_3$, δ): 7.99 (d, $^3J_{9,10}$ = 9.0 Hz, *H10,* 2H), 7.81 (m, $^3J_{8,9}$ = 7.5 Hz, *H8, H3,* 4H), 7.18 (t, $^3J_{8,9}$ = 7.5 Hz, $^3J_{9,10}$ = 9.0 Hz, *H9,* 2H), 6.65 (d, $^3J_{2,3}$ = 8.4 Hz, *H2,* 2H), 3.99 (s, *H13,* 6H), 3.92 (s, *H6,* 4H), 3.58 (s, *H5,* 2H). ^{13}C NMR (75 MHz, $CDCl_3$, δ): 165.1 (*C12*), 160.9 (*C7*), 147.5 (*C11*), 145.8 (*C1*), 137.5 (*C4*), 130.3 (*C9*), 126.9 (*C3*) , 126.1 (*C8*), 123.7 (*C10*), 115.2 (*C2*), 59.8 (*C6*), 58.5 (*C5*), 53.1 (*C13*). HR-ESI-MS calcd. for $C_{23}H_{24}NaN_4O_4$: 443.1686, found: 443.1695 $[M + Na]^+$.

6-[(4-Amino- benzylamido-biotinyl)-methyl]-di-pyridine-2-carboxylic acid methyl ester (5, Me_2dipin-biotin).

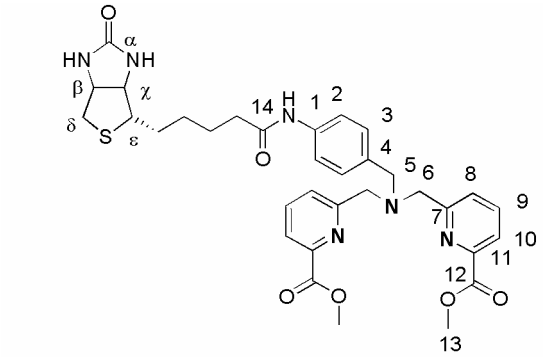

6-[(4-Amino-benzylamino)-methyl]-di-pyridine-2-carboxylic acid methyl ester (**4**, 173 mg, 0.4 mmol) and triethylamine (173 μL, 1.245 mmol) were stirred in DMF (6 mL), biotin-TFP (181 mg, 0.461 mmol) was added, and the mixture was stirred overnight at 60°C. The solvent was removed and the product was precipitated with THF as a white solid (105 g, 0.163 mmol, yield 40 %) which was collected by filtration. ^{1}H NMR (300 MHz, CD_3OD, δ): 7.95 (m, *H8*, *H9*, *H10*, *H11*, 6H), 7.54 (d, $^3J_{2,3}$ = 8.4 Hz, *H2*, 2H), 7.35 (d, $^3J_{2,3}$ = 8.4 Hz, *H3*, 2H), 4.30 (m, *Hβ*, 1H), 4.15 (m, *Hχ,* 1H), 3.87 (s, *H13*, 6H), 3.77 (s, *H6*, 4H), 3.60 (m, *H5*, 4H), 2.9 (dd, $^3J_{\varepsilon, CH_2}$ = 5.1 Hz, *Hε*, 2H), 2.72 (m, *Hδ*, 2H), 2.28 (m, *CH_2*, 2H), 1.85 – 1.40 (m, 6H). ^{13}C NMR (75 MHz, CD_3OD, δ): 174.4 (*C14*), 165.3 (*C12*), 162.7 (*Cα*), 159.7 (*C7*), 146.7 (*C11*), 137.9 (*C1*), 129.2 (*C10*), 126.2 (*C4*), 123.3 (*C3*), 118.9 (*C8*), 67.0 (*C6*), 61.1 (*Cχ*), 59.2 (*Cβ*), 55.4 (*C5*), 52.4 (*C13*), 33.5, 28.2, 28.1, 25.1, 24.5. IR (neat, cm^{-1}): 1697 (w), 1428 (m), 1313 (w). HR-ESI-MS calcd. for $C_{33}H_{39}N_6O_6S$: 647.2652, found: 647.2645 $[M + H]^+$.

6-[(4-Aminobenzylamidobiotinyl)methyl]-di-pyridine-2-carboxylic acid (6, H_2dipin-biotin).

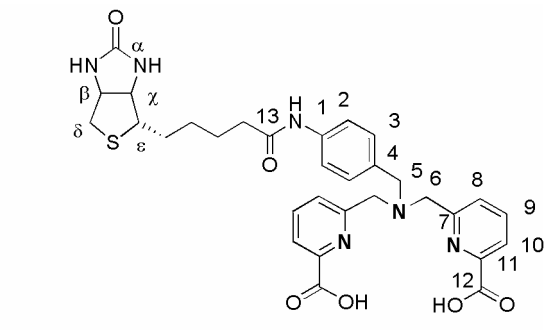

5 (8 mg, 0.012 mmol) was dissolved in THF/ H_2O / CH_2Cl_2 (1:2:1, 4 mL). LiOH (2 mg, 0.08 mmol) was added and the reaction was monitored by TLC (20% CH_3OH in CH_2Cl_2). After the reaction was found to be complete, the solvent was removed *in vacuo* to afford a yellow solid which was redissolved in CH_3OH and filtered to remove insoluble impurities. The product was isolated as a light yellow solid, (6.8 mg, 0.011 mmol, yield 91 %) ^{1}H NMR

(300 MHz, d_6-DMSO, δ): 8.06 (d, $^3J_{9,10}$ = 7.7 Hz, *H10*, 2H), 7.87 (d, $^3J_{9,10}$ = 7.7 Hz, $^3J_{8,9}$ = 7.7 Hz, *H9*, 2H), 7.53 (d, $^3J_{2,3}$ = 8.5 Hz, *H2*, 2H), 7.41 (d, $^3J_{8,9}$ = 7.7 Hz, *H8*, 2H), 7.32 (d, $^3J_{2,3}$ = 8.5 Hz, *H3*, 2H), 4.44 (m, *Hβ*, 1H), 4.27 (m, *Hχ*, 1H), 3.73 (s, *H6*, 4H), 3.60 (m, *H5*, 2H), 3.19 (m, *Hε*, 1H), 2.88 (dd, *Hδ*, 2H), 2.65 (m, CH_2, 2H), 2.13 (m, CH_2, 2H), 1.51 (m, 6H) ^{13}C NMR (75 MHz, CD_3OD, δ): 183.0 (*C12*), 172.4 (*C13*), 166.3 (*Cα*), 158.7 (*C7*), 139.5 (*C11*), 136.5 (*C1*), 131.0 (*C9*), 127.6 (*C4*), 123.8 (*C3*), 121.5 (*C8*), 115.9 (*C2*), 63.4 (*C6*), 61.8 (*C5*), 41.2 (*Cχ*), 39.1 (*Cβ*), 30.31 (*Cδ*), 29.9, 29.7, 27.7. IR (neat, cm^{-1}): 1682 (w, amide), 1636 (w), 1567 (w), 1429 (m). HR-ESI-MS calcd. for $C_{31}H_{32}Li_3N_6O_6S$: 623.2264, found: 623.2274 $[M - 2H + 3\ Li]^+$.

3.2.3 Coordination Chemistry

[Re(CO)$_3$(2)]Br ([Re(CO)$_3$(Me$_2$dipin-NO$_2$)]Br).

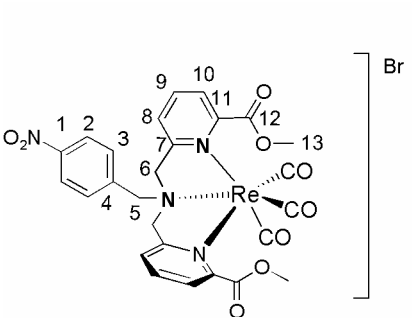

2 (44 mg, 0.098 mmol) was dissolved in dichloromethane (5 mL). $[Re(CO)_3(Br)_3][N(Et)_4]_2$ (76 mg, 0.98 mmol) was dissolved in CH_3OH (5 mL) and added dropwise to the ligand solution. The reaction mixture was heated for 18 h at 40°C. Subsequently, the solvent was removed and the crude mixture was triturated with dichloromethane (to remove unreacted ligand) and extracted with CH_3OH (to precipitate most of the $[N(Et)_4]Br$) to afford the product after removal of the solvent *in vacuo* as a white solid (32 mg, 0.043 mmol, yield 44 %). ^{1}H NMR (300 MHz, CD_3OD, δ): 8.41 (d, $^3J_{9,10}$ = 8.7 Hz, *H10,* 2H), 8.09 (d, $^3J_{8,9}$ = 8,7 Hz, $^3J_{9,10}$ = 8.7 Hz, *H9,* 2H), 8.01 (d, $^3J_{8,9}$ = 8.7 Hz, *H8*, 2H), 7.79 (d, $^3J_{2,3}$ = 7.8 Hz, *H2,* 2H), 7.69 (d, $^3J_{2,3}$ = 7.8 Hz, *H3*, 2H), 5.16-5.11 (m, *H6*, 4H), 4.57 (d, *H5*, 2H), 4.06 (s, *H13*, 6H). ^{13}C NMR (75 MHz, CD_3OD, δ): 195.7 (*C*O), 191.6 (*C*O), 163.4 (*C12*), 142.7(*C7*), 140.8 (*C11*), 139.6 (*C6*), 135.0 (*C9*), 131.4 (*C4*), 126.8 (*C3*), 125.2 (*C8*), 124.7 (*C2*), 70.7 (*C6*), 64.1 (*C5*), 59.7 (*C13*). IR (neat, cm^{-1}): 2034 (s, ν_{CO}) 2011 (s, ν_{CO}), 1895 (s, ν_{CO}), 1867 (m), 1728 (w). HR-ESI-MS calcd. for $C_{26}H_{22}N_4O_9{}^{185}Re$: 719.0917, found: 719.0906 $[M + H]^+$.

[Re(CO)$_3$(5)]Br ([Re(CO)$_3$(Me$_2$dipin-biotin)]Br).

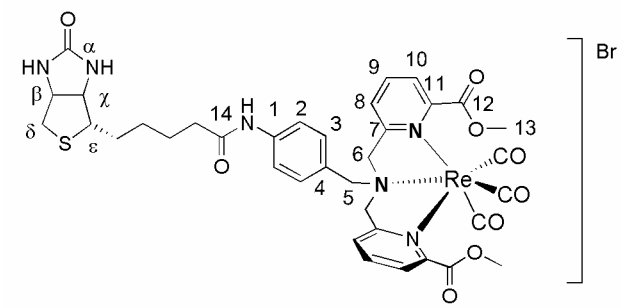

5 (5 mg, 0.007 mmol) was dissolved in CH_3OH (2 mL). $[Re(CO)_3(Br)_3][N(Et)_4]_2$ (6 mg, 0.007 mmol) was added to the ligand solution. The reaction mixture was heated for 18 h at 60°C. Subsequently, the solvent was removed and the crude product was purified by reversed phase HPLC. The solvent was removed and the product was afforded as a colourless solid (1 mg, 0.001 mmol, yield 14 %). ^{1}H NMR (300 MHz, CD_3OD, δ), 8.09 (m, *H10,* 2H), 7.79 (m, *H9,H8,* 4H), 7.65 (m, *H2, H3,* 4H), 5.11-4.94 (m, *H6,* 4H), 4.60 (d, *H5*, 2H), 4.48 (m, *Hβ*, 1H), 4.30 (m, *Hχ*, 1H), 3.21 (m, *Hε*, 1H), 2.93 (dd, *Hδ*, 2H), 2.69 (m, C*H*$_2$, 2H), 2.21 (m, C*H*$_2$, 2H), 1.78-1.41 (m, 6H). ^{13}C NMR (75 MHz, CD_3OD, δ): 195.5 (*C*O), 191.8 (*C*O), 177.9 (*C*), 174.1, 166.9 (*C12*), 166.5 (*Cα*), 163.9 (*C11*), 155.0 (*C6*), 142.9 (*C9*), 134.5 (*C4*), 134.5 (*C3*), 126.9 (*C8*), 121.8 (*C2*), 67.1 (*C6*), 63.7 (*C5*), 57.4 (*C13*), 44.3 (*Cχ*), 41.5 (*Cβ*), 35.1 (*Cδ*), 30.2, 29.9, 26.9, 26.4, 25.9. IR (neat, cm^{-1}): 2033 (s, ν_{CO}), 2011 (s, ν_{CO}), 1722 (m), 1698 (w). HR-ESI-MS calcd. for $C_{36}H_{38}N_6O_9{}^{185}Re\ {}^{32}S$: 915.1951, found: 915.1964 $[M]^+$.

[Cu(3)]·EtOH ([Cu(dipin-NO$_2$)]·EtOH).

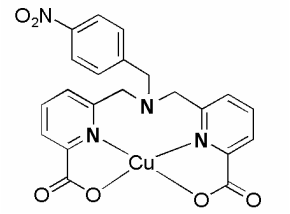

3 (5 mg, 0.0126 mmol) was stirred in CH_3OH /H_2O (1:1). The pH was adjusted with 0.1 M HCl to 2-3. $Cu(C_2H_3O_2)\cdot H_2O$ (2.5 mg, 0.0126 mmol, in 2:1 CH_3OH /H_2O) was added, and the solution turned clear green. The pH was raised to 7-8 with 0.1 M NaOH, and a solid precipitated. The mixture was left to stir for 3 hours, and the solvent was removed by rotary evaporation to give a green solid (5 mg, 0.007 mmol, yield 58 %). Small green plates suitable for X-ray diffraction were afforded through slow evaporation of a solution of the complex in a water-methanol mixture (1:3) in order to remove salts, which precipitate together with the product; the crude product is

purified using a C18 cartridge. The cartridge is rinsed thoroughly with H_2O before the product is eluted using EtOH. IR (neat, cm^{-1}): 1639 (m,br), 1513 (s), 1344 (s). HR-ESI-MS calcd. for $C_{21}H_{16}{}^{63}CuN_4O_6$: 506.0264, found: 506.0272 $[M]^+$. Elemental Analysis calcd. (found) for $C_{21}H_{16}CuN_4O_6 \cdot EtOH$: C, 52.12 (52.04); H, 4.18 (4.30); N, 10.57 (10.36).

[Cu(6)]·2 H_2O ([Cu(dipin-biotin)]·2H_2O).

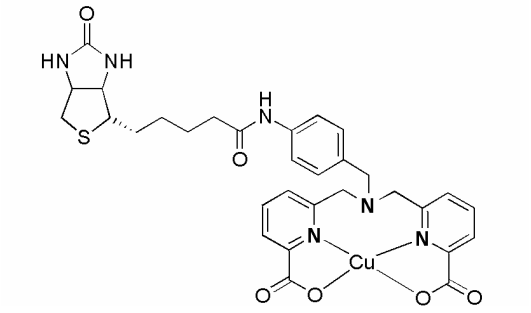

The biotinylated complex was afforded through the same synthetic procedure as [Cu(**dipin-NO_2**)]·EtOH but using **6** (6 mg, 0.0097 mmol) as the starting material. The product is eluted using CH_3OH. The product was afforded as a light green solid (4 mg, 0.0058 mmol, 89 %). IR (neat, cm^{-1}): 1684 (s), 1636 (w), 1551 (m), 1410. HR-ESI-MS calcd. for $C_{31}H_{32}{}^{63}CuN_6NaO_6S$: 702.1398, found: 702.1406 $[M + Na]^+$. Elemental Analysis calcd. (found) for $C_{31}H_{34}CuN_6O_7 \cdot 2H_2O$: C, 51.98 (51.73); H, 5.07 (5.28); N, 11.63 (11.15).

3.2.4 X-Ray Diffraction Structural Characterization

For [Cu(**dipin-NO_2**)]·EtOH, a green plate crystal of $C_{21}H_{18}CuN_4O_7$ having approximate dimensions of 0.02 x 0.15 x 0.25 mm was mounted on a glass fiber. All measurements were made on a Bruker DUO APEX II diffractometer with graphite monochromated Mo-Kα radiation. The data were collected at a temperature of -183.0 ± 0.1°C to a maximum 2θ value of 45.2°. Data were collected in a series of ϕ and ω scans in 0.50° oscillations with 60.0-second exposures. The crystal-to-detector distance was 40.00 mm. Of the 6190 reflections that were collected, 2560 were unique (R_{int} = 0.072); equivalent reflections were merged. Data were collected and integrated using the Bruker SAINT[78] software package. The linear absorption coefficient μ for Mo-Kα radiation is 11.55 cm^{-1}. Data were corrected for absorption effects using the multi-scan technique (SADABS[79]), with

minimum and maximum transmission coefficients of 0.730 and 0.977, respectively. The data were corrected for Lorentz and polarization effects.

For [$Re(CO)_3$(**2**)]Br, a colourless blade crystal of $C_{26}H_{22}N_4O_9Re.½Re(CO)_3Br_3$ having approximate dimensions of 0.02 x 0.10 x 0.40 mm was mounted on a glass fiber. All measurements were made on a Bruker APEX DUO diffractometer with graphite monochromated Mo-Kα radiation. The data were collected at a temperature of -183.0 ± 0.1 °C to a maximum 2θ value of 58.4°. Data were collected in a series of ϕ and ω scans in 0.5 oscillations using 20.0-second exposures. The crystal-to-detector distance was 40.00 mm. Of the 50217 reflections that were collected, 8033 were unique (R_{int} = 0.048); equivalent reflections were merged. Data were collected and integrated using the Bruker SAINT[78] software package. The linear absorption coefficient, μ, for Mo-Kα radiation is 81.83 cm^{-1}. Data were corrected for absorption effects using the multi-scan technique (SADABS[79]), with minimum and maximum transmission coefficients of 0.611 and 0.849, respectively. The data were corrected for Lorentz and polarization effects. The collection and analysis of the data were done by Dr. Brian O. Patrick.

3.2.5 Radiolabelling with ^{99m}Tc

The organometallic precursor $[^{99m}Tc(H_2O)_3(CO)_3]^+$ was prepared from a saline solution of $Na[^{99m}TcO_4]$ (1 mL, 2.7 mCi) using the Isolink kit. A solution of $Na[^{99m}TcO_4]$ (1 mL) was added to the Isolink kit, and the vial was heated to reflux for 40 min. Upon cooling, 0.1 M HCl solution (1 mL) was added to adjust the pH to approximately 7. $[^{99m}Tc(H_2O)_3(CO)_3]^+$ (10 MBq, in 0.2 mL) was added to a 10^{-4} M solution of ligand (0.8 mL) in a sealed vial and heated to reflux for 40 min. TLCs were developed with a 4:1 mixure of dichloromethane and methanol as mobile phase.

3.2.6 Cysteine and Histidine Challenge

To evaluate complex stability, an aliquot (0.5 mL) of ^{99m}Tc-complex was challenged with a 0.1 M solution of cysteine and histidine (0.5 mL). The mixture was incubated at 37°C and analyzed by TLC after 24 h.

3.2.7 Radiolabelling with ^{64}Cu

A solution of ^{64}Cu (non-carrier added, 0.4 – 0.7 mCi, in 50 μL) was added to a 10^{-5} M solution (pH 5, sodium acetate buffer, 0.95 mL) of ligand. The reaction mixture was analyzed after 10 minutes at room temperature by HPLC (gradient: A: H_2O, 0.1 % TFA, B: CH_3CN. 5-100% B linear gradient 30 min). R_t of [^{64}Cu(**dipin-NO_2**)] radiolabelled product on HPLC: 10.9 minutes. Stability versus serum (1 h; in % complex intact): 22. R_t of [^{64}Cu(**dipin-biotin**)] radiolabelled product on HPLC: 8.1 minutes. Stability versus serum (1 h; in % complex intact): 48.

3.2.8 Serum Challenge

To evaluate complex stability, an aliquot (500 μL) of the reaction was added to a solution of mouse serum (pH 5 buffer, 500 μL). The mixture was incubated at 37°C and analyzed by HPLC (gradient: A: H_2O, 0.1 % TFA, B: CH_3CN. 5-100% B linear gradient 30 min) after 1h.

3.3 Results and Discussion

3.3.1 Chelate Synthesis

A double reductive amination reaction was chosen to join the two functional ends of the proposed bifunctional chelate. Commercially available dipicolinic acid can be converted into **1** using a three-step literature procedure.[108,109]

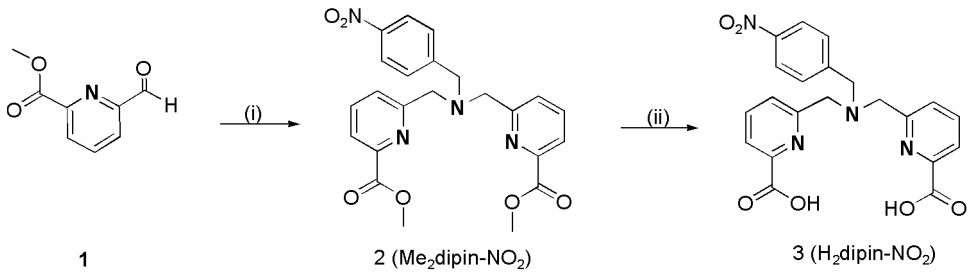

Scheme 3.1 Synthetic scheme for the synthesis of **2** and **3** (i) 0.5 eq 4-Nitrobenzylamine**,** $NaBH(OAc)_3$, DCE, reflux, overnight (ii) 4 eq LiOH, in THF/H_2O.

Aldehyde **1** can be reacted with a benzylamine derivative and undergoes a double reductive amination to form the framework of the intended chelate.[42] For the model chelate, a benzyl nitro derivative is used, which was initially supposed to act also as an intermediate to prepare an easy-to-couple phenyl amine.

This synthetic strategy involved use of a 4-nitrobenzylamine fragment to form **2** (Me_2dipin, Scheme 3.1). Sodium triacetoxyborohydride is routinely used as a mild reducing agent for double reductive amination, strong enough to reduce the imine intermediate, but not too strong to reduce the methyl ester. Since 4-nitrobenzylamine was purchased as the hydrochloride salt, basifying the salt with sodium hydroxide was initially performed to form the corresponding amine. The reductive amination reaction was performed overnight and quenched with saturated aqueous Na_2CO_3. Since the product was minimally soluble in methanol, it was found that recrystallization of the crude product mixture was possible with a 4:1 mixture of CH_3OH / CH_2Cl_2, affording the pure product **2** as brown needle-like crystals. Subsequent deprotection of the methyl ester protection group with LiOH afforded the desired model compound **3** (H_2dipin) quantitatively.

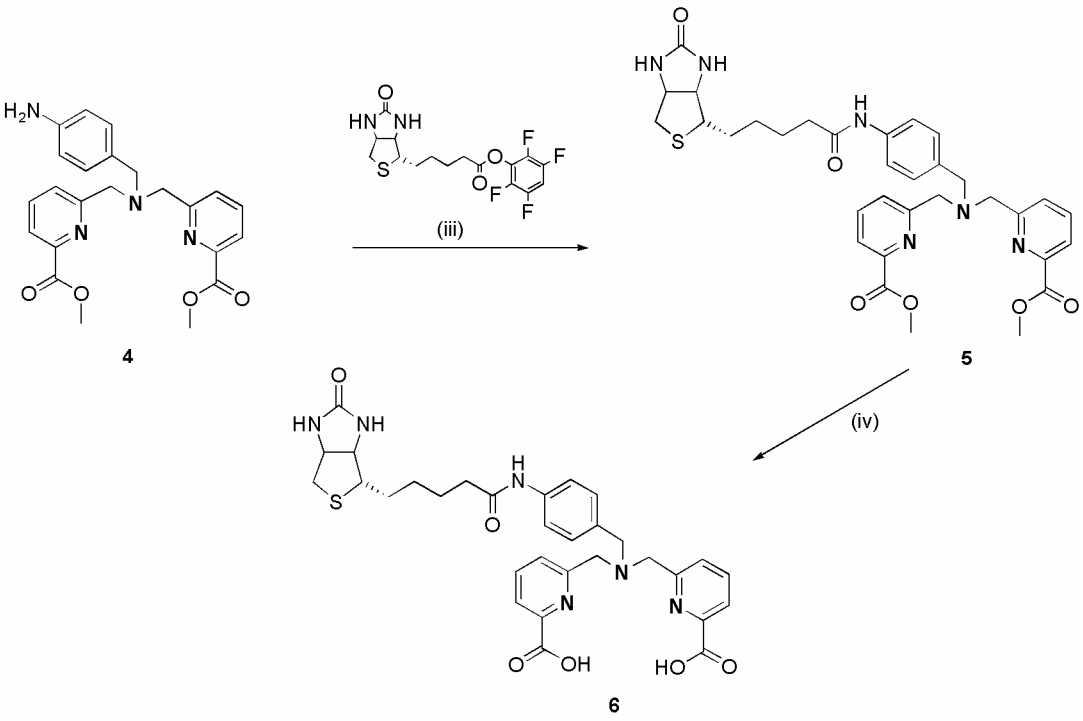

Scheme 3.2 Synthetic scheme for the synthesis of **5** and **6** (iii) NEt_3, DMF, 60 °C, overnight (iv) 5 eq LiOH, THF/ H_2O / CH_2Cl_2 (1:2:1).

To afford the easily derivatized phenylamine, however, reducing the nitro group of **2** to form **4** proved to be unsuccessful. Initially, reduction using hydrazine with Raney nickel as the catalyst was attempted. Formation of the product was evidenced by ESI-MS, but the ^{1}H NMR spectrum showed broadened peaks, suggesting possible coordination of the chelate to Ni(II). The same reduction reaction was attempted again using H_2 with Pd/C catalyst. Low to moderate pressure of H_2 did not drive the reaction to a significant yield, whereas higher pressure (70 psi) led to cleavage of the nitrobenzylamine fragment, as suggested by both ^{1}H NMR spectroscopy and ESI-MS. Hence, the reduction method for this specific nitro group was concluded to be ineffective.

The second, more successful strategy involved Fmoc-protected 4-aminobenzylamine as the starting material. 4-Aminobenzylamine can be selectively protected by Fmoc at the phenylamine position to produce 4-(aminomethyl)-N-(9-fluorenylmethoxycarbonyl)phenylamine as a hydrochloride salt.[106] Basic extraction was then performed to obtain the corresponding free amine. This was reacted with 2 equivalents of **1** to form the Fmoc-protected version of **4** via a double reductive

amination reaction. The product was purified by column chromatography. Finally, deprotection with 20% piperidine in DMF afforded the intended product **4** in 92 %.

To synthesize the biotin-conjugated fragment, the terminal carboxylic acid of commercially available D(+)-biotin was first activated using a tetrafluorophenyl ester following literature conditions.[104] The strong electron-withdrawing ability of the tetrafluorophenyl (TFP) group transforms the -OH into O-TFP, which serves as a convenient leaving group, making the carbonyl particularly susceptible to nucleophilic attack by the benzyl amine functionality of **4**.

Once biotin-TFP was prepared, it was reacted with **4** in DMF (Scheme 3.2). Triethylamine was added to maintain the basic condition that would be ideal for the coupling reaction (Scheme 3.2).[104] After overnight stirring at 60°C, the product was identified by ESI-MS; the crude solid was triturated with THF according to the literature[42] to remove impurities and to afford **5** (Me_2dipin-biotin) as a yellow solid. Compound **6** (H_2dipin-biotin) was prepared through LiOH deprotection of the methyl esters and extracted with CH_3OH, since the protected starting material and the salts present have low solubility in this solvent. Removal of the solvent *in vacuo* yielded the desired, deprotected product **6**.

3.3.2 Coordination Complexes

To synthesize the copper and rhenium complexes, the chelate was mixed with the corresponding precursor metal complex to form the desired product complex via a ligand substitution reaction. Copper(II) acetate was used as the starting material of copper complex formation. Copper(II) acetate is a dark green crystalline solid. To synthesize copper complexes, **3** or **6** was acidified in a CH_3OH/ H_2O mixture. The initial acidic condition prevents the hydrolysis of copper to form insoluble copper hydroxides. The solution was then neutralized to pH 7-8 after addition of complex precursors. Upon addition of the chelate, an immediate colour change was observed, and the colour of the solution intensified as the pH was increased. When **3** was added to the chelate solution, the product complex precipitated, forming a cloudy suspension. Evaporation of the solvent gave the light green copper complex mixed with NaCl. In order to remove excess

salt and confirm bulk composition of the complex by elemental analysis, both copper complexes were purified using C18 cartridges. [Cu(**dipin-biotin**)] readily elutes using MeOH and can be confirmed as the dihydrate salt. In the case of [Cu(**dipin-NO_2**)], a large amount of EtOH is used to elute the sparingly soluble complex from the cartridge. Presence of the complexes in solution was confirmed with high resolution mass spectrometry, which shows the characteristic isotope pattern for copper with corresponding masses $[M + H]^+$ and $[M + Na]^+$ for both Cu(II) complexes.

Table 3.1 Summarized relevant IR stretching frequencies for Cu complexes and the corresponding ligands.

	IR stretching frequency of diagnostic functional groups [cm^{-1}]		
Compound	Amido	Nitro	Carboxylate
H_2**dipin-NO_2**	-	1340	1739
H_2**dipin-biotin**	1684	-	1710
[Cu(**dipin-NO_2**)]	-	1344	1639
[Cu(**dipin- biotin**)]	1682	-	1636

Table 3.1 summarizes diagnostic IR frequencies observed. While the nitro group on the H_2dipin-NO_2 ligand system remains virtually uninfluenced by the coordination of the Cu ion, similar to the amido group on the H_2dipin-biotin ligand system, the stretching frequency of the carboxylate functional group strongly decreases upon coordination.

Compounds **2** and **5** were used for the coordination of the $[Re(CO)_3]^+$ core.[110,111] While the carboxylates remain protected and could only act as poor binding groups, the two pyridyl nitrogens together with the aliphatic nitrogen form the widely explored and popular dpa (dipicolylamine) ligand system. To afford [Re(Me_2**dipin-NO_2**)$(CO)_3$]Br, equimolar amounts of $[Re(CO)_3(H_2O)_3]$Br and ligand were stirred over night at 60°C in a 1:1 methanol/dichloromethane mixture. Excess ligand was removed from the crude product through trituration with dichloromethane to give the corresponding tridentate rhenium complex. In the case of [Re(Me_2**dipin-biotin**)$(CO)_3$]Br, reactants were stirred in methanol overnight at 60°C. The crude reaction mixture was purified using preparative HPLC.

Table 3.2 Summarized relevant IR stretching frequencies for Re complexes and the corresponding ligands.

Compound	IR stretching frequency of diagnostic functional groups [cm^{-1}]		
	Amido	Ester	Re-Carbonyl
Me_2**dipin-NO_2**	-	1717	-
Me_2**dipin-biotin**	1698	n. o.	-
$[Re(CO)_3(Me_2$**dipin-NO_2**$)]Br$	-	1728	2034, 2011
$[Re(CO)_3(Me_2$**dipin- biotin**$)]Br$	1687	n. o.	2033, 2011

Again, IR spectroscopy served as a good tool for confirming which donor atoms were involved in coordination (Table 3.2). The amide bond in both ligand and complex of the biotin conjugate remains unchanged, confirming the great distance from the coordination sphere for this specific functional group. The ester functionality is not observed in the case of the biotin conjugate due to overlap with the stronger amido peak, but for the nitro derivatized compounds a slight increase in wave number is observed. The characteristic metal bound carbonyl frequencies are observed and confirm coordination of identical ligand spheres in both cases.

Metal ion coordination of the tridentate ligands could be further verified by shifts in peaks in both the ^{1}H and ^{13}C NMR spectra. The summarized ^{1}H NMR spectra of ligands including the Re complexes are shown in Figures 3.4 and 3.5.

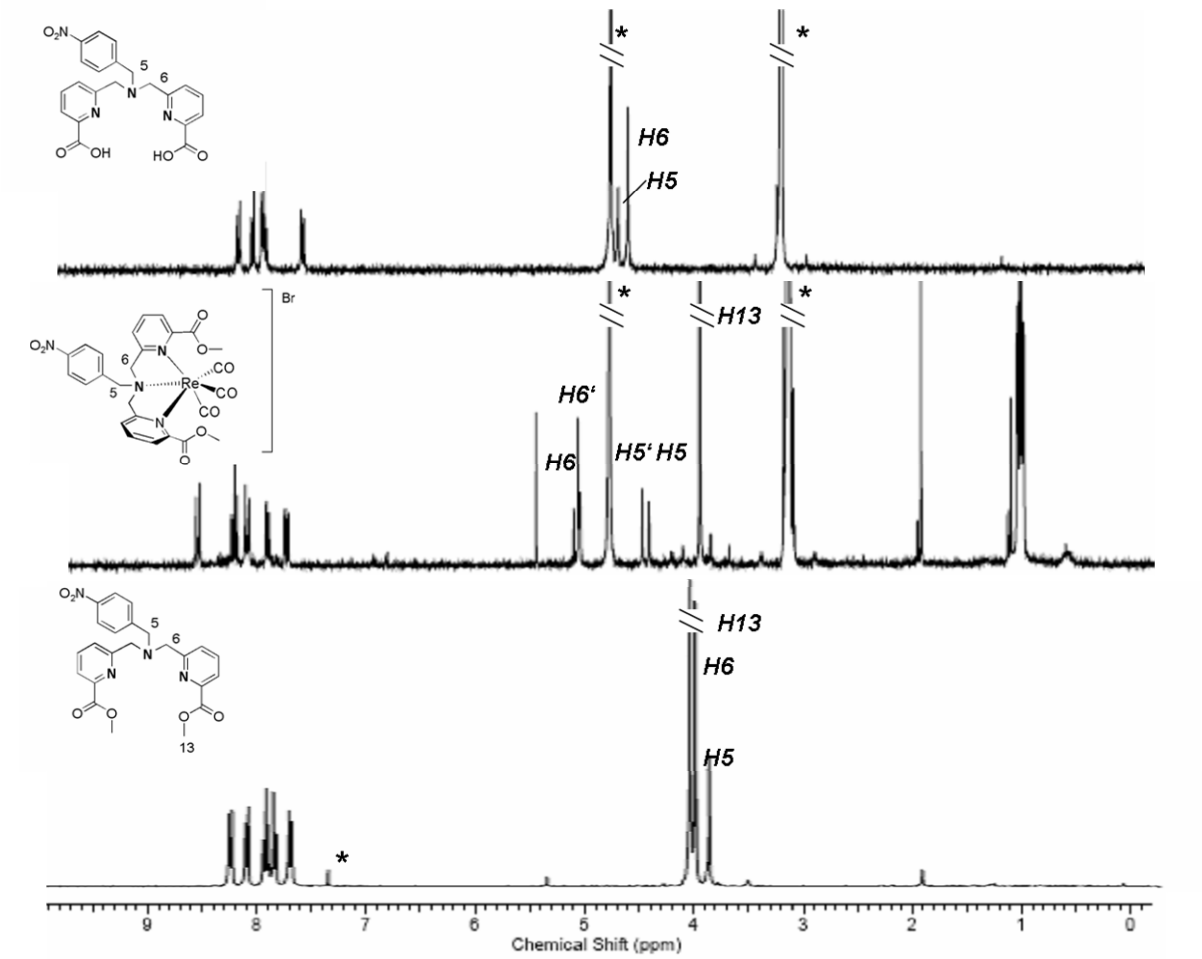

Figure 3.4 ^{1}H NMR spectra (300 MHz, $CDCl_3/CD_3OD$, 298 K) of the benzylnitro derivatized compounds synthesized, * denotes residual solvent peaks, presence of residual $N(Et)_4Br$ is observed for the Re complex (1.2 and 3.2 ppm).

As clearly recognizeable from the presented spectral data (Figures 3.4, 3.5), the coordination of the metal leads to observation of diasterotopic protons around the coordination sphere. The methylene groups 6 show a characteristic splitting pattern observed for coordination of the *fac*-$[Re(CO)_3]^+$ core, which was already described in Chapter 2. Due to coordination of the tertiary amine, methylene group 5 becomes fixed in its confirmation and splitting of the formerly singlet peak into two distinct peaks is observed; however, methyl group 13 maintains its free rotation, appearing as a defined singlet peak in both ligand and complex systems.

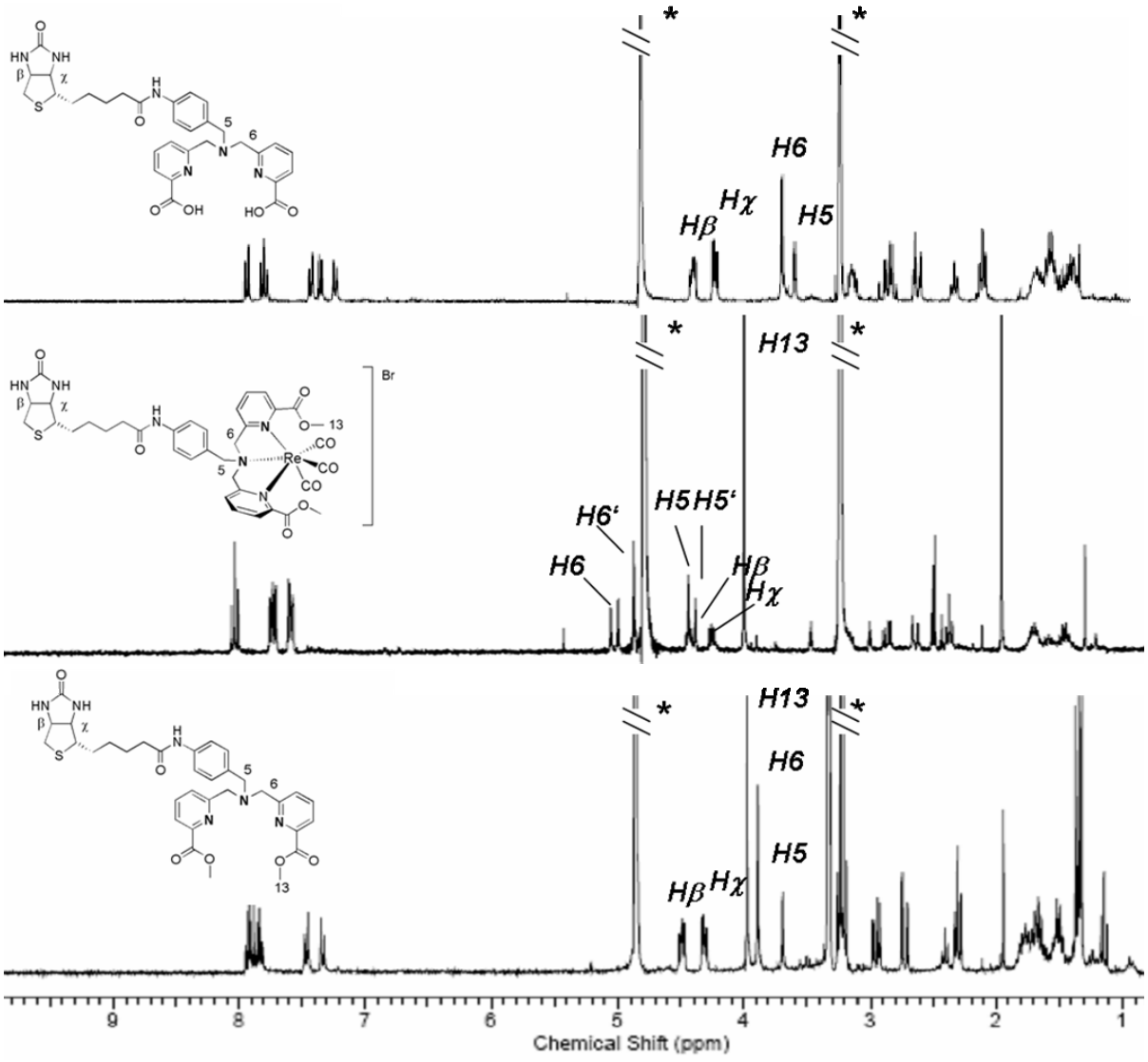

Figure 3.5 ^{1}H NMR spectra (300 MHz, CD_3OD, 298 K) of the biotin derivatized compounds synthesized, * denotes residual solvent peaks.

The mass spectrometry data confirmed the predicted coordination product by appearance of the mass of complex cations [M^+] with the characteristic isotope splitting pattern observed for Re.

3.3.3 X-Ray Diffraction Structural Characterization of [Cu(dipin-NO_2)H_2O] and [$Re(CO)_3$(Me_2dipin-NO_2)]$^+$

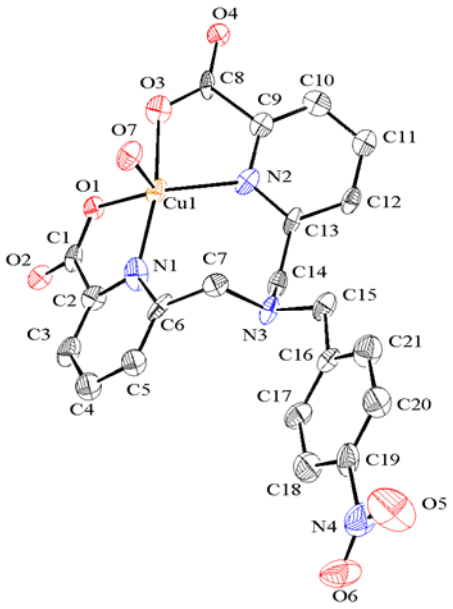

Figure 3.6 ORTEP drawing of [Cu(**dipin-NO_2**)(H_2O)], showing the atom numbering scheme (50% thermal ellipsoids).

The pale green solid [Cu(**dipin-NO_2**)] was dissolved in a CH_2Cl_2/CH_3OH mixture, and crystals were obtained by slow evaporation (Figure 3.6). The complex has a strongly distorted square pyramidal geometry and the four donor atoms from the chelate are sitting on the distorted square plane. The bond length between Cu and any of the 4 donor atoms of the chelate is roughly the same; however, the Cu-N bond lengths are slightly longer than the Cu-O bond lengths. The bond length between Cu and the apical water oxygen atom is longer than the other coordinate bonds, suggesting that the water molecule may be loosely coordinated to the metal centre. The axial elongation is typical of the Jahn Teller distortion observed for Cu(II) complexes and is also in agreement with previously reported square pyramidal Cu(II) complexes. The axially coordinated water molecule could be another indicator for the instability of this particular ligand system *in vitro*, since it could be easily displaced by serum proteins facilitating the transchelation

of the metal out of the dipin ligand (*vide infra*).

Table 3.3 Selected bond lengths in [Cu(dipin-NO_2)(H_2O)] ([Å]) and angles ([°]).

bond	length [Å]	angle	degree [°]
N(1) – Cu(1)	2.005(10)	O(3)- Cu(1)- O(1)	90.7(3)
N(2) – Cu(1)	2.061(9)	O(1)- Cu(1)- N(1)	81.3(3)
O(1) – Cu(1)	1.988(7)	O(3)- Cu(1)- N(2)	82.9(4)
O(3) – Cu(1)	1.927(8)	O(3)- Cu(1)- O(7)	86.5(3)
O(7) – Cu(1)	2.155(8)	N(1)- Cu(1)- O(7)	90.1(4)

For the structure of $[Re(CO)_3(Me_2$**dipin-NO_2**$)]^+$ (Figure 3.7), the colorless crude solid was dissolved in CH_3OH and crystals were obtained by slow evaporation. The complex co-crystallized with $[Re(CO)_3Br_3]^{2-}$ as the counter ion for two molecules of $[Re(CO)_3($**2**$)]^+$.

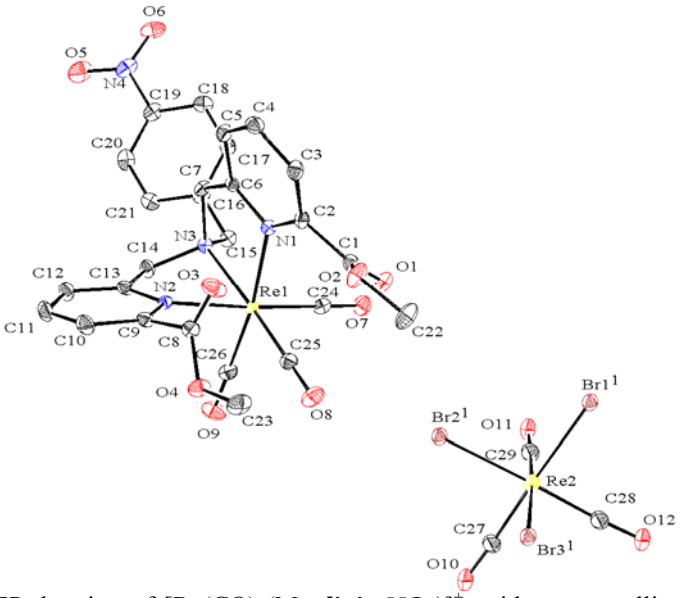

Figure 3.7 ORTEP drawing of $[Re(CO)_3(Me_2$**dipin-NO_2**$)]^+$, with co-crystallized counter ion $[Re(CO)_3Br_3]^{2-}$ shown is the atom numbering scheme (50% thermal ellipsoids).

The structure displays a distorted octahedral geometry. With all Re-N bond lengths close to 2.2 Å (Table 3.4), which is characteristic for bipyridyl complexes of the $[Re(CO)_3]^+$ core.[112] This is one indication that the stable coordination of this scaffold is not influenced by the two adjacent methyl ester functionalities.

Table 3.4 Selected bond lengths in $[Re(CO)_3(Me_2\textbf{dipin-NO}_2)]^+$ ([Å]) and angles ([°]).

bond	length [Å]	angle	degree [°]
N(1) – Re(1)	2.201(2)	C(26)- Re(1)- C(2)	90.62(12)
N(2) – Re(1)	2.209(2)	C(24)- Re(1)- N(1)	95.68(11)
N(3) – Re(1)	2.240(2)	C(25)- Re(1)- N(2)	100.24(11)
C(24) – Re(1)	1.929(3)	C(26)- Re(1)- N(2)	89.26(11)
C(25) – O(8)	1.161(4)	N(1)- Re(1)- N(2)	84.06(9)
C(25) – Re(1)	1.902(3)	C(26)- Re(1)- N(3)	96.51(11)
C(26) – O(9)	1.153(4)	C(24)- Re(1)- N(3)	98.66(11)
C(26) – Re(1)	1.915(3)	N(1)- Re(1)- N(3)	78.85(9)

3.3.4 Radiolabelling and Stability of ^{99m}Tc Complexes

The structural investigation of the Re complexes provided insight into the radiochemical complexes formed with ^{99m}Tc. In order to synthesize the ^{99m}Tc complexes, the organometallic precursor $[^{99m}Tc(H_2O)_3(CO)_3]^+$ was synthesized via heating, using the Isolink kit. When the mixture was cool, the pH was adjusted to approximately 7. A 10^{-4} M solution of ligand was mixed with $[^{99m}Tc(H_2O)_3(CO)_3]^+$ in a sealed vial and heated to reflux for 40 min. Reaction monitoring was performed by radio-TLC (Figure 3.8). Labeling with **2** was performed in a 1:1 acetonitrile/water mixture due to poor solubility of the ligand in protic solvents, yielding 72% product after reaction, with $R_f = 0.8$.

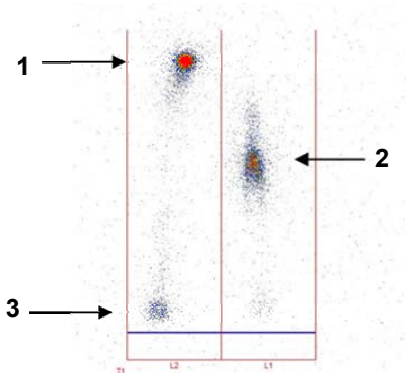

Figure 3.8 TLC labelling traces of $[^{99m}Tc(CO)_3(Me_2\textbf{dipin-NO}_2)]^+$ (left, spot 1) and $[^{99m}Tc(CO)_3(Me_2\textbf{dipin-biotin})]^+$ (right, spot 2); bottom spots indicate unreacted $[^{99m}Tc(CO)_3(H_2O)_3]^+$ (bottom, spot 3).

Due to increased solubility of **5** in protic solvents, labeling for this ligand was performed in a 3:7 methanol/water mixture, yielding 85% product with an R_f of 0.57. Both complexes were stirred in 0.1 M solution of histidine and cysteine at 37°C for 24 h, and were found to be fully stable against decomposition.

3.3.5 Radiolabelling and Stability of ^{64}Cu Complexes

A solution of ^{64}Cu was added to a 10^{-4} M solution of ligand (H_2**dipin-NO$_2$** or H_2**dipin-biotin**, both in aqueous solutions) at pH 5. The reaction was analyzed by HPLC after 10 minutes at room temperature. [^{64}Cu(**dipin-NO$_2$**)] was found to form in a 95 % yield with R_t = 10.9 min. [^{64}Cu(**dipin-biotin**)] was found to form in a 91% yield with R_t = 8.1 min (Figure 3.9). To evaluate complex stability, an aliquot of the reaction was added to a solution of mouse serum. The mixture was incubated at 37°C and analyzed by HPLC after 1h. For [^{64}Cu(**dipin-NO$_2$**)], 78% serum binding was found after 1h, while in the case of [^{64}Cu(**dipin-biotin**)], 52% activity was found to be bound to serum after the same incubation time.

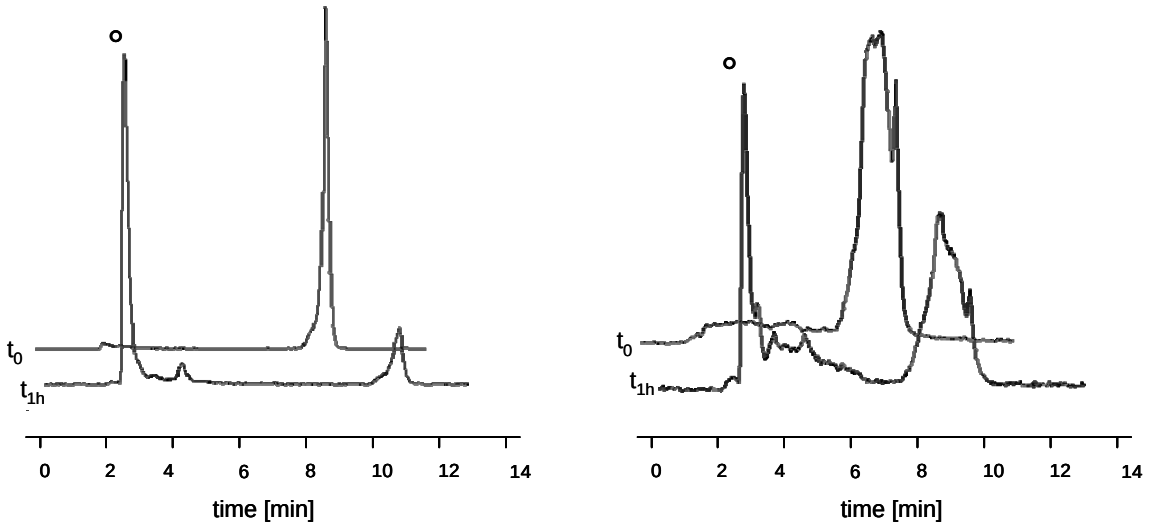

Figure 3.9 Labelling traces of ^{64}Cu copper complex [t_0] and trace after 1h serum challenge experiment [t_{1h}]. Left shows Cu complex with [^{64}Cu(**dipin-NO$_2$**)], right shows Cu complex with [^{64}Cu(**dipin-biotin**)], ° denotes transchelation of ^{64}Cu to serum proteins.

The HPLC labelling peak observed for the two complexes correlate with their polarity. Due to increased water solubility of the biotinylated complex, the retention time is shorter than the retention time of the model complex. [^{64}Cu(**dipin-biotin**)] appears as multiple peaks, suggesting formation of different coordination modes in solution. This was not observed in the cold coordination reaction, hence it could be an effect of the great excess of ligand used for the radiochemical coordination reaction.

3.4 Conclusions

Successful synthesis of the model ligands Me$_2$**dipin-NO$_2$** and H$_2$**dipin-NO$_2$** as well as the corresponding conjuguate versions Me$_2$**dipin-biotin** and H$_2$**dipin-biotin** are outlined in this chapter. Corresponding cold complexes with copper(II) and tricarbonylrhenium(I) were prepared in satisfying yields; the intended mode of coordination was confirmed by IR and NMR spectroscopy (for diamagnetic Re(I)) as well as solid state structural elucidation of both benzyl-nitro derivatives with the corresponding metal. In the case of the Cu complex, the coordination of an apical H_2O molecule is observed, which indicates potential destabilization of the chelation scaffold. Radiolabelling, while fast and efficient with ^{64}Cu, confirms this worry, since neither [^{64}Cu(**dipin-NO$_2$**)] nor [^{64}Cu(**dipin-biotin**)] proves to withstand serum competition tests. This renders the dipin ligand system unstable and not worthy of further investigations for the purpose of labelling with ^{64}Cu. The acyclic, tetradentate coordination mode of the dip ligand system was shown to be a non ideal chelation scaffold, despite the use of strong donor atoms as ligands. It is also suggested that the formation of an 8-membered ring upon coordination leads to destabilization of this complex in solution, also caused by the enhanced mobility and twisting of the chelate arms.[113]

[^{99m}Tc(CO)$_3$]$^+$ complexes with both Me$_2$**dipin-NO$_2$** and Me$_2$**dipin-biotin** were synthesized under standard labelling conditions, showing satisfactory stability of the [^{99m}Tc(CO)$_3$]$^+$ complexes. The solid state structure of [Re(CO)$_3$(Me$_2$**dipin-NO$_2$**)]$^+$ confirms feasibility and compares well to other complexes of similar make-up. It appears to be the case that the methyl ester functionalities do not influence the coordination chemistry in a negative way. This approach could bring opportunities to further functionalize SAAC type

chelates, as outlined similarly by Babich and coworkers,[114] where pyrazolyl ligands were functionalized with a carboxylic acid moiety to enhance the clearance properties for the otherwise quite lipophilic $[^{99m}Tc(CO)_3]^+$ core.

Chapter 4: A Novel Chelate for ^{68}Ga Imaging Agent Elaboration ‡

4.1 Introduction: Prior Art on $^{67/68}$Ga Chelates

The disruptions in the supply chain of ^{99}Mo, the parent of the clinically important daughter isotope ^{99m}Tc, has had worldwide effects on diagnostic nuclear medicine and has turned many researchers' attention to other generator-produced isotopes.[91] Among attractive alternatives to ^{99}Mo/^{99m}Tc is the ^{68}Ge/^{68}Ga generator system,[22] which has the potential to be eluted for up to one year due to the long half-life ($t_{1/2}$ = 271 d) of the parent radionuclide ^{68}Ge. The ^{68}Ga generator has been used to prepare ^{68}Ga radiopharmaceuticals for clinical imaging in Europe for several years,[115] but the development of a generator with regulatory approval for human use would further facilitate the transition of ^{68}Ga based agents into the clinic in North America. One of the most sophisticated commercially available generator systems is based on titanium dioxide (Cyclotron Co., Ltd., Obninsk, Russia) and is currently used worldwide.

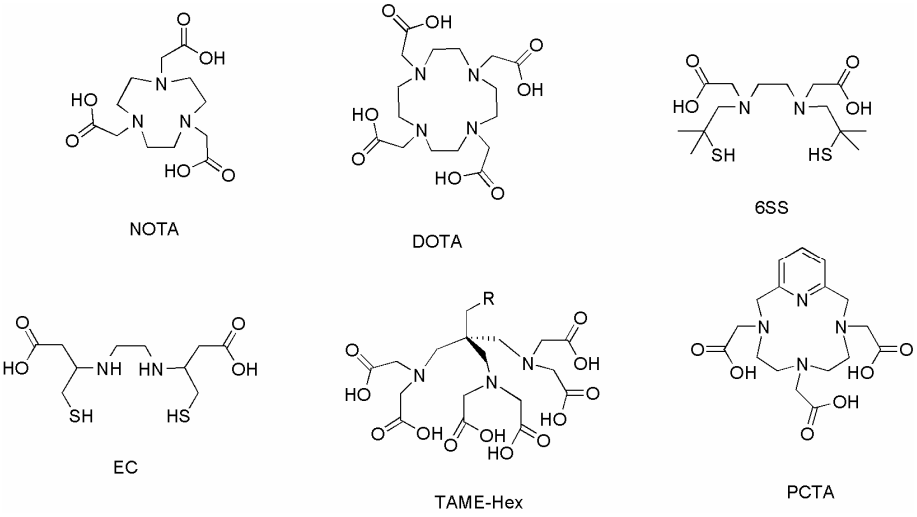

Figure 4.1 Structures of some previously investigated chelate systems for ^{68}Ga.

‡ Parts of this chapter have been published: "Acyclic Chelate with Ideal Properties for ^{68}Ga PET Imaging Agent Elaboration", E. Boros, C. L. Ferreira, J. F. Cawthray, E. W. Price, B. O. Patrick, D. W. Wester, M. J. Adam, C. Orvig , *J. Am. Chem. Soc.* **132** , 15726-15733 (2010).

The advantages of this particular generator include the use of a nontoxic packing material and, most importantly, the elution of free, cationic ^{68}Ga with low acid concentration of 0.1 M HCl, allowing universal application for radiopharmaceutical preparations. Other advantages include low ^{68}Ge breakthrough, which is reported to be between 0.001 and 0.005%.[60] Ga(III) forms stable complexes with many multidentate ligands,[116] and the radionuclide ^{68}Ga has suitable properties for high-quality positron-emission tomography (PET) imaging including a short half-life ($t_{1/2}$ = 68 min), decay by 89% positron emission and a maximum positron energy of 1.899 keV.[60,117,118] While Ga(I) is only stable in non aqueous media, under physiological conditions Ga(III) is the only stable and relevant oxidation state.

The free hydrated Ga(III) cation is only stable under acidic conditions, while above pH 4 formation of hydroxide species $Ga(OH)_3$ (pH 4 – 7) and $[Ga(OH)_4]^-$ (> pH 7) occurs.[119] To make the metal ion available for ligand systems that coordinate preferentially at pH < 5, a pre-labelling strategy uses a weakly coordinating ligand such as citrate, which is then easily replaced by a stronger ligand system.[120] This strategy is not compatible with the short $t_{1/2}$ of ^{68}Ga, hence a direct labelling strategy is preferred, which can be executed at a pH compatible with biomolecules. An additional non-negligible factor includes kinetic stability of the formed complex towards the iron sequestering protein transferrin, which is capable of transchelating weakly bound Ga(III) due to the similarity between the charge to size ratio of Ga(III) and Fe(III).[57]

Table 4.1 Summary of some investigated chelates for labelling of $^{67/68}$Ga

Ligand	Log K_{ML}	Labelling conditions (yield)
DOTA	21.33[121]	5 min, 80°C (95 %)[58]
NOTA	30.98[122]	10 min, room temperature, (> 98 %)[58]
6SS	41.0[60]	60 min, 90 °C (> 90 %)[60]
EC	31.5[51]	5 min, room temperature, (> 90 %)[51]
TAME-Hex	n. d.	10 min, 100 °C (99 %)[60]
PCTA	19.37[123]	10 min, room temperature, (> 98 %)[58]
apo-transferrin	20.3[57]	

The efficient and strong chelation of radiometals of Ga(III) has been investigated for the past 40 years with high hopes for potentially useful complexes in radiopharmacy.[124,125] The sustained efforts of Martell and Welch over several decades[126] have been succeeded by the significant progress of Maecke and co-workers in the late 1990s. Bifunctional versions of the tri- and tetra-aza-based aminocarboxylate macrocyclic chelates 1,4,7-triazacyclononane-1,4,7-triacetic acid (NOTA) and 1,4,7,10-tetraazacyclododecane-1,4,7,10-tetraacetic acid (DOTA) were able to deliver highly promising results not only for the isotopes $^{67/68}$Ga and ^{111}In but also for a wide range of radiolanthanides.[55] Many attempts to find chelates of comparable kinetic and thermodynamic stability for ^{68}Ga have been less successful.[51,127,128] The macrocyclic chelates themselves are challenging to synthesize as selectively functionalized analogues, thus most research groups in need of bifunctional derivatives of NOTA or DOTA are supplied by a commercial source. An array of previously investigated chelates for Ga(III), including thermodynamic stability constants and optimal labelling conditions, is summarized in Table 4.1 and Figure 4.1. In order to furnish the ideal bifunctional chelate for ^{68}Ga, rapid coordination under mild conditions (pH > 4, room temperature, labelling within 15 minutes), high kinetic stability (stable versus *apo*-transferrin challenge and *in vivo* conditions) and simple synthesis and functionalization (for applications for peptide labelling) are key. A thermodynamic stability constant log K_{ML} above the value found for the main *in vivo* competitor, transferrin (log K_{ML} = 20.3) is strongly desired. The 3+ charge is preferentially reduced to 1+, 1- or neutral in order to avoid high kidney uptake and accelerated excretion.

In this chapter, the synthesis of a series of acyclic chelates with pyridyl and carboxylate donor arms is described, as well as screening for their capability to label $^{67/68}$Ga under the ideal conditions outlined above.

4.2 Pyridine Carboxylate Chelates and Their Relevance for Chelation of Ga(III)

Ga(III) is often classified as hard Lewis acid because of its high charge density and small ionic radius (0.62 Å), having a preference for ligands of highly ionic, non-polarizable hard Lewis base nitrogen and oxygen donors (mainly as in aliphatic amines and

carboxylates). However, it was also found that much softer donors such as thiols and pyridyls (a softer type of nitrogen donor atom) have been used in order to form stable complexes with Ga(III).[120,129]

This observation leads to the conclusion that a combination of hard and soft donor atoms within one ligand system could result in a rather successful ligand design for Ga(III). Phenolates are less attractive, since the deprotonation of the phenolic proton requires a pH at which Ga(III) preferentially forms insoluble $Ga(OH)_3$, while thiols have a strong tendency to form disulfide bonds in the presence of O_2 as an oxidant. Pyridine-containing ligand systems however have no obvious drawbacks. The directed lone pair of the nitrogen serves as a convenient donor atom and a wide variety of chelates has been explored with pyridines as donors; a variety of building blocks can be synthesized or is even commercially available. PCTA, a macrocyclic chelate bearing one pyridyl group has been shown to chelate Ga(III) efficiently.[58]

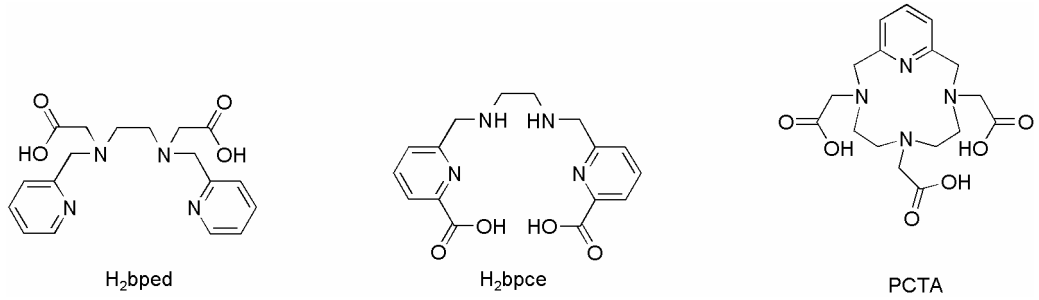

Figure 4.2 Previously reported pyridyl containing ligand systems.

Some of the compounds outlined in this chapter have been investigated before. The acyclic, tripodal chelate H_2bped has been investigated for its chelation properties with Ga(III) previously in the Orvig group and found to have moderate thermodynamic stability (log K_{ML} = 19.9).[130] A permutation of this system is H_2bpce (in this work referred to as H_2dedpa), where all donors are aligned in a linear manner (Figure 4.2).[131] This chelate has not been investigated previously for its coordination properties with Ga(III). An advantage of these acyclic systems is the simple synthesis. Extension of denticity or bite angle is easily achieved, as opposed to more sophisticated macrocyclic systems which have been widely explored and are assembled over many synthetic steps. Macrocyclic chelates are typically kinetically slow to bind, while acyclic chelates

coordinate fast. This is another key feature of successful chelate design for a short-lived radioisotope such as ^{68}Ga.[118]

4.3 Experimental

4.3.1 Materials and Methods

All solvents and reagents were from commercial sources and were used as received unless otherwise indicated. Human serum *apo*-transferrin was purchased from Sigma-Aldrich (St. Louis, MO). Refer to Chapter 2.2 for general information. The HPLC system used for analysis consisted of a Waters Alliance HT 2795 separation module equipped with a Raytest Gabbistar NaI detector and a Waters 996 photodiode array (PDA) detector. ^{67}Ga was obtained as a 0.1 M HCl solution, and ^{68}Ga (5-10 mCi/mL) (both from Nordion Inc.) was obtained from a generator constructed of titanium dioxide sorbent that was charged with ^{68}Ge and eluted with aqueous HCl (0.1 M).[132] The generator has been previously used for radiolabelling NOTA- and DOTA-based chelate systems and the resulting radiochemical yields and specific activities achievable for these chelates using this generator have been reported.[58]

4.3.2 General Synthesis Procedures

(i) Reductive amination: Two equivalents of the aldehyde were dissolved in CH_3OH (80 mL). The solution was heated to reflux and one equivalent of the corresponding diamine was added dropwise into the hot reaction solution and refluxing continued for 30 minutes. Subsequently, the reaction was filtered hot and cooled to 0°. $NaBH_4$ (1.2 eq) was slowly added into the solution. The mixture was then stirred for 2 h at 0°C and subsequently quenched with a saturated solution of $NaHCO_3$ and extracted three times with CH_2Cl_2.

(ii) Alkylation: One equivalent of diamine was dissolved in CH_3CN (100 mL). Two equivalents of *tert*-butyl bromoacetic acid were added dropwise into the solution, as well as 5-10 equivalents of Na_2CO_3. The white slurry was then stirred overnight at 70 °C. The reaction mixture was then cooled, filtered through a filter paper and the solvent was

removed *in vacuo* to afford the crude product as an oil, which was subsequently purified with column chromatography (silica, 10% CH_3OH in CH_2Cl_2).

(iii) Acid-catalyzed deprotection: The starting material was dissolved in a 1:1 mixture of CH_2Cl_2 and TFA (total volume 10 mL) and stirred until no more starting material was visible by TLC. The solvent of the reaction mixture was subsequently removed *in vacuo* to afford the product.

(iv) Base-catalyzed deprotection: The starting material was dissolved in a 3:1 mixture of THF and water (total volume 10 mL). LiOH (2-4 eq) was added and the reaction was monitored by TLC until no more starting material was detectable (30 min – 2 h). The solvent was removed *in vacuo* to afford the product as a Li^+ salt. In order to afford the HCl salt, 12 M HCl was added to the solid dissolved in minimal amount of water and the dihydrochloride salt was produced as a precipitate and collected by filtration.

4.3.3 Ligand Synthesis

6-Propylaminomethyl-di-pyridine-2-carboxylic acid methyl ester.

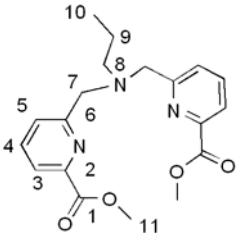

N-propylamine (7 mg, 10 µL, 0.119 mmol) was dissolved in CH_2Cl_2, together with 2 equivalents of 6-bromomethyl-pyridine-2-carboxylic acid methyl ester and 5 equivalents of Na_2CO_3. The mixture was stirred overnight and subsequently filtered. The solvent was removed *in vacuo* and the product was purified using column chromatography (silica, 20% CH_3OH in CH_2Cl_2) to afford the product as a yellow oil which crystallizes upon standing (27 mg, 0.08 mmol, yield 64 %). R_f = 0.72. ^{1}H NMR (400 MHz, $CDCl_3$, δ): 7.87 (m, *H3, H4,* 4H), 7.78 (d, $^3J_{4,5}$ = 5.2 Hz, *H5,* 2H), 3.87 (s, *H11,* 6H), 3.83 (s, *H7,* 4H), 2.43 (t, $^3J_{8,9}$ = 7.2 Hz, *H8,* 2H), 1.44 (qt, $^3J_{8,9}$ = 7.2 Hz, $^3J_{9,10}$ = 7.3 Hz, *H9,* 2H), 0.75 (t, $^3J_{9,10}$ = 7.3 Hz, *H10,* 3H). ^{13}C NMR (100 MHz, $CDCl_3$, δ): 165.8 (*C1*), 160.8 (*C6*), 147.2 (*C2*), 137.4 (*C4*), 124.4 (*C5*), 121.1 (*C3*), 60.4 (*C7*), 56.7 (*C8*), 52.8 (*C11*), 20.4 (*C9*), 11.8 (*C10*). (HR-ESI-MS calcd. for $C_{19}H_{23}N_3NaO_4$: 380.1586, found: 380.1589 $[M + Na]^+$.

6-Propylaminomethyl-di-pyridine-2-carboxylic acid.

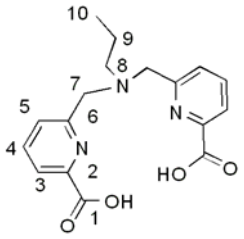

6-Propylaminomethyl-di-pyridine-2-carboxylic acid methyl ester was dissolved in a 3:1 mixture of THF and water, following procedure (iv) to afford the product quantitatively (83 mg, 0.25 mmol). ^{1}H NMR (300 MHz, CD_3OD, δ): 8.04 (d, $^{3}J_{3,4}$ = 7.5 Hz, *H3,* 2H), 7.9 (m, $^{3}J_{3,4}$ = 7.5 Hz, $^{3}J_{4,5}$ = 7.5 Hz, *H4,* 2H), 7.56 (d, $^{3}J_{4,5}$ = 7.5 Hz, *H5,* 2H), 3.83 (s, *H7,* 4H), 2.51 (t, $^{3}J_{8,9}$ = 7.6 Hz, *H8,* 2H), 1.63 (qt, $^{3}J_{8,9}$ = 7.6 Hz, $^{3}J_{9,10}$ = 7.2 Hz, *H9,* 2H), 0.93 (t, $^{3}J_{9,10}$ = 7.2 Hz, *H10,* 3H) ^{13}C NMR (75 MHz, CD_3OD, δ): 172.6 (*C1*), 156.7 (*C6*), 151.9 (*C2*), 137.5 (*C4*), 125.7 (*C5*), 121.6 (*C3*), 58.9 (*C7*), 56.9 (*C8*), 18.4 (*C9*). 10.6 (*C10*). IR (neat, cm^{-1}): 1620 (m), 1586 (s), 1397 (m). HR-ESI-MS calcd. for $C_{17}H_{17}LiN_3O_4$: 334.1379, found: 334.1378 $[M + Li]^+$.

N-N'-Bis(2-pyridylmethyl)ethylenediamine-N-N'-diacetic acid (H_2bped).

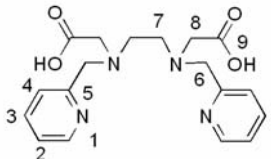

Using the original reference,[130] the compound was synthesized affording the reported compound. ^{1}H NMR (300 MHz, CD_3OD, δ): 8.73 (d, $^{3}J_{1,2}$ = 5.5 Hz, *H1,* 2H), 8.36 (m, $^{3}J_{3,4}$ = 7.5 Hz, $^{3}J_{3,4}$ = 8.2 Hz, *H3,* 2H), 7.96 (d, $^{3}J_{3,4}$ = 8.2 Hz, *H4,* 2H), 7.82 (m, 3.83 $^{3}J_{1,2}$ = 5.5 Hz, *H2,* 2H), 4.58 (s, *H6,* 4H), 3.91 (s, *H8,* 4H), 3.45 (s, *H7,* 4H). ^{13}C NMR (75 MHz, CD_3OD, δ): 171.7 (*C9*), 151.0 (*C5*), 147.3 (*C1*), 144.5 (*C4*), 129.5 (*C2*), 128.1 (*C3*), 56.4 (*C8*), 55.2 (*C6*), 52.9 (*C7*). IR (neat, cm^{-1}): 1719 (s), 1633 (m), 1408 (m). HR-ESI-MS calcd. for $C_{18}H_{22}NaN_4O_4$: 381.1539, found: 381.1532 $[M + Na]^+$.

N-N'-Bis(2-pyridylmethyl)propylenediamine-N-N'-diacetic acid *tert*-butyl ester.

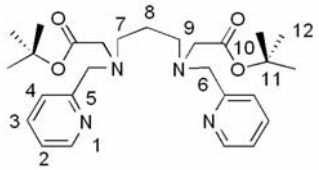

Using methods (i) and (ii) in sequence, the title compound was afforded from 1,3-diaminopropane, 2-pyridinecarboxaldehyde and tert-butyl bromoacetate after column chromatography (20 mg, 0.041 mmol, yield 12 %). ^{1}H NMR (300 MHz, $CDCl_3$, δ): 8.38 (d, $^{3}J_{1,2}$ = 4.8 Hz, *H1,* 2H), 7.49 (m, $^{3}J_{3,4}$ = 7.8 Hz, *H3,* 2H), 7.25 (d, $^{3}J_{3,4}$ = 7.8 Hz, *H4,* 2H), 7.00 (m, $^{3}J_{1,2}$ = 4.8 Hz, *H2,* 2H), 3.76 (s, *H6,* 4H), 3.14 (s, *H9,* 4H), 2.57 (t, $^{3}J_{7,8}$ = 7.2 Hz, *H7,* 4H), 1.57 (quin, $^{3}J_{7,8}$ = 7.2 Hz, *H8,* 2H),

1.32 (s, *H12,* 18H). ^{13}C NMR (75 MHz, $CDCl_3$, δ): 170.3 (*C10*), 159.6 (*C5*), 148.6 (*C1*), 136.1 (*C3*), 122.6 (*C2*), 121.6 (*C4*), 80.42 (*C11*), 59.9 (*C6*), 55.6 (*C7*), 51.83 (*C9*), 27.9 (*C12*), 25.5 (*C8*). HR-ESI-MS calcd. for $C_{27}H_{41}N_4O_4$: 485.3128, found: 485.3131 $[M + H]^+$.

N-N'-Bis(2-pyridylmethyl)propylenediamine-N-N'-diacetic acid.

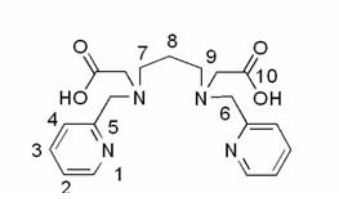

Using method (iii), the title compound was afforded quantitatively from N-N'-bis(2-pyridylmethyl) propylenediamine-N-N'-diacetic acid *tert*-butyl ester (13 mg, 0.035 mmol). ^{1}H NMR (300 MHz, CD_3OD, δ): 8.70 (d, $^3J_{1,2}$ = 5.3 Hz, *H1,* 2H), 8.21 (m, $^3J_{3,4}$ = 7.9 Hz, *H3,* 2H), 7.76 (d, $^3J_{3,4}$ = 7.9 Hz, *H4,* 2H), 7.71 (m, $^3J_{1,2}$ = 5.3 Hz, *H2,* 2H), 4.48 (s, *H6,* 4H), 3.92 (s, *H9,* 4H), 3.15 (t, $^3J_{7,8}$ = 7.5 Hz, *H7,* 4H), 2.02 (quin, $^3J_{7,8}$ = 7.5 Hz, *H8,* 2H). ^{13}C NMR (75 MHz, CD_3OD, δ): 170.2 (*C10*), 152.5 (*C5*), 145.8 (*C1*), 141.7 (*C4*), 125.4 (*C2*), 124.9 (*C3*), 56.7 (*C9*), 54.2 (*C6*), 52.8 (*C7*) 21.8 (*C8*). IR (neat, cm^{-1}): 1674 (s), 1434 (w), 1202 (s). HR-ESI-MS calcd. for $C_{19}H_{25}N_4O_4$: 373.1876, found: 373.1877 $[M + H]^+$.

1,2-[{6-(Carboxylato)pyridin-2-yl}methylamino]ethane (H_2dedpa).

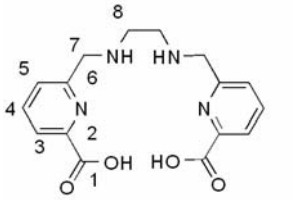

Protected precursor 1,2-[{6-(methoxycarbonyl)pyridin-2-yl} methylamino]ethane was synthesized according to the literature.[108] Deprotection of the precursor was achieved using method (iv) to afford the product as a white solid (24 mg, 0.059 mmol, yield 59 %). ^{1}H NMR (d_6-DMSO, 300 MHz): 8.12-8.09 (m, $^3J_{4,5}$ = 6.8 Hz, $^4J_{3,5}$ = 1.8 Hz, *H3, H4*, 4H), 7.78 (dd, $^3J_{4,5}$ = 6.8 Hz, $^4J_{3,5}$ = 1.8 Hz, *H5*, 2H), 4.52 (s, *H7* ,2H), 3.51 (d, *H8*, 2H). ^{13}C NMR (d_6-DMSO, 150 MHz, δ): 166.1 (*C1*), 153.5 (*C6*), 148.1 (*C2*), 139.7 (*C4*), 127.2 (*C5*), 124.9 (*C3*), 50.7 (*C7*), 43.8 (*C8*). IR (neat, cm^{-1}): 1761 (s), 1749 (s), 1599 (m). HR-ESI-MS calcd. for $C_{16}H_{19}N_4O_4$: 331.1406, found: 331.1329 $[M + H]^+$. Elemental analysis: calcd. (found) for H_2dedpa·2HCl: C 47.65 (47.30), H 5.00 (5.11), N 13.81 (13.38).

1,2-[{6-(Methoxycarbonyl)pyridin-2-yl}methylamino]propane.

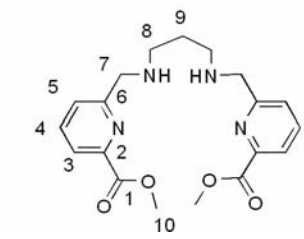

The product was synthesized using method (i) using 6-formyl-pyridine-2-carboxylic acid methyl ester and 1,3-diaminopropane. The procedure afforded the product as a colourless oil (69 mg, 0.18 mmol, yield 17 %). ^{1}H NMR (300 MHz, $CDCl_3$, δ): 7.98 (m, $^{3}J_{3,4}$ = 8.2 Hz, *H3*, 2H), 7.78 (m, $^{3}J_{4,5}$ = 7.6 Hz, $^{3}J_{3,4}$ = 8.2 Hz, *H4*, 2H), 7.55 (d, $^{3}J_{4,5}$ = 7.6 Hz, *H5*, 2H), 3.96 (s, *H7*, 4H), 3.94 (s, *H10*, 6H), 2.75 (t, $^{3}J_{8,9}$ = 6.8 Hz, *H8,* 4H), 2.02 (quin, $^{3}J_{8,9}$ = 6.8, *H9,* 2H). ^{13}C NMR (75 MHz, $CDCl_3$, δ) δ: 161.2 (*C1*), 160.5 (*C6*), 148.0 (*C2*), 137.9 (*C4*), 126.2 (*C5*), 124.0 (*C3*), 55.73 (*C10*), 53.4 (*C7*), 48.6 (*C8*), 29.8 (*C9*). HR-ESI-MS calcd. for $C_{19}H_{24}NaN_4O_4$: 395.1695, found: 395.1699 [M + Na]$^{+}$.

1,2-[{6-(Carboxylato)pyridin-2-yl}methylamino]propane.

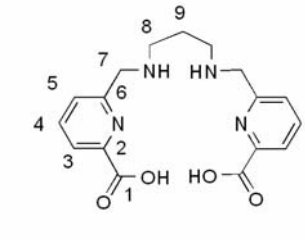

Using method (iv), the title compound was afforded quantitatively from 1,2-[{6-(Methoxycarbonyl)pyridin-2-yl}methylamino]propane after deprotection (62 mg, 0.18 mmol). ^{1}H NMR (300 MHz, CD_3OD, δ): 7.92 (m, $^{3}J_{3,4}$ = 8.2 Hz, *H3, H4*, 4H), 7.51 (m, $^{3}J_{4,5}$ = 7.4 Hz, $^{4}J_{3,5}$ = 1.5 Hz, *H5*, 2H), 3.88 (s, *H7*, 4H), 2.61 (t, $^{3}J_{7,8}$ = 6.9 Hz, *H8,* 4H), 1.75 (quin, $^{3}J_{8,9}$ = 6.9, *H9,* 2H). ^{13}C NMR (125 MHz, CD_3OD, δ): 170.7 (*C1*), 159.5 (*C6*), 152.8 (*C2*), 137.1 (*C4*), 121.8 (*C5*), 121.7 (*C3*), 63.3 (*C7*), 53.1 (*C8*), 27.3 (*C9*). IR (neat, cm^{-1}): 1614 (m), 1433 (m), 1383 (m). HR-ESI-MS calcd. for $C_{17}H_{20}LiN_4O_4$: 351.1645, found: 351.1637 [M + Li]$^{+}$.

N,N'-Bis(6-carboxy-2-pyridylmethyl)ethylenediamine-N,N'-diacetic acid

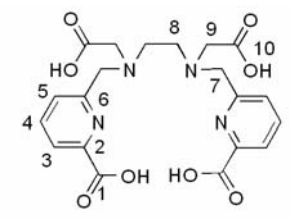

Using the original reference,[108] the desired compound was synthesized. ^{1}H NMR (300 MHz, CD_3OD, δ): 8.12 (d, $^{3}J_{3,4}$ = 7.8 Hz, *H3,* 2H), 7.97 (m, $^{3}J_{3,4}$ = 7.8 Hz, $^{3}J_{4,5}$ = 7.5 Hz, *H4*, 2H), 7.78 (d, $^{3}J_{4,5}$ = 7.5 Hz, *H5*, 2H), 4.7 (s, *H8,* 4H), 4.10 (s, *H7,* 4H), 3.68 (s,

H9, 4H). HR-ESI-MS calcd. for $C_{20}H_{23}N_4O_8$: 447.1516, found: 447.1511 $[M + H]^+$.

N,N'-Bis(6-carboxy-2-pyridylmethyl)propylenediamine-N,N'-diacetic acid *tert*-butyl ester

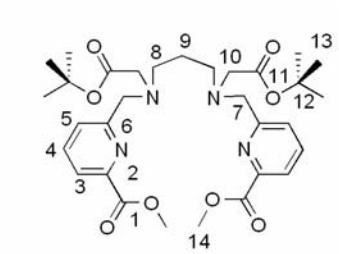

1,2-[{6-(Methoxycarbonyl)pyridin-2-yl} methylamino]propane was alkylated using method (ii) to afford the product after column chromatography (24 mg, 0.04 mmol, yield 8 %). ^{1}H NMR (300 MHz, $CDCl_3$, δ): 7.98 (m, *H4*, 2H), 7.76 (m, *H3, H5*, 4H), 3.99 (s, *H14,* 6H), 3.97 (s, *H7,* 4H), 3.25 (s, *H10,* 4H), 2.67 (t, $^3J_{8,9}$ = 7.2 Hz, *H8,* 4H), 2.02 (quin, $^3J_{8,9}$ = 7.2, *H9,* 2H), 1.44 (s, *H13*, 18H). HR-ESI-MS calcd. for $C_{31}H_{44}N_4NaO_8$: 623.3057, found: 623.3057 $[M + Na]^+$.

N,N'-Bis(6-carboxy-2-pyridylmethyl)propylenediamine-N,N'-diacetic acid

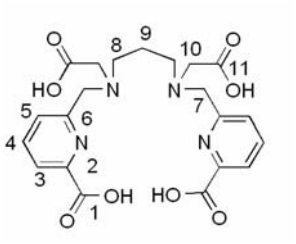

The product was afforded from 1,3-propylenediamine and methyl 6-formylpyridine-2-carboxylate using methods (iii) and (iv) sequentially (11 mg, 0.023 mmol, yield 57 %). ^{1}H NMR (300 MHz, CD_3OD, δ): 8.17 (d, $^3J_{3,4}$ = 7.2 Hz, *H3,* 2H), 8.08 (m, $^3J_{3,4}$ = 7.2 Hz, $^3J_{4,5}$ = 7.8 Hz, *H4*, 2H), 7.72 (d, $^3J_{4,5}$ = 7.56 Hz, *H5*, 2H), 4.78 (s, *H10,* 4H), 4.27 (s, *H7,* 4H), 3.55 (t, $^3J_{8,9}$ = 7.2 Hz, *H8,* 4H), 2.43 (quin, $^3J_{8,9}$ = 7.2, *H9,* 2H). ^{13}C NMR (125 MHz, CD_3OD, δ): 178.2 (*C11*), 171.0 (*C1*), 157.5 (*C6*), 152.7 (*C2*), 137.8 (*C4*), 123.3 (*C5*), 121.1 (*C3*), 69.3 (*C10*), 58.9 (*C7*), 52.5 (*C8*), 25.7 (*C9*). IR (cm^{-1}): 1679 (w), 1417 (s). HR-ESI-MS calcd. for $C_{21}H_{25}N_4O_8$: 461.1672, found: 461.1662 $[M + H]^+$.

(1,2-[N,N'-{*p*-Nitrobenzyl}methyl]-N,N'-[6-{methoxycarbonyl}-pyridin-2-yl] methylamino)ethane (Me_2dp-N-NO_2).

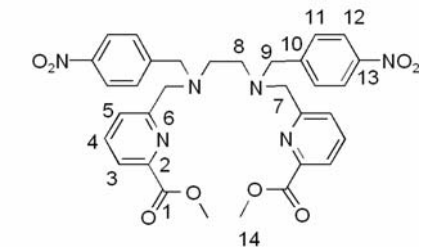

N,N'-[6-{Methoxycarbonyl}-pyridin-2-yl]methyl amino)ethane was synthesized according to the literature.[108] 4-Nitrobenzyl bromide (135 mg, 0.625 mmol) was dissolved in 20 mL acetonitrile together with 1,2-[{6-(methoxycarbonyl)pyridin-2-yl}methyl amino] ethane (105 mg, 0.293 mmol). Na_2CO_3 (400 mg) was added into the solution and the reaction

was stirred overnight at 70 °C. Subsequently, the suspension was filtered and the solvent removed *in vacuo*. The resulting orange oil was purified by column chromatography (silica, CH_2Cl_2); the product was eluted with 5% CH_3OH, and isolated as an orange oil (60 mg, 0.095 mmol, 33%, R_f: 0.6). ^{1}H NMR (300 MHz, $CDCl_3$, δ): 8.01 (d, $^3J_{11,\ 12}$ = 8.9 Hz, *H11*, 4H), 7.98 (d, $^3J_{3,\ 4}$ = 7.7 Hz, *H3*, 2H), 7.76 (m, $^3J_{3,\ 4}$ = 7.7 Hz, , $^3J_{4,\ 5}$ = 7.8 Hz, *H4*, 2H), 7.59 (d, $^3J_{4,\ 5}$ = 7.8 Hz, *H5*, 2H), 7.46 (d, $^3J_{11,\ 12}$ = 8.9 Hz, *H12*, 4H), 4.98 (s, *H14*, 6H) 3.83 (s, *H7*, 4H), 3.69 (s, *H9*, 4H), 2.71 (s, *H8*, 4H). ^{13}C NMR (75 MHz, $CDCl_3$, δ): 165.8 (*C1*), 160.1 (*C6*), 147.6 (*C2*), 147.3 (*C13*), 137.6 (*C10*), 129.3 (*C4*), 125.9 (*C5*), 123.8 (*C3*), 123.7 (*C11*), 60.6 (*C7*), 58.7 (*C9*), 53.1 (*C14*), 52.3 (*C8*). IR (neat, cm^{-1}): 1734 (s), 1515 (s), 1342 (s). HR-ESI-MS calcd. for $C_{32}H_{32}NaN_6O_8$: 651.2179, found: 651.2289 $[M + Na]^+$.

(1,2-[N,N'-{*p*-Nitrobenzyl}methyl]-N,N'bis-[6-carboxy-2-pyridylmethyl] ethylene diamine (H_2dp-N-NO_2).

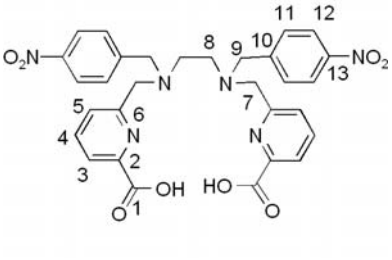

The starting material (**14**, 27 mg, 0.042 mmol) was dissolved in 4 mL of a 3:1 mixture of THF and water. LiOH (5 mg, 0.21 mmol) was added to the solution resulting in an immediate colour change of the solution. The reaction was monitored by TLC and found to be complete after 45 min. The solvent was removed *in vacuo* to afford a white solid (25 mg, 0.041 mmol, 97%). ^{1}H NMR (400 MHz, CD_3OD, δ): 8.12 (d, $^3J_{3,\ 4}$ = 8.7 Hz, *H3*, 2H), 8.10 (d, $^3J_{4,\ 5}$ = 7.8 Hz, *H5*, 2H), 7.91 (t, $^3J_{3,\ 4}$ = 8.7 Hz, $^3J_{4,\ 5}$ = 7.8 Hz, *H4*, 2H), 7.42 (d, $^3J_{11,\ 12}$ = 7.8 Hz, *H11*, 4H), 7.36 (d, $^3J_{11,\ 12}$ = 7.8 Hz, *H12*, 4H), 3.88 (s, *H7*, 4H), 3.56 (s, *H9*, 4H), 2.41 (s, *H8*, 4H). ^{13}C NMR (100 MHz, CD_3OD, δ): 172.5 (*C1*), 159.2 (*C6*), 155.0 (*C2*), 148.78 (*C13*), 145.0 (*C10*), 139.9 (*C4*), 132.2 (*C5*), 125.9 (*C3*), 124.4 (*C11*), 123.4 (*C12*), 61.0 (*C7*), 57.6 (*C9*), 31.1 (*C8*). IR (neat, cm^{-1}): 1621 (w), 1512 (s), 1345 (s). HR-ESI-MS calcd. for $C_{30}H_{27}N_6O_8$: 599.1890, found: 599.1887 $[M - H]^-$.

2-(*p*-Nitrobenzyl)-N,N'-[6-{methoxycarbonyl}-pyridin-2-yl]methylamino)ethane (Me_2dp-bb-NO_2).

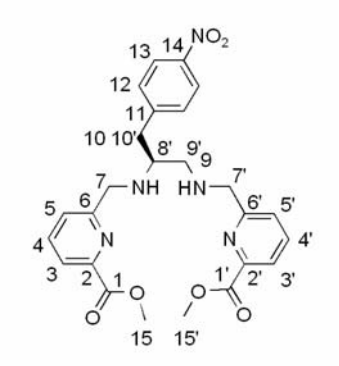

3-(4-Nitrophenyl)-propane-1,2-diaminemethane and 6-formyl-pyridine-2-carboxylic acid methyl ester were synthesized according to the literature.[108,133] To a mixture of 3-(4-nitrophenyl)-propane-1,2-diaminemethane (0.46 g, 2.36 mmol) in methanol (50 mL), 6-formyl-pyridine-2-carboxylic acid methyl ester (0.78 g, 4.72 mmol) was added. The mixture was refluxed for 2 h and then cooled to 0 °C in an ice bath. After cooling, $NaBH_4$ (0.139 g, 3.67 mmol) was added slowly and stirred at 0 °C for 2 h. Saturated aqueous $NaHCO_3$ was then added (150 mL) and the mixture stirred for 15 min, followed by extraction with dichloromethane (5 x 80 mL). The combined dichloromethane fractions were dried over $MgSO_4$ and evaporated to give 0.96 g of crude yellow oil. Subsequent purification of a 50 mg aliquot with column chromatography (10% CH_3OH in dichloromethane) afforded the product as a colourless oil (5 mg, 0.012 mmol, 8%, R_f: 0.05). ^{1}H NMR (300 MHz, $CDCl_3$, δ): 8.12 (d, $^3J_{11,\ 12}$ = 8.0 Hz, *H12*, 2H), 7.99 (m, *H3*, *H3'*, 2H), 7.78 (m, *H4, H4'*, 2H), 7.54 (m, *H5, H5'*, 2H), 7.35 (d, $^3J_{11,\ 12}$ = 8.0 Hz, *H13*, 2H), 4.06 – 4.03 (m, *H7, H7'*, 4H), 3.97 (s, *H15, H15'*, 6H), 3.04 (m, *H8'*,1H), 2.97 (m, *H9, H9'*, 2H), 2.60 (m, $^2J_{10,\ 10'}$ = 12.0 Hz, *H10, H10'*, 2H). ^{13}C NMR (75 MHz, $CDCl_3$, δ): 165.9 (*C1, C1'*), 160.8 (*C6, C6'*), 147.7 (*C2, C2'*), 147.6 (*C14*), 147.4 (*C4, C4'*), 146.8 (*C5, C5'*), 137.7 (*C11*), 130.4 (*C3, C3'*), 125.9 (*C12*), 123.8 (*C13*), 58.5 (*C7, C7'*), 53.1 (*C15, C15'*), 52.6 (*C8*), 52.1 (*C9*), 39.6 (*C10*). HR-ESI-MS calcd. for $C_{25}H_{28}N_5O_6$: 494.2040, found 494.2049 $[M + H]^+$.

2-(*p*-Nitrobenzyl)-(1,2-[N,N'-{*p*-nitrobenzyl}methyl]-N,N'bis-[6-carboxy-2-pyridyl methyl] ethylenediamine (H_2dp-bb-NO_2).

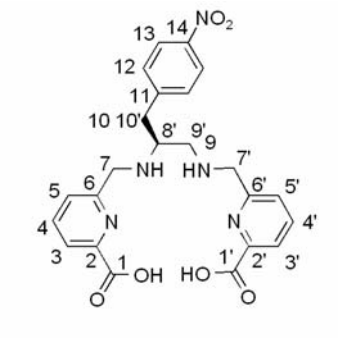

2-(*p*-Nitrobenzyl)-N,N'-[6-{methoxycarbonyl}-pyridin-2-yl] methylamino)ethane (5 mg, 0.012 mmol) was dissolved in 2 mL of a 3:1 mixture of THF and water. LiOH (1 mg, 0.04 mmol) was added into the solution. The reaction was monitored by TLC and found to be complete after 30 minutes. The solvent was removed *in vacuo* to afford a light yellow solid (4 mg, 0.01 mmol, 83%). ^{1}H NMR (400 MHz, CD_3OD, δ): 8.15 (d, $^3J_{12,\ 13}$ = 8.0 Hz, *H13*, 2H), 7.99 (d, $^3J_{3,\ 4}$ = 7.9, *H3, H3'*, 2H), 7.88 (m $^3J_{3,\ 4}$ = 7.9, *H4, H4'*, 2H), 7.41 (m, *H12, H5, H5'*,4H), 4.12 - 3.91 (m, $^2J_{7,\ 7}$ = 16.0, *H7, H7'*, 4H), 2.75 - 2.17 (m, *H8', H9, H9', H10, H10'*, 5H). ^{13}C NMR (100 MHz, CD_3OD, δ): 165.0 (*C1, C1'*), 160.2 (*C6, C6'*), 155.2 (*C2, C2'*), 149.0 (*C4, C4'*), 148.1 (*C14*), 139.5 (*C5, C5'*), 131.6 (*C11*), 125.6 (*C3, C3'*), 124.6 (*C12*), 123.4 (*C13*), 59.5 (*C7, C7'*), 51.9(*C9*), 39.9 (*C8*), 39.7 (*C10*). HR-ESI-MS calcd. for $C_{23}H_{22}N_5O_6$: 464.1570; found: 464.1581 $[M - H]^-$.

4.3.4 Coordination Chemistry with Ga

1,2-[{6-(Carboxylato-)pyridin-2-yl}methylamino]ethane gallium(III) perchlorate ([Ga(dedpa)][ClO_4]).

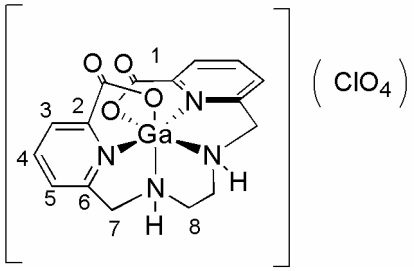

H_2**dedpa**·2HCl (21 mg, 0.052 mmol) was dissolved in a CH_3OH-water mixture (1:2, total volume 5 mL). $Ga(ClO_4)_3$·$6H_2O$ (24 mg, 0.052 mmol) was added and the pH was adjusted to 4.5 by addition of 0.1 M NaOH. The reaction mixture was heated for 30 minutes and then set aside in the fumehood for slow evaporation. After 72 h, rhombic colorless crystals suitable for X-ray diffraction had precipitated in quantitative yield. ^{1}H NMR (300 MHz, d_6-DMSO, δ): 8.59 (d, $^3J_{4,\ 5}$ = 7.6 Hz, *H5*, 2H), 8.29 (d, $^3J_{3,\ 4}$ = $^3J_{4,\ 5}$ = 7.6 Hz, *H4*, 2H), 8.09 (d, $^3J_{3,\ 4}$ = 7.6 Hz, *H3*, 2H), 4.60-4.32 (dd, $^2J_{7,\ 7'}$ = 17.4 Hz, *H7, H7'*, 4H), 3.06 (dd, $^2J_{8,\ 8'}$ = 10.0 Hz, *H8*, 2H), 2.4 (dd, $^2J_{8,\ 8'}$ = 10.0 Hz, *H8'*, 2H). ^{13}C NMR (75

MHz, d_6-DMSO, δ): 162.0 (*C1*), 150.4 (*C6*), 145.2 (*C4*), 144.1 (*C2*), 126.5 (*C5*), 122.0 (*C3*), 48.2 (*C7*), 46.0 (*C8*). IR (neat, cm^{-1}): 1695, 1664, 1606. HR-ESI-MS calc. for $C_{16}H_{16}{}^{69}GaN_4O_4$: 397.0427, found: 397.0431 $[M]^+$.

(1,2-[N,N'-{*p*-Nitrobenzyl}methyl]-N,N'bis-[6-carboxy-2-pyridylmethyl]ethylene diamine gallium(III) nitrate ([Ga(dp-N-NO_2)][NO_3]).

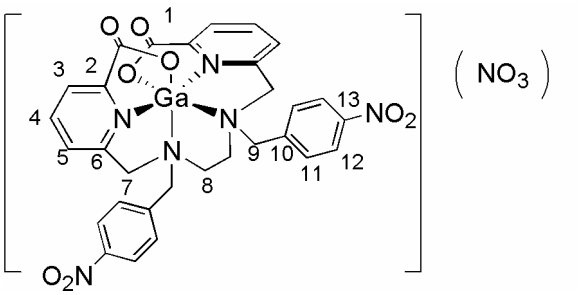

H_2dp-N-NO_2 (7 mg, 0.011 mmol) was dissolved in a CH_3OH-water mixture (1:2, total volume 2 mL). $Ga(NO_3)_3 \cdot 6H_2O$ (4 mg, 0.011 mmol) was added and the pH was adjusted to 4.5 by addition of 0.1 M NaOH. The reaction mixture was stirred at 60 °C for 2 h. The solvent was removed *in vacuo* to afford a white solid in quantitative yield. The solid was redissolved in a mixture of water and methanol (1:2). Colourless plates suitable for X-ray diffraction were obtained by slow evaporation of the solvent mixture. ^{1}H NMR (400 MHz, CD_3OD, δ): 8.71 (m, $^3J_{3,4}$ = 7.6 Hz, $^3J_{4,5}$ = 7.9 Hz, *H4*, 2H), 8.49 (d, $^3J_{3,4}$ = 7.6 Hz, *H3*, 2H), 8.32 (d, $^3J_{11,12}$ = 8.5 Hz, *H11*, 2H), 8.18 (d, $^3J_{4,5}$ = 7.9 Hz, *H5*, 2H), 7.72 (d, $^3J_{11,12}$ = 8.5 Hz, *H12*, 2H), 5.03-4.34 (dd, $^2J_{7,7'}$ = 16.8 Hz, *H7, H7'*, 4H), 4.18-3.87 (dd, $^2J_{8,8'}$ = 17.4 Hz, *H8, H8*, 4H), 3.13 (dd, $^2J_{7,7'}$ = 17.4 Hz, *H9 H9',* 4H). ^{13}C NMR (150 MHz, CD_3OD, δ): 165.1 (*C1*), 152.0 (*C6*), 150.3 (*C4*), 148.3 (*C13*), 145.7 (*C10*), 138.1 (*C2*), 134.5 (*C5*), 129.8 (*C11*), 125.6 (*C3*), 124.8 (*C12*), 57.7 (*C7*), 55.4 (*C9*), 48.1 (*C8*). IR (neat, cm^{-1}): 1607 (w), 1519 (s), 1346 (s). HR-ESI-MS calcd. for $C_{30}H_{26}N_6O_8{}^{69}Ga$: 667.1068, found: 667.1075 $[M]^+$.

2-(*p*-Nitrobenzyl)-(1,2-[N,N'-{*p*-nitrobenzyl}methyl]-N,N'bis-[6-carboxy-2-pyridyl methyl] ethylenediamine gallium(III) nitrate ([Ga(dp-bb-NO_2)][NO_3]).

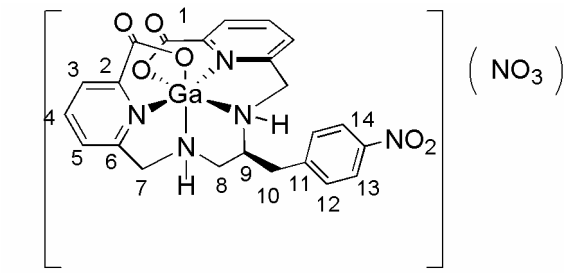

H_2dp-bb-NO_2 (2.5 mg, 5.3 μmol) was dissolved in water (1 mL). $Ga(NO_3)_3 \cdot 6H_2O$ (2 mg, 5.5 μmol, in 0.5 mL water) was added and the pH was adjusted to 5 by addition of 0.1 M NaOH. The reaction mixture was stirred at 60 °C for 2 h. The solvent was removed *in vacuo* to afford an off-white solid in quantitative yield. ^{1}H NMR (300 MHz, CD_3OD, δ): 8.62 (m, $^3J_{3,4}$ = 7.5 Hz, *H3*, 2H), 8.36 (d, $^3J_{12,13}$ = 8.7 Hz, *H12*, 2H), 8.20 - 8.09 (d, $^3J_{3,4}$ = 7.5 Hz, *H4, H5*, 4H), 7.53 (d, $^3J_{12,13}$ = 8.7 Hz, *H13*, 2H), 4.81 - 4.39 (dd, $^2J_{7,7'}$ = 17.4/ 16.8 Hz, *H7, H7'*, 4H), 3.59 - 2.21 (m, $^2J_{8,8'}$ = 12.3 Hz, , $^3J_{8,9}$ = 3 Hz, *H8, H8', H9, H10, H10'*, 5H). ^{13}C NMR (150 MHz, CD_3OD, δ): 165.5 (*C1*), 165.4 (*C1'*), 152.1 (*C6*), 151.6 (*C6'*), 148.8 (*C14*), 147.4 (*C4*), 147.3 (*C4'*), 146.1 (*C10*), 145.9 (*C2*), 145.3 (*C2'*), 131.8 (*C5*), 129.1 (*C5'*), 129.0 (*C13*), 125.1 (*C3*), 124.7 (*C3'*), 124.6 (*C12*), 58.9 (*C7, C7'*), 53.7 (*C9*), 51.5 (*C8*), 37.6 (*C10*). HR-ESI-MS calcd. for $C_{23}H_{21}{}^{69}GaN_5O_6$: 532.0748, found: 532.0743 $[M]^+$.

4.3.5 Labelling with $^{67/68}$Ga

$^{67}GaCl_3$ (100 μL, 1 mCi) or $^{68}Ga^{3+}$(100 μL, 1 mCi) in a 0.1 M HCl solution was added to 900 μL of a 10^{-4} M solution of ligand in 10 mM NaOAc solution (pH 4.5) and left for 10 minutes at RT. The reaction progress was monitored by analytical HPLC to evaluate yield of the coordination reaction. [$^{67/68}$Ga(**dedpa**)]$^+$: t_R on HPLC: 6.1 minutes (gradient: A: 10 mM NaOAc buffer, pH 4.5, B: CH_3OH. 0-5% B linear gradient 20 min). Ligand concentrations of up to 10^{-7} M are capable of coordinating the radionuclide to above 96% (under the same labeling conditions, 10 min, room temperature). The high specific activity of 9.8 mCi/nmol was achieved with 900 μL of a 10^{-7} M solution of H_2**dedpa** in 10 mM NaOAc solution (pH 4.5) and 100 μL of $^{68}Ga^{3+}$ in a 0.1 M HCl solution (0.98 mCi) under standard labelling conditions (10 min, room temperature). Analysis of radiolabelled complexes was done using reversed phase HPLC, on a Phenomenex Hydrosynergy RP C18 4.6 × 150 mm analytical

column ([Ga(**dedpa**)]$^+$), Phenomenex Jupiter 5u C18 300 A 4.6 × 100 mm analytical column (transferrin challenge with [Ga(**dedpa**)]$^+$, NOTA versus H_2**dedpa** challenge, H_2dedpa challenge of Ga(NOTA), retention time of ^{67}Ga-Tf: 10.7 min) and Waters XBridge BEH130 4.6 × 150 mm ([Ga(**dp-bb-NO$_2$**)]$^+$, [Ga(**dp-N-NO$_2$**)]$^+$, as well as the transferrin challenges thereof, retention time of ^{67}Ga-Tf: 2.5 min).

R_t of [$^{67/68}$Ga(**dedpa**)]$^+$ on HPLC: 5.5 minutes (gradient: A: NaOAc buffer, pH 4.5, B: CH_3OH. 0-5 % B linear gradient 20 min). Stability versus transferrin (10 min/1 h/ 2 h; in % complex intact): 99/ 99/ 99.

R_t of [$^{67/68}$Ga(**dp-N-NO$_2$**)]$^+$ on HPLC: 10.8 minutes (gradient: A: NaOAc buffer, pH 4.5, B: CH_3OH. 0-100 % B linear gradient 20 min). Stability versus transferrin (10 min/1 h/ 2 h; in % complex intact): 88/ 69/ 51.

R_t of [$^{67/68}$Ga(**dp-bb-NO$_2$**)]$^+$ on HPLC: 7.7 minutes (gradient: A: NaOAc buffer, pH 4.5, B: CH_3OH. 0-100 % B linear gradient 20 min). Stability versus transferrin (10 min/1 h/ 2 h; in % complex intact): 98/ 97/ 97.

4.3.6 *In Vitro* Stability: Transferrin Challenge and Challenge against NOTA

Analysis of radiolabelled complexes Both the NOTA versus H_2**dedpa** challenge, H_2**dedpa** challenge of Ga(NOTA), retention time of ^{67}Ga-Tf: 10.7 min) and ([Ga(**dp-bb-NO$_2$**)]$^+$, [Ga(**dp-N-NO$_2$**)]$^+$, as well as the transferrin challenges thereof, retention time of ^{67}Ga-Tf: 2.5 min) were done using reversed phase HPLC, using a Waters XBridge BEH130 4.6 × 150 mm analytical column.

For *apo*-transferrin competition, $^{67}GaCl_3$ was added to a 10^{-4} M solution of ligand in 10 mM NaOAc solution (pH 4.5). Complex formation was checked by HPLC. A 400 µL aliquot was added to 1 mg/mL *apo*-transferrin in a $NaHCO_3$ solution (10 mM, 600 µL) and incubated at 37° C (water bath). Complex stability was checked at time points 10 minutes, 1 h and 2 h via analytical HPLC.

$^{67}GaCl_3$ was added to 10^{-4} M solution of both NOTA and H_2dedpa in 10 mM NaOAc solution (pH 4.5). After a reaction time of 10 minutes at room temperature the reaction

mixture was checked for the formed complex by analytical HPLC. Over 98% of the ^{67}Ga-dedpa complex was detected opposed to 0.2 % Ga-NOTA.

4.3.7 X-Ray Diffraction Structural Characterization of [Ga(dedpa)][ClO_4] and [Ga(dp-N-NO_2)] [ClO_4]

Data for compound [Ga(**dedpa**)][ClO_4] were collected with graphite-monochromated Mo-Kα radiation (0.71073 Å) at -17˚C on a Bruker X8 APEX II diffractometer. The structure was solved using direct methods using SIR-97[134] and refined using SHELXL-97.[135] All non-hydrogen atoms were refined anisotropically. All N-H hydrogen atoms were located in a difference map and refined isotropically. All other hydrogen atoms were placed in calculated positions and refined using a riding model. Data for compound [Ga(**dp-N-NO_2**)][ClO_4] were collected with graphite-monochromated Mo- Kα radiation at -183˚C on a Bruker APEX DUO diffractometer. The structure was solved using direct methods using SIR-97[134] and refined using SHELXL-97.[135] The material crystallizes with two crystallographically independent moieties in the asymmetric unit. One perchlorate anion is disordered and was modeled in two orientations, with restraints used to maintain reasonable geometries. Finally, CH_3OH solvent was found in the lattice. Two molecules of solvent were located and modeled, however one region within the asymmetric unit had residual electron density that could not be properly modeled. The SQUEEZE[136] program was used to generate a data set free of residual electron density in that region. All non-hydrogen atoms were refined anisotropically. All hydrogen atoms were placed in calculated positions and refined using a riding model. The collection and analysis of the data was done by Dr. Brian O. Patrick.

4.3.8 Biodistribution of [^{67}Ga (dedpa)]$^+$, [^{67}Ga(dp-bb-NO_2)]$^+$ and [^{67}Ga(dp-N-NO_2)]$^+$

The protocol used for the animal studies was approved by the Institutional Animal Care Committee of the University of British Columbia and was performed in accordance with the Canadian Council on Animal Care Guidelines. A total of 16 female ICR (20-30 g)

mice were used for the animal study of each of the three compounds. [^{67}Ga(**dedpa**)]$^{+}$, [^{67}Ga(**dp-bb-NO$_2$**)]$^{+}$ and [^{67}Ga(**dp-N-NO$_2$**)]$^{+}$ were each prepared as described above and then diluted in phosphate buffered saline to a concentration of 100 μCi/mL. Each mouse was i.v. injected with ~10 μCi (100 μL) of the ^{67}Ga complex and then sacrificed by CO_2 inhalation at 30 min, 1 h, 2 h, or 4 h after injection (n=4 at each time point). Blood was collected by cardiac puncture and plasma was separated from whole blood by centrifuging (2500 rpm, 15 min). Urine was collected from the bladder. Tissues collected included kidney, liver, spleen, femur, muscle, heart, lung, intestine and brain. Tissues were weighed and counted on a gamma counter and the counts were converted to % injected dose/gram (%ID/g). The collection of the data was done by Dr. Dawn Waterhouse.

4.4 Results and Discussion

4.4.1 Ligand Synthesis

In order to find a novel chelate for fast, clean and mild labelling with the radioisotope ^{68}Ga, a library of chelates with the same set of donor atoms was first established. The compounds outlined in this chapter have denticities reaching from tetradentate to octadentate, while bearing permutations of pyridyl, aliphatic amino- and carboxylato donor atoms. Bridging units can be varied in a simple manner and reach from no bridging unit to three carbon bridges.

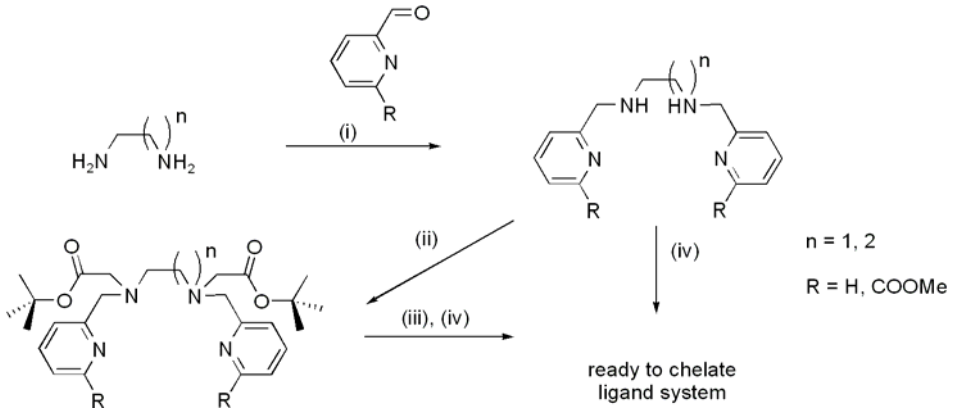

Scheme 4.1 Schematic overview of synthesis methodology used to synthesize chelates of library (i) 1. CH_3OH, reflux, 30 min 2. $NaBH_4$, CH_3OH, 0°C, 2 h (ii) *tert*-butyl bromoactetic acid, Na_2CO_3, CH_3CN, 70 °C, o.n. (iii) TFA/ CH_2Cl_2, 30 min (iv) LiOH, THF/ H_2O, 30 min – 2 h.

The assembly of these chelates was simple. The primary amines are commercially available and were reacted with the pyridyl unit using reductive amination to afford the pyridyl functionalized secondary amine. This approach afforded either an already protected chelate scaffold, or provided a protected intermediate, which could be further functionalized by alkylation with additional carboxylate arms. In all cases, deprotection of the carboxylate functionalities constituted the last synthetic step furnishing a selection of simple chelation scaffolds. The facile assembly of the chelate library compounds is shown with the general reaction Scheme 4.1. Some chelates were synthesized using a variation of this methodology, such as direct alkylation with the pyridyl fragment. Syntheses of a variety of fragments, such as N-N'-bis(2-pyridylmethyl) ethylenediamine-N-N'-diacetic acid,[130] 1,2-[{6-(carboxylato-)pyridin-2-yl}methylamino] ethane[131] and N,N'-bis(6-carboxy-2-pyridylmethyl)ethylenediamine-N,N'-diacetic acid[108] have been reported previously. All chelates included in this chapter have an even number of donor atoms. While some heptadentate chelates were afforded as byproducts of the alkylation reaction, none of them was found to have particularly favourable characteristics.

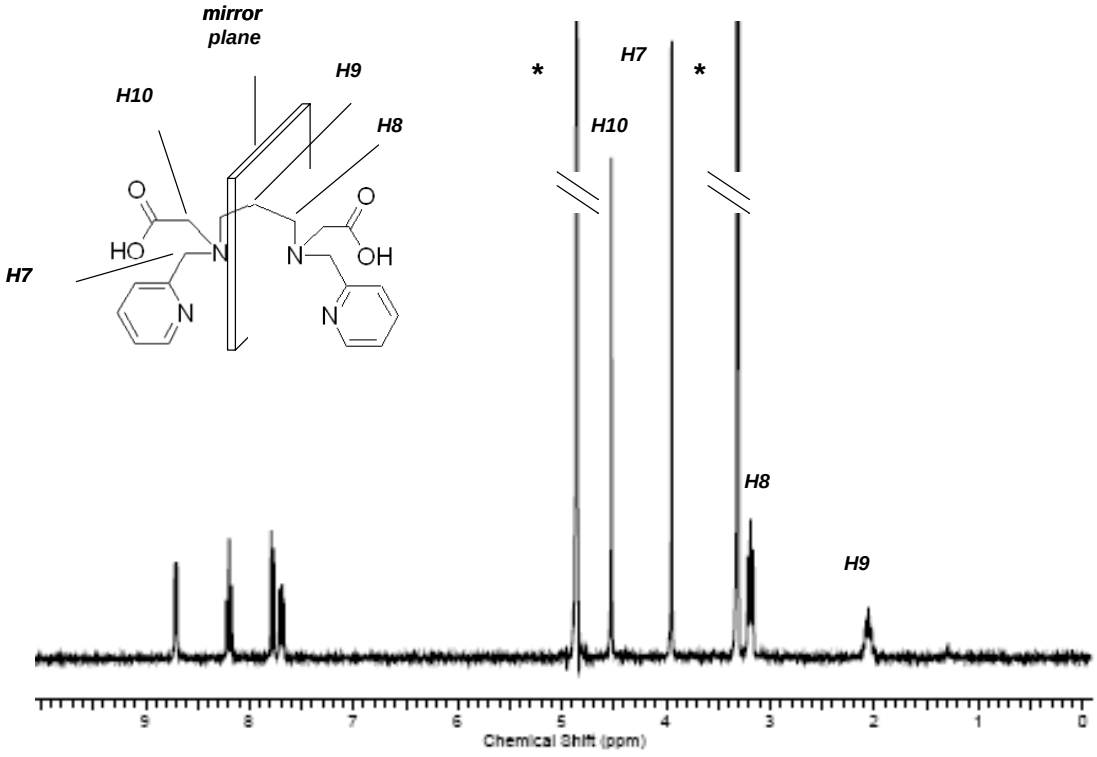

Figure 4.3 ^{1}H NMR spectrum (300 MHz, CD_3OD, 298 K) of a propyl bridged chelate, * denotes residual solvent peaks.

All final compounds were characterized using ^{1}H and ^{13}C NMR spectroscopy, mass spectrometry and IR. Previously synthesized compounds and protected intermediates were characterized using ^{1}H NMR spectroscopy and mass spectrometry. Characterisic spectroscopic features include aromatic ^{1}H NMR peaks in the low field region between $\delta = 7 - 8.2$, as well as peaks of bridging methylene groups neighboring secondary and tertiary amines, which appear as singlets, either due to the lack of vicinal protons or due to the mirror plane present in these ligand systems. The only multiplets observed in the non-aromatic region were found for propyl bridged ligand systems and for the aliphatic chain on the low denticity ligand 6-propylaminomethyl-di-pyridine-2-carboxylic acid. An example of an ^{1}H NMR spectrum of a propyl bridged ligand, N-N'-bis(2-pyridylmethyl) propylenediamine-N-N'-diacetic acid, is shown in Figure 4.3.

4.4.2 Screening with ^{67}Ga

After establishing the ligand library, the ligands were screened for radiolabelling properties. Since the most successful chelate systems for the coordination of the radioisotope ^{67}Ga will label at room temperature, pH 4.5 and within 10 minutes,[58] the chelate systems were tested under these labelling conditions as well. Reaction monitoring was performed with analytical HPLC. Chelates yielding below 95 % were additionally heated in order to drive the coordination reaction to completion. In all cases where heating was employed, additional side product formation was observed. The results from the screening procedure are summarized in Table 4.2. The ligand concentration was kept at 10^{-4} M in all cases. One lead compound was clearly identified. 1,2-[{6-(Carboxylato)pyridin-2-yl}methylamino]ethane (H_2**dedpa**) shows excellent labelling yields of 99 % and shows quantitative, clean labelling under the mild conditions outlined above with no residual free metal detectable. Concentration dependent coordination of H_2dedpa at concentrations as low as 10^{-7} M with both ^{68}Ga and ^{67}Ga showed quantitative conversion to the desired product. When coordinating to ^{68}Ga, high specific activities (as high as 9.8 mCi $nmol^{-1}$) were obtainable without any purification steps. This is the highest specific activity measured for any chelate with ^{68}Ga when neither heating nor ^{68}Ga pre-purification is used.[137]

Table 4.2 Summarized results from initial labeling experiments with the synthesized chelates. HPLC gradients include: A: 0 to 5% in 10 mM NaOAc (pH 4.5), 20 min. B: 0 to 100% CH_3OH in 10 mM NaOAc (pH 4.5), 20 min**.**

Chelate	Retention time (Gradient)	Temp.	Purity
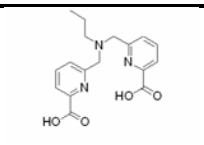	8.9 min (B)	RT Heating	73% mixture of products
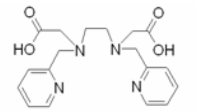	7.7 min (B)	RT Heating	70% 88%,impurities
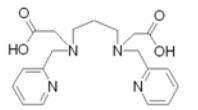	5.3 min (B)	RT Heating	92% 72%,impurities
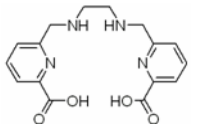	6.19 min (A)	RT	99%
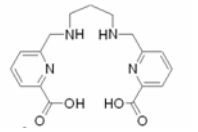	7.6 min (A)	RT Heating	44 % 44%
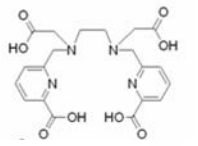	6.29 min (B)	RT	95 %
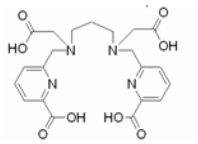	7.5 min (B)	RT	95%

4.4.3 *In Vitro* stability of Select Ligand Candidate

After identification of H_2dedpa as the clear lead chelate, further investigations were made to examine the potential of the chelate as a viable alternative to the gold standard NOTA. To investigate the stability of the $[^{67}Ga(\mathbf{dedpa})]^+$ radiochemical complex, a 2 h competition experiment was conducted in the presence of excess human *apo*-transferrin, the iron sequestering/transport protein that has very high affinity for Ga(III).[57] $[^{67}Ga(\mathbf{dedpa})]^+$ was fully intact after 2 h, suggesting that it should have very high *in vivo* stability, similar to that reported for Ga(NOTA) complexes.[58] The corresponding labelling traces are shown in Figure 4.4.

In order to compare the radiolabelling efficiency of NOTA and H_2**dedpa**, a direct competition for chelation of ^{67}Ga was done using equal concentrations (10^{-4} M) of both NOTA and H_2**dedpa**, over 96% was coordinated by $(\mathbf{dedpa})^{2-}$, less than 1 % by NOTA, demonstrating the expected faster Ga complexation with the acyclic H_2dedpa compared with the macrocyclic NOTA.

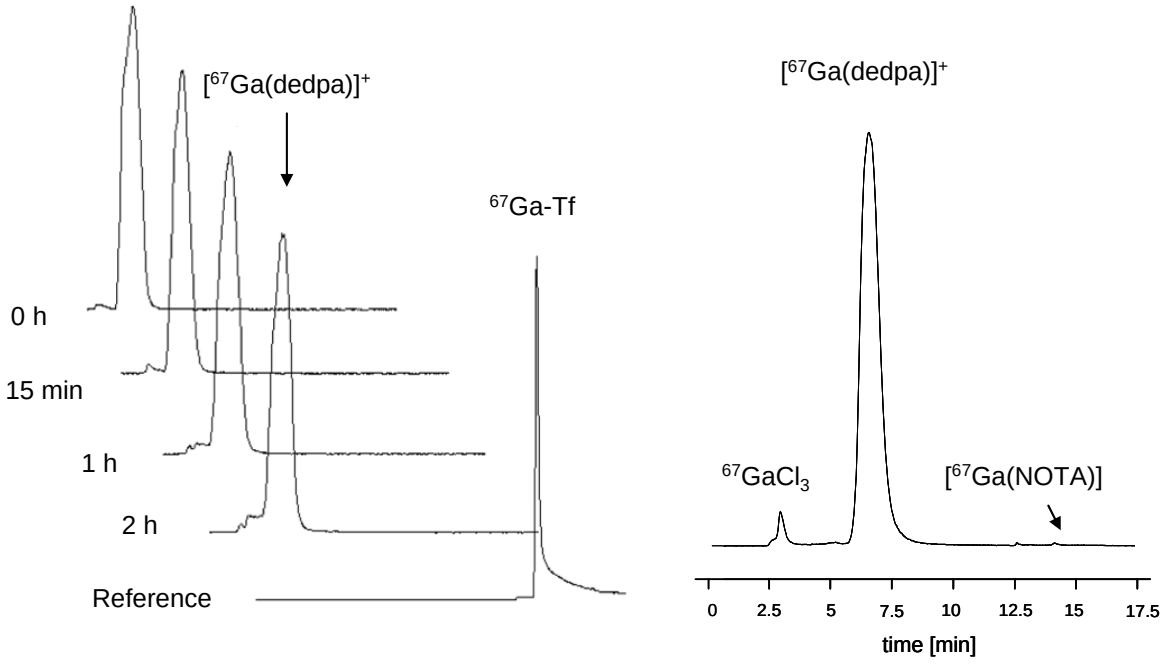

Figure 4.4 Labelling traces from transferrin challenge experiment (left) and NOTA versus H_2dedpa challenge (right).

4.4.4 Coordination Chemistry with Non-radioactive Ga and X-Ray Diffraction Structural Characterization of [Ga(dedpa)][ClO_4]

In order to characterize the formed Ga complex macroscopically, [Ga(**dedpa**)][ClO_4] was prepared. Due to formation of insoluble $Ga(OH)_3$ at pH > 4.5, which can be observed by characteristic cloudiness of an aqueous solution, the ligand and the $Ga(ClO_4)_3$ salt were mixed at pH ~ 2 in a 1:1 solution of water and CH_3OH. The pH was subsequently raised slowly by dropwise addition of 0.1 M NaOH to pH 4.2 – 4.5 and then stirred at 70 °C for 30 minutes to guarantee complex formation. The solution was set aside in the fume hood for slow evaporation of solvent, which led to the formation of crystals suitable for X-ray diffraction structural characterization. [Ga(**dedpa**)][NO_3] is formed using the analogous procedure, affording a salt which is more soluble in protic solvents and therefore more suitable for spectroscopic characterization; however, the crystals formed from this salt were never suitable for X-ray diffraction. The solid state X-ray crystal structure (Figure 4.5) provides significant insight into the coordination environment of [Ga(**dedpa**)]$^+$. In comparison with the crystallized Ga complexes of NOTA[55] and DOTA,[138] which have widely dispersed metal-to-ligand bond distances, [Ga(**dedpa**)]$^+$ has a more equally distributed array of bond lengths (Table 4.3), suggesting that the unusually high stability of the complex is due to a near-perfect fit with the Ga^{3+} ion.

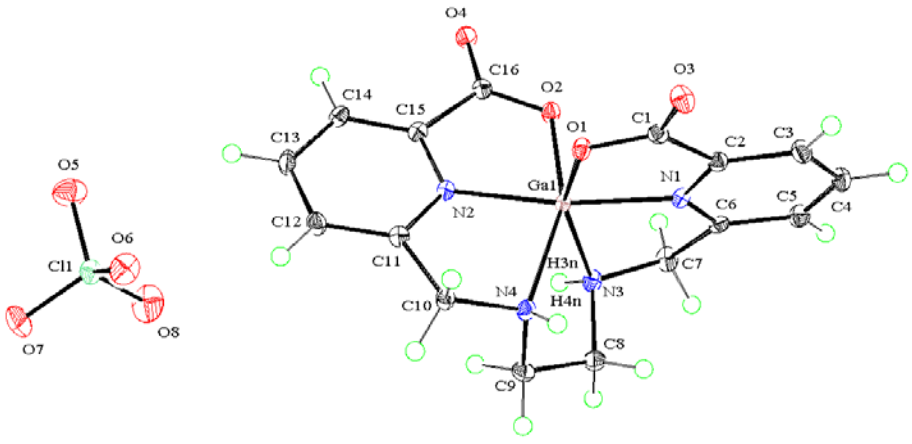

Figure 4.5 ORTEP drawing of [Ga(**dedpa**)][ClO_4]. Shown is the atom numbering scheme (50% thermal ellipsoids).

Table 4.3 Selected bond lengths in [Ga(**dedpa**)][ClO_4] , ([Å]) and angles ([°]).

bond	length [Å]	angle	degree [°]
N1-Ga	1.9866(16)	O(1)- Ga(1)- O(2)	101.39(6)
N2-Ga	1.9902(16)	O(1)- Ga(1)- N(1)	80.14(6)
N3-Ga	2.1115(16)	O(2)- Ga(1)- N(1)	94.02(6)
N4-Ga	2.1132(16)	O(1)- Ga(1)- N(2)	94.72(6)
O1-Ga	1.9708(13)	O(2)- Ga(1)- N(3)	94.78(6)
O2-Ga	1.9828(13)	N(1)- Ga(1)- N(3)	77.82(6)

Another characteristic that clearly differentiates [Ga(**dedpa**)]$^+$ from complexes with the macrocyclic chelates, is the C_2 rotational axis, which has also been confirmed in solution through ^{13}C NMR spectroscopy, where only one signal is observed per type of carbon in the ligand molecule. Other information that can be easily gained from spectroscopy is the conversion from homotopic protons on the non-metal bound ligand to diastereotopic protons with individual shifts and large geminal coupling constants within the complex. This is a phenomenon observed and described also in previous chapters and, along with the shift of aromatic protons to lower field upon metal binding to the pyridyl unit, it gives a good indication of completion of the coordination reaction (Figure 4.6).

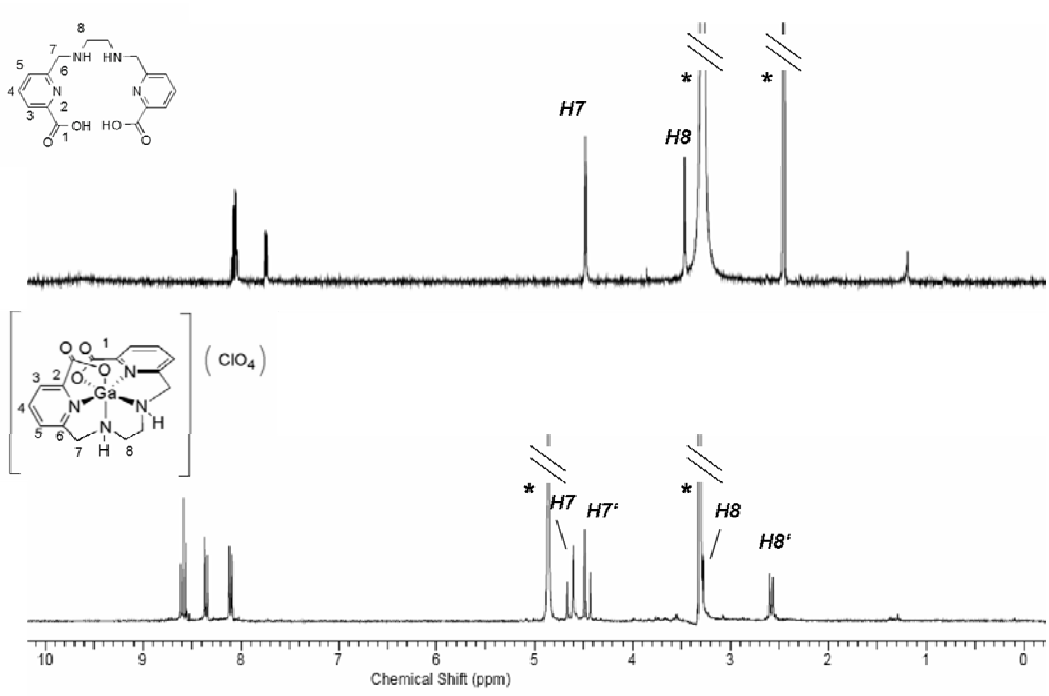

Figure 4.6 ^1H NMR spectra (300 MHz, d_6-DMSO/CD_3OD, 298 K) of H_2dedpa and [Ga(**dedpa**)][NO_3], * denotes residual solvent peaks.

4.4.5 Potentiometric Measurements on [Ga(dedpa)]$^+$

Solution thermodynamic investigations of the corresponding cold complex [Ga(**dedpa**)]$^+$ provided a complex stability constant of log K_{ML} = 28.11(8),[139] obtained by ligand-ligand competition with EDTA using potentiometric titration (performed by Dr. J. Cawthray). A more relevant indicator of the extent to which a metal complex is stable in solution is given by pM (-log[free M]), which considers the influence of ligand basicity and chelate hydrolysis. The values of log K_{ML} and pM of the Ga(III) complexes of **dedpa**$^{2-}$ and other relevant multidentate ligands are shown in Table 4.4. The high value of log K_{ML} and pM for [Ga(**dedpa**)]$^+$ confirms the high affinity of **dedpa**$^{2-}$ for Ga(III) as well as high thermodynamic stability.[139]

Table 4.4 Formation constants (log K_{ML}) and pM[a] of Ga(III) complexes. [a] Calculated for 10 μM total ligand and 1 μM total metal at pH 7.4 and 25°C. [b] Conditional constant for log K_{ML} from Ref [57].

Ligand	log K_{ML}	pM
dedpa^{2-}	28.11	27.4
EDTA[140]	21.7	18.3
DOTA[121]	21.33	18.5
NOTA[122]	30.98	27.9
Transferrin[b]	20.3	21.3

4.4.6 Model Functionalization of the H_2dedpa Scaffold

While the close investigation of the chelation scaffold H_2dedpa was able to show very promising results, the derivatization of H_2dedpa to allow conjugation to a potential biomolecule had not yet been explored. To investigate different modes of functionalization analogous to the bifunctional versions of the macrocyclic chelates, two model compounds H_2**dp-N-NO$_2$** and H_2**dp-bb-NO$_2$** were synthesized (Scheme 4.2).

H_2**dp-N-NO$_2$** displays derivatization through the two aliphatic nitrogens, affording a scaffold capable of carrying two targeting molecules, while compound H_2**dp-bb-NO$_2$** is derivatized through the backbone of the ethylenediamine (en) component of the basic ligand structure, retaining the original coordination environment more closely, but only allowing the attachment of one targeting molecule.

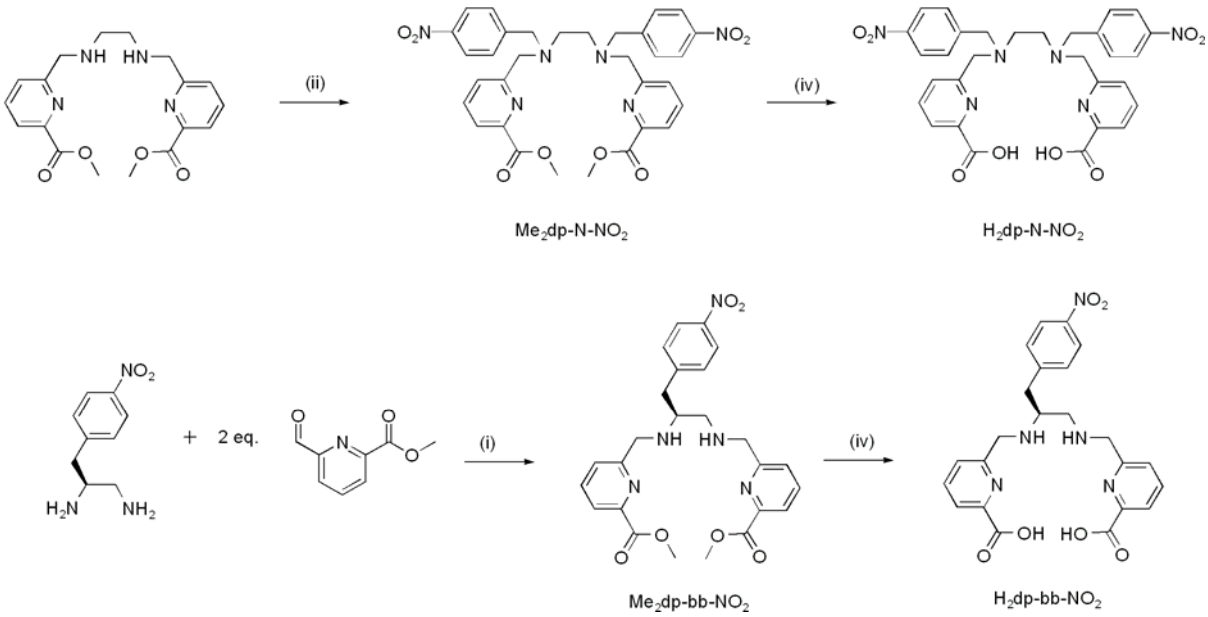

Scheme 4.2 Syntheses of H_2**dp-N-NO$_2$** and H_2**dp-bb-NO$_2$**: (i) 1. CH_3OH, reflux, 2h, 2. $NaBH_4$, 0°C, 2h (ii) 4-nitrobenzyl bromine, Na_2CO_3, CH_3CN, 18 h (iv) LiOH, THF/water (3:1), 45 min.

Both H_2**dp-N-NO$_2$** and H_2**dp-bb-NO$_2$** incorporate the nitrobenzyl functionality, which can be converted easily into the corresponding amino- or isothiocyanato-benzyl coupling moieties frequently employed for conjugation to target molecules via a free carboxylate or primary amine, respectively.[141,142] H_2**dp-N-NO$_2$** is synthesized from 1,2-[{6-(methoxycarbonyl)pyridin-2-yl}methylamino]ethane,[108] which is then subsequently alkylated with 4-nitrobenzyl bromide. Intermediate Me_2**dp-N-NO$_2$** is purified and the carboxylates are deprotected under standard conditions to afford the clean product H_2**dp-N-NO$_2$** as a white solid, characterized using ^{1}H and ^{13}C NMR spectroscopy, mass spectrometry and IR. Compound H_2**dp-N-NO$_2$** is furnished through a different route; 3-(4-nitro-phenyl)-propane-1,2-diaminemethane is derived from 4-nitro-L-phenylalanine,[133] while 6-formyl-pyridine-2-carboxylic acid methyl ester is afforded through a four step

synthesis from 2,6-pyridinedicarboxylic acid.[108] A one-pot reductive amination process produces Me_2**dp-bb-NO_2** in moderate yields, along with a mixture of impurities, which can be separated from the product through column chromatography. The subsequent deprotection leads to H_2**dp-bb-NO_2** as a light orange solid characterized using ^{1}H and ^{13}C NMR spectroscopy, and mass spectrometry. Since only a very small amount of compound H_2**dp-bb-NO_2** was isolated, no IR spectroscopy was performed.

4.4.7 ^{67}Ga Labelling of the Model Bifunctionals H_2dp-bb-NO_2 and H_2dp-N-NO_2 and Transferrin Challenge Experiments of [^{67}Ga(dp-bb-NO_2)]$^+$ and [^{67}Ga(dp-N-NO_2)]$^+$

Coordination of H_2**dp-N-NO_2** to ^{67}Ga or ^{68}Ga affords the complex within 10 minutes at room temperature in 98 % radiochemical yield. The subsequent *apo*-transferrin challenge experiment revealed that 51 % of the radiolabeled complex remained intact after 2 h in the presence of excess *apo*-transferrin, a stability inferior to that of [Ga(**dedpa**)]$^+$, but comparable to that of Ga-DOTA.[58] In the case of H_2**dp-bb-NO_2**, the ^{67}Ga and ^{68}Ga complexes are formed within 10 minutes at room temperature in 97 % radiochemical yield. The subsequent *apo*-transferrin challenge experiment reveals a stability comparable to that of [Ga(**dedpa**)]$^+$, with over 97 % of the complex remaining intact after 2 h (Figure 4.7). Concentration-dependent coordination to ^{68}Ga showed that both (**dp-N-NO_2**)$^{2-}$ and (**dp-bb-NO_2**)$^{2-}$ are capable of coordinating under mild conditions at concentrations as low as 10^{-6} M.

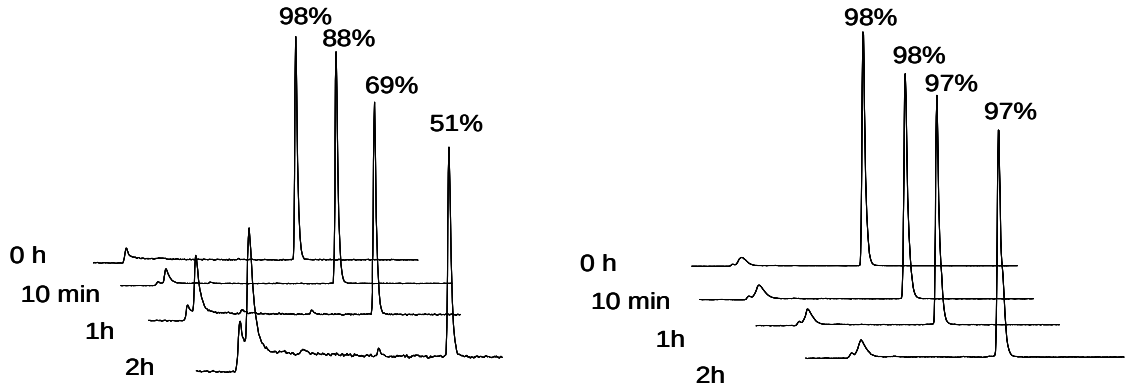

Figure 4.7 Stacked HPLC monitoring traces of [^{67}Ga(**dp-N-NO_2**)]$^+$ (left) and [^{67}Ga(**dp-bb-NO_2**)]$^+$ (right) over 2 h stability experiment against *apo*-transferrin.

4.4.8 Coordination Chemistry of the Model Bifunctionals with Cold Ga and X-Ray Diffraction Structural Characterization of [Ga(dp-N-NO_2)][ClO_4]

The complex with cold Ga is formed within 2 h at pH 4-5 under gentle heating and again the C_2 rotational axis was confirmed in both the solid-state structure and the solution NMR. The same procedure as for [Ga(**dedpa**)][ClO_4] was employed. For both model compounds, the complex was formed with $(NO_3)^-$ as the counter ion, since this salt provides better solubility in protic solvents. In the case of [Ga(**dp-N-NO_2**)][NO_3], information that can be easily extracted from ^{1}H NMR spectroscopy includes the conversion from homotopic protons on the non-metal bound ligand to diastereotopic protons with individual shifts and large geminal coupling constants upon complexation of Ga(III) within the complex, analogous to the previously described [Ga(**dedpa**)]$^+$ complex (Figure 4.8).

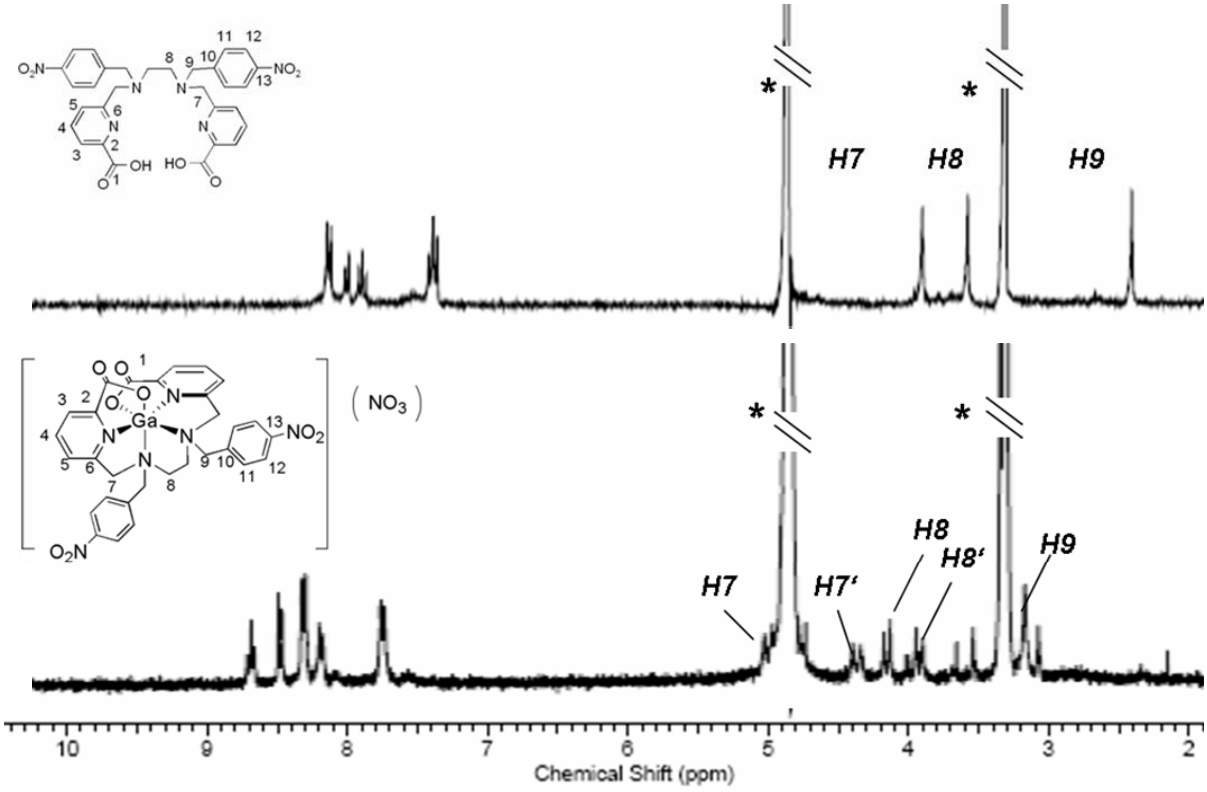

Figure 4.8 ^{1}H NMR spectra (300 MHz, CD_3OD, 298 K) of H_2**dp-N-NO_2** and [Ga(**dp-N-NO_2**)][NO_3]. * denotes residual solvent peaks.

For H_2**dp-bb-NO_2** however, where all protons appear already as diastereotopic

protons within the ligand due to the asymmetry of this ligand system, the coordination reaction can be traced using the ^{1}H NMR spectrum mainly through the shift of the aromatic protons and bridging methylene protons to lower field, as well as increased splitting between geminal protons upon coordination (Figure 4.9).

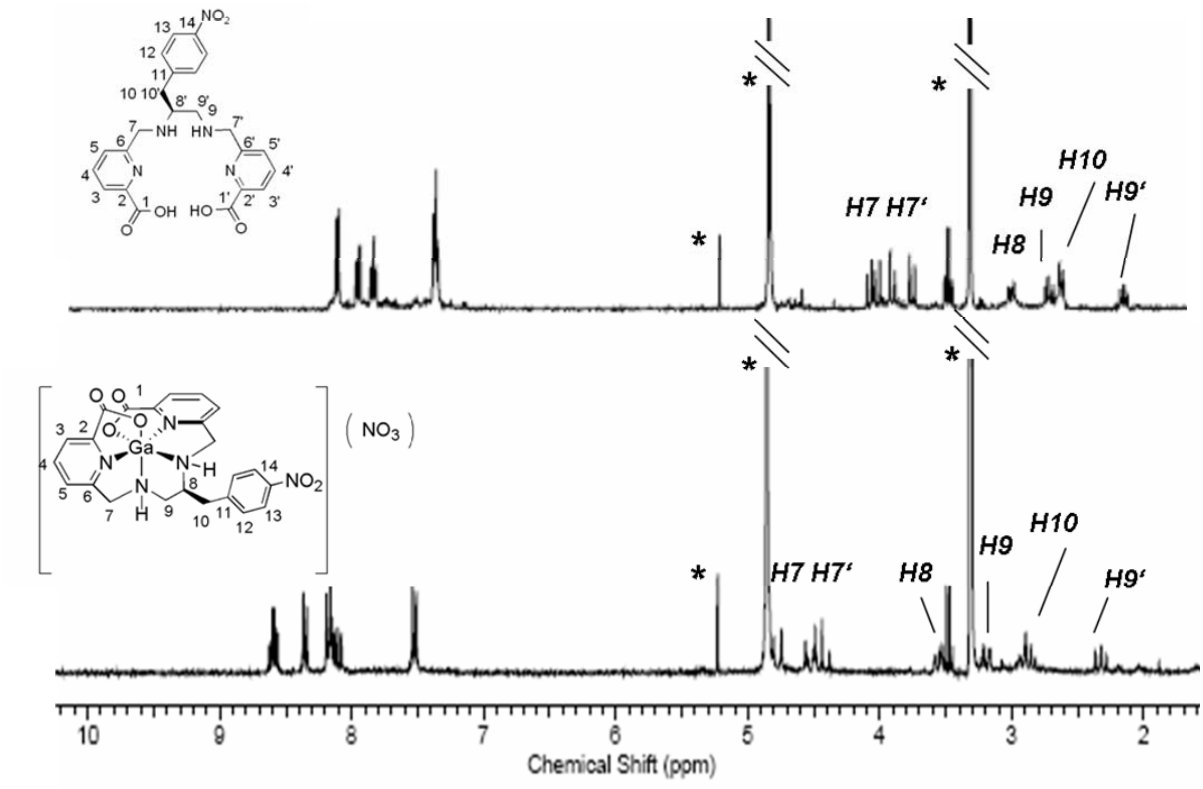

Figure 4.9 ^{1}H NMR spectra (300 MHz, CD_3OD, 298 K) of H_2**dp-bb-NO$_2$** and [Ga(**dp-bb-NO$_2$**)][NO_3]. * denotes residual solvent peaks.

In order to afford crystals suitable for X-ray diffraction structural characterization of the Ga complex with H_2**dp-N-NO$_2$**, the complex with $(ClO_4)^-$ as the counter ion was prepared and, after slow evaporation, crystals suitable for X-ray diffraction were formed. The solid state structure (Figure 4.10) shows similar bond lengths as for [Ga(**dedpa**)][ClO_4], however the N3-Ga and the N4-Ga bond lengths appear to be slightly elongated compared to the non-derivatized structure, which could be an indication as to why the corresponding radiochemical complex exhibited decreased stability in the *apo*-transferrin challenge experiment.

Table 4.5 Selected bond lengths in [Ga(**dp-N-NO$_2$**)][ClO_4] (bold), compared to selected bond lengths in [Ga(**dedpa**)][ClO_4], ([Å]).

bond	length [Å]	length [Å]
N1-Ga	**1.992(5)**	1.9866(16)
N2-Ga	**1.981(5)**	1.9902(16)
N3-Ga	**2.188(5)**	2.1115(16)
N4-Ga	**2.159(5)**	2.1132(16)
O1-Ga	**1.967(4)**	1.9708(13)
O2-Ga	**1.976(4)**	1.9828(13)

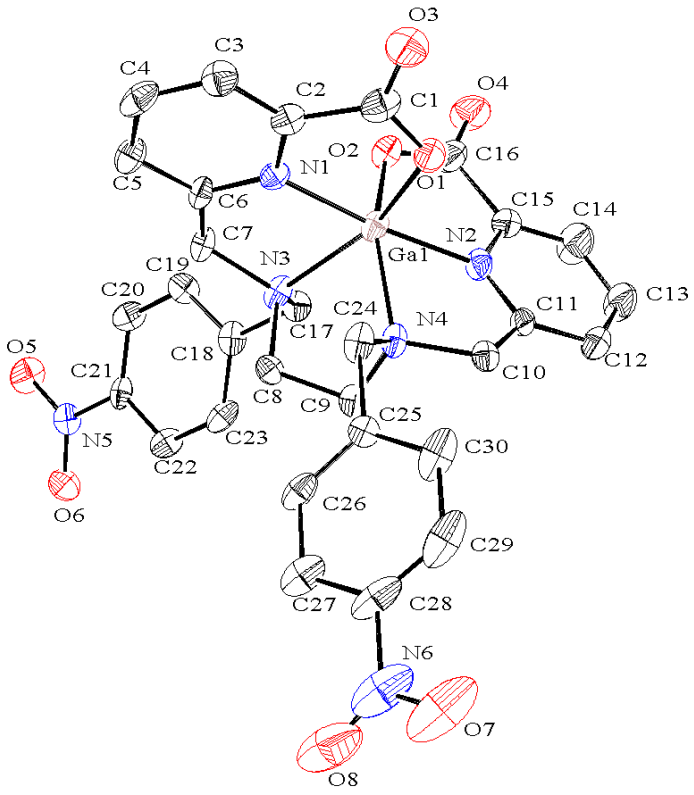

Figure 4.10 ORTEP drawing of [Ga(**dp-N-NO$_2$**)][ClO_4] (50% thermal ellipsoids); H atoms and the (ClO_4) counter ion are omitted for clarity.

4.4.9 Biodistribution of ^{67}Ga Complexes of $(dedpa)^{2-}$ and the Model Bifunctionals

The biodistribution study in mice (Figure 4.11, appendix Tables B) indicated that $[^{67}Ga(\mathbf{dedpa})]^{+}$ cleared from the background tissue, such as muscle, within the first 30 min and was excreted mainly through the kidneys. The *in vivo* stability of $[^{67}Ga(\mathbf{dedpa})]^{+}$ was supported by the low uptake in bone, which is known to be a site of increasing accumulation for weakly chelated ^{67}Ga.[143] The overall biodistribution profile compares well to macrocyclic chelates evaluated in a similar study,[58] also exhibiting the low uptake in liver and intestines characteristic of ionic compounds such as $[^{67}Ga(\mathbf{dedpa})]^{+}$. The persistent high uptake in the blood serum was not confirmed with the derivatized compounds, suggesting that added functionality influences biodistribution.

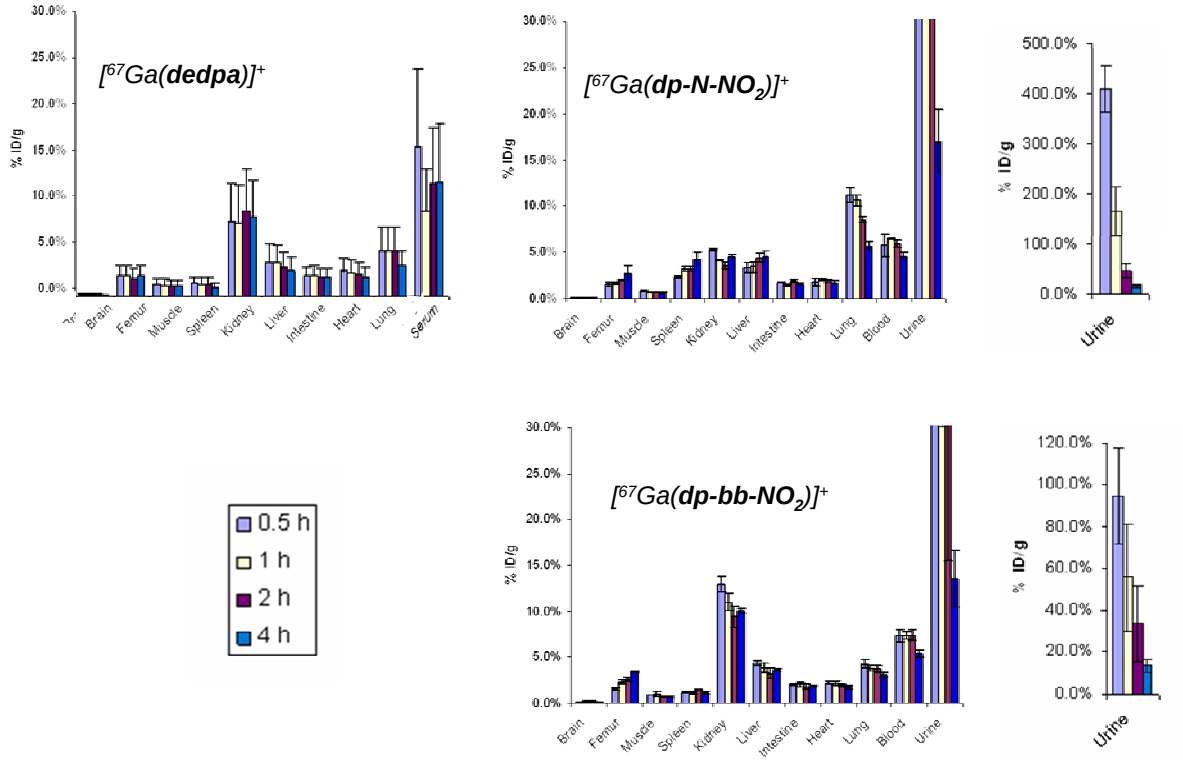

Figure 4.11 Biodistribution of $[^{67}Ga(\mathbf{dedpa})]^{+}$, $[^{67}Ga(\mathbf{dp\text{-}N\text{-}NO_2})]^{+}$ and $[^{67}Ga(\mathbf{dp\text{-}bb\text{-}NO_2})]^{+}$ in female ICR mice over 4h; complete data of the latter two compounds for urine is shown also in separate diagrams to the right.

In the biodistribution studies for [^{67}Ga(**dp-N-NO$_2$**)]$^+$and [^{67}Ga(**dp-bb-NO$_2$**)]$^+$, whole blood was collected instead of serum, and urine was collected as an additional data point (Figure 4.11, Table A.1). Both [^{67}Ga(**dp-N-NO$_2$**)]$^+$and [^{67}Ga(**dp-bb-NO$_2$**)]$^+$ exhibit improved clearance from all organs, low bone uptake (indicator for complex stability) and excretion through urine. Despite lower *in vitro* stability, the biodistribution of [^{67}Ga(**dp-N-NO$_2$**)]$^+$ suggests high stability *in vivo* and shows better clearance from blood and kidneys than either [^{67}Ga(**dp-bb-NO$_2$**)]$^+$ or [^{67}Ga(**dedpa**)]$^+$. It is possible that compounds containing secondary amines associate more strongly with blood serum proteins and kidney tissue; however, the difference in biodistribution of [^{67}Ga(**dp-bb-NO$_2$**)]$^+$and [^{67}Ga(**dedpa**)]$^+$ shows that added functionalities, such as peptides or other targeting vectors, should have a great impact on the interaction of these compounds with *in vivo* systems.

4.5 Conclusions

A set of easily assembled acyclic chelates was synthesized and screened for their ability to chelate $^{67/68}$Ga under mild conditions (pH 4.5, room temperature) and short reaction time. The hexadentate H_2dedpa ligand complexes quickly with Ga, forming complexes of very high stability, comparing well to the widely used macrocyclic chelate NOTA and exceeding the properties of DOTA. The mild conditions used, combined with the high radiochemical yields make this ligand system an ideal scaffold for applications with more sensitive biomolecules such as peptides and antibodies. The direct labelling, high radiochemical yield and high specific activity of the products could obviate the need for time consuming HPLC purification, a major advantage when using the short lived isotope ^{68}Ga. Two model derivatives were synthesized in order to predict the most optimal mode of conjugation to a biomolecule. While the backbone derivatization gave rise to a complex with higher stability, the N-derivative complex showed slightly decreased *in vitro* stability. The biodistributions of [^{67}Ga(**dedpa**)]$^+$, [^{67}Ga(**dp-N-**

NO_2)]$^+$and [^{67}Ga(**dp-bb-NO_2**)]$^+$ confirmed the stability of the complexes measured *in vitro* with general clearance rendering these frameworks a good basis for elaboration of new Ga bioconjugates.

It is important to note that many of the advantageous properties described for H_2**dedpa** have been observed previously with only one macrocyclic chelate (NOTA), and they are unexpected for an acyclic system. Chapter 6 elaborates further on the functionalization of the H_2**dedpa** scaffold with biomolecules, as well as the properties of the corresponding bioconjugates.

Chapter 5: Viability of H_2dedpa for Labelling with ^{64}Cu

5.1 Introduction: Prior Art in ^{64}Cu Chelates

A wide variety of Cu isotopes applicable to diagnostic imaging and radiotherapy has been the subject of extensive research. ^{64}Cu ($t_{1/2}$=12.7 h, β^+ 17.4 %, E_{max} = 0.656 MeV, β^- 39 %, E_{max} = 0.573 MeV) is of high current interest for both positron emission tomography (PET) and radiotherapy.[48] The longer half-life is more applicable to developing PET agents with larger biomolecules, such as monoclonal antibodies that may require longer circulation times before imaging to achieve optimal target uptake.[95] While not available as a generator produced isotope, the longer half-life allows for shipment of the isotope to remote areas where no cyclotron is available.[118]

As opposed to the non-redox active Ga(III), three oxidation states (+1, +2, +3) are accessible for copper in aqueous solution. The d^9 Cu(II) configuration is predominant in aqueous solution and prefers square planar and Jahn-Teller distorted octahedral geometries. The ligand exchange kinetics of Cu(II) are particularly rapid, therefore kinetically inert ligand systems with strong crystal field stabilization for complexation are preferred for incorporation into radiopharmaceuticals.[49] Cu(II) is a borderline soft metal center, with preferences for donor atoms similar to the preferences of Ga(III): amines, imines, pyridines and carboxylates.[143]

Among the bifunctional ligand systems investigated and previously reported for the purpose of targeted delivery of ^{64}Cu, a strong preference for hexadentate cage-like poly-aza macrocyclic ligands can be found. Preferred properties for good ^{64}Cu bifunctional chelates include: complex stability against serum over the course of 24 h, and *in vivo* inertness toward transchelation, which can be monitored by liver uptake, negative complex reduction potentials well below -0.4 V (NHE),[49] as well as reversibility of the reduction reaction without loss of ligand.[144] The metal ion 2+ charge is preferentially reduced to a 1+, -1 or neutral charge of the complex in order to minimize high kidney uptake and accelerate excretion. Mild labelling conditions are preferred, despite the long half-life, since heat- and pH- sensitive biomolecules such as antibodies are used preferentially with this isotope.

Thermodynamic stability is a consideration when designing Cu chelates; however, it does not necessarily correlate with *in vivo* complex stability.[49] In Figure 5.1 and Table 5.1, a selection of important chelate structures and some of their relevant characteristics such as labelling conditions, reduction potential and thermodynamic stability constant log K_{ML} are shown.

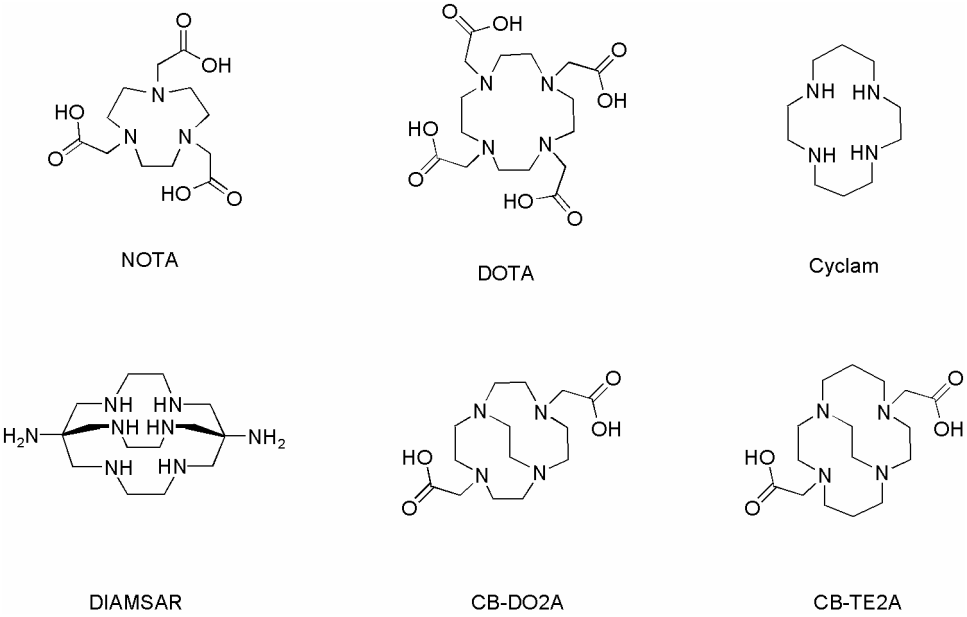

Figure 5.1 Structures of selected, previously investigated chelate systems for labelling with ^{64}Cu.

Table 5.1 Summary of relevant properties of previously investigated chelates for labelling of ^{64}Cu

Ligand system	Labelling conditions	log K_{ML}	E_{red} (vs NHE)
NOTA[145]	30 min, room temp.	19.8, 21.6	-0.7 (irrev.)
DOTA[146]	5 min, room temp.	22.7	-0.74 (irrev.)
Cyclam[147]	10 min, room temp.	27	-0.48 (irrev.)
DIAMSAR[148]	1h, room temp.	n. d.	-0.90 (irrev.)
CB-TE2A[149]	1 h, 95 °C	n. d.	-0.88 (q-rev.)
CB-DO2A[149]	30 min, 80 °C	n. d.	-0.72 (irrev.)

5.2 Experimental

5.2.1 Materials and Methods

Refer to Chapter 2.2 for general information. H_2dedpa was prepared according to Chapter 4. A Phenomenex Synergi 4 μm Hydro-RP 80A column (250 × 4.6 mm) was used to monitor decomplexation in 6 M HCl at 90 °C. HPLC solvents consisted of 0.1% trifluoroacetic acid in water (solvent A) and acetonitrile (solvent B). Samples were analyzed with a linear gradient method (100 % solvent A to 100 % solvent B over 30 min). ^{64}Cu was obtained as a dilute HCl solution (Nordion); it was commercially available from Nordion at the time of the ^{64}Cu experiments. Product specification reported the specific activity of the ^{64}Cu to be > 5000Ci/g with < 0.2 micrograms of Cu per mCi. The HPLC system used for analysis of the ^{64}Cu labelled compounds consisted of a Waters Alliance HT 2795 separation module equipped with a Raytest Gabbistar NaI detector and a Waters 996 photodiode array (PDA) detector. ^{64}Cu labelled compounds and their serum stability were analyzed on a Waters XBridge BEH130 4.6 mm × 150 mm column. Samples were analyzed with a linear gradient method (95 % solvent A to 100 % solvent B over 30 min).

5.2.2 Coordination Chemistry with Non-radioactive Cu

1,2-[{6-(Carboxylato)pyridin-2-yl}methylamino]ethane copper(II) trihydrate [Cu(dedpa)]·3H_2O.

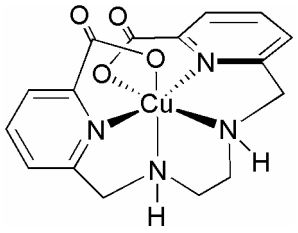

H_2dedpa·2 HCl (5.8 mg, 0.023 mmol) was dissolved in 1 mL H_2O. $Cu(Cl)_2 \cdot H_2O$ (2.4 mg, 0.023 mmol) is dissolved in a 1:1 mixture of CH_3OH / H_2O (2 mL total volume) and added dropwise to the ligand solution. The color of the mixture intensified to a greenish blue indicating coordination of the ligand. The pH was adjusted to 6-7 by dropwise addition of an aqueous solution of 0.1 M NaOH. Subsequently, the solvent was removed and the blue crude residue is redissolved

in minimal amounts of H_2O and loaded onto a C18 Waters sep-pak column cartridge. The column was flushed with 20 mL H_2O and the complex was eluted with EtOH as a clear blue solution, which was set aside for slow evaporation in the fumehood. IR (neat, cm^{-1}): 1621 (w), 1574 (s, br), 1410 (m), 1362 (m). HR-ESI-MS calcd. for $C_{16}H_{16}CuN_4NaO_4$: 414.0365, found: 414.0374 $[M + Na]^+$. Elemental analysis: calcd. (found) for Cu(**dedpa**)·$3H_2O$: C 43.0 (42.58), H 4.97 (4.67), N 12.56 (12.04).

5.2.3 Labelling with ^{64}Cu and *In Vitro* Stability

$^{64}Cu^{2+}$ in dilute HCl (100 µL, 0.7 mCi) was added to 900 µL of a 10^{-5} M solution of H_2dedpa in 10 mM NaOAc solution (pH 5.5) and left to react for 10 minutes at RT. The reaction progress was monitored by analytical HPLC to evaluate yield of the coordination reaction. [^{64}Cu(**dedpa**)]. t_R on HPLC: 5.2 minutes (gradient: A: 0.1 % TFA in H_2O, B: CH_3CN 5-100% B linear gradient 30 min), yield: 99 %. Ligand concentrations as low as 10^{-6} M were capable of coordinating the radionuclide with a 63 % yield (under these labelling conditions).

To evaluate complex stability, an aliquot (500 µL) of the reaction was added to a solution of mouse serum (500 µL). The mixture was incubated at 37°C and analyzed by PD-10 column filtration after 2 h and 24 h. Aliquots of reaction mixtures were loaded onto the pre-rinsed PD-10 columns (total loading volume: 2.5 mL). Subsequently, the column was rinsed with 3.5 mL PBS. The resulting eluate was collected and measured for radioactivity. The activity eluted corresponds to serum-bound ^{64}Cu. Stability versus serum (2 h/ 24 h; in % complex intact): 97/ 77.

5.2.4 X-Ray Diffraction Structural Characterization of [Cu(dedpa)]·$3H_2O$

A blue prism crystal of $C_{16}H_{16}Cu\ N_4O_4·3H_2O$ having approximate dimensions of 0.11 x 0.15 x 0.21 mm was mounted on a glass fiber. All measurements were made on a Bruker APEX DUO diffractometer with graphite monochromated Mo-Kα radiation. Data were collected and integrated using the Bruker SAINT[78] software package. The linear absorption

coefficient, μ, for Mo-Kα radiation is 12.07 cm^{-1}. Data were corrected for absorption effects using the multi-scan technique (SADABS[79]), with minimum and maximum transmission coefficients of 0.808 and 0.876, respectively. The data were corrected for Lorentz and polarization effects. The structure was solved by direct methods. The material crystallizes with three molecules of H_2O in the asymmetric unit. All non-hydrogen atoms were refined anisotropically. All hydroxyl hydrogen atoms and N-H hydrogen atoms were located in difference maps and refined isotropically. The hydrogen atoms of each water molecule were disordered in three orientations, each orientation taking advantage of a possible hydrogen bond interaction. The excellent quality of the data made it possible to refine the positions and occupancies of the hydrogen fragments on each water molecule; however, the isotropic thermal parameters were constrained to be 1.5 times the thermal parameter of its associated oxygen. All other hydrogen atoms were placed in calculated positions. Finally, the material crystallizes as a racemic twin, in an approximately 80:20 ratio between the two twin volumes. The collection and analysis of the data was done by Dr. Brian O. Patrick.

5.2.5 Cyclic Voltammetry Measurements on [Cu(dedpa)]

Cyclic voltammetry was carried out using an Autolab potentiostat. A glassy carbon electrode (MF 2012, 3 mm diameter) was used as the working electrode, the reference electrode was Ag/AgCl (sat.), and the counterelectrode was platinum mesh. Cyclic voltammetry was carried out in 0.1 M NaOAc, pH 7 (adjusted with glacial acetic acid), with a 0.1 M solution of [Cu(**dedpa**)] at scan rates 100 mV/s and 10 mV/s. A 100 mV/s scan was applied to a solution of solvent between 2 and -2 V in order to establish solvent reduction and oxidation. This was found to be 0.5 to -1.25 V and should not lead to solvent redox behaviour. Subsequently, the ligand or complex was dissolved in the previously measured solvent solution and the cyclic voltammogram was measured within a variety of electrochemical potential windows (0.5 to -1.25 V, as well as 0.5 to -0.5 V). It was found that the one electron reduction of the copper complex could be observed at -1.12 V (normal hydrogen electrode, NHE: 0.92 V) with re-oxidation at 0.02 V (NHE: 0.22). The afforded voltammogram is reproducible upon cycling.

5.3 Results and Discussion

5.3.1 Cu(II) Coordination Chemistry and X-Ray Diffraction Structural Characterization of [Cu(dedpa)]·3H_2O

Formation of the copper complex with H_2dedpa can be followed by the strong, obvious color change of the reaction mixture upon mixing of ligand and metal solution. A variety of copper salts was evaluated as starting material for complex formation: $Cu(OAc)_2 \cdot H_2O$, $CuCl_2 \cdot 2H_2O$, as well as $Cu(ClO_4)_2 \cdot 6H_2O$. The resulting complex is only soluble in protic solvents despite its neutral nature, hence the product cannot be precipitated or extracted. Separation from salts was done with purification using C18 reversed phase cartridge. The paramagnetic nature of the Cu(II) metal center hinders NMR spectroscopic investigations, hence the product was characterized through elemental analysis, IR spectroscopy and mass spectrometry. IR spectral data show a characteristic decrease of carboxylate stretching frequencies upon metal coordination. In the mass spectrum, diagnostic $[M + Na]^+$ peaks were easily identified and displayed the characteristic isotope distribution of $^{63}Cu/^{65}Cu$.

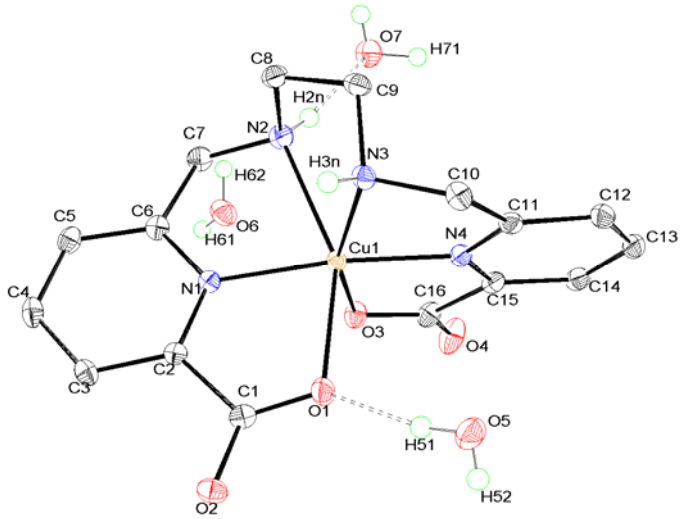

Figure 5.2 ORTEP drawing of [Cu(**dedpa**)]; shown is the atom numbering scheme (50% thermal ellipsoids) and hydrogen atoms within the complex structure are omitted for clarity.

The product crystallizes forming small blue prism crystals suitable for X-ray diffraction. The complex co-crystallizes with three water molecules in the lattice (Figure 5.2). Bond length comparisons between the metal complex and the ligand provides insight into the coordination environment (Table 5.2).

Table 5.2 Selected bond lengths in [Cu(**dedpa**)] (bold), compared to selected bond lengths in [Ga(**dedpa**)][ClO_4], ([Å]). Select bond angles are given [°].

bond	length [Å] (M = Cu)	length [Å] (M = Ga)	angle	degree [°]
N1-M	**2.0008(12)**	1.992(5)	N(4)- Cu(1)- O(3)	81.17(5)
N2-M	**2.3171(13)**	1.981(5)	N(4)- Cu(1)- N(3)	78.65(5)
N3-M	**2.1364(13)**	2.188(5)	N(1)- Cu(1)- N(3)	104.83(5)
N4-M	**1.9386(13)**	2.159(5)	N(4)- Cu(1)- O(1)	97.86(5)
O1-M	**2.3014(11)**	1.967(4)	N(1)- Cu(1)- O(1)	76.23(4)
O2-M	**2.0430(10)**	1.976(4)	N(1)- Cu(1)- N(2)	76.82(5)

Most bond lengths in [Cu(**dedpa**)] are between 1.93 – 2.04 Å, except N2-Cu and O1-Cu, which at 2.30 Å show a Jahn-Teller type distortion, typical for octahedral Cu(II) complexes and similarly observed for [Cu(CB-TE2A)].[144] In order to illustrate the elongation of the axial bonds, a side-on view in Figure 5.3 is provided, with comparison to [Ga(**dedpa**)]$^+$.

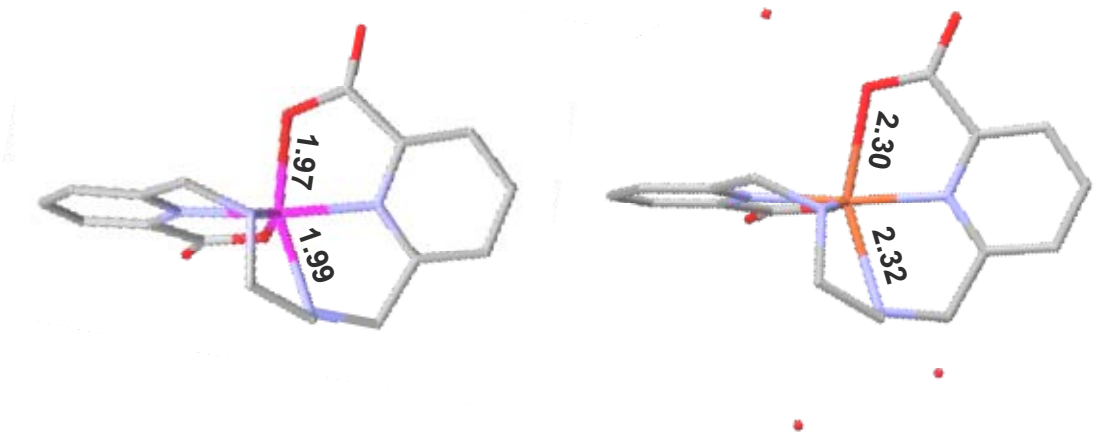

Figure 5.3 Side-on view of [Cu(**dedpa**)] (right), compared to selected bond lengths in [Ga(**dedpa**)]$^+$ (left), H atoms and $(ClO_4)^-$ counter ion of Ga complex omitted for clarity. Graphic generated using Mercury 2.2.[150]

By looking at another side-on view of both complexes, the degree of distortion of both complexes is illustrated. The Cu(II) complex appears to be closer to octahedral geometry; however, both complexes are strongly distorted. The H_2dedpa ligand system shows great flexibility in terms of metal ion tolerance. A possible reason for this could be the enhanced intrinsic rigidity of the carboxylate subunit, which is fixed in conformation with regard to the pyridine ring (Figure 5.4), while the aliphatic units of the chelate regulate the bite angle with which it wraps around the metal center.

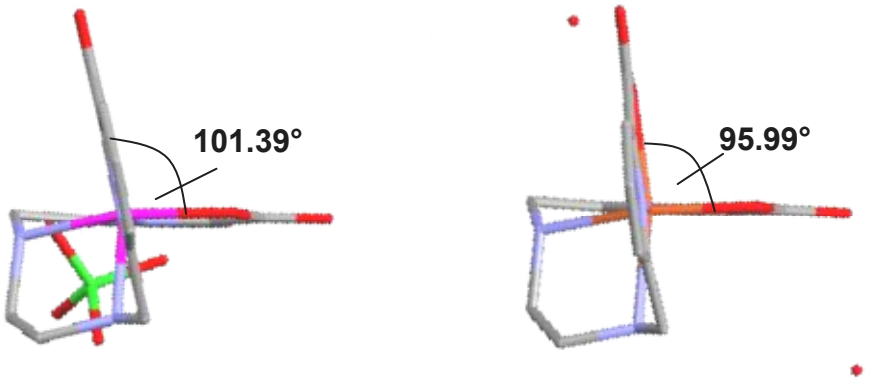

Figure 5.4 Side-on view of [Cu(**dedpa**)] (right), compared to compared to selected bond lengths in [Ga(**dedpa**)]$^+$ (left), H atoms omitted for clarity. Graphic generated using Mercury 2.2.[150]

5.3.2 Cyclic Voltammetry

In order to evaluate the capability of the complex to withstand bio-reductive conditions without reduction of Cu(II) to Cu(I) and subsequent decomplexation, a cyclic voltammogram was measured. A reduction process was observed at -1.12 V (-0.92 V vs. NHE, Figure 5.5), and an oxidation process was observed at 0.02 V (0.22 V vs. NHE, Figure 5.5). The cyclic voltammogram, while irreversible, was found to be reproducible over multiple cycles without decrease of intensities of either peak. In order to show that the two distinct, dissimilar peaks observed are related, a smaller electrochemical potential window was chosen, which excludes the reduction process found at -1.12 V. Subsequently, the oxidation peak at 0.02 was not observed (Figure 5.6); hence, the two peaks are assumed to be related. Due to dissimilar peak shape, it is likely that the coordination mode of **dedpa**$^{2-}$ changes upon reduction.

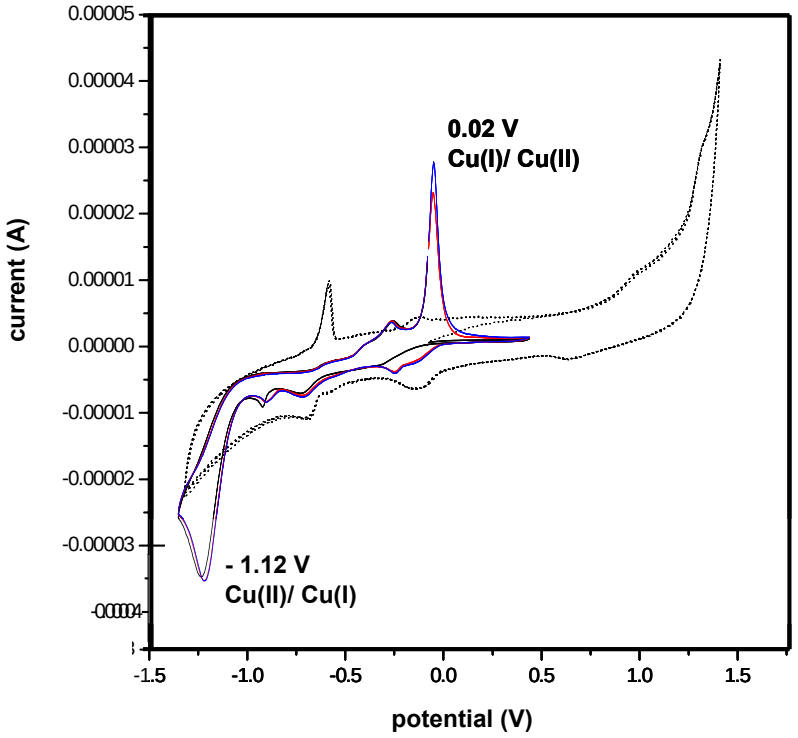

Figure 5.5 Cyclic voltammogram of [Cu(**dedpa**)], -1.25 and 0.5 V (solid line). Also shown is the blank voltammogram with solvent only (dotted, -1.25 – 1.5 V). Potential values are given with reference electrode Ag/AgCl (sat.).

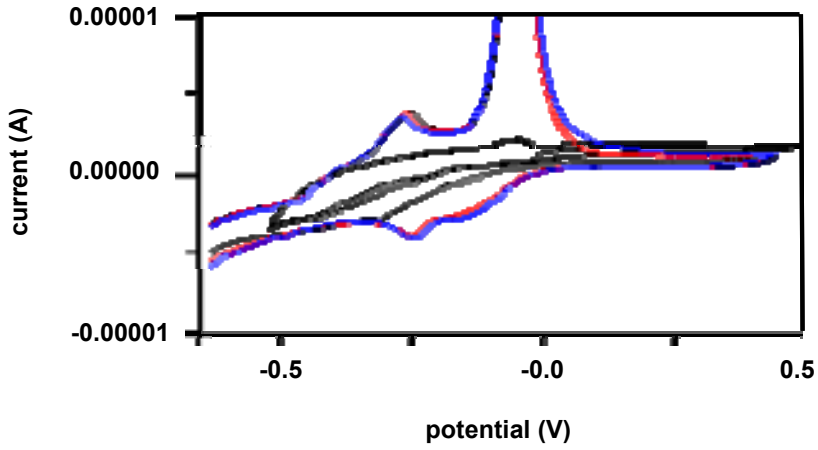

Figure 5.6 [Cu(**dedpa**)], -0.5 and 0.5 V(solid, black line), overlayed with full range voltammogram. Note, how the oxidation peak at 0.02 V is not observed, therefore it could be related to observed reduction peak at -1.12 V. Potential values are given with reference electrode Ag/AgCl (sat.).

Previously reported CV data on Cu(II) complexes with ligands DOTA, TETA, CB-DO2A and CB-TE2A indicate that complexes, which are found to dissociate *in vivo* are also found to produce irreversible voltammograms indicating loss of the metal upon reduction (TETA, CB-DO2A).[149] This was not observed for **dedpa**$^{2-}$, hence no copper is lost in the course of multiple reduction and re-oxidation cycles. The reduction potential well below the -0.4 V (NHE) threshold for bioreductants, suggests that [Cu(**dedpa**)] could have high complex stability *in vivo*.[118]

5.3.3 Labelling with ^{64}Cu and *In Vitro* Stability

Labelling of ^{64}Cu with H_2dedpa proceeds quantitatively with ligand concentrations of 10^{-5} M in ten minutes at room temperature. The stability of the radiochemical complex was measured by a competition experiment in mouse serum. While the complex remains relatively stable over the first two hours (only 3 % transchelation), over the course of 24 h, 23 % of the ^{64}Cu previously coordinated to dedpa^{2-} is associated with serum. It cannot be determined if actual transchelation has happened, or if the complex is still intact but associated with serum proteins as a whole entity. In a related study, the thermodynamic stability constant was found to be log K_{ML} = 20.43.[151] This value is found to be much lower than values determined for stronger chelates such as cyclam, indicating that a transchelation event after 24 h is plausible.

5.4 Conclusions

Evidently H_2dedpa has many promising properties for the coordination of Cu(II) and its radionuclide of interest, ^{64}Cu. The solid state structure shows similarities to the CB-TE2A coordination sphere. Investigations on redox properties of [Cu(**dedpa**)] yielded a reproducible, irreversible cyclic voltammogram with a reduction event at -0.92 V and oxidation at 0.22 V (vs. NHE). While the two events are related but show dissimilar peak shape, it is likely that the ligand system changes its coordination sphere according to the predominant redox species. Labelling of ^{64}Cu proceeds within 10 minutes at room temperature, unlike some of the established ligand systems that require heat and

prolonged reaction times. In a related study, the thermodynamic stability constant was found to be log K_{ML} = 20.76.[151] Together with the reasonable kinetic stability over 2 h in the presence of serum (less than 3 % transchelated), this chelate is likely to have favourable properties for coordination and target specific delivery of ^{64}Cu when conjugated to a targeting molecule. Chapter 6 investigates bifunctional versions of H_2dedpa and its coordination to ^{64}Cu. Once target specific chelates are evaluated *in vivo*, the liver uptake (indicative of transchelated ^{64}Cu) will provide insight into the *in vivo* stability of this scaffold.

Chapter 6: Functionalization of the H_2**dedpa** Scaffold (1): Bioconjugation and Multifunctionality

6.1 Introduction

6.1.1 Modes of Bioconjugation

Chapters 4 and 5 have given a detailed description of the required criteria for an optimal metal chelate with radiometals. In order to achieve target specific delivery of a radionuclide, an actual targeting moiety must be attached to the radiochemical complex in a covalent manner (for receptor mediated delivery) or the chemical and physical properties must be modified to direct the biodistribution of the radiochemical complex. This chapter focuses on conjugation of the H_2**dedpa** scaffold to targeting biomolecules. Many biomolecules have been successfully conjugated to chelate systems and have been used to deliver a radioactive payload; examples are ^{111}In-DTPA-Octreotide and ^{90}Y-Ibitumomab Tiuxetan (Zevalin®), both FDA approved agents.[62] ^{68}Ga-DOTANOC is currently in clinical trials.[152] The main difficulty in conjugating a biomolecule to a chelate system lies in the selective coupling of functional groups, which are non-essential to the coordination chemistry, without interfering with functional groups necessary for coordination. One solution is to coordinate the metal first and conjugate the targeting moiety second. This pre-labelling approach has been explored for isotopes that require reduction using strong agents prior to conjugation, such as ^{99m}Tc and ^{188}Re.[153,154] This is not an option for short-lived radionuclides such as ^{68}Ga. In order to design kit-formulations suitable for clinical applications, which can be used with a variety of radioisotopes, the post-labelling approach is more desirable. The two approaches are summarized in Scheme 6.1 with a hypothetical H_2**dedpa** derivative as the chelate example.

Since post-labelling was selected as the more viable option, orthogonal protection of functional groups must be carried out to promote controlled reaction of specific functional groups. Selective amide coupling (Scheme 6.1) is difficult to control when multiple free carboxylate functionalities are present on the same molecule.

pre-labelling

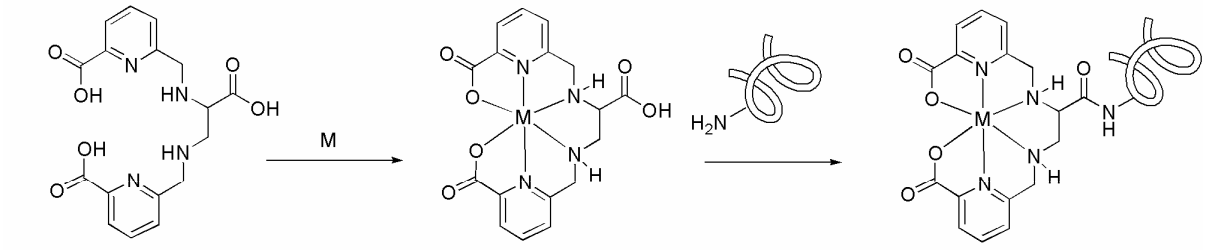

post-labelling

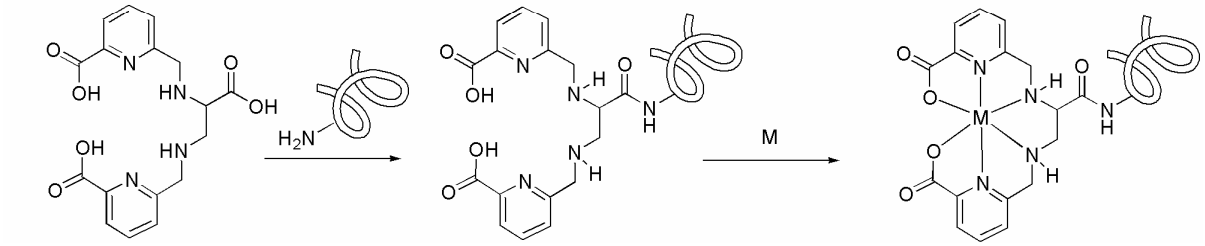

Scheme 6.1 Scheme illustrating pre- and post-labelling approach based on H_2dedpa.

As an added difficulty, the final deprotection step cannot interfere with potentially sensitive functional groups on the targeting biomolecule, and must be done either before coupling of the latter or under conditions mild enough to preserve the native form of the biomolecule. Scheme 6.2 elaborates on possible combinations of functional groups and their corresponding protecting group chemistry combined with different coupling methodologies relevant for H_2dedpa-type chelate systems. Approach ***a*** is a frequently employed coupling method,[155] which requires a *tert*-butyl protection group on the pyridine carboxylate subunit. The synthesis of this fragment failed since this protection group was found to be too labile. Method ***b*** was used with slight modifications in Chapter 3 and is further elaborated in this chapter.[42]

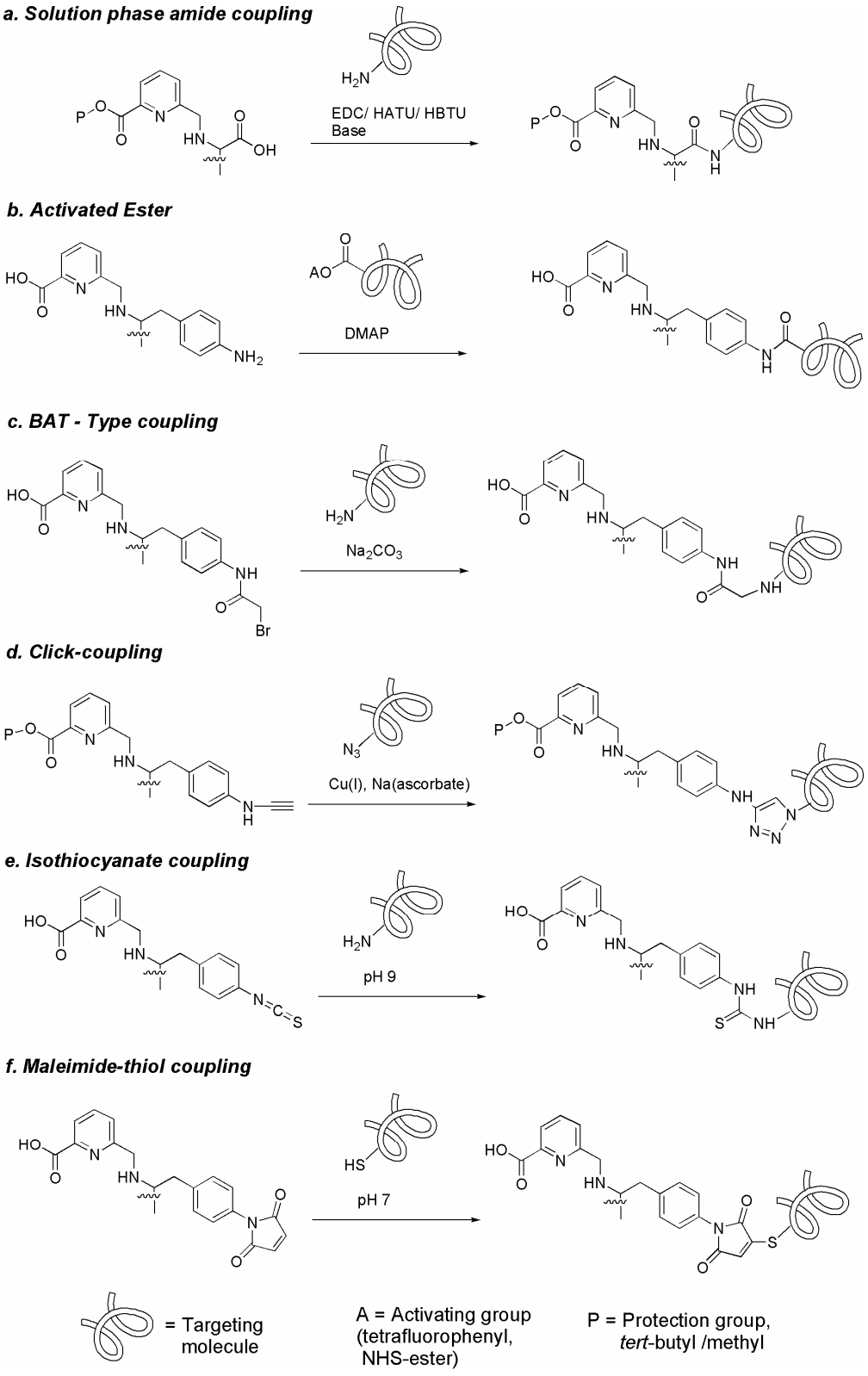

Scheme 6.2 Possible conjugation strategies using H_2dedpa to couple a bifunctional chelate with a targeting molecule.

Method ***c*** has been used previously for conjugation of antibodies to macrocyclic chelates.[156] Because the backbone derivatized H_2**dedpa** derivative contains secondary amines, which could be easily alkylated, this method appears to be a less viable possibility. Method ***d*** entails the currently very popular, Cu(I) catalyzed, Huisgen 1,3-dipolar cycloaddition forming 1,2,3-triazoles. This reaction has been used successfully to furnish a wide variety of chelates, especially for the coordination of the $[^{99m}Tc(CO)_3]^+$ core.[157] The synthesis of a corresponding derivatized alkyne was successfully realized; however, the affinity of the H_2**dedpa/** Me_2**dedpa** scaffold to both Cu(I) and Cu(II) species impedes a clean coupling reaction. A subsequent treatment with highly acidic conditions, in order to remove Cu(II) is not in accordance with the presence of a sensitive biomolecule, hence this route was also abandoned. Method ***e*** has been widely explored and is employed among others, for the formation of Zevalin®.[158] Isothiocyanates are somewhat more shelf stable then NHS-esters, while they display a strong preference for reaction with primary amines to form the thiourea functional group in aqueous media with pH 9-9.5.[159] The successful synthesis and coupling of H_2**dedpa**-isothiocyanato derivatives is described in this chapter. Method ***f*** is limited to targeting molecules containing thiols; however, since optimal reaction conditions are found at pH 7 this is the coupling condition of choice for molecules sensitive to pH > 8.[160]

6.1.2 Convenient Biomolecules for Proof of Principle

In order to prove that a bifunctional chelate is able to deliver its radioactive payload successfully, the chelate must be attached to a targeting molecule with a known target and evaluated for maintained binding efficiency. A variety of benchmark targeting molecules are used for this purpose (Table 6.1), with corresponding assays and animal models readily available. Biotin was also used as bioconjugation proof of principle in Chapter 3. Due to its small size and chemical robustness, it is a convenient moiety for preliminary, simple proof of principle. The corresponding target (avidin, $K_d \sim 10^{-15}$) is readily available and inhibitory assays are, especially in the presence of a radioactively labelled species, straightforward.[42]

For evaluation of targeting molecules with potential applications for tumor imaging, small polypeptides such as c(RGDyK) provide a convenient tool. c(RGDyK) (further referred to as RGD) is a cyclic pentapeptide targeting the vitronectin receptor $\alpha_v\beta_3$, a membrane protein which has been linked to tumor growth and metastatic potential, since it is highly expressed in tissues undergoing angiogenesis.[161] A variety of *in vitro* assays are available, as are animal models where angiogenesis can be easily induced by artery ablation.[162] Since RGD exhibits fast localization and excellent organ clearance, it is well suited for shorter lived radioisotopes such as ^{68}Ga and serves as a convenient tool to investigate chelate induced effects such as poor clearance or organ-specific uptake. Conjugation of a chelate molecule to RGD can be done conveniently using either of methods ***a*** or ***e*** via the primary amine of the Lys residue, because it is not essential for binding to the integrin membrane protein. Other RGD derivatives such as cRGDfD (Asp instead of Lys in the non-binding position) are available, but require additional synthetic steps for conjugation due to necessary orthogonal protection of two Asp residues.[142] Other frequently used target molecules, together with target, structural features and preferred conjugation method are summarized in Table 6.1. While not investigated in this thesis, they might become relevant for future work with the H_2**dedpa** chelate system.

Table 6.1 Summary of frequently used target molecules for imaging and therapy with radiometals.

Target molecule	***In vivo* target**	**Features**	**Conjugation method**
Biotin	Avidin	Small molecule	***a,***[104] ***b,***[42] ***d, e***[163]
RGD	$\alpha_v\beta_3$ integrin	Peptide (5 mer)	***a,***[142] ***b,***[142] ***e***[162]
Bombesin	GRP-receptor	Peptide (8-14 mer)	***a,***[164] ***d***[165]
Somatostatin (OC, TATE, Octreotide)	Somatostatin receptor	Peptide (14 mer)	***a***[166], ***e***[167]

Target molecule	*In vivo* target	Features	Conjugation method
EGF, hEGF Cetuximab	EGF-receptor	Peptide (53 mer) Antibody	***a*[168], *b, e, f***
HER-2/neu Fab4D5	HER-2/neu receptor	Antibody Antibody-fragment	***a*[169], *e, f***

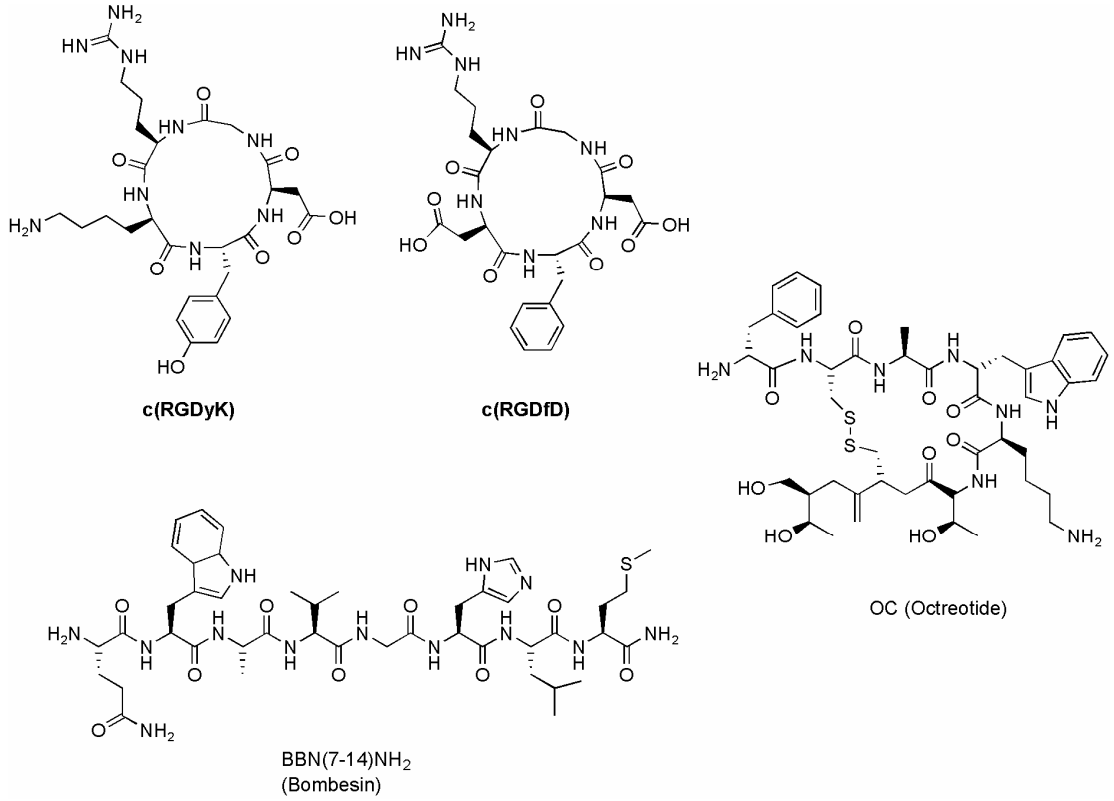

Figure 6.1 Structures of frequently used target molecules for imaging and therapy with radiometals.

6.2 Experimental

6.2.1 Synthesis of Fragments for Coupling

Materials and Methods:

Refer to Chapter 2.2 for general information. HPLC analysis or purification of non-radioactive compounds was done on a Phenomenex Jupiter 5µ C18 300 Å (100 x 4.6 mm) in a Waters WE 600 HPLC system equipped with a 2478 dual wavelength absorbance UV detector controlled by the Empower software package. The HPLC system used for analysis of the radiochemical complexes consists of a Waters Alliance HT 2795 separation module equipped with a Raytest Gabbistar NaI detector and a Waters 996 photodiode array (PDA) detector. Analysis of radiolabeled complexes was done on a Waters XBridge BEH130 4.6 × 150 mm (retention time of ^{67}Ga-Tf: 2.5 min). If not mentioned otherwise, the R_f values are measured on standard TLC plates with 10% CH_3OH in CH_2Cl_2 as the mobile phase.

Common starting materials such as the protected precursor 1,2-[{6-(methoxycarbonyl)pyridin-2-yl}methylamino]ethane[108] were synthesized according to the literature. 6-Bromomethylpyridin-2-carboxylic acid methyl ester was synthesized according to the literature.[170] The synthesis of biotin-TFP has been reported,[104] as has the synthesis of the precursor 3-(4-nitro-phenyl)-propane-1,2-diamine.[133]

General procedure for synthesis of non-radioactive Ga complexes: the ligand was dissolved in a CH_3OH-water mixture (1:2) and acidified to pH 2 by addition of 0.1 M HCl. $Ga(NO_3)_3 \cdot 6H_2O$ (1 eq) was added and the pH was adjusted by addition of 0.1 M NaOH to 4.5. The reaction mixture was stirred at 60 °C for 2 h. The solvent was removed *in vacuo* to afford the complex as a white solid in quantitative yield.

(1,2-[N, N'-{*p*-Benzylamino-*tert*-butyl carbamato} methyl]-N, N'-[6-{methoxycarbonyl} -pyridin-2-yl] methylamino)ethane (1).

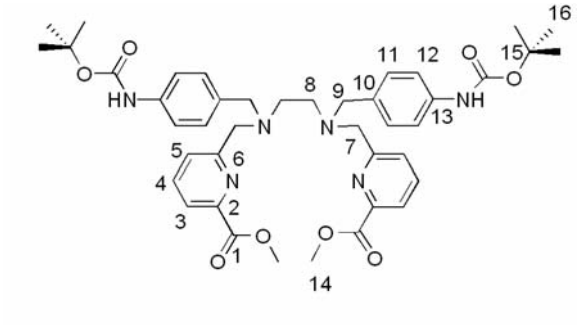

1,2-[{6-(Methoxycarbonyl)pyridin-2-yl}methylamino]ethane (23 mg, 0.064 mmol) and (4-bromomethyl-phenyl)-carbamic acid tert-butyl ester (38 mg, 0.135 mmol, 2.1 eq) were dissolved in acetonitrile (80 mL). Na_2CO_3 (400 mg) was added into the reaction mixture and it was stirred at 60°C over night (Scheme 6.3). The resulting milky solution was filtered and the solvent was removed *in vacuo* to afford the crude product as an oil, which was subsequently purified by column chromatography (10% CH_3OH in CH_2Cl_2) to afford **1** as a very viscous, colourless oil (19 mg, 0.024 mmol, 38 % R_f: 0.5). ^{1}H NMR ($CDCl_3$, 400 MHz, δ): 7.97 (d, $^3J_{4,5}$ = 7.1 Hz, *H5*, 2H), 7.70 (d, $^3J_{4,5}$ = 7.1 Hz, *H4*, 2H), 7.24 – 7.14 (m, $^3J_{11,12}$ = 7.7 Hz, *H3, H11*, *H12*, 10H), 6.58 (s, CO-N*H*, 2H), 3.98 (s, *H14,* 6H), 3.81 (s, *H7,* 4H), 3.49 (s , *H9,* 4H), 2.62 (s, *H8,* 4H), 1.52 (s, *H16,* 18H).^{13}C NMR ($CDCl_3$, 100 MHz, δ): 163.1 (*C*O-NH), 161.5 (*C1*), 158.3 (*C6*), 153.0 (*C2*), 147.3 (*C13*), 137.5 (*C10*), 129.5 (*C4*), 118.8 (*C11*), 58.7 (*C7*), 58.6 (*C9*), 53.6 (*C14*), 53.1 (*C15*), 28.6 (*C16*). IR (neat, cm^{-1}): 1716 (s), 1525 (m), 1313 (s), 1232 (s), 1157 (s). HR-ESI-MS: *m/z* calcd. for $C_{42}H_{52}N_6NaO_8$: 791.3744, found: 791.3730 $[M + Na]^+$. Elemental Analysis: calcd. (found) for for **1**·CH_3OH: C: 64.74 (64.49), H: 6.65 (6.73), N: 10.53 (10.31).

(1,2-[N,N'-{*p*-Benzylamino}methyl]-N,N'-[6-{methoxycarbonyl}-pyridin-2-yl] methylamino)ethane (2).

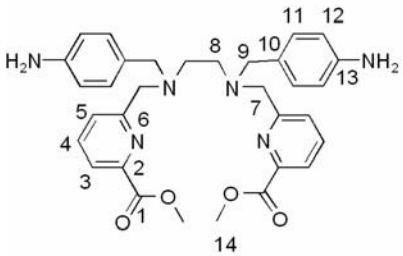

1 (20 mg, 0.026 mmol) was dissolved in 2 mL CH_2Cl_2. TFA (0.5 mL) was added and the reaction mixture was stirred for 1 h. The acid was then quenched with saturated $NaHCO_3$ (20 mL) and the aqueous solution was then extracted twice with EtOAc (20 mL) and twice with CH_2Cl_2 (20 mL). All organic fractions were collected and dried over $MgSO_4$. The solvent was removed *in vacuo* to subsequently afford the free

amine **2** as a yellow oil which was immediately used in the follow-up reaction (3 mg, 0.005 mmol, 22 % R_f: 0.1). ^{1}H NMR ($CDCl_3$, 400 MHz, δ): 7.98 (d, $^3J_{4,5}$ = 6 Hz, *H5*, 2H), 7.71 (m, $^3J_{4,5}$ = 6 Hz, *H3*, *H4,* 4H), 7.06 (d, $^3J_{11,12}$ = 8 Hz, *H11*, 4H), 6.59 (d, $^3J_{11,12}$ = 8 Hz, *H12*, 4H), 4.02 (s, *H14,* 6H), 3.81 (s, *H7,* 4H), 3.47 (s, *H9,* 4H), 2.65 (s, *H8,* 4H). HR-ESI-MS: *m/z* calcd. for $C_{32}H_{37}N_6O_4$: 569.2869, found: 569.2869 $[M + H]^+$.

(1,2-[N,N'-{*p*-Benzyl-isothiocyanato}-methyl]-N,N'-[6-{carboxylato}-pyridin-2-yl] methylamino)ethane (3, H_2dp-N-NCS).

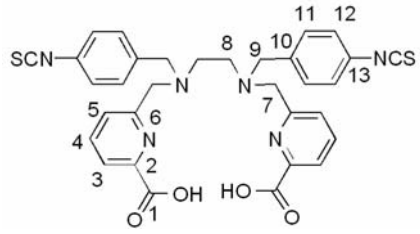

Compound **1** (13 mg, 0.069 mmol) was dissolved in a 3:1 mixture of THF and H_2O. LiOH (8 mg, 0.3 mmol) was added to the reaction mixture and the reaction was stirred for 1 h at room temperature to afford the free carboxylate intermediate. Reaction monitoring was performed via TLC and analytical HPLC ($R_{t(\mathbf{1})}$ = 18.3 minutes, $R_{t(intermediate)}$ = 15.8 minutes). The solvent was removed *in vacuo* and the intermediate was redissolved in 3 M HCl solution (2 mL) and stirred for 2 h to remove the *t*-Boc protecting groups. Again, HPLC was used to confirm full conversion of the intermediate into the fully deprotected second intermediate ($R_{t(sec.\ intermediate)}$ = 9.4 minutes). $CHCl_3$ (1 mL) and $SCCl_2$ (106 µL, 20 eq) were added and the biphasic reaction was stirred vigorously for 18 h at room temperature to afford the final product **3** as a white precipitate; it was collected by vacuum filtration to yield 11 mg (0.017 mmol, 24 %, $R_{t(\mathbf{3})}$ = 18.0 minutes). ^{1}H NMR (400 MHz, CD_3OD, δ): 8.11 (d, $^3J_{3,4}$= 7.5 Hz, *H3,* 2H), 8.02 (m, $^3J_{3,4}$= 7.5 Hz, $^3J_{4,5}$= 7.9 Hz, *H4,* 2H) 7.59 (d, $^3J_{4,5}$= 7.9 Hz, *H5,* 2H), 7.50 (d, $^3J_{11,12}$= 8.5 Hz, *H12,* 2H), 7.21 (d, $^3J_{11,12}$= 8.5 Hz, *H11,* 2H), 4.52 (s, *H7*, 4H), 4.32 (s, *H9*, 4H), 3.65 (s, *H8*, 4H). ^{13}C NMR (100 MHz, CD_3OD, δ): 165.6 (*C1*), 154.2 (*C6*), 147.5 (*C2*), 138.5 (*C10*), 136.2 (N*C*S), 133.9 (*C4*), 131.8 (*C5*), 130.1 (*C13*), 126.9 (*C3*), 125.9 (*C12*), 123.9 (*C11*), 57.0 (*C7*), 56.3 (*C9*), 49.0 (*C8*). IR (neat, cm^{-1}): 2023 (s, br), 1731 (m), 1595 (w), 1505 (m), 1344 (m). HR-ESI-MS: *m/z* calcd. for $C_{32}H_{27}N_6O_4{}^{32}S_2$: 623.1535, found: 623.1542 $[M - H]^-$.

[N, N'-Bis{benzylamino}] 3-(4-Nitrophenyl)-propane-1,2-diamine (4).

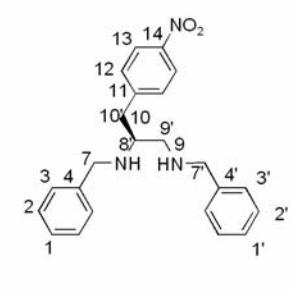

3-(4-Nitrophenyl)-propane-1,2-diamine (204 mg, 1.046 mmol) was dissolved in 40 mL EtOH together with benzaldehyde (221 mg, 0.213 mL, 2.084 mmol) and the flask was cooled in an ice bath (Scheme 6.4). After two hours of reaction, the imine intermediate was confirmed through mass spectrometry. $NaBH_4$ (80 mg, 2.5 mmol) was added to the reaction mixture at 0 °C and the reaction was stirred for another two hours. Subsequently the reaction was quenched with a saturated aqueous solution of NH_4Cl (20 mL) and the product was extracted with 200 mL CH_2Cl_2. After removal of the solvent, **4** was afforded as an orange oil (378 mg, 1.01 mmol, 97% R_f: 0.1). ^{1}H NMR ($CDCl_3$, 400 MHz, δ): 8.13 (d, $^3J_{12,\ 13}$ = 8.2 Hz, *H13,* 2H), 7.38 – 7.27 (m, $^3J_{12,\ 13}$ = 8.2 Hz, *H1-H3, H1'-H3',H12,* 12H), 3.79 - 3.70 (d, $^2J_{7,\ 7}$ = 13.2 Hz, *H7, H7',* 4H), 2.96 (m, $^3J_{8,\ 9}$ = 8.8 Hz, $^2J_{9,\ 9'}$ = 15.2 Hz, *H8', H9,* 2H), 2.81 (dd, $^3J_{8,\ 9'}$ = 8.8 Hz, $^2J_{9,\ 9'}$ = 15.2 Hz, *H9',* 1H), 2.63 (dd, $^3J_{8,\ 10}$ = 3.6 Hz, $^2J_{10,\ 10'}$ = 12.0 Hz, *H10,* 1H), 2.52 (dd, $^3J_{8,\ 10'}$ = 6.9 Hz, $^2J_{10,\ 10'}$ = 12.0 Hz, *H10',* 1H). ^{13}C NMR ($CDCl_3$, 100 MHz, δ): 147.2 (*C14*), 146.4 (*C11*), 141.0, (*C4*) 139.9 (*C12*), 129.9 (*C3*), 128.4 (*C3'*), 128.3 (*C2*), 128.0 (*C2'*), 127.4 (*C1*), 127.0 (*C1'*), 123.5 (*C13*), 64.9 (*C7*), 57.5 (*C7'*), 53.6 (*C8*), 51.3 (*C9*), 38.9 (*C10*). HR-ESI-MS: *m/z* calcd. for $C_{32}H_{26}N_3O_2$: 376.2025, found: 376.2019 $[M + H]^+$.

[N,N'-Bis{benzylamino}]3-(4-nitrophenyl)-propane-1,2-diamino-N,N'-[6-methoxycarbonyl}-pyridin-2-yl]methylamine (5).

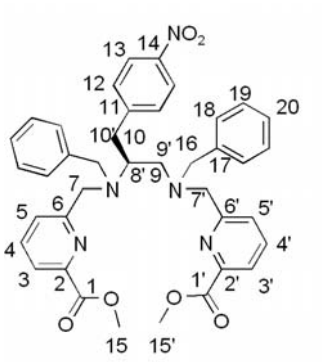

Compound **4** (181 mg, 0.48 mmol) and 6-bromomethyl-pyridine-2-carboxylic acid methyl ester (225 mg, 0.97 mmol, 2 eq) were dissolved in acetonitrile (35 mL). Na_2CO_3 (0.5 g) was added and stirred overnight at 70 °C. The milky yellow solution was filtered and the solvent was removed from the filtrate. The crude product was purified with column chromatography (5 % CH_3OH in CH_2Cl_2) to afford **5** as a yellow solid (78 mg, 0.12 mmol, 25 % R_f: 0.6). ^{1}H NMR ($CDCl_3$, 400 MHz, δ): 8.02 (d, $^3J_{12,\ 13}$ = 8.5 Hz, *H13,* 2H), 8.00 – 7.08 (m, *H18-20, H3/3'-H5/5',*16H), 7.05 (d, $^3J_{12,\ 13}$ =

8.5 Hz, *H12,* 2H), 4.01 (s, *H15/H15',* 6H), 3.94 (s, *H16/H16',* 6H), 3.90 – 3.48 (d, $^{2}J_{7,\ 7}$ = 10.8 Hz, $^{2}J_{7',\ 7'}$ = 13.7 Hz, *H7/H7',* 4H), 3.18 (m, $^{3}J_{8,\ 9}$ = 8.7 Hz, $^{3}J_{8,\ 9'}$ = 8.2 Hz, $^{3}J_{8,\ 10'}$ = 5.3 Hz , *H8',* 1H), 2.97 (dd, $^{2}J_{10,\ 10'}$ = 13.2 Hz, $^{3}J_{8,\ 10'}$ = 5.3 Hz, *H10/10',* 2H), 2.58 (dd, $^{2}J_{9,\ 9'}$ = 13.4 Hz, $^{3}J_{8,\ 9}$ = 8.7 Hz, *H9,* 1H), 2.53 (dd, $^{2}J_{9,\ 9'}$ = 13.4 Hz, $^{3}J_{8,\ 9'}$ = 8.2 Hz, *H9',* 1H). ^{13}C NMR ($CDCl_3$, 100 MHz, δ): 165.6 (*C1/1'*), 160.5 (*C6*), 160.4 (*C6'*), 148.9 (*C2/2'*), 146.9 (*C14*), 146.1 (*C11*), 138.8 (*C4/4'*), 138.6 (*C17*), 130.0 (*C12*), 128.8 (*C18*), 128.4 (*C19*), 128.2 (*C20*), 127.4 (*C5*), 126.8 (*C5'*), 125.6 (*C13*), 123.5 (*C3*), 123.1 (*C3'*), 65.2 (*C7'*), 61.0 (*C16*), 59.6 (*C8*), 58.6 (*C9*), 53.9 (*C7*), 53.7 (*C16*), 53.4 (*C15*), 52.8 (*C15'*), 35.8 (*C10*). IR (neat, cm^{-1}): 1719 (s), 1514 (m), 1342 (s), 1315 (m). HR-ESI-MS: *m/z* calcd. for $C_{39}H_{40}N_5O_6$: 674.2979, found: 674.2960 $[M + H]^+$. Elemental Analysis calcd. (found) for **6**·$2CH_2Cl_2$: C: 58.37 (58.36), H: 5.10 (5.05), N: (8.30)8.72.

3-(4-Aminophenyl)-1,2-diamino-N,N'-bis[6-{methoxycarbonyl}-pyridin-2-yl] methylamino-propane (6, Me_2dp-bb-NH_2).

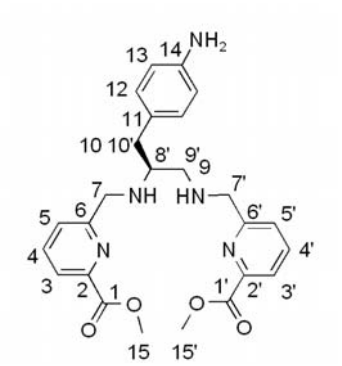

Compound **5** (302 mg, 0.44 mmol) was dissolved in glacial acetic acid (20 mL). Pd/C (10% w/w, 80 mg) was added and the mixture was charged with H_2 in a balloon and stirred overnight at room temperature. The reaction was found to be complete according to TLC (product stains bright purple with ninhydrin). $Pd(OH)_2$ was filtered off and the solvent was removed *in vacuo* to afford the pure product **6** as the tri-acetate salt (149 mg, 0.32 mmol, 72 %, R_f: 0.05). ^{1}H NMR ($CDCl_3$, 400 MHz, δ): 8.00 – 7.62 (m, *H5/5', H4,* 3H), 7.56 (m, $^{3}J_{3,\ 4}$ = 7.6 Hz, *H3,* 1H), 7.46 (m, $^{3}J_{3,\ 4}$ = 7.6 Hz, *H3',* 1H), 7.32 (m, *H4',* 1H), 6.91 (d, $^{3}J_{12,\ 13}$= 7.9 Hz, *H12,* 2H), 6.56 (d, $^{3}J_{12,\ 13}$= 7.9 Hz, *H13,* 2H), 4.76 – 4.09 (dd, $^{2}J_{7,\ 7}$ = 16.5 Hz, $^{2}J_{7',\ 7'}$ = 17.1 Hz, *H7/H7',* 4H), 3.95 (s, N*H*$_2$, 2H), 3.81 (s, *H15,* 3H), 3.79 (s, *H15',* 3H), 3.63 (m*, H8',* 1H), 3.02 (dd, $^{3}J_{8,\ 10'}$ = 6.9 Hz, *H10/10',* 2H), 3.04 (dd, $^{2}J_{9,\ 9'}$ = 14.0 Hz, $^{3}J_{8,\ 9'}$ = 6.4 Hz, *H9',* 1H), 2.72 (dd, $^{2}J_{9,\ 9'}$ = 14.0 Hz, $^{3}J_{8,\ 9}$ = 8.2 Hz, *H9,* 1H), 2.61 (s, N*H*, 2H). ^{13}C NMR ($CDCl_3$, 100 MHz, δ): 164.9 (*C1'*), 164.7 (*C1*), 146.9 (*C2'*), 146.6 (*C2*), 144.7 (*C14*), 138.3 (*C4*), 137.2 (*C4'*), 129.9 (*C11*), 126.9 (*C6*), 126.2 (*C6'*), 126.0 (*C12*), 125.8 (*C5*), 124.3 (*C5'*), 124.0 (*C3*), 122.3 (*C3'*), 115.7 (*C13*), 57.1 (*C7'*), 53.5 (*C9*), 52.7 (*C8*), 52.6

(*C7*), 49.7 (*C15*), 48.7 (*C15'*), 35.9 (*C10*). HR-ESI-MS: *m/z* calcd. for $C_{25}H_{29}N_5O_4Na$: 486.2117, found: 486.2111 $[M + Na]^+$.

3-(4-Isothiocyanatophenyl)-propane-1,2-diamino-N,N'-bis[6-{carboxylato}-pyridin-2-yl] methylamine (7, H_2dp-bb-NCS).

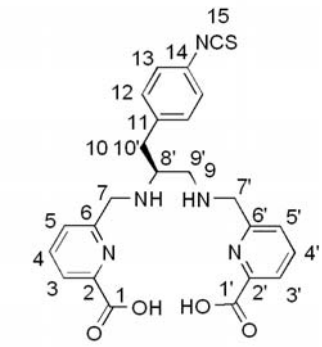

Compound **6** (10 mg, 0.023 mmol) was dissolved in 3 M HCl (1 mL) to which $CHCl_3$ (1 mL) and $SCCl_2$ (19 µL, 10 eq) were added. The biphasic reaction was stirred vigorously for 18 h at room temperature. Subsequently, the solvent was removed and the crude was purified by preparative HPLC. The clean fractions were pooled and lyophilized to afford the final product as a yellow solid (3 mg, 0.006 mmol, 26 % $R_{t(7)}$= 13 minutes. ^{1}H NMR (400 MHz, CD_3OD, δ): 8.17 – 8.06 (m, *H3/3', H4/4',* 4H), 7.70 (m, *H5/5',* 2H), 7.08 (d, $^3J_{12,\ 13}$= 8.4 Hz, *H13,* 2H), 7.26 (d, $^3J_{12,\ 13}$= 8.4 Hz, *H12,* 2H), 4.78 – 4.59 (dd, $^2J_{7,\ 7}$ = 16 Hz, *H7/H7',* 4H), 3.69 (m*, H8',* 1H), 3.37 (dd, $^3J_{8,\ 10'}$ = 3.2 Hz, *H10/10',* 2H), 3.32 – 2.85 (dd, $^2J_{9,\ 9'}$ = 13.7 Hz, $^3J_{8,\ 9}$ = 9.7 Hz, *H9,* 1H). ^{13}C NMR (125 MHz, CD_3OD, δ): 168.8 (*C1'*), 168.2 (*C1*), 162.7 (*C6*), 162.4 (*C6'*), 150.0 (*C2*), 149.6 (*C2'*), 139.6 (*C4*), 139.1 (*C4'*), 134.2 (N*C*S) , 133.1 (*C11*), 129.9 (*C12*), 129.8 (*C5*), 129.6 (*C14*), 125.9 (*C5'*), 125.8 (*C13*), 125.4 (*C3*), 124.3 (*C3'*), 56.7 (*C8*), 49.6 (*C7'*), 47.0 (*C9*), 46.3 (*C7*), 34.0 (*C10*). IR (neat, cm^{-1}): 2076 (s, br), 1634 (m), 1505 (w), 1394 (m), 1346 (w). HR-ESI-MS: *m/z* calcd. for $C_{24}H_{22}N_5O_4{}^{32}S$: 476.1393, found: 476.1405 $[M - H]^-$.

Me_2dp-N-biotin (8).

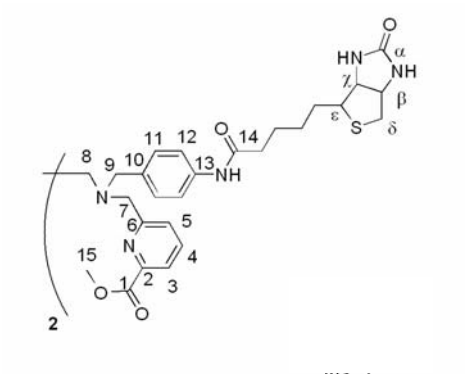

2 (48 mg, 0.084 mmol) was dissolved in DMF (5 mL) together with biotin-TFP (76 mg, 0.19 mmol, 2 equ.) and NEt_3 (73 µL) and stirred at 55 °C for 20 h. Subsequently, the solvent was removed and the resulting colourless solid was purified by column chromatography (aluminium oxide, 10% CH_3OH in CH_2Cl_2) to afford the dialkylated product **8** as a white solid (9 mg, 0.009 mmol, 10 % R_f: 0.5 on aluminium oxide, 10% CH_3OH in CH_2Cl_2). ^{1}H NMR (d_6-DMSO, 400 MHz, δ): 9.80 (s, CO-N*H*, 2H), 7.87 (m, $^3J_{3,4}$ = 5.7 Hz, $^3J_{3,5}$ = 3.2 Hz, *H5, H4*, 2H), 7.62 (d, $^3J_{3,4}$ = 5.7 Hz, $^4J_{3,5}$ = 3.2 Hz, *H3*, 2H), 7.47 (d, $^3J_{11,12}$ = 8.5 Hz, *H12*, 4H), 7.16 (d, $^3J_{11,12}$ = 8.5 Hz, *H11*, 4H), 6.42 – 6.35 (s, CO-N*H*, 4H), 4.29 (m, $^3J_{\delta,\beta}$ = 5.0 Hz, *Hβ*, 2H), 4.06 (m, *Hχ,* 2H), 3.85 (s, *H15*, 6H), 3.65 (s, *H7*, 4H), 3.45 (s, *H9*, 4H), 3.16 (m, *Hε*, 2H), 2.83 – 2.79 (dd, $^2J_{\delta,\delta}$ = 12.6 Hz, $^3J_{\delta,\beta}$ = 5.0 Hz, *Hδ*, 4H), 2.56 (m, *H9*, 4H), 2.28 (m, CH_2, 4H), 1.63 – 1.23 (m, CH_2, 10H). ^{13}C NMR (d_6-DMSO, 100 MHz, δ): 171.0 (*C*O-NH), 162.7 (*Cα*), 160.3 (*C1*), 138.1 (*C6*), 137.7 (*C13, C4*), 133.3 (*C10*), 129.0 (*C11*), 126.0 (*C5*), 123.2 (*C12*), 118.8 (*C3*), 61.0 (*C7*), 59.2 (*Cχ*), 57.7 (*Cβ*), 55.4 (*Cε*), 54.9 (*Cβ*), 52.4 (*C8*), 50.8 (*C15*), 40.0 (*Cδ*), 36.2, 28.3, 28.1, 25.2. HR-ESI-MS: *m/z* calcd. for $C_{52}H_{65}N_{10}O_8{}^{32}S$: 1021.4428, found: 1021.4451 $[M + H]^+$.

H_2dp-N-biotin (9).

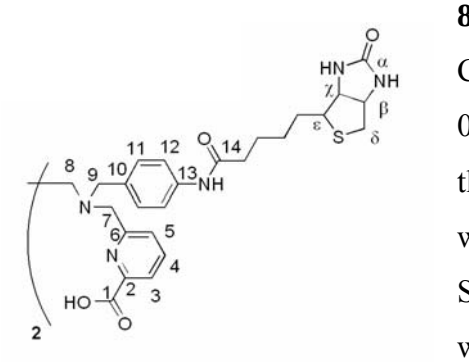

8 (7 mg, 0.007 mmol) was dissolved in a 1:3 mixture of CH_3OH and H_2O (2 mL total volume). LiOH (1 mg, 0.041 mmol, 6 eq) was added to the solution which was then stirred at room temperature for 2 h. The reaction was found to be complete after 2 h according to TLC. Subsequently, the solvent was removed to afford **9** as a white solid (yield: 6 mg, 0.006 mmol, 85 %, R_f: 0.15). ^{1}H NMR (d_6-DMSO, 400 MHz, δ): 9.83 (s, 2H, CO-N*H*), 7.87 (m, $^3J_{3,4}$ = 7 Hz, $^4J_{3,5}$ = 1.2

Hz, *H5, H4*, 4H), 7.47 (d, $^{3}J_{11,\,12}$ = 8.2 Hz, *H12*, 4H), 7.33 (d, $^{3}J_{3,\,4}$ = 7 Hz, $^{4}J_{3,\,5}$ = 1.2 Hz, *H3*, 2H), 7.06 (d, $^{3}J_{11,\,12}$ = 8.2 Hz, *H11*, 4H), 6.43 – 6.34 (d, 4H, CO-N*H*), 4.30 (m, $^{3}J_{\delta,\,\beta}$ = 4.8 Hz, *Hβ*, 2H), 4.19 (m, *Hχ*, 2H), 3.59 (s, *H7,* 4H), 3.38 (s, *H9,* 4H), 3.24 (m, CH_2, 4H), 2.83 – 2.81 (dd, $^{3}J_{\delta,\,\beta}$ = 4.8 Hz, $^{2}J_{\delta,\,\delta}$ = 12.3 Hz, *Hδ*, 2H), 2.57 (d, $^{2}J_{\delta,\,\delta}$ = 12.3 Hz, *Hδ*, 2H), 2.30 (d, $^{3}J_{CH_2}$= 7.7 Hz, CH_2, 2H), 2.23 (s, *H8,* 4H), 1.62 – 1.29 (m, CH_2, 12H).^{13}C NMR (d_6-DMSO, 100 MHz, δ): 171.0 (*C*O-NH), 167.6 (*Cα*), 162.8 (*C1*), 157.5 (*C12*), 155.8 (*C13*), 138.2 (*C6*), 137.9 (*C4*), 131.8 (*C10*), 129.5 (*C11*), 124.0 (*C12*), 121.6 (*C5*), 118.8 (*C3*), 61.0 (*C7*), 59.2 (*Cχ*), 58.7 (*Cβ*), 56.9 (*Cε*), 55.4 (*C8*), 40.0 (*Cβ*), 36.2 (*Cδ*), 29.5, 28.3, 28.1, 25.2. IR (neat, cm^{-1}): 1667 (s), 1573 (m), 1512 (s), 1428 (s), 1382 (s). HR-ESI-MS: *m/z* calcd. for $C_{50}H_{58}{}^{7}LiN_{10}O_8{}^{32}S$: 997.4041 found: 997.4065 $[M -2H + Li]^+$.

6.2.2 Thiourea Coupling with [c(RGDyK)]

General procedure for RGD coupling: the cyclic RGD peptide (3 mg, 0.0048 mmol) was dissolved in aqueous buffered solution (0.1 M $NaHCO_3$, pH 9 - 9.5, 1.5 mL). The isothiocyanate (H_2**dp-bb-NCS**: 1.9 mg, 0.004 mmol or H_2**dp-N-NCS:** 1.3 mg, 0.0022 mmol) was dissolved in CH_3OH (0.5 mL). The two solutions were mixed and stirred at room temperature for 18 h in the dark. The solvent was subsequently removed and the crude product was redissolved in a minimal amount of a MeCN/H_2O mixture (1:2) and then purified via semi-preparative HPLC. A Phenomenex Jupiter 5u C18 300 A 4.6 × 100 mm HPLC column was used. The gradient consisted of A(100%) – B(100%) in 25 minutes at 1mL/ min flow rate (A: H_2O, 0.1 % TFA; B: MeCN).The fractions containing the desired product were pooled and the solvent was removed to afford the RGD conjugates as white solids in approximately 45 % yield. The product was analyzed with ESI-MS.

H_2**dp-bb-NCS-RGD:** R_t: 10.5 min; $[M - H]^-$ = 1862.0 (calculated for $C_{87}H_{110}N_{23}O_{20}S_2$: 1861.8).

H_2**dp-N-NCS-RGD:** R_t: 11.5 min; $[M + H]^+$ = 1097.6 (calculated for $C_{51}H_{65}N_{14}O_{12}S$: 1097.5).

6.2.3 Coordination Chemistry with Ga

[Ga(dp-N-biotin)](NO$_3$).

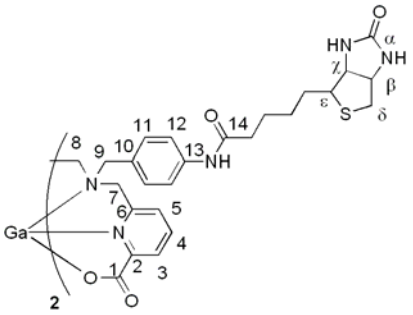

The Ga complex of **4** was synthesized according to general procedure (see 6.2.1). ^{1}H NMR (d$_6$-DMSO, 400 MHz, δ): 10.13 (s, 2H, CO-N*H*), 8.67 (m, $^{3}J_{3,4}$ = 8.2 Hz, $^{3}J_{4,5}$ = 7.5 Hz, *H4*, 2H), 8.36 (m, $^{3}J_{4,5}$ = 7.5 Hz, *H5,* 2H), 8.23 (m, $^{3}J_{3,4}$ = 8.2 Hz, *H3*, 2H), 7.64 (d, $^{3}J_{11,12}$ = 8.6 Hz, *H12*, 4H), 7.36 (d, $^{3}J_{11,12}$ = 8.6 Hz, *H11*, 4H), 6.41 – 6.36 (d, 4H, CO-N*H*), 4.98 – 4.06 (dd, $^{2}J_{7,7}$ = 16.3 Hz, *H7,* 4H), 4.31 (m, $^{3}J_{\chi,\beta}$ = 7.8 Hz, $^{3}J_{\delta,\beta}$ = 4.4 Hz, *Hβ*, 2H), 4.21 (m, $^{3}J_{\chi,\beta}$ = 7.8 Hz, $^{3}J_{\chi,\varepsilon}$ = 4.1 Hz, *Hχ*, 2H), 3.78 – 3.75 (dd, $^{3}J_{9.9}$ = 12.9 Hz, *H9,* 4H), 3.16 (m, $^{3}J_{\chi,\varepsilon}$ = 4.1 Hz, *Hδ,* 2H) 3.04 – 2.85 (dd, $^{3}J_{8.8}$ = 11.2 Hz, *H8,* 4H), 2.83 – 2.81 (m, 6H), 2.81 – 2.55 (dd, $^{3}J_{\delta,\beta}$ = 4.4 Hz, $^{2}J_{\delta,\delta}$ = 12.3 Hz, *Hδ*, 2H), 2.31 (d, $^{3}J_{CH_2}$= 7.5 Hz, C*H*$_2$, 2H), 1.62 – 1.32 (m, C*H*$_2$, 12H). ^{13}C NMR (d$_9$-DMSO, 75 MHz, δ): 171.5 (*C*O-NH), 162.7 (*Cα*), 162.4 (*C1*), 151.0 (*C12*), 146.5 (*C13*), 143.6 (*C6*), 140.1 (*C4*), 132.7 (*C10*), 128.4 (*C11*), 124.4 (*C12*), 123.3 (*C5*), 118.7 (*C3*), 61.1 (*C7*), 59.2 (*Cχ*), 55.9 (*Cβ*), 55.4 (*Cε*), 53.7 (*C8*), 46.1 (*Cβ*), 40.0 (*Cδ*), 36.3, 29.8, 28.2, 28.1, 25.1. HR-ESI-MS: *m/z* calcd. for $C_{50}H_{58}{}^{69}GaN_{10}O_8{}^{32}S$: 1059.3136, found: 1059.3145 $[M]^+$.

6.2.4 Radiolabelling with $^{67/68}$Ga, and Transferrin Stability

General procedure for labelling with $^{67/68}$Ga: 100 µL of $^{67}Ga^{3+}$ (1 mCi, in 0.01 N HCl) or $^{68}Ga^{3+}$ (0.1 M HCl) was added into 10^{-4} M or 10^{-6} M solution of ligand in 10 mM NaOAc solution (pH 4.5, 950 µL) and left to react for 10 minutes at room temperature. The reaction was monitored by analytical HPLC (gradient: A: NaOAc buffer, pH 4.5, B: CH_3CN. 0-100% B linear gradient 20 min). Transferrin competition: $^{67}GaCl_3$ was added into 10^{-4} M (H$_2$**dp-N-biotin)** or 10^{-6} M (H$_2$**dp-bb-NCS-RGD,** H$_2$**dp-N-NCS-RGD**) solution of ligand in 10 mM NaOAc solution (pH 4.5, 950 µL). Complex formation was followed by HPLC. A 400 µL aliquot was added to 1 mg/ mL apo-transferrin in a

$NaHCO_3$ solution (10 mM, 600 µL) and incubated at 37 °C (water bath). Complex stability was followed at time points 10 minutes, 1 h and 2 h via analytical HPLC (for biotin-conjugate). PD-10 size-exclusion columns were used to determine the stability of the RGD conjugates, since the decomposition product could not be observed with previously used HPLC methods. Reaction mixtures were loaded onto the pre-rinsed PD-10 columns (total loading volume: 2.5 mL). Subsequently, the column was rinsed with 3.5 mL PBS. The resulting eluate was collected and measured for radioactivity. The activity eluted corresponds to transferrin-bound ^{67}Ga.

[^{67}Ga(dp-N-Biotin)]$^+$: R_t of radiolabelled product on HPLC (gradient: A: NaOAc buffer, pH 4.5, B: CH_3CN. 0-100% B linear gradient 20 min): 9.1 minutes. Stability versus transferrin (10 min/1 h/ 2 h; in % complex intact): 76/ 55/ 43.
[$^{67/68}$Ga(dp-bb-NCS-RGD)]$^+$: R_t of ^{67}Ga radiolabelled product on HPLC (gradient: A: NaOAc buffer, pH 4.5, B: CH_3CN. 0-100% B linear gradient 20 min): 6.4 minutes. Stability versus transferrin (10 min/1 h/ 2 h; in % complex intact): 96/ 93/ 92.
[$^{67/68}$Ga(dp-N-NCS-RGD)]$^+$: R_t of ^{67}Ga radiolabelled product on HPLC (gradient: A: NaOAc buffer, pH 4.5, B: CH_3CN. 0-100% B linear gradient 20 min): 7.6 minutes. Stability versus transferrin (10 min/1 h/ 2 h; in % complex intact): 92/ 73/ 73.

6.2.5 Radiolabelling with ^{64}Cu, and Serum Stability

100 µL of $^{64}Cu^{2+}$ (0.7 mCi, in dilute HCl) was added to 900 µL of a 10^{-5} or 10^{-6} M solution of ligand in 10 mM NaOAc solution (pH 5.5, 950 µL) and left to react for 10 minutes at RT. The reaction progress was monitored by analytical HPLC (gradient: A: H_2O, 0.1 % TFA, B: CH_3CN. 5-100% B linear gradient 30 min). Ligand concentrations of 10^{-6} M are capable of coordinating the radionuclide with an 82 % (H_2**dp-bb-NCS–RGD)** to 97 % (H_2**dp-N-NCS–RGD)** yield. Serum challenge: to evaluate complex stability, an aliquot (500 µL) of the reaction was added to a solution of mouse serum (500 µL). The mixture was incubated at 37 °C and analyzed by PD-10 column filtration after 15 min, 2 h and 24 h. PD-10 size-exclusion columns were used to determine the stability of the RGD conjugates because the decomposition product could not be observed with

previously used HPLC methods. Reaction mixtures were loaded onto the pre-rinsed PD-10 columns (total loading volume: 2.5 mL). Subsequently, the column was rinsed with 3.5 mL PBS. The resulting eluate was collected and measured for radioactivity. The activity eluted corresponds to serum-bound ^{64}Cu.

[^{64}Cu(dp-bb-NCS-RGD)]: R_t of ^{64}Cu radiolabelled product on HPLC (gradient: A: H_2O, 0.1 % TFA, B: CH_3CN. 5-100% B linear gradient 30 min): 8.4 minutes. Stability versus serum (15 min/ 2 h/ 24 h; in % complex intact): 94/ 90/ 72.
[^{64}Cu(dp-N-NCS-RGD)]: R_t of ^{64}Cu radiolabelled product on HPLC (gradient: A: H_2O, 0.1 % TFA, B: CH_3CN. 5-100% B linear gradient 30 min): 9.2 minutes. Stability versus serum (15 min/ 2 h/ 24 h; in % complex intact): 98/ 94/ 88.

6.2.6 Avidin binding

In order to evaluate target specific binding capabilities of conjugate [^{67}Ga**(dp-N-Biotin)**]$^{+}$, an avidin blocking experiment was conducted in the following manner. The radiolabelled complex was incubated with a 10 fold excess of avidin for 30 minutes at 37 °C. As the corresponding control experiment, avidin was also pre-incubated with the corresponding 10 fold excess of native biotin for 30 minutes at 37 °C and subsequently incubated with the radiolabeled complex for 30 minutes at 37 °C. Subsequently, the reaction mixture was loaded onto a 30 kD MW cutoff separation filter and separated by centrifugation and washed three times with 1 mL of PBS pH 7.2. Avidin binding was determined as the percent radioactivity retained on the filter as compared to the total radioactivity.

6.3 Results and Discussion

6.3.1 Synthesis of H_2dp-bb-NH_2, H_2dp-N-NH_2, H_2dp-bb-NCS and H_2dp-N-NCS

In order to successfully furnish building blocks which connect H_2**dedpa** to a biomolecule, different methodologies were taken into consideration. The synthesis of building blocks consistent with conjugation methods ***a***, ***b***, ***d*** and ***e*** (Scheme 6.2) were all attempted, but some proved unsuccessful. In the case of method ***a***, orthogonal protection of the two different carboxylates is required. A hypothetical molecule **A** is shown in Figure 6.2.

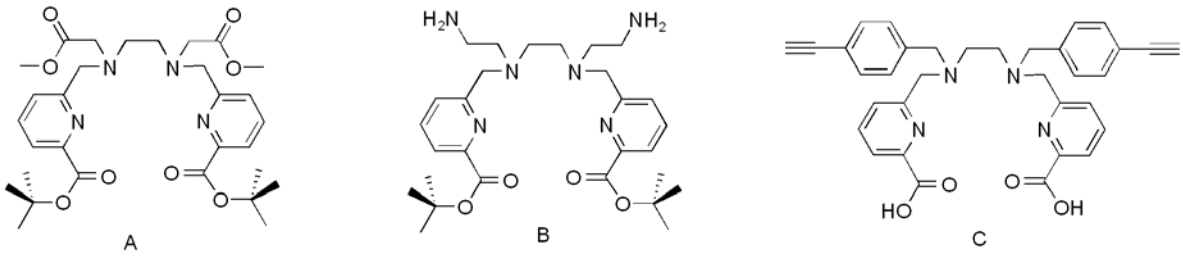

Figure 6.2 Hypothetical, postulated building blocks for functionalization of the H_2dedpa scaffold.

Synthesis of a *tert*-butyl protected pyridine carboxylate fragment was attempted (also as a convenient building block for compounds described in Chapter 3) but the corresponding molecule turned out to be extraordinarly acid-labile. Hence, synthesis of molecule **B** (compatible with method ***b***) was also dismissed. Compound C was synthesized as a building block compatible with method ***b***; however, attempted click-coupling with both the free carboxylate, as well as the methyl-protected precursor, led to incorporation of the catalytically active Cu(I) with oxidation to Cu(II). This result prompted investigations of the H_2dedpa scaffold for the purpose of coordination of both these Cu oxidation states on the macroscopic scale, and with ^{64}Cu (Chapter 5), but also led to dismissal of this type of conjugation method.

After careful evaluations of possible syntheses and remaining possible coupling

methodologies, the benzylamino- as well as the benzylisothiocyanato- derivatives were chosen. While their syntheses differs only by one step, they allow for conjugation to different functional groups.

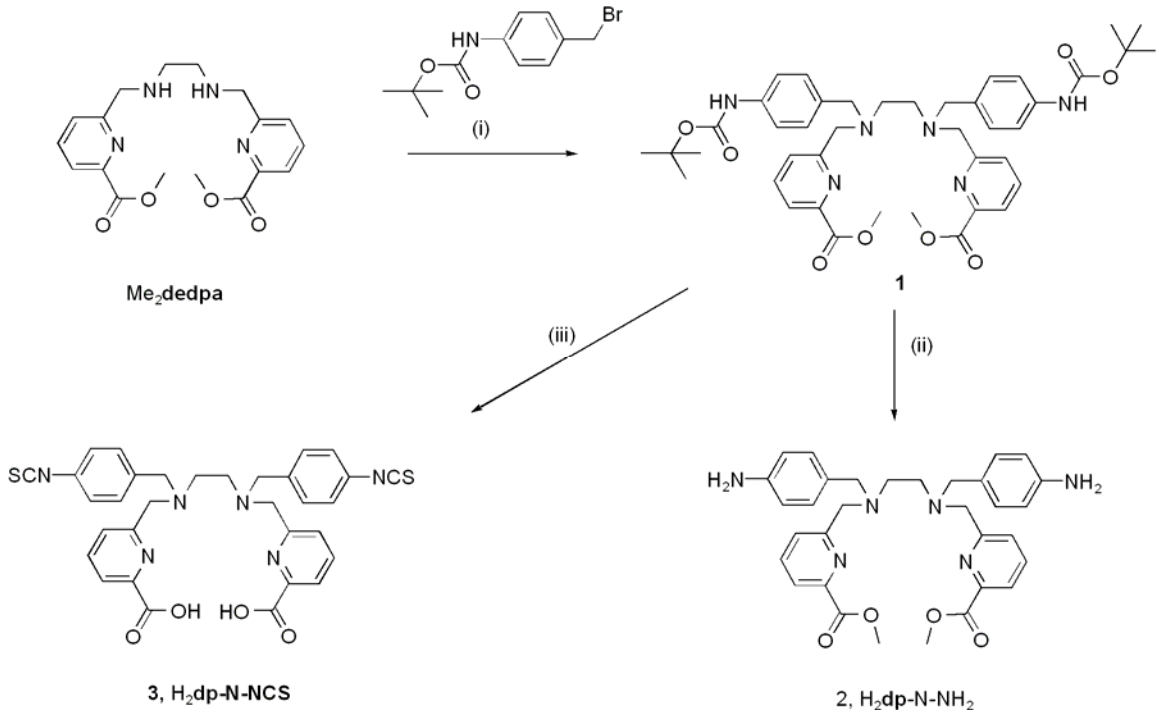

Scheme 6.3 Synthesis scheme for compounds **1, 2** and **3**. (i) Na_2CO_3, CH_3CN, 70 °C, 18 h (ii) CH_2Cl_2/TFA, 30 min (iii) 1. LiOH (4 eq), THF/H_2O (3:1), 2. HCl (3 M), 2 h, 3. $SCCl_2$, 18 h.

For the N-derivative, which has a somewhat simpler chemical makeup due to a lack of secondary amines and an inherent C_2 symmetry, initial reduction of compound Me_2**dp-N-NO$_2$** was attempted but (similar to reactivity of compounds reported in Chapter 3) led to complete debenzylation. Instead, the amine was introduced via alkylation of Me_2**dedpa** with Boc-protected *p*-anilino fragment to form **1**. **1** can be subsequently deprotected to afford **2**, which can be used immediately for conjugation following method ***b***. In order to furnish the corresponding isothiocyanato derivative, however, *t*-Boc-deprotection and extraction work-up was avoided since a large amount of the diamine **2** would be lost to the aqueous phase. Instead, an alternative sequence of deprotection conditions was sought to yield clean intermediate products. The synthesis was optimized to avoid tedious, low yielding purification steps of these highly polar compounds. Best results were obtained following a three-step one-pot reaction. First, the methyl esters

were removed under the usual basic conditions. Then, the intermediate was redissolved in 3 M HCl, leading to cleavage of the *t*-Boc protection groups. The reaction was monitored by analytical HPLC and was found to be complete after approximately 2 h. Subsequently, without isolation of the diamino-intermediate, $SCCl_2$ was added to the reaction mixture and left to react overnight to form the di-SCN fragment **3** (H_2**dp-N-NCS**) which, when the reaction is carried out on a larger scale, precipitates from the aqueous solution.

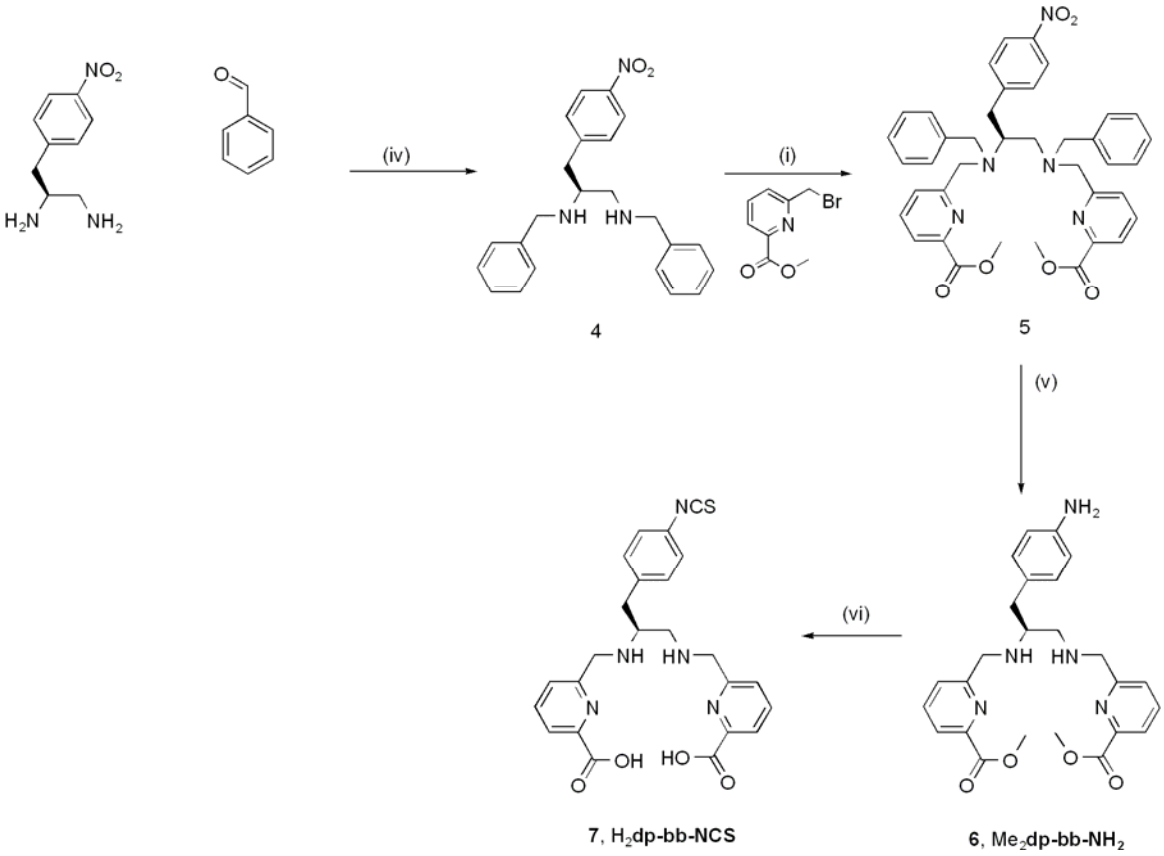

Scheme 6.4 Synthesis scheme for compounds **4, 5, 6** and **7**. (iv) 1. EtOH, 0 °C, 2 h, 2. $NaBH_4$, 0°C, 2 h (i) Na_2CO_3, MeCN, 70 °C, 18 h (v) Pd/C, AcOOH, 18 h (vi) 1. LiOH (4 eq), THF/H_2O (3:1), 2. HCl (3 M), $SCCl_2$, 18 h.

For the backbone derivatized fragments **6** and **7**, the main difficulty was to overcome purification issues and the extremely low yielding reductive amination encoutered with compound Me_2**dp-bb-NO$_2$** (see Chapter 4). To circumvent this reaction, the reductive amination was carried out with benzaldehyde first in order to generate **4**, which can be easily alkylated using 6-bromomethyl-pyridine-2-carboxylic acid methyl ester forming **5**, which can be purified in large quantities using column chromatography

(Scheme 6.4). One-pot debenzylation and transformation of the nitro functional group with Pd/C in one step yielded **6** (Me_2**dp-bb-**NH_2) as the triacetate salt. Subsequent one-pot sequential deprotection and functional group transformation was monitored by analytical HPLC. In contrast to **3**, **7** (H_2**dp-bb-NCS**) did not precipitate out of the reaction solution and required purification by HPLC, which has been previously reported for this type of chelate building block.[158] All products were thoroughly characterized by ^{1}H and ^{13}C NMR spectroscopy, as well as mass spectrometry. Notable spectroscopic features of compounds H_2**dp-bb-NCS** and H_2**dp-N-NCS** include the characteristic ^{13}C NMR resonances for the NCS carbon atoms, which are typically found around 135 ppm. ^{1}H NMR spectra of both isothiocyanato compounds are shown in Figure 6.3.

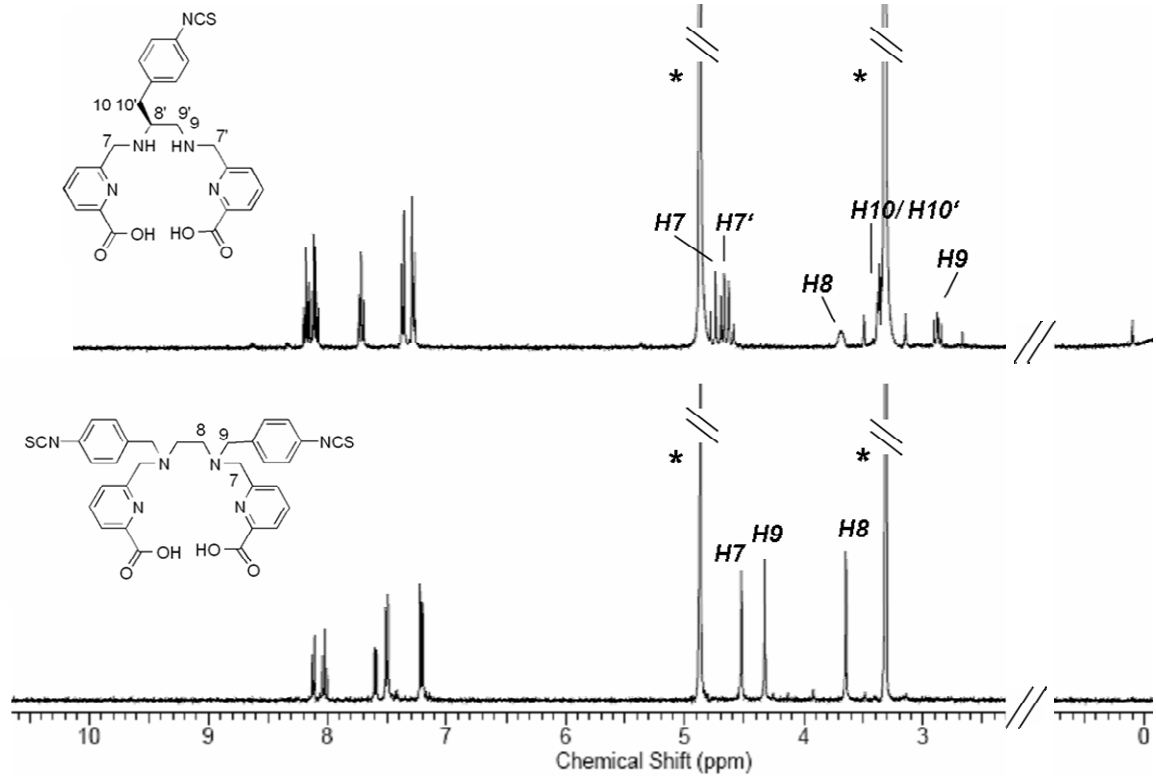

Figure 6.3 ^{1}H NMR spectra (300 MHz, CD_3OD, 298 K) of H_2**dp-bb-NCS** and H_2**dp-N-NCS**, * denotes residual solvent peaks.

The NCS functional group can also be identified by its characteristic stretching frequency. For both compounds H_2**dp-bb-NCS** and H_2**dp-N-NCS,** the corresponding broad peaks were found between 2020 – 2100 cm^{-1}, a typical value for the NCS functionality.

6.3.2 Amide Coupling with Biotin

In order to show the viability of coupling method ***b***, biotin-TFP was synthesized and mixed with either Me_2**dp-bb-NH_2** or Me_2**dp-N-NH_2** under standard coupling conditions. Initial reaction control with mass spectrometry seemed promising. Me_2**dp-N-Biotin** was easily purified by column chromatography using aluminium oxide, then characterized and identified as the desired product. Deprotection yielded the desired compound H_2**dp-N-Biotin**, which was also characterized and identified by ^{1}H and ^{13}C NMR spectroscopy, IR spectroscopy and mass spectrometry.

In contrast, the identification of the product from the conjugation with the backbone derivatized ligand system proved to be rather problematic. After purification via preparative TLC and HPLC, the product was identified and was subsequently deprotected. Structural characterization using the 2D NMR techniques HMBC and HSQC suggested that the amido-carbon of the biotin fragment and the chelate backbone were covalently associated (Figure 6.4). This assumption was further confirmed when the corresponding coordination reactions with both non-radioactive Ga and ^{67}Ga remained unsuccessful. In retrospect, the molecular connectivity observed is not surprising, because aliphatic, secondary amines are much stronger nucleophiles than aromatic amines under the chosen, basic reaction conditions. Hence, this coupling methodology, while efficient for the N-derivative, was abandoned for the backbone derivatized fragment.

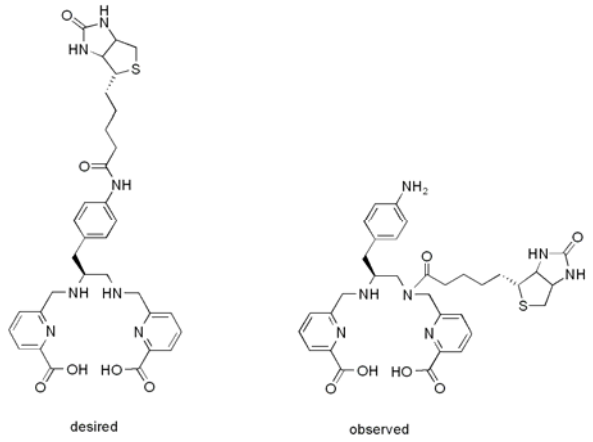

Figure 6.4 Desired and observed products from coupling of biotin-TFP and **Me_2**dp-bb-NH_2.

6.3.3 Coordination Chemistry of Ga with H_2dp-N-Biotin

The biotin conjugated fragment Me_2**dp-N-Biotin** was successfully synthesized and characterized. Base catalyzed saponification of the methyl esters provides the ready-to chelate fragment H_2**dp-N-Biotin**. The coordination reaction proceeds smoothly, as with all H_2dedpa derivatives. Since biotin is a reasonably small molecule, NMR spectroscopic methods were employed for complete identification of all hydrogens and carbon atoms of the complex structure. The observed coordination mode mirrors what was predicted by observations made on the model compound H_2**dp-N-NO$_2$** and its corresponding Ga(III) coordination complex. The ligand adopts a C_2 symmetric coordination mode upon chelation of the metal. Characteristic geminal splitting patterns are observed for the previously homotopic methylene hydrogens, that are rendered diastereotopic upon coordination (Figure 6.5).

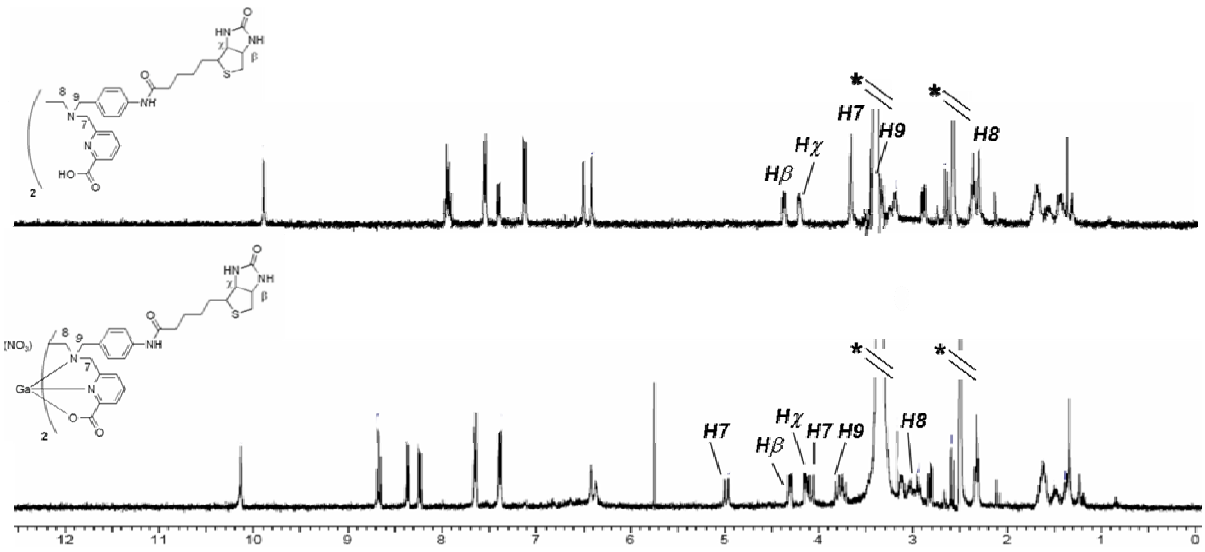

Figure 6.5 ^{1}H NMR spectra (300 MHz, d_6-DMSO, 298 K) of H_2**dp-N-Biotin** and [Ga(**dp-N-Biotin**)]$^+$, * denotes residual solvent peaks.

6.3.4 Radiolabelling of H_2dp-N-Biotin with ^{67}Ga and Avidin Binding

Radiolabelling of H_2**dp-N-Biotin** with ^{67}Ga proceeds within 10 minutes at room temperature in 98 % radiochemical yield. The subsequent *apo*-transferrin challenge experiment (Figure 6.6) revealed that 43 % of the radiolabelled complex remained intact after 2 h in the presence of excess *apo*-transferrin, a stability inferior to that of [Ga(**dedpa**)]$^+$, but similar to the model derivative H_2**dp-N-NO$_2$**.

To evaluate the affinity of the radiolabelled biotin conjugate for the target protein avidin, the radiochemical complex was incubated with the target protein for 30 minutes at 37 °C and the reaction mixture was subsequently filtered through a 30 kD cutoff filter. Any radiochemical complex associated with avidin is retained in the filter. Of the full amount of radiochemical complex added to avidin, 58 % was found to be bound to avidin. The corresponding blocking experiment, where the same amount of avidin was pre-incubated with a 10 fold excess of native biotin before incubation with the radiolabelled complex for 30 minutes at 37 °C, resulted in only 21 % of the biotin conjugate binding to avidin. Despite derivatization of the original biotin structure upon conjugation, the targeting moiety retains its affinity for the target molecule.[42]

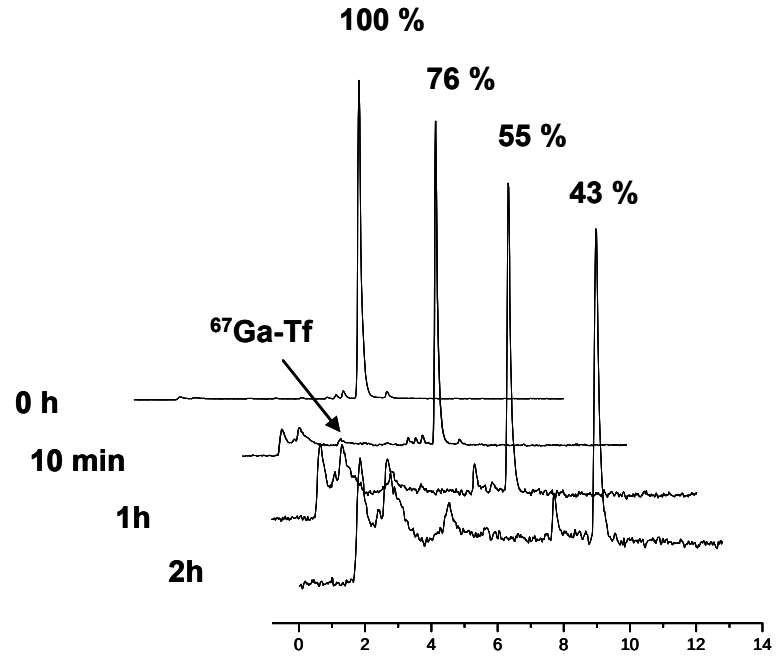

Figure 6.6 Stacked HPLC monitoring traces of transferrin challenge experiment for [^{67}Ga(**dp-N-Biotin**)]$^+$.

6.3.5 Thiourea Coupling with [c(RGDyK)]

The great advantage of using an isothiocyanate functional group for the coupling of chelate to biomolecule, especially for the H_2**dedpa** scaffold, is that under the chosen reaction conditions only primary amines are transformed into the NCS functional group. Also, the NCS functional group will only react with primary amines to form the thiourea functional group. This solves the problem encountered with the secondary amine of Me_2**dp-bb-NH$_2$**, which interfered with the coupling reactions using amines as nucleophiles. H_2**dp-bb-NCS** or H_2**dp-N-NCS,** dissolved in a minimal amount of CH_3OH, was successfully coupled by addition of a slight excess of RGD peptide in pH 9 -9.5 aqueous solution (0.1 M $NaHCO_3$), a condition key for efficient thiourea coupling. The coupled products H_2**dp-bb-NCS-RGD** and H_2**dp-N-NCS-RGD** were purified via preparative HPLC. It was noted that the reaction only proceeds if the NCS derivative is reasonably solubilized with CH_3OH. The use of other solvents such as DMSO yielded no peptide-chelate coupling product.

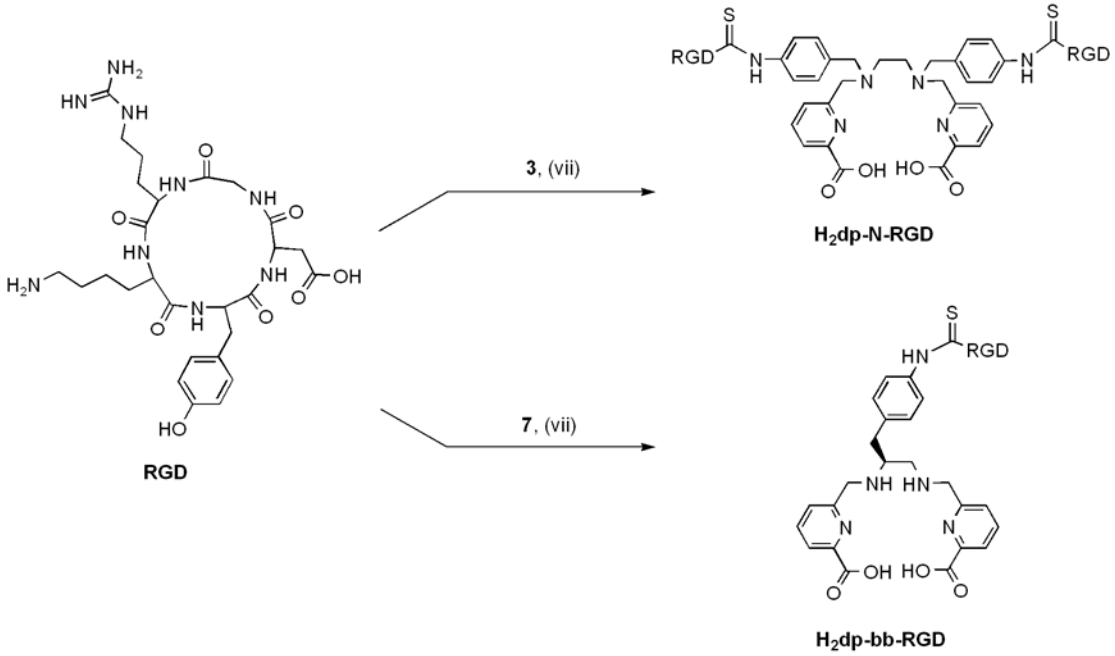

Scheme 6.5 Synthesis scheme for compounds H_2**dp-bb-RGD** and H_2**dp-N-RGD**. (vii). 0.1 M $NaHCO_3$ (pH 9 - 9.5)/ CH_3OH (3:1), room temperature, under light exclusion, 18 h.

6.3.6 Radiolabelling and Stability of RGD Conjugates with $^{67/68}$Ga

Coordination of H_2**dp-bb-RGD** to ^{67}Ga or ^{68}Ga affords the complex within 10 minutes at room temperature in 97 % radiochemical yield (Figure 6.7). As an added difficulty, HPLC turned out to be uninformative for the RGD transchelation experiments with *apo*-transferrin. Instead, PD-10 columns were used to filter off any transferrin-bound ^{67}Ga. The subsequent *apo*-transferrin challenge experiment revealed that 92 % of the radiolabeled complex remained intact after 2 h in the presence of excess *apo*-transferrin. In the case of H_2**dp-N-RGD**, the ^{67}Ga and ^{68}Ga complexes are formed within 10 minutes at room temperature in 99% radiochemical yield (trace Figure 6.7). The subsequent *apo*-transferrin challenge experiment yields 73 % of the complex remaining intact after 2 h. Both radiochemical coordination experiments are in accordance with what was observed with the model compounds H_2**dp-bb-NO$_2$** and H_2**dp-N-NO$_2$** (Chapter 4), including the high-yielding labelling at low ligand concentrations (1 nmol).

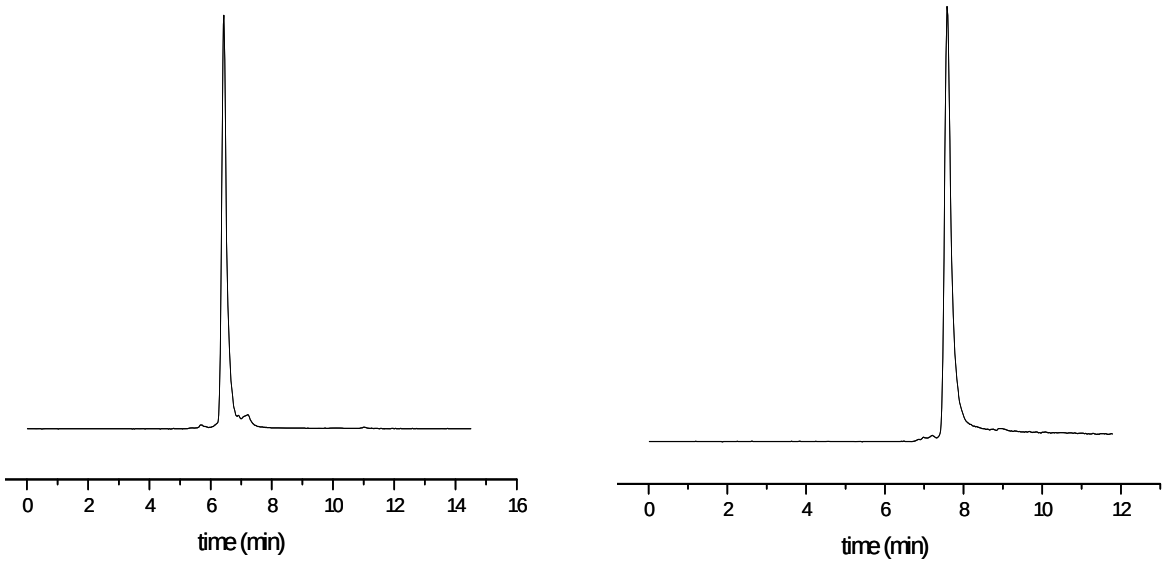

Figure 6.7 HPLC monitoring traces of labelling traces for $[^{67}$Ga(**dp-bb-RGD**)$]^+$ (left) and $[^{67}$Ga(**dp-N-RGD**)$]^+$ (right).

6.3.7 Radiolabelling and Stability of RGD Conjugates with ^{64}Cu

Coordination of H_2**dp-bb-RGD** to ^{64}Cu affords the complex within 10 minutes at room temperature in 97 % radiochemical yield. The subsequent serum challenge experiment revealed 72 % of the radiolabeled complex remained intact after 24 h in the presence of excess serum. PD-10 columns were used to filter off any serum-bound ^{64}Cu. In the case of H_2**dp-N-RGD**, the ^{64}Cu complexes are formed within 10 minutes at room temperature in 96 % radiochemical yield (Figure 6.8). The subsequent serum challenge experiment yields over 88 % of the complex remaining intact after 24 h. Both radiochemical coordination experiments are in accordance with what was observed with H_2**dedpa** (Chapter 5), efficient labelling with radiochemical yields > 92 % can be observed with ligand concentrations as low as 10 nmol. Decrease of radiochemical yield at lower concentrations is due to the lower specific activity (compared to ^{67}Ga) of the ^{64}Cu stock solution and also corresponds to the H_2**dedpa** labelling experiment (Chapter 5).

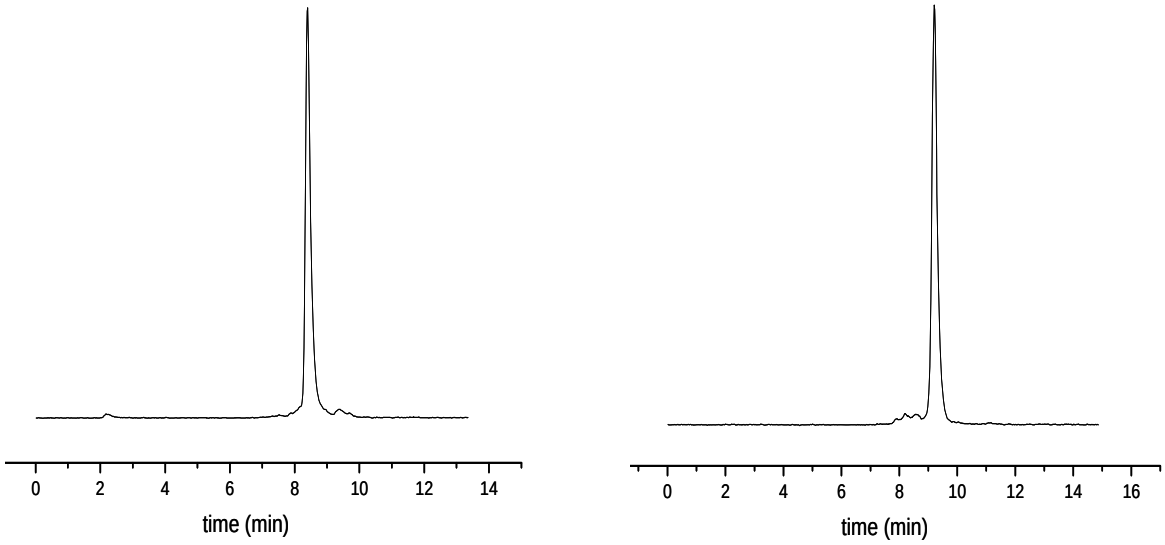

Figure 6.8 Radioabelling traces for $[^{64}Cu(\mathbf{dp\text{-}bb\text{-}RGD})]^+$ (left) and $[^{64}Cu(\mathbf{dp\text{-}N\text{-}RGD})]^+$ (right).

^{64}Cu labelled bioconjugates show a non-negligible percentage of ^{64}Cu transchelated with serum proteins after 24 hours, which might impose limitations for the use of slowly localizing biomolecules such as antibodies. For imaging with fast localizing

biomolecules such as RGD, the stability may be sufficient; *in vivo* experiments will provide further indication of the potential of these chelates for ^{64}Cu labelling. The finding that the N-derivative is slightly more stable then the bb-derivative could be due to Cu(II) being a softer metal, which prefers softer, tertiary amines as donor ligands, compared to the harder Ga(III), which prefers harder, secondary amine ligand systems.

6.4 Conclusions

In this chapter, the H_2**dedpa** scaffold was successfully functionalized with targeting biomolecules. While conjugation using a conventional amide coupling was only successful using the N-derivative, the cyclic peptide RGD was successfully conjugated with both derivatization modes using a thiourea forming coupling reaction. The novel isothiocyanato compounds necessary for this conjugation reaction were synthesized and characterized. Radiolabelling with radioisotopes $^{67/68}$Ga and ^{64}Cu was successful under the same mild conditions described previously for the model compounds H_2**dedpa**, H_2**dp-N-NO$_2$**)]$^+$and H_2**dp-bb-NO$_2$**. *In vitro* stability evaluations also confirm findings from previous Chapters 4 and 5, establishing the benzyl nitro derivatives as good models for the derivatization with actual biomolecules. Successful bioconjugation of a novel chelate, as well as confirmation of preliminary labelling results with the latter is a great step towards the actual application of a novel chemical entity for clinical purposes. The ability of the H_2**dedpa** derivatives, to coordinate the two PET isotopes ^{68}Ga and ^{64}Cu, both of interest to the radiopharmaceutical community, in a fast and efficient manner renders this acyclic bifunctional chelate truly unique for its labelling properties. Due to decreased stability with ^{64}Cu at the 24 h *in vitro* competition timepoint, the complex might be more suitable for targeted imaging with small, fast localizing biomolecules. *In vivo* evaluation, planned after submission of this thesis, will provide information on the potential of this chelate for the purpose of imaging with either radionuclide.

Chapter 7: Functionalization of the H_2dedpa Scaffold (2): Small Lipophilic Cations for Potential Imaging of Myocardial Bloodflow[§]

7.1 Introduction: Cardiac Imaging Agents

Evaluation of myocardial perfusion is done routinely with SPECT agents such as ^{201}Tl, ^{99m}Tc-sestamibi (trade name Cardiolite) or ^{99m}Tc-tetrofosmin (brand name Myoview, Figure 7.1). Due to the great importance of early detection of coronary artery disease in the clinic, limitations such as low first-pass extraction and high liver uptake of such agents have been recognized.[171] One way to improve upon the current ^{99m}Tc agents, which are believed to be targeting mitochondrial uptake, is the development of new, lipophilic, cationic ^{99m}Tc complexes with improved *in vivo* properties.[39] Another approach focuses on using PET in order to increase spatial resolution. This can be done by ^{11}C-labelling of aliphatic carbon chains with terminal carboxylates, which subsequently show increased retention in the myocardium since they function as metabolites for the heart muscle;[172] however, the short 20 minute half-life and the need for a cyclotron to produce the radioisotope in this case imposes significant limitations.

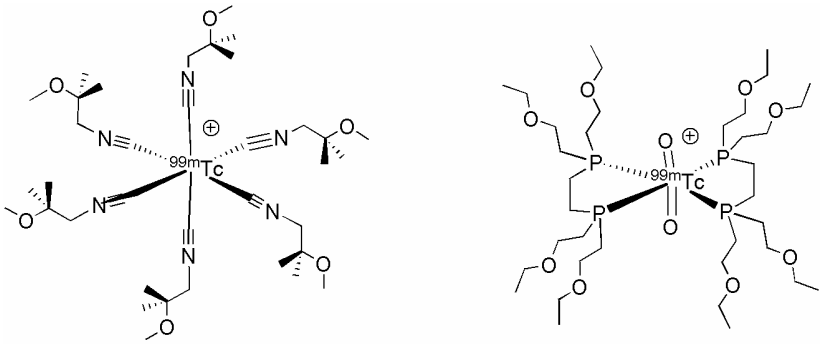

Figure 7.1 Some commercially approved radiopharmaceuticals for heart imaging.

[§] Work presented in this chapter has accepted for publishing: "New Ga Derivatives of the H_2dedpa Scaffold with Improved Clearance and Persistent Heart Uptake", E. Boros, C. L. Ferreira, B. O. Patrick, M. J. Adam, C. Orvig, *Nucl. Med. Biol.*, in press (2011).

^{82}Rb, a generator produced PET isotope, has been in use in the clinic for perfusion imaging; however, the emission properties of this radionuclide are not ideal and the liver uptake is high.[173] ^{68}Ga, also a generator produced PET isotope, has potential for developing a ^{68}Ga based cardiac imaging agent.

Ga(III) forms stable complexes with many multidentate ligands (see Chapter 4), and a myriad of capable ligand systems has been reviewed recently;[60,90] however, very few of the investigated ligands exhibit favourable properties such as high thermodynamic stability and kinetic inertness, as well as fast labelling under favourable conditions of room temperature and mild pH. Fulfillment of these criteria is crucial for a ^{68}Ga based compound with potential use in clinical settings. From the findings described in Chapter 4 for the H_2**dedpa** scaffold, it was concluded that through thoughtful functionalization of the chelate the physical properties, and biodistribution of the radiochemical complex should be modified accordingly. As [Ga(**dedpa**)]$^+$ is a cation, investigations of more lipophilic derivatives could be of great interest and could potentially lead to compounds with increased and prolonged myocardial retention.

Other ligand systems for ^{68}Ga have been investigated previously for this purpose, ranging from tetra- to hexadentate, forming neutral or mono-cationic complexes upon coordination.[51,52] Green and coworkers have investigated potential myocardial imaging agents based on acyclic bis(salicylaldimine) type chelates over the past decade (Figure 7.2).[174]

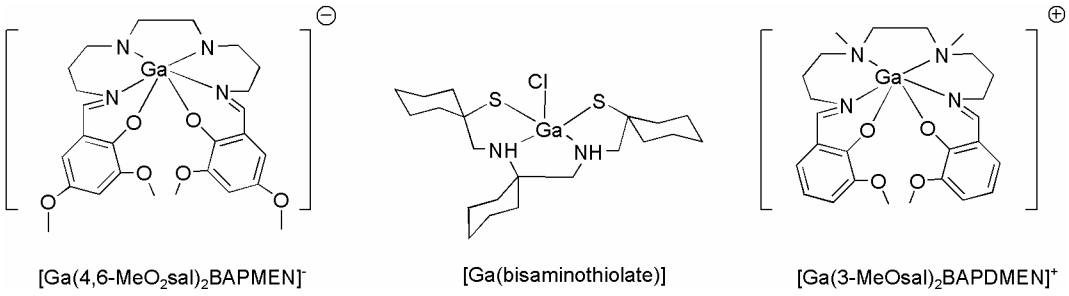

Figure 7.2 Previously investigated Ga-based compounds for heart imaging.

Despite recent, highly promising results, inferior heart-to-blood and heart-to-lung ratios compared to ^{99m}Tc-sestamibi, and a non-optimal, carrier-added labelling procedure remain to be improved upon.[173]

In this chapter, seven new derivatives of the H_2**dedpa** scaffold are described and investigated for their labelling properties, *in vitro* stability, log $P_{o/w}$ and biodistribution. All compounds bear two phenyl residues, which are derivatized with a varying number of methoxy or ethoxy groups. In the case of two ligands, an additional methoxy group was incorporated via derivatization of the pyridyl ring.

7.2 Experimental

7.2.1 Materials and Methods

All solvents and reagents were used as received. Refer to Chapter 2.2 for general information. The HPLC system used for analysis consisted of a Waters Alliance HT 2795 separation module equipped with a Raytest Gabbistar NaI detector and a Waters 996 photodiode array (PDA) detector. Analysis of radiolabeled complexes was done on a Waters XBridge BEH130 4.6 × 150 mm column (retention time of ^{67}Ga-Tf: 2.5 min). If not stated otherwise, the R_f values are measured on standard TLC plates with 10% CH_3OH in CH_2Cl_2 as the mobile phase.

7.2.2 Chemical Synthesis

Common starting materials for synthetic precursors such as **1, 3, 6, 9** and **10** were synthesized according to the literature references.[108,170,175,176]

Alkylation A (step 1, synthesis of **14** and **15,** Scheme 7.1): Both secondary amine and 2.1 equivalents of the bromoaryl were dissolved in acetonitrile (100 mL). Na_2CO_3 (20 eq) was added into the reaction mixture and the reaction was stirred at 70 °C overnight. The resulting milky solution was filtered and the solvent was removed *in vacuo* to afford the crude product as an oil. This was then subsequently purified by column chromatography (10% CH_3OH in CH_2Cl_2) to afford the product as a viscous oil that solidifies upon standing.

Alkylation B (step 1, synthesis of **13**, **16**, **17**, **18** and **19**): Both secondary amine and 2.1 equivalents of 6-bromomethyl-pyridine-2-carboxylic acid methyl ester or **9** were dissolved in acetonitrile (100 mL). Na_2CO_3 (20 eq) was added to the reaction mixture and the reaction was stirred at 70 °C overnight. The resulting milky solution was filtered and the solvent was removed *in vacuo* to afford the crude product as an oil. This was then subsequently purified by column chromatography (10% CH_3OH in CH_2Cl_2) to afford the product as a very viscous oil that solidifies upon standing.

Deprotection procedure (step 2): The methylester-protected starting material was dissolved in 6 mL of a 3:1 mixture of THF and water (4 mL total volume). LiOH (4 eq) was added into the solution and the reaction mixture was stirred at room temperature until the reaction was determined to be complete by TLC (10% CH_3OH in CH_2Cl_2). The solvent was removed *in vacuo* to afford the product as a white solid.

7.2.3 Synthesis of Lipophilic Ligand Systems

1,2-[N,N'-Bis(phenylmethyl)]-N,N'-bis[6-{methoxycarbonyl}-pyridin-2yl] methylamino)ethane (2).

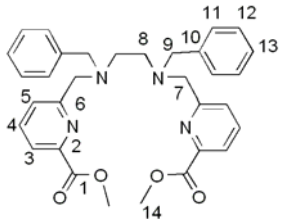

Precursors **1** and 6-bromomethyl-pyridine-2-carboxylic acid methyl ester were used according to alkylation method B to synthesize **2**. Yield: 52 mg, 0.096 mmol, 46 %. R_f: 0.45. ^{1}H NMR ($CDCl_3$, 400 MHz, δ): 7.96 – 7.94 (dd, $^3J_{3,4}$ = 5.2 Hz, $^4J_{3,5}$ = 2 Hz, *H3*, 2H), 7.72 – 7.68 (m, $^3J_{4,5}$ = 5.2 Hz, $^4J_{3,5}$ = 2 Hz, *H4, H5*, 4H), 7.26 – 7.19 (m, *H11-H13*, 10H), 3.97 (s, *H14*, 6H), 3.81 (s, *H7*, 4H), 3.57 (s, *H9*, 4H), 2.68 (s, *H8*, 4H). ^{13}C NMR ($CDCl_3$, 75 MHz, δ): 166.0 (*C1*), 161.3 (*C6*), 147.2 (*C2*), 139.1 (*C4*), 137.4 (*C10*), 128.8 (*C11*), 127.2 (*C12*), 125.9 (*C13*), 123.6 (*C3*), 60.7 (*C7*), 59.3 (*C9*), 53.0 (*C14*), 52.2 (*C8*). HR-ESI-MS: *m/z* calcd. for $C_{32}H_{35}N_4O_4$: 539.2658, found: 539.2645 $[M + H]^+$.

1,2-[N,N'-Bis{3-methoxybenzyl}methyl]-N,N'-bis[6-{methoxycarbonyl}-pyridin-2-yl] methylamino)ethane (4).

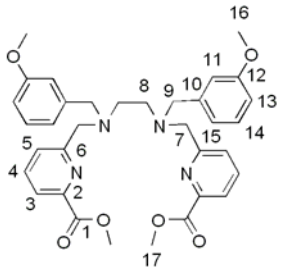

Precursors **3** and 1-(bromomethyl)-3-methoxybenzene were used according to alkylation method A to synthesize **4**. Yield: 50 mg, 0.083 mmol, 59 %. R_f: 0.5. ^{1}H NMR ($CDCl_3$, 400 MHz, δ): 7.98 (d, $^3J_{3,4}$ = 4 Hz, *H3*, 2H), 7.73 – 7.72 (m, *H14, H15*, 4H) 7.18 (t, $^3J_{3,4}$ = 4 Hz, , $^3J_{4,5}$ = 5.6 Hz, *H4*, 2H), 6.89 (m, *H11, H12*, 4H), 6.71 (d, $^3J_{4,5}$ = 5.6 Hz, *H5*, 2H), 4.0 (s, *H17*, 6H) , 3.85 (s, *H7*, 4H), 3.78 (s, *H16*, 6H), 3.58 (s, *H9*, 4H), 2.71 (s, *H8*, 4H). ^{13}C NMR ($CDCl_3$, 75 MHz, δ): 166.0 (*C1*), 161.3 (*C12*), 159.8 (*C6*), 147.3 (*C2*), 140.9 (*C4*), 137.5 (*C10*), 129.4 (*C14*), 126.0 (*C5*), 123.7 (*C3*), 121.2 (*C15*), 114.4 (*C12*), 112.4 (*C13*), 60.7 (*C7*), 59.3 (*C9*), 55.3 (*C16*), 53.0 (*C8*), 52.3 (*C17*). HR-ESI-MS: *m/z* calcd. for $C_{34}H_{39}N_4O_6$: 599.2870, found: 599.2882 $[M + H]^+$.

(1,2-[N,N'-Bis{3,5-dimethoxybenzyl}methyl]-N,N'-bis[6-{methoxycarbonyl}-pyridin-2-yl] methylamino)ethane (5).

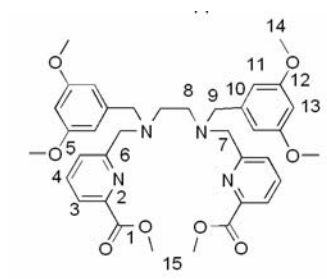

Precursors **3** and 3,5-dimethoxybenzyl bromide were used according to alkylation method A to synthesize **5**. Yield: 51 mg, 0.077 mmol, 56 %. R_f: 0.45. ^{1}H NMR ($CDCl_3$, 400 MHz, δ): 7.96 (m, *H4*, 2H), 7.70 (m, *H3, H5*, 4H), 6.46 (s, *H11*, 4H), 6.30 (s, *H13*, 2H), 3.97 (s, *H9*, 6H) , 3.83 (s, *H7*, 4H), 3.73 (s, *H14*, 12H), 3.53 (s, *H15*, 4H), 2.69 (s, *H8*, 4H). ^{13}C NMR ($CDCl_3$, 75 MHz, δ): 165.9 (*C1*), 161.2 (*C12*), 160.9 (*C6*), 147.3 (*C2*), 141.8 (*C4*), 137.4 (*C10*), 126.0 (*C5*), 123.6 (*C3*), 106.6 (*C11*), 98.9 (*C12*), 60.7 (*C3*), 59.4 (*C9*), 55.4 (*C14*), 52.9 (*C15*), 52.4 (*C8*). HR-ESI-MS: *m/z* calcd. for $C_{36}H_{43}N_4O_8$: 659.3081, found: 659.3068 $[M + H]^+$.

(1,2-[N,N'-Bis{2,4,6-trimethoxybenzyl}methyl]-N,N'-bis[6-{methoxycarbonyl}-pyridin-2-yl] methylamino)ethane (7).

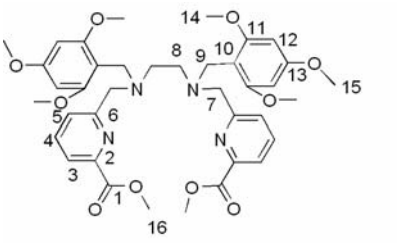

Precursors **6** and 6-bromomethyl-pyridine-2-carboxylic acid methyl ester were used according to alkylation method B to synthesize **7**. Yield: 79 mg, 0.11 mmol, 55 %. R_f: 0.4. ^{1}H NMR ($CDCl_3$, 300 MHz, δ): 8.27 (d, $^3J_{3,4}$ = 8.4 Hz, *H3*, 2H), 7.99 (d, $^3J_{4,5}$ = 7.5 Hz, *H5*, 2H), 7.86 (m, $^3J_{3,4}$ = 8.4 Hz, $^3J_{4,5}$ = 7.5 Hz, *H4*, 2H), 6.02 (s, *H12*, 4H), 4.31 (s, *H7*, 4H), 3.96 (s, *H16*, 6H), 3.94 (s, *H9*, 4H), 3.78 (s, *H15*, 6H), 3.68 (s, *H14*, 12H), 3.19 (s, *H8*, 4H) . ^{13}C NMR ($CDCl_3$, 75 MHz, δ): 165.2 (*C1*), 161.9 (*C6*), 159.9 (*C11, C13*), 146.8 (*C2*), 137.9 (*C4, C10*), 127.9 (*C5*), 124.2 (*C3*), 90.2 (*C12*), 58.5 (*C7*), 55.5 (*C14*), 55.3 (*C15*), 52.7 (*C9*), 50.4 (*C8*), 45.5 (*C16*). HR-ESI-MS: *m/z* calcd. for $C_{38}H_{47}N_4O_{10}$: 719.3292, found: 719.3303 $[M + H]^+$.

(1,2-[N,N'-Bis{2,4,6-trimethoxybenzyl}methyl]-N,N'-bis[4-methoxy-6-{methoxy-carbonyl}pyridin-2-yl]methylamino)ethane (8).

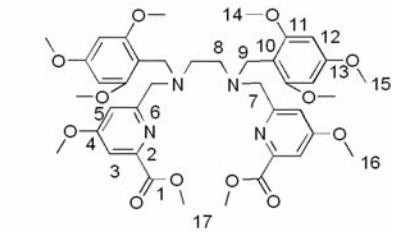

Precursors **1** and **9** were used according to alkylation method B to synthesize **8**. Yield: 311 mg, 0.4 mmol, 70 %. R_f: 0.4. ^{1}H NMR ($CDCl_3$, 400 MHz, δ): 7.32 (s, *H3, H5*, 4H), 5.89 (s, *H12*, 4H), 4.08 (s, *H7*, 4H), 3.83 (s, *H9*, 4H), 3.78 (s, *H17*, 6H), 3.64 (s, *H16*, 6H) 3.55 (s, *H14*, 12H), 3.25 (s, *H15*, 6H), 3.03 (s, *H8*, 4H). ^{13}C NMR ($CDCl_3$, 100 MHz, δ): 167.3 (*C1*), 165.3 (*C4*), 162.3 (*C11*), 160.1 (*C13*), 157.9 (*C6*), 148.4 (*C2*), 112.9 (*C5*), 111.3 (*C3*), 101.2 (*C10*), 90.5 (*C12*), 58.3 (*C7*), 56.3 (*C15*), 55.7 (*C14'*), 55.5 (*C14*), 52.9 (*C16*), 50.0 (*C17*), 49.2 (*C8*), 45.9 (*C9*). IR (neat, cm^{-1}): 1721 (m), 1593 (m), 1455 (m), 1335 (m). HR-ESI-MS: *m/z* calcd. for $C_{40}H_{51}N_4O_{12}$: 779.3503, found: 779.3493 $[M + H]^+$.

6-Bromomethyl-4-methoxy-pyridine-2-carboxylic acid methyl ester (9).

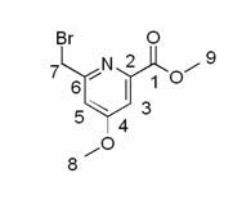

The title compound was synthesized in 4 steps.[170] The fist two steps include a two-step methylation of the two carboxylates and the alcohol, followed by a standard partial reduction as done for 1,2-[{6-(methoxycarbonyl)pyridin-2-yl}methylamino]ethane, followed by bromination of the alcohol to afford the product **9**. Yield: 31 % (overall yield). ^{1}H NMR ($CDCl_3$, 400 MHz, δ): 7.46 (d, $^{4}J_{3,5}$ = 2.4 Hz, *H3,* 2H), 7.06 (d, $^{4}J_{3,5}$ = 2.4 Hz, *H5,* 2H), 4.73 (s, *H7*, 2H), 3.88 (s, *H9*, 3H), 3.82 (s, *H8*, 6H). ^{13}C NMR ($CDCl_3$, 100 MHz, δ): 167.4 (*C1*), 165.4 (*C4*), 158.6 (*C6*), 149.3 (*C2*), 112.81 (*C5*), 110.9 (*C3*), 55.86 (*C8*), 53.15 (*C9*), 33.5 (*C7*). IR (neat, cm^{-1}): 1731 (s), 1591 (m), 1439 (w), 1246 (m), 1043 (s). HR-ESI-MS: *m/z* calcd. for $C_9H_{10}N^{79}BrNaO_3$: 281.9742, found: 281.9739 $[M + Na]^+$. Elemental Analysis calcd. (found) for for $C_9H_{10}{}^{79}BrNO_3$: C: 41.56 (41.7), H: 3.88 (3.88), N: 5.31 (5.79).

2,4,6-Triethoxybenzaldehyde

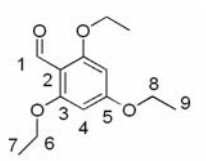

2,4,6-Trihydroxybenzaldehyde (1.88 g, 9.9 mmol) was dissolved in DMF. NaH (0.960 g, 0.024 mol, in 60 % dispersion in mineral oil) was added, followed by EtBr (16.240 g, 11.05 mL, 0.149 mol). The mixture was stirred overnight at room temperature. After no tri-alkylated product was afforded, another batch of NaH (0.301 g, 0.0125 mol, in 60 % dispersion in mineral oil) was added, together with more EtBr (2.05 g, 1.397 mL, 0.0188 mol). The mixture was stirred overnight at 60 °C and quenched with H_2O (50 mL). The crude product was extracted with CH_2Cl_2, and the organic phase was washed twice with saturated brine. Subsequently, the solvent was removed and the residual crude product was purified with column chromatography (SiO_2, 3:2 mixture of hexanes/EtOAc) to afford the clean product as a colorless solid. Yield: 0.970 g, 3.4 mmol, 34 %. R_f = 0.21. ^{1}H NMR ($CDCl_3$, 400 MHz, δ): 10.34 (s, *H1*, 1H), 5.99 (s, *H4*, 2H), 4.03 (m, *H6, H8*, 6H), 1.39 (m, *H7, H9*, 9H) . ^{13}C NMR ($CDCl_3$, 100 MHz, δ): 187.9 (*C1*), 165.5 (*C3*), 163.5 (*C5*), 109.1 (*C2*), 91.6 (*C4*), 64.6 (*C6*), 63.9 (*C8*), 14.65 (*C7, C9*). IR (neat, cm^{-1}): 1672 (m), 1599 (m), 1565 (s). HR-ESI-MS: *m/z* calcd. for $C_{13}H_{19}O_9$: 239.1283, found:

239.1286 $[M + H]^+$. Elemental Analysis calcd. (found) for for $C_{13}H_{18}O_9$: C: 65.53 (65.37), H: 7.61 (7.48).

N,N'-Bis-(2,4,6-triethoxybenzyl)ethane1,2-diamine (10).

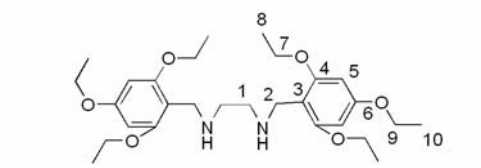

This compound was synthesized according to a literature procedure.[176] ^{1}H NMR ($CDCl_3$, 400 MHz, δ): 6.01 (s, *H5*, 4H), 4.08 (s, *H2*, 4H), 3.91 (m, *H7, H9*, 12H), 3.74 (s, *H1*, 4H), 1.30 (m, *H8, H10*, 18H). ^{13}C NMR ($CDCl_3$, 100 MHz, δ): 159.9 (*C4*), 158.8 (*C6*), 107.3 (*C3*), 92.04 (*C5*), 91.8 (*C5'*), 63.8 (*C7, C9*), 46.0 (*C1*), 40.3 (*C2*), 14.9 (*C8, C10*). IR (neat, cm^{-1}): 1592 (m), 1438 (m). HR-ESI-MS: *m/z* calcd. for $C_{28}H_{45}N_2O_6$: 505.3278, found: 505.3269 $[M + H]^+$.

(1,2-[N,N'-Bis{2,4,6-triethoxybenzyl}methyl]-N,N'-bis[6-{methoxycarbonyl}-pyridin 2-yl]methylamino)ethane (11).

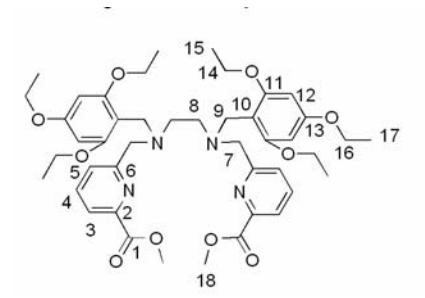

Precursors **10** and 6-bromomethyl-pyridine-2-carboxylic acid methyl ester were used according to alkylation method B to synthesize **11**. Yield: 112 mg, 0.13 mmol, 52 %. R_f: 0.2. ^{1}H NMR ($CDCl_3$, 400 MHz, δ): 8.01 (d, $^3J_{3,4}$ = 7.6 Hz, *H3*, 2H), 7.94 (d, $^3J_{4,5}$ = 7.6 Hz, *H5*, 2H), 7.82 (d, $^3J_{3,4}$ = $^3J_{4,5}$ = 7.6 Hz, *H4*, 2H), 5.94 (s, *H12*, 4H), 4.30 (s, *H7*, 4H), 3.94 (s, *H9*, 4H), 3.88 (m, $^3J_{16,17}$ = $^3J_{14,15}$ = 6.8 Hz, *H14, H16, H18*, 18H), 3.11 (s, *H8*, 4H), 1.35 (t, $^3J_{16,17}$ = 6.8 Hz, *H17*, 6H), 1.09 (m, $^3J_{14,15}$ = 6.8 Hz, *H15*, 12H). ^{13}C NMR ($CDCl_3$, 100 MHz, δ): 165.4 (*C1*), 161.5 (*C13*), 159.6 (*C11*), 156.2 (*C6*), 147.1 (*C2*), 138.4 (*C4*), 128.2 (*C5*), 124.7 (*C3*), 101.2 (*C10*), 91.7 (*C12*), 64.1 (*C14*), 63.7 (*C16*), 58.7 (*C7*), 52.9 (*C18*), 48.9 (*C8*), 45.6 (*C9*), 14.8 (*C15, C17*). HR-ESI-MS: *m/z* calcd. for $C_{44}H_{59}N_4O_{10}$: 803.4231, found: 803.4248 $[M + H]^+$.

(1,2-[N, N'-Bis{2,4,6-triethoxybenzyl}methyl]-N,N'-bis[4-methoxy-6-{methoxy-carbonyl}-pyridin-2-yl] methylamino)ethane (12).

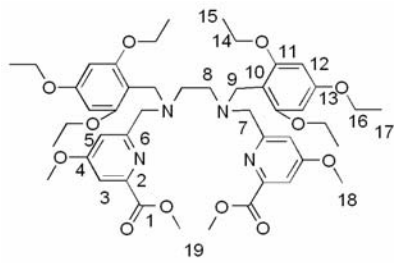

Precursors **9** and **10** were used according to alkylation method B to synthesize **12**. Yield: 116 mg, 0.13 mmol, 52 %. R_f: 0.4. ^{1}H NMR ($CDCl_3$, 400 MHz, δ): 7.57 (s, *H3,* 2H), 7.47 (s, *H5,* 2H), 5.96 (s, *H12,* 4H), 4.24 (s, *H7,* 4H), 3.96 (s, *H9,* 4H), 3.91 (m, $^3J_{16,\ 17} = {}^3J_{14,\ 15}$ = 6.8 Hz, *H14, H16, H18, H19*, 24H), 3.07 (s, *H8,* 4H), 1.35 (t, $^3J_{16,\ 17}$ = 6.8 Hz, *H17*, 6H), 1.09 (t, $^3J_{14,\ 15}$ = 6.8 Hz, *H15*, 12H). ^{13}C NMR ($CDCl_3$, 100 MHz, δ): 167.4 (*C1*), 165.4 (*C4*), 161.5 (*C11*), 159.6 (*C13*), 158.3 (*C6*), 148.5 (*C2*), 113.1 (*C5*), 111.9 (*C3*), 101.4 (*C10*), 91.8 (*C12*), 64.1 (*C14*), 63.8 (*C16*), 58.9 (*C7*), 56.5 (*C15*), 53.0 (*C18*), 48.9 (*C8*), 45.6 (*C9*), 14.8 (*C15*), 14.4 (*C17*). HR-ESI-MS: *m/z* calcd. for $C_{46}H_{63}N_4O_{12}$: 863.4405, found: 863.4424 $[M + H]^+$.

(1,2-[N,N'-Bis{3-methoxybenzyl}methyl]-N,N'-bis[6-{carboxyato}-pyridin-2-yl] methyl amino)ethane (13, 0MeO).

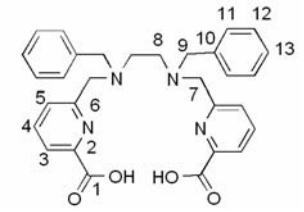

The general deprotection procedure was used with **2** as the starting material. Yield: 41 mg, 0.082 mmol, 85 %. R_f: 0.02. ^{1}H NMR (CD_3OD, 400 MHz, δ): 8.01 (d, $^3J_{3,\ 4}$ = 7.6 Hz, *H3*, 2H), 7.89 (m, $^3J_{3,\ 4}$ = 7.6 Hz, $^3J_{4,\ 5}$ = 6.8 Hz, *H4*, 2H), 7.37 (d, $^3J_{4,\ 5}$ = 6.8 Hz, *H5*, 2H), 7.25 – 7.21 (m, *H11, H12,* 6H), 7.04 (m, *H13,* 4H), 3.87 (s, *H7,* 4H), 3.41 (s, *H9,* 4H), 2.31 (s, *H8,* 4H). ^{13}C NMR (CD_3OD, 100 MHz, δ): 172.5 (*C1*), 159.5 (*C6*), 154.7 (*C2*), 139.8 (*C4*), 136.3 (*C10*), 131.4 (*C11*), 129.2 (*C12*), 128.5 (*C13*), 125.7 (*C5*), 123.2 (*C3*), 61.0 (*C7*), 57.6 (*C9*), 48.5 (*C8*). IR (neat, cm^{-1}): 1616 (m), 1583 (m), 1433 (w), 1386 (m). HR-ESI-MS: *m/z* calcd. for $C_{30}H_{29}N_4O_4$: 509.2189, found: 509.2193 $[M - H]^-$.

(1,2-[N,N'-Bis{3-methoxybenzyl}methyl]-N,N'-bis[6-{carboxyato}-pyridin-2-yl] methylamino)ethane (14, 2MeO).

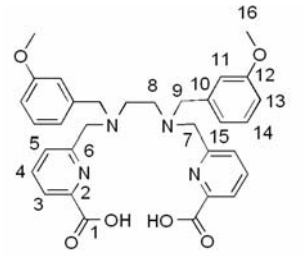

The general deprotection procedure was used with **4** as the starting material. Yield: 37 mg, 0.065 mmol, 78 %. R_f: 0.1. ^{1}H NMR (CD_3OD, 400 MHz, δ): 7.99 (d, $^3J_{3,\,4}$ = 7.6 Hz, *H3*, 2H), 7.89 (m, $^3J_{3,\,4}$ = 7.6 Hz, $^3J_{4,\,5}$ = 7.2 Hz, *H4*, 2H), 7.39 (d, $^3J_{4,\,5}$ = 7.2 Hz, *H5*, 2H), 7.15 (m, $^3J_{14,\,15}$ = 9.2 Hz, *H14,* 2H), 6.79 (d, $^3J_{14,\,15}$ = 9.2 Hz, *H15,* 2H), 6.61 (m, *H13,H11,* 4H), 3.89 (s, *H7,* 4H), 3.73 (s, *H16,* 6H), 3.38 (s, *H9,* 4H), 2.38 (s, *H8,* 4H). ^{13}C NMR (CD_3OD, 100 MHz, δ): 172.5 (*C1*), 160.8 (*C12*), 159.4 (*C6*), 154.6 (*C2*), 139.6 (*C4*), 137.7 (*C10*), 130.0 (*C14*), 125.5 (*C3*), 123.6 (*C13*), 122.9 (*C5*), 116.9 (*C11*), 113.5 (*C15*), 60.9 (*C7*), 57.2 (*C9*), 55.6 (*C16*), 47.5 (*C8*). IR (neat, cm^{-1}): 1614 (m), 1584 (m), 1434 (w), 1387 (m). HR-ESI-MS: *m/z* calcd. for $C_{32}H_{33}N_4O_6$: 569.2400, found: 569.2396 $[M - H]^-$.

(1,2-[N,N'-Bis{3,5-dimethoxybenzyl}methyl]-N,N'-bis[6-{carboxylato}-pyridin-2-yl] methylamino)ethane (15, 4MeO).

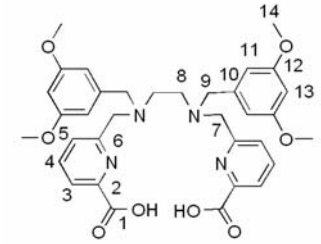

The general deprotection procedure was used with **5** as the starting material. Yield: 42 mg, 0.063 mmol, 83 %. R_f: 0.15. ^{1}H NMR (CD_3OD, 400 MHz, δ): 7.99 (d, $^3J_{3,\,4}$ = 8.0 Hz, *H3*, 2H), 7.88 (m, $^3J_{3,\,4}$ = 8.0 Hz, $^3J_{4,\,5}$ = 7.6 Hz, *H4*, 2H), 7.41 (d, $^3J_{4,\,5}$ = 7.6 Hz, *H5*, 2H), 6.35 (s, *H13,* 2H), 6.32 (s, *H11,* 4H), 3.89 (s, *H7,* 4H), 3.69 (s, *H14,* 12H), 3.34 (s, *H9,* 4H), 2.36 (s, *H8,* 4H). ^{13}C NMR (CD_3OD, 100 MHz, δ): 173.0 (*C1*), 162.2 (*C12*), 159.7 (*C6*), 154.8 (*C2*), 139.8 (*C4*), 138.8 (*C10*), 125.7 (*C3*), 123.1 (*C5*), 109.4 (*C11*), 100.1 (*C13*), 61.1 (*C7*), 56.8 (*C9*), 55.8 (*C14*), 47.8 (*C8*). IR (neat, cm^{-1}): 1585 (m), 1428 (w), 1387 (m). HR-ESI-MS: *m/z* calcd. for $C_{34}H_{37}N_4O_8$: 629.2611. found: 629.2615 $[M - H]^-$.

(1,2-[N,N'-Bis{2,4,6-trimethoxybenzyl}methyl]-N,N'-bis[6-{carboxylato}-pyridin-2-yl] methylamino)ethane (16, 6MeO).

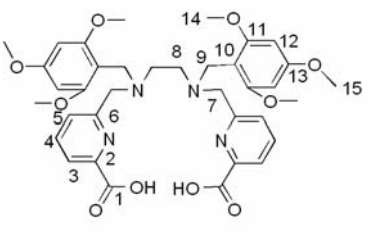

The general deprotection procedure was used with **7** as the starting material. Yield: 61 mg, 0.088 mmol, 80 %. R_f: 0.2. ^{1}H NMR (CD_3OD, 400 MHz, δ): 7.95 (d, $^3J_{3,4}$ = 7.6 Hz, *H3*, 2H), 7.84 (m, $^3J_{3,4}$ = 7.6 Hz, $^3J_{4,5}$ = 7.2 Hz, *H4*, 2H), 7.30 (d, $^3J_{4,5}$ = 7.2 Hz, *H5*, 2H), 6.12 (s, *H12,* 4H), 3.93 (s, br, *H7* 4H), 3.62 (s, *H15,* 6H), 3.63 (s, *H14,* 12H), 3.41 (s, *H8,* 4H), 2.19 (s, *H8,* 4H). ^{13}C NMR (CD_3OD, 100 MHz, δ): 172.6 (*C1*), 162.4 (*C13*), 161.7 (*C11*), 160.9 (*C6*), 154.7 (*C2*), 139.5 (*C4*), 125.2 (*C3*), 122.6 (*C5*), 105.7 (*C10*), 91.5 (*C12*), 61.9 (*C7*), 55.9 (*C14*), 55.8 (*C15*), 48.7 (*C8*), 43.6 (*C9*). IR (neat, cm^{-1}): 1585 (m), 1455 (m), 1434 (w), 1390 (m). HR-ESI-MS: *m/z* calcd. for $C_{36}H_{41}N_4O_{10}$: 689.2823, found: 689.2812 $[M + H]^+$.

1,2-[N,N'-Bis{2,4,6-trimethoxybenzyl}methyl]-N,N'-bis[4-methoxy-6-{carboxylato} pyridin-2-yl]methylamino)ethane (17, 8MeO).

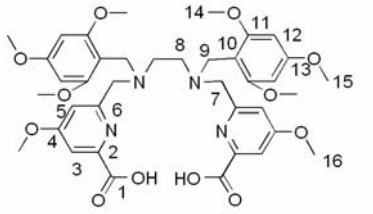

The general deprotection procedure was used with **8** as the starting material. Yield: 61 mg, 0.088 mmol, 87 %. R_f: 0.35. ^{1}H NMR (CD_3OD, 300 MHz, δ): 7.50 (d, $^4J_{3,5}$ = 2.1 Hz, *H3*, 2H), 6.84 (d, $^4J_{3,5}$ = 2.1 Hz, *H5*, 2H), 6.13 (s, *H12,* 4H), 3.89 (s, *H16,* 6H), 3.77 (s, *H15,* 6H) 3.61 (s, *H14,* 12H), 3.41 (s, *H7,* 4H), 3.34 (s, *H9,* 4H), 2.10 (s, *H8,* 4H). ^{13}C NMR (CD_3OD, 100 MHz, δ): 172.4 (*C1*), 169.6 (*C4*), 162.7 (*C13*), 161.7 (*C11*), 156.7 (*C6, C2*), 110.9 (*C5*), 108.5 (*C3*), 106.0 (*C10*), 91.5 (*C12*), 65.1 (*C7*), 56.0 (*C16*), 55.8 (*C14, C15*), 48.7 (*C8*), 43.8 (*C9*). IR (neat, cm^{-1}): 1585 (m), 1455 (m), 1433 (w), 1390 (m). HR-ESI-MS: *m/z* calcd. for $C_{38}H_{46}N_4O_{12}{}^7Li$: 757.3272, found: 757.3260 $[M + Li]^+$.

(1,2-[N,N'-Bis{2,4,6-triethoxybenzyl}methyl]-N,N'-bis[6-{carboxylato}-pyridin-2-yl] methylamino)ethane (18, 6EtO).

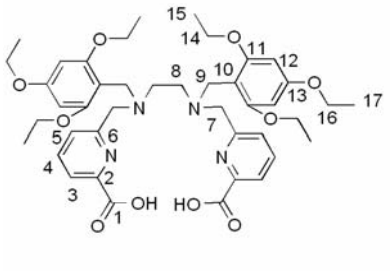

The general deprotection procedure was used with **11** as the starting material. Yield: 91 mg, 0.12 mmol, 92 %. R_f: 0.2. ^{1}H NMR (CD_3OD, 400 MHz, δ): 7.97 (d, $^3J_{3,4}$ = 7.6 Hz, *H3*, 2H), 7.87 (m, $^3J_{3,4}$ = $^3J_{4,5}$ = 7.6 Hz, *H4*, 2H), 7.29 (d, $^3J_{4,5}$ = 7.6 Hz, *H5*, 2H), 6.06 (s, *H12,* 4H), 3.97-3.81 (m, $^3J_{16,17}$ = $^3J_{14,15}$ = 6.8 Hz, *H14, H16,H7,* 16H), 3.43 (s, *H9,* 4H), 2.21 (s, *H8,* 4H), 1.38 (t, $^3J_{16,17}$ = 6.8 Hz, *H17*, 6H), 1.16 (t, $^3J_{14,15}$ = 6.8 Hz, *H15*, 12H). ^{13}C NMR (CD_3OD, 100 MHz, δ): 171.2 (*C1*), 160.0 (*C13, C11*), 159.8 (*C6*), 153.4 (*C2*), 138.2 (*C4*), 123.9 (*C3*), 121.4 (*C5*), 104.7 (*C10*), 91.3 (*C12*), 63.5 (*C15*), 63.3 (*C16*), 61.5 (*C7*), 42.7 (*C8*), 28.7 (*C9*), 14.1 (*C15, C17*). IR (neat, cm^{-1}): 1583 (m), 1434 (w), 1390 (m). HR-ESI-MS: *m/z* calcd. for $C_{42}H_{53}N_4O_{10}$: 773.3762, found: 773.3744 $[M + H]^+$.

(1,2-[N,N'-Bis{2,4,6-triethoxy-benzyl}methyl]-N,N'-bis[4-methoxy-6-{carboxylato} pyri-din-2-yl]methylamino)ethane (19, 6EtO·2MeO).

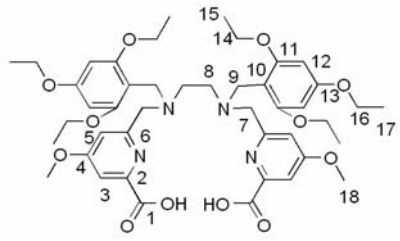

The general deprotection procedure was used with **12** as the starting material. Yield: 92 mg, 0.11 mmol, 84 %. R_f: 0.35. ^{1}H NMR (CD_3OD, 400 MHz, δ): 7.54 (d, $^4J_{3,5}$ = 2 Hz, *H3*, 2H), 6.82 (d, $^4J_{3,5}$ = 2.1 Hz, *H5*, 2H), 6.06 (s, *H12,* 4H), 3.97-3.84 (q, $^3J_{16,17}$ = $^3J_{14,15}$ = 6.8 Hz, *H14, H16,H7,* 12H), 3.89 (s, *H18,* 6H), 3.41 (s, *H9,* 4H), 2.20 (s, *H8,* 4H), 1.33 (t, $^3J_{16,17}$ = 6.8 Hz, *H17*, 6H), 1.18 (t, $^3J_{16,17}$ = 6.8 Hz, *H15*, 12H). ^{13}C NMR (CD_3OD, 100 MHz, δ): 171.0 (*C1*), 168.2 (*C4*), 161.3 (*C13*), 159.9 (*C11*), 159.8 (*C6*) , 155.3 (*C2*), 109.7 (*C5*), 107.0 (*C3*), 104.8 (*C10*), 91.3 (*C12*), 63.5 (*C14*), 63.2 (*C16*), 61.7 (*C7*), 42.8 (*C8*), 29.5 (*C9*), 14.1 (*C5, C17*). IR (neat, cm^{-1}): 1587 (m), 1435 (w), 1390 (m). HR-ESI-MS: *m/z* calcd. for $C_{44}H_{57}N_4O_{12}$: 833.3973, found: 833.3979 $[M - H]^-$.

7.2.4 Coordination Chemistry

General procedure for synthesis of non-radioactive Ga complexes: The ligand was dissolved in a CH_3OH-water mixture (1:2, 6 mL total volume) with adjustment to pH 2 by addition of 0.1 M HCl. $Ga(NO_3)_3 \cdot 6H_2O$ (1 eq) was added and the pH was adjusted by addition of 0.1 M NaOH to 4.5. The reaction mixture was stirred at 60 °C for 2 h. The solvent was removed *in vacuo* to afford the complex as a white solid in quantitative yield.

(1,2-[N,N'-Bis{3-methoxybenzyl}methyl]-N,N'-bis[6-{carboxylato}-pyridin-2-yl]methyl- amino)ethane gallium(III) nitrate ([Ga(13)][NO_3], [Ga(0MeO)][NO_3]).

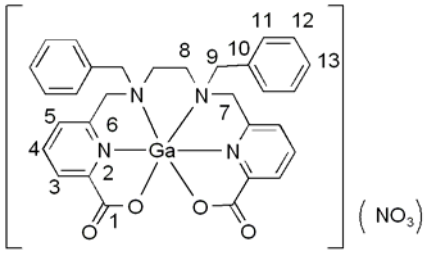

The general complex synthesis procedure was used with **13** as the starting material. ^{1}H NMR (CD_3OD, 400 MHz, δ): 8.69 (m, $^3J_{3,4}$ = 7.6 Hz, $^3J_{4,5}$ = 8 Hz, *H4*, 2H), 8.48 (d, $^3J_{3,4}$ = 7.6 Hz, *H3*, 2H), 8.21 (d, $^3J_{4,5}$ = 8 Hz, *H5*, 2H), 7.45 (s, *H11, H12, H13,* 10H), 4.94 (d, $^3J_{7,7'}$ = 16.4 Hz, *H7*, 2H), 4.32 (d, $^3J_{7,7'}$ = 16.4 Hz, *H7*, 2H), 4.05 (d, $^3J_{9,9'}$ = 14 Hz, *H9*, 2H), 3.81 (d, $^3J_{9,9'}$ = 14 Hz, *H9*, 2H), 3.20 (dd, $^3J_{8,8'}$ = 10.8 Hz, *H8*, 4H). ^{13}C NMR (CD_3OD, 75 MHz, δ): 165.3 (*C1*), 152.3 (*C6*), 148.0 (*C2*), 145.5 (*C4*), 133.3 (*C10*), 130.9 (*C11, C12*), 130.3 (*C13*), 130.0 (*C5*), 125.3 (*C3*), 57.8 (*C7*), 56.6 (*C9*), 47.9. (*C8*) IR (neat, cm^{-1}): 1686 (m), 1609 (m), 1345 (w), 1264 (m). HR-ESI-MS: *m/z* calcd. for $C_{30}H_{28}{}^{69}GaN_4O_4$: 577.1366, found: 577.1368 $[M]^+$.

(1,2-[N,N'-Bis{3-methoxybenzyl}methyl]-N,N'-bis[6-{carboxylato}-pyridin-2-yl] methyl-amino)ethane gallium(III) nitrate ([Ga(14)][NO_3], [Ga(2MeO)][NO_3]).

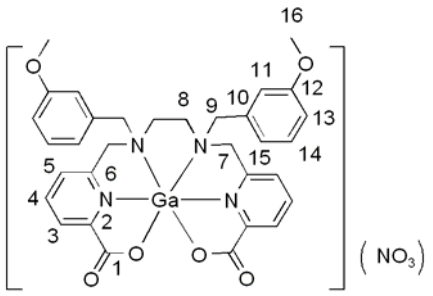

The general complex synthesis procedure was used with **14** as the starting material. ^{1}H NMR (CD_3OD, 600 MHz, δ): 8.62 (m, $^3J_{3,4}$ = 9.6 Hz, $^3J_{4,5}$ = 7.2 Hz, *H4*, 2H), 8.41 (d, $^3J_{3,4}$ = 9.6 Hz, *H3*, 2H), 8.09 (d, $^3J_{4,5}$ = 7.2 Hz, *H5*, 2H), 7.36 (m, *H14*, 2H), 7.05 (m, *H15*, 2H), 6.86 (m, *H11,*

H13, 4H), 4.86 (d, $^{3}J_{7,\,7'}$ = 16.4 Hz, *H7*, 2H), 4.36 (d, $^{3}J_{7,\,7'}$ = 17.8 Hz, *H7*, 2H), 4.01 (d, $^{3}J_{9,\,9'}$ = 15.2 Hz, *H9*, 2H), 3.78 (s, *H16*, 6H), 3.59 (d, $^{3}J_{9,\,9'}$ = 15.2 Hz, *H9*, 2H), 3.02 (dd, $^{3}J_{8,\,8'}$ = 12 Hz, *H8*, 4H). ^{13}C NMR (CD_3OD, 125 MHz, δ): 164.7 (*C1*), 158.7 (*C12*), 147.8 (*C6*), 142.8 (*C2*), 130.0 (*C4*), 129.7 (*C10*), 128.3 (*C14*), 124.1 (*C5*), 124.0 (*C3*), 123.9 (*C15*), 117.1 (*C11*), 114.5 (*C13*), 55.8 (*C7*), 54.9 (*C16*), 54.7 (*C9*), 46.2 (*C8*). IR (neat, cm^{-1}): 1681 (m), 1601 (m), 1346 (w). HR-ESI-MS: *m/z* calcd. for $C_{32}H_{32}{}^{69}GaN_4O_6$: 637.1578, found: 637.1566 $[M]^+$.

(1,2-[N,N'-Bis{3,5-dimethoxybenzyl}methyl]-N,N'-bis[6-{carboxylato}-pyridin-2-yl] methylamino)ethane gallium(III) nitrate ([Ga(15)][NO_3], [Ga(4MeO)][NO_3]).

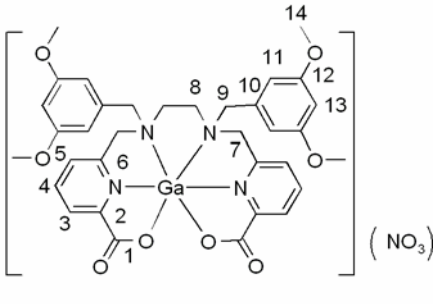

The general complex synthesis procedure was used with **15** as the starting material. ^{1}H NMR (CD_3OD, 400 MHz, δ): 8.69 (m, $^{3}J_{3,\,4}$ = 7.9 Hz, $^{3}J_{4,\,5}$ = 7.5 Hz, *H4*, 2H), 8.49 (d, $^{3}J_{3,\,4}$ = 7.9 Hz, *H3*, 2H), 8.20 (d, $^{3}J_{4,\,5}$ = 7.5 Hz, *H5*, 2H), 6.61 (br, s, *H11, H13*, 6H), 4.98 (d, $^{3}J_{7,\,7'}$ = 16.7 Hz, *H7*, 2H), 4.37 (d, $^{3}J_{7,\,7'}$ = 16.7 Hz, *H7*, 2H), 3.98 (d, $^{3}J_{9,\,9'}$ = 14 Hz, *H9*, 2H), 3.81 (s, *H14*, 6H), 3.67 (d, $^{3}J_{9,\,9'}$ = 14 Hz, *H9*, 2H), 3.18 (dd, $^{3}J_{8,\,8'}$ = 11.6 Hz, *H8*, 4H). ^{13}C NMR (CD_3OD, 75 MHz, δ): 165.3 (*C1*), 162.9 (*C12*), 152.5 (*C6*), 147.9 (*C2*), 145.6 (*C4*), 132.8 (*C10*), 129.8 (*C3*), 125.3 (*C5*), 111.2 (*C11*), 102.3 (*C13*), 58.1 (*C7*), 56.8 (*C9*), 56.1 (*C14*), 47.9 (*C8*). IR (neat, cm^{-1}): 1694 (m), 1596 (m), 1356 (w). HR-ESI-MS: *m/z* calcd. for $C_{34}H_{36}{}^{69}GaN_4O_8$: 697.1789, found: 697.1803 $[M]^+$.

(1,2-[N,N'-Bis{2,4,6-trimethoxybenzyl}methyl]-N,N'-bis[6-{carboxylato}-pyridin-2-yl]methylamino)ethane gallium(III) nitrate ([Ga(16)][NO_3], [Ga(6MeO)][NO_3]).

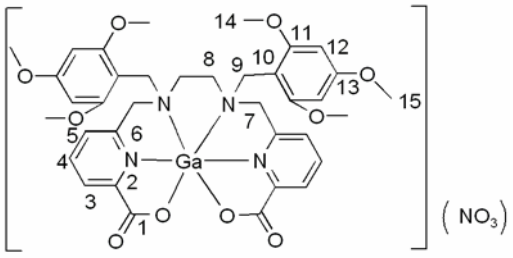

The general complex synthesis procedure was used with **16** as the starting material. ^{1}H NMR (CD_3OD, 400 MHz, δ): 8.68 (m, $^{3}J_{3,\,4}$ = $^{3}J_{4,\,5}$ = 7.6 Hz, *H4*, 2H), 8.48 (d, $^{3}J_{3,\,4}$ = 7.6 Hz, *H3*, 2H), 8.18 (d, $^{3}J_{3,\,4}$ = 7.6 Hz, *H5*, 2H), 6.31 (br, s, *H12*, 4H), 4.92 (d, $^{3}J_{7,\,7'}$ =

16.8 Hz, *H7*, 2H), 4.45 (d, $^3J_{7,7'}$ = 16.8 Hz, *H7*, 2H), 4.07 (d, $^3J_{9,9'}$ = 14 Hz, *H9*, 2H), 3.85 (s, *H15*, 6H), 3.79 (s, *H14*, 12H), 3.46 (d, $^3J_{9,9'}$ = 14 Hz, *H9*, 2H), 3.84 (dd, $^3J_{8,8'}$ = 11.4 Hz, *H8*, 4H). ^{13}C NMR (CD_3OD, 75 MHz, δ): 164.8 (*C1*), 163.2 (*C13*), 162.0 (*C11*), 153.2 (*C2*), 148.1 (*C6*), 145.9 (*C4*), 129.7 (*C3*), 125.2 (*C5*), 100.2 (*C10*), 92.2 (*C12*), 57.9 (*C7*), 56.5 (*C14, C15*), 56.2 (*C8*), 45.5 (*C9*). IR (neat, cm^{-1}): 1689 (m), 1607 (m), 1352 (w). HR-ESI-MS: *m/z* calcd. for $C_{36}H_{40}N_4O_{10}{}^{69}Ga$: 757.2000, found: 757.2005 $[M]^+$.

1,2-[N,N’-Bis{2,4,6-trimethoxybenzyl}methyl]-N,N’-[4-methoxy-6-{carboxylato} pyri-din-2-yl]methylamino)ethane gallium(III) nitrate ([Ga(17)][NO$_3$], [Ga(8MeO)][NO$_3$]).

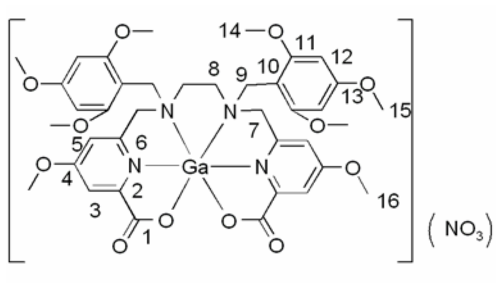

The general complex synthesis procedure was used with **17** as the starting material. ^{1}H NMR (CD_3OD, 400 MHz, δ): 7.85 (d, $^4J_{3,5}$ = 2.1 Hz, *H3*, 2H), 7.62 (d, $^4J_{3,5}$ = 2.1 Hz, *H5*, 2H), 6.27 (br, s, *H12*, 4H), 4.73 (d, $^3J_{7,7'}$ = 16.5 Hz, *H7*, 2H), 4.24 (d, $^3J_{7,7'}$ = 16.5 Hz, *H7*, 2H), 4.15 (s, *H16*, 6H), 4.00 (d, $^3J_{9,9'}$ = 13.8 Hz, *H9*, 2H), 3.43 (d, $^3J_{9,9'}$ = 13.8 Hz, *H9*, 2H), 3.82 (s, *H15*, 6H), 3.76 (s, *H14*, 12H), 2.99-2.77 (dd, $^3J_{8,8'}$ = 10.8 Hz, *H8*, 4H). ^{13}C NMR (CD_3OD, 75 MHz, δ): 175.6 (*C4*), 165.5 (*C1*), 164.9 (*C13*), 162.1 (*C11*), 154.6 (*C6*), 147.8 (*C2*), 113.9 (*C5*), 111.9 (*C3*), 100.4 (*C10*), 92.3 (*C12*), 58.8 (*C7*), 57.9 (*C16*), 56.6 (*C14*), 56.3 (*C15*), 49.9 (*C8*), 45.5 (*C9*). IR (neat, cm^{-1}): 1667 (m), 1611 (m), 1372 (w). HR-ESI-MS: *m/z* calcd. for $C_{38}H_{44}{}^{69}GaN_4O_{12}$: 817.2212, found: 817.2220 $[M]^+$.

(1,2-[N,N’-Bis{2,4,6-triethoxybenzyl}methyl]-N,N’-bis[6-{carboxylato}-pyridin-2-yl] methylamino)ethane gallium(III)nitrate ([Ga(18)][NO$_3$], [Ga(6EtO)][NO$_3$]).

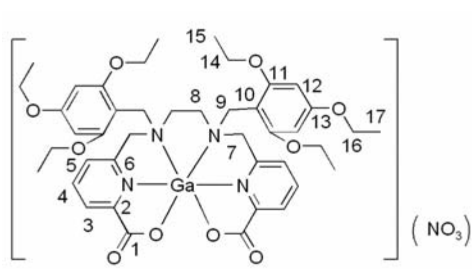

The general complex synthesis procedure was used with **18** as the starting material. ^{1}H NMR (CD_3OD, 400 MHz, δ): 6.69 (m, $^3J_{3,4}$ = 7.2 Hz, $^3J_{4,5}$ = 7.8 Hz, *H4*, 2H), 8.45 (d, $^3J_{3,4}$ = 7.2 Hz, *H3*, 2H), 8.19 (d, $^3J_{3,4}$ = 7.8 Hz, *H5*, 2H), 6.22 (s, *H12*, 4H), 4.97 (d, $^3J_{7,7'}$ = 17.4 Hz, *H7*, 2H), 4.43 (d, $^3J_{7,7'}$ = 17.4 Hz,

H7, 2H), 4.09 (d, $^{3}J_{9,\ 9'}$ = 13.8 Hz, *H9*, 2H), 3.43 (d, $^{3}J_{9,\ 9'}$ = 13.8 Hz, *H9*, 2H), 4.01 (q, $^{3}J_{16,\ 17} = {}^{3}J_{14,\ 15}$ = 7.2 Hz, *H14, H16,* 12H), 3.29-2.84 (dd, $^{3}J_{8,\ 8'}$ = 10.2 Hz, *H8*, 4H), 1.37 (t, $^{3}J_{16,\ 17}$ = 7.2 Hz, *H17*, 6H), 1.17 (t, $^{3}J_{14,\ 15}$ = 7.2 Hz, *H15*, 12H). ^{13}C NMR (CD_3OD, 75 MHz, δ): 163.1 (*C1*), 161.9 (*C13*), 159.4 (*C11*), 150.9 (*C6*), 146.4 (*C2*), 144.1 (*C4*), 127.4 (*C3*), 123.3 (*C5*), 98.4 (*C10*), 91.4 (*C12*), 63.7 (*C15*), 62.9 (*C16*), 56.0 (*C7*), 48.4 (*C8*), 43.8 (*C9*), 13.3 (*C15, C17*). IR (neat, cm^{-1}): 1693 (m), 1606 (m), 1586 (w), 1339 (w). HR-ESI-MS: *m/z* calcd. for $C_{42}H_{52}{}^{69}GaN_4O_{10}$: 841.2939, found: 841.2953 $[M]^+$.

(1,2-[N,N'-Bis{2,4,6-triethoxybenzyl}methyl]-N,N'-bis[4-methoxy-6-{carboxylato}-pyri-din-2-yl]methylamino)ethane gallium(III) nitrate ([Ga(19)][NO_3]), [Ga(6EtO·2MeO)][NO_3]).

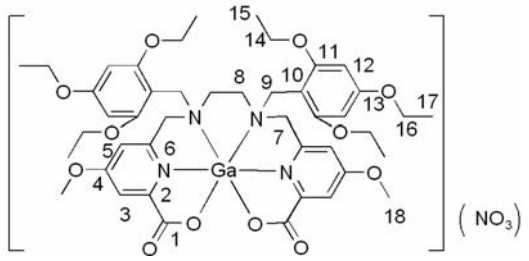

The general complex synthesis procedure was used with **19** as the starting material. ^{1}H NMR (CD_3OD, 400 MHz, δ): 7.87 (s, *H3*, 2H), 7.68 (s, *H5*, 2H), 6.22 (s, *H12*, 4H), 5.12-4.80 (d, $^{3}J_{7,\ 7'}$ = 16.8 Hz, *H7*, 2H), 4.15 (s, *H18*, 6H), 4.09 (d, $^{3}J_{9,\ 9'}$ = 13.8 Hz, *H9*, 2H), 3.43 (d, $^{3}J_{9,\ 9'}$ = 13.8 Hz, *H9*, 2H), 4.03 (q, $^{3}J_{16,\ 17} = {}^{3}J_{14,\ 15}$ = 6.6 Hz, *H14, H16,* 12H), 3.10-2.80 (dd, $^{3}J_{8,\ 8'}$ = 10.8 Hz, *H8*, 4H), 1.37 (t, $^{3}J_{16,\ 17}$ = 6.6 Hz, *H17*, 6H), 1.25 (t, $^{3}J_{14,\ 15}$ = 6.6 Hz, *H15*, 12H). ^{13}C NMR (CD_3OD, 75 MHz, δ): 175.5 (*C4*), 165.2 (*C1*), 165.1(*C11*), 163.6 (*C13*), 154.1 (*C2*), 147.6 (*C3*), 134.1 (*C6*), 113.6 (*C5*), 111.7 (*C10*), 93.2 (*C12*), 65.6 (*C18*), 63.2 (*C16*), 58.7 (*C14*), 57.5 (*C7*), 49.4 (*C8*), 45.4 (*C9*), 15.2 (*C15*), 15.0 (*C17*). IR (neat, cm^{-1}): 1687 (m), 1607 (m), 1583 (w), 1357 (w). HR-ESI-MS: *m/z* calcd. for $C_{44}H_{56}{}^{69}GaN_4O_{12}$: 901.3151, found: 901.3138 $[M]^+$.

7.2.5 X-Ray Diffraction Structural Characterization of [Ga(6EtO·2MeO)][ClO_4]

A colourless tablet crystal of $C_{44}H_{56}N_4O_{16}GaCl.[1.28MeOH][1.18H_2O]$ having approximate dimensions of 0.10 x 0.29 x 0.29 mm was mounted on a glass fiber. All measurements were made on a Bruker APEX DUO diffractometer with graphite

monochromated Mo-Kα radiation. The data were collected at a temperature of -183.0 ± 0.1° C to a maximum 2θ value of 52.1 °. Data were collected in a series of ϕ and ω scans in 0.5 ° oscillations using 20.0-second exposures. The crystal-to-detector distance was 40.11 mm. Of the 57970 reflections that were collected, 9817 were unique (R_{int} = 0.043); equivalent reflections were merged. Data were collected and integrated using the Bruker SAINT[78] software package. The linear absorption coefficient, μ, for Mo-Kα radiation is 6.82 cm^{-1}. Data were corrected for absorption effects using the multi-scan technique (SADABS),[79] with minimum and maximum transmission coefficients of 0.815 and 0.934, respectively. The data were corrected for Lorentz and polarization effects. The collection and analysis of the data was done by Dr. Brian O. Patrick.

7.2.6 Radiolabelling with $^{67/68}$Ga, Log $P_{o/w}$ Measurements and Transferrin Stability

General procedure for labelling with $^{67/68}$Ga: $^{67}GaCl_3$ (100 μL, 1 mCi) in 0.01 M HCl or $^{68}Ga^{3+}$ in a 0.1 M HCl solution was added into 10^{-4} M solution of ligand in 10 mM or 200 mM NaOAc solution (pH 4.5, 950 μL) respectively and left to react for 10 minutes at room temperature. The reaction was monitored by analytical HPLC (gradient: A: NaOAc buffer, pH 4.5, B: CH_3OH. 0-100% B linear gradient 20 min). Radioactivity for ^{68}Ga labelling decay corrected to elution time.

Transferrin competition was done by addition of $^{67}GaCl_3$ into a 10^{-4} M solution of ligand in 10 mM NaOAc solution (pH 4.5, 950 μL). Complex formation was confirmed by HPLC. A 400 μL aliquot was added to 1 mg/mL *apo*-transferrin in a $NaHCO_3$ solution (10 mM, 600 μL) and incubated at 37° C (water bath). Complex stability was checked at time points 10 minutes, 1 h and 2 h via analytical HPLC.

Log $P_{o/w}$ measurements entail addition of a 20 μL aliquot of labelling solution to a mixture of 500 μL octanol and 480 μL aqueous PBS solution. The biphasic mixture was agitated for 30 seconds and subsequently centrifuged to separate the two layers. Aliquots (100 μL) of each phase were isolated and radioactivity was measured. Log $P_{o/w}$ measurements were executed in triplicate.

[^{67}Ga(0MeO)]$^{+}$: R_t of radiolabeled product on HPLC: 9.9 minutes. Stability versus transferrin (10 min/1 h/ 2 h; % complex intact): 96/ 74/ 66. ^{68}Ga labelling: 10^{-6} M ligand, 97 %, 0.45 mCi/ nmol. Log $P_{o/w}$: -1.25.

[^{67}Ga(2MeO)]$^{+}$: R_t of radiolabeled product on HPLC: 10.8 minutes. Stability versus transferrin (10 min/1 h/ 2 h; % complex intact): 95/ 66/ 55. ^{68}Ga labelling: 10^{-6} M ligand, 96.5 %, 0.45 mCi/ nmol. Log $P_{o/w}$: -0.83.

[^{67}Ga(4MeO)]$^{+}$: R_t of radiolabeled product on HPLC: 11.6 minutes. Stability versus transferrin (10 min/1 h/ 2 h; % complex intact): 76/ 59/ 52. ^{68}Ga labelling: 10^{-6} M ligand, 95 %, 0.45 mCi/ nmol. Log $P_{o/w}$: -0.32.

[^{67}Ga(6MeO)]$^{+}$: R_t of radiolabelled product on HPLC: 11.8 minutes. Stability versus transferrin (10 min/1 h/ 2 h; % complex intact): 86/ 85/ 82. ^{68}Ga labelling: 10^{-6} M ligand, 94 %, 0.45 mCi/ nmol. Log $P_{o/w}$: -0.03.

[^{67}Ga(8MeO)]$^{+}$: R_t of radiolabelled product on HPLC: 12.4 minutes. Stability versus transferrin (10 min/1 h/ 2 h; % complex intact): 97/ 96/ 96. ^{68}Ga labelling: 10^{-5} M ligand, 98.5 %, 0.45 mCi/ nmol. Log $P_{o/w}$: 0.66.

[^{67}Ga(6EtO)]$^{+}$: R_t of radiolabelled product on HPLC: 14.6 minutes. Stability versus transferrin (10 min/1 h/ 2 h; % complex intact): 95/ 92/ 91. ^{68}Ga labelling: 10^{-5} M ligand, 97.9 %. Log $P_{o/w}$: 1.10.

[^{67}Ga(6EtO·2MeO)]$^{+}$: R_t of radiolabeled product on HPLC: 15.4 minutes. Stability versus transferrin (10 min/1 h/ 2 h; % complex intact): 94/ 93/ 93. ^{68}Ga labelling: 10^{-5} M ligand, 98.3 %. Log $P_{o/w}$: 1.16.

7.2.7 *In Vivo* Evaluation

The protocol used in the animal studies was approved by the Institutional Animal Care Committee of the University of British Columbia and was performed in accordance with the Canadian Council on Animal Care Guidelines. A total of 16 female ICR (20-30 g) mice were used for the animal study of each of the seven compounds. ^{67}Ga monocationic complexes of **0MeO, 2MeO, 4MeO, 6MeO, 6EtO** and **6EtO·2MeO** were prepared as described above and then diluted in phosphate buffered saline to a concentration of 100 μCi/mL. Each mouse was i.v. injected with ~10 μCi (100 μL) of the

^{67}Ga complex and then sacrificed by CO_2 inhalation at 2 min, 30 min, 1 h or 2 h after injection (n = 4 at each time point). Blood was collected by cardiac puncture. Tissues collected included kidney, liver, spleen, femur, muscle, heart, lung, intestine and brain. Tissues were weighed and counted on a gamma counter and the counts were converted to % injected dose/gram (% ID/ g). The collection of the data was done by Dr. Dawn Waterhouse.

7.3 Results and Discussion

7.3.1 Ligand Synthesis

The seven ligand systems are synthesized using analogous synthetic pathways (Scheme 7.1), derived from methodology used for compounds reported in Chapter 4 and Chapter 6. For **0MeO, 6MeO** and **6EtO**, the corresponding benzaldehyde reacted with the ethylenediamine by reductive amination.

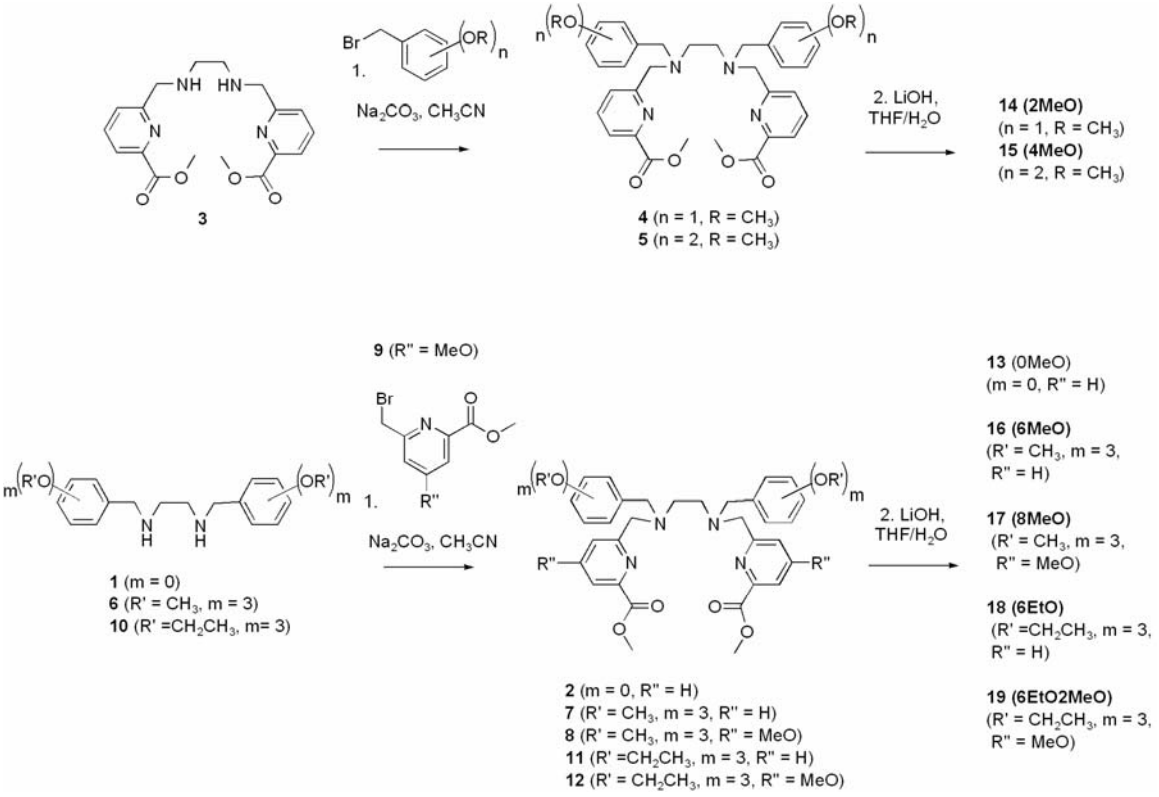

Scheme 7.1 General synthetic scheme for all compounds synthesized and reported in this chapter.

Then, 6-bromomethylpyridin-2-carboxylic acid methyl ester was used to alkylate the secondary amine to afford the desired scaffolds with methyl-protected carboxylates. **8MeO** and **6EtO·2MeO** were synthesized using the same methodology, using **9** as the alkylating agent. For the preparation of **2MeO** and **4MeO**, **3** was synthesized according to the literature.[131] The secondary amines of **3** were alkylated with the corresponding bromo-methyl-phenyl derivatives to give rise to the corresponding methyl-protected carboxylate-bearing ligand scaffolds. Deprotection of all methyl esters was achieved using base-catalyzed saponification (Scheme 7.1). All chelates were characterized using ^{1}H and ^{13}C NMR spectroscopic methods, mass spectrometry and IR spectroscopy.

7.3.2 Non-radioactive Complexes with Ga

The corresponding non-radioactive Ga complexes were formed by mixing $Ga(NO_3)_3 \cdot 6H_2O$ with the ligand of interest. The pH was adjusted to 4.5 and the reaction mixture was stirred at 60 °C for 2 h in order to afford the desired complex quantitatively. ^{1}H NMR spectroscopy is used to determine complete chelation; a low field shift and simultaneous splitting of the methylene protons can be observed. Two examples of ^{1}H NMR spectra of ligand and corresponding Ga complex are shown (Figures 7.3 and 7.4). Geminal protons are easily identified by the characteristic, large geminal ^{2}J coupling constants, which are found to be > 11 Hz for **dedpa**-type ligand systems.

All complexes were characterized using ^{1}H and ^{13}C NMR spectroscopic methods, mass spectrometry and IR spectroscopy. One interesting observation from the spectroscopic data is the strong broadening of the methylene peaks, when the ligand is not complexed. This could be due to the fast rotation of the molecule in an attempt to decrease repulsion of hydrophilic and hydrophobic functional groups. This is supported by the observation that this effect increases with enhanced lipophilicity of the corresponding chelate.

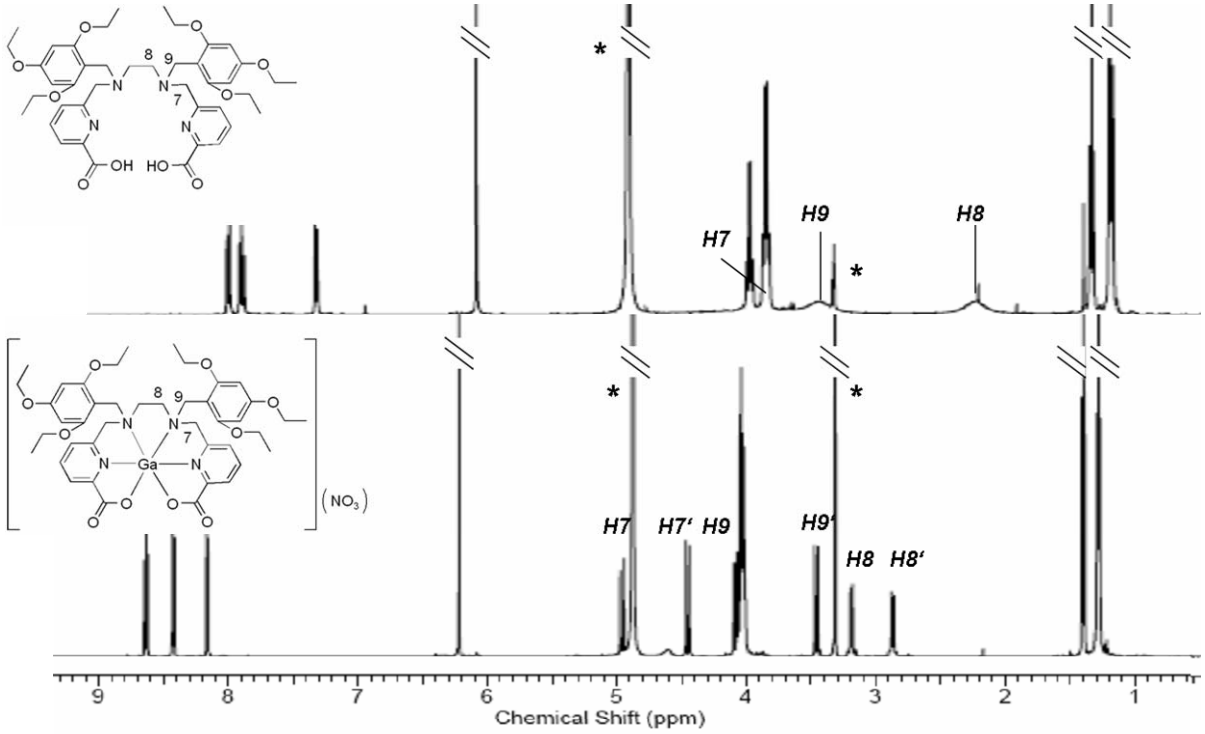

Figure 7.3 ^{1}H NMR (300 MHz, CD_3OD, 298 K) spectra of **6EtO** and [Ga(**6EtO**)][NO_3]. * denotes residual solvent peaks.

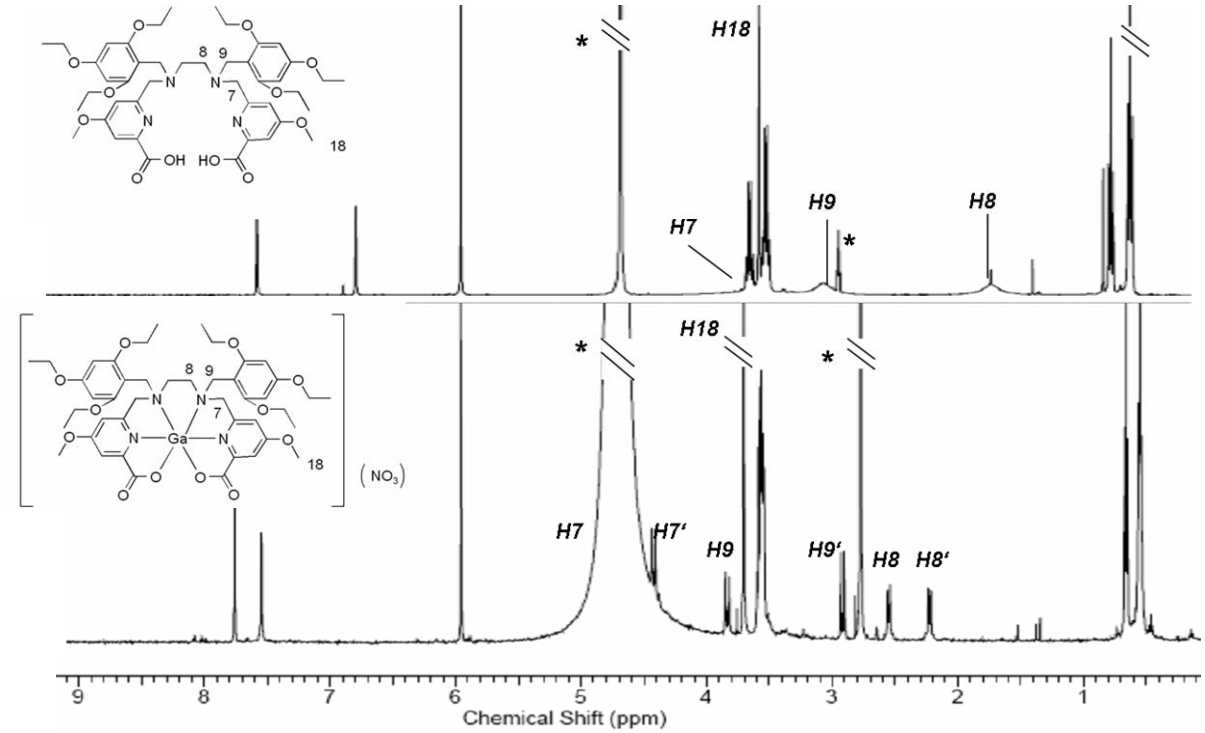

Figure 7.4 ^{1}H NMR spectra (300 MHz, CD_3OD, 298 K) of **6EtO·2MeO** and [Ga(**6EtO·2MeO**)][NO_3]. * denotes residual solvent peaks.

7.3.3 X-Ray Diffraction Structural Characterization of [Ga(6EtO·2MeO)][ClO_4]

To afford crystals suitable for solid state structure determination, $Ga(ClO_4)_3 \cdot 6H_2O$ was used as starting material in place of the nitrate salt. The complex was dissolved in a H_2O-CH_3OH mixture and was left for slow solvent evaporation. After 5 days, crystals suitable for X-ray diffraction had formed. The solid state structure of complex [Ga(**6EtO·2MeO**)][ClO_4] was determined by X-ray diffraction and is shown in Figure 7.5. When compared to the structural information for [Ga(**dedpa**)]$^+$ (Chapter 4), a complex of similar structural composition with no overall increase in metal to ligand bond lengths was observed, despite the greatly increased steric bulk and additional functionality on the pyridyl moiety (Table 7.1).

Table 7.1 Selected bond lengths in [Ga(**6EtO·2MeO**)][ClO_4] (bold), compared to selected bond lengths in [Ga(**dedpa**)][ClO_4], ([Å]).

bond	length [Å]	length [Å]	angle	degree [°]
N1-Ga	**1.969(3)**	1.992(5)	N(1)- Ga(1)- O(1)	80.25(12)
N2- Ga	**2.163(3)**	2.159(5)	O(1)- Ga(1)- O(3)	100.76(12)
N3- Ga	**2.171(3)**	2.188(5)	O(3)- Ga(1)- N(2)	92.12(12)
N4-Ga	**1.970(3)**	1.981(5)	N(1)- Ga(1)- N(3)	104.78(13)
O1- Ga	**1.980(3)**	1.967(4)	N(4)- Ga(1)- N(3)	78.98(13)
O2- Ga	**1.998(3)**	1.976(4)	O(1)- Ga(1)- N(3)	90.65(12)

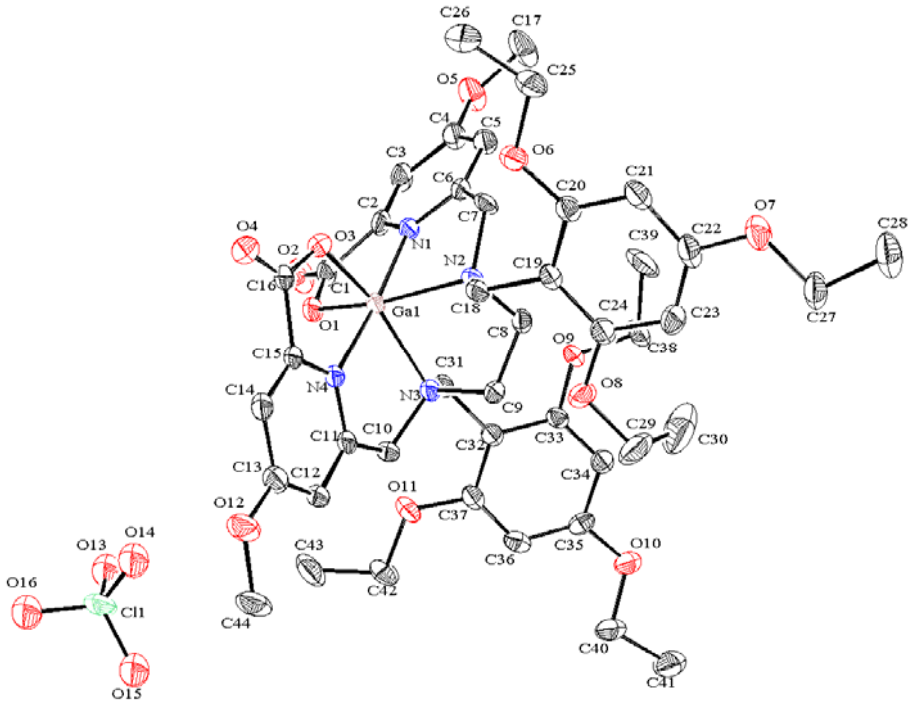

Figure 7.5 ORTEP representation of [Ga(**6EtO·2MeO**)][ClO_4], with corresponding molecular drawing. Shown is the atom numbering scheme (50% thermal ellipsoids). Hydrogen atoms are omitted for clarity.

7.3.4 Radiolabelling with $^{67/68}$Ga and *In Vitro* Stability

To investigate the viability of these new ligand systems for the purpose of labelling with ^{68}Ga, the ligands were subjected to extensive labelling studies with ^{67}Ga. All chelates labelled in close to quantitative radiolabelling yields at concentrations as low as 10^{-6} M under the mild labelling conditions of only 10 minutes at room temperature. The labelling proceeds non-carrier added, which is advantagous compared to previously reported small cationic ^{67}Ga complexes.[173,177] When the radiochemical complexes were investigated for their stability to transferrin challenge, an unexpected trend was observed. Stability decreased from [^{67}Ga(**0MeO**)]$^+$ to [^{67}Ga(**2MeO**)]$^+$ to [^{67}Ga(**4MeO**)]$^+$, which was the complex with the lowest *in vitro* stability. [^{67}Ga(**6MeO**)]$^+$ however, showed increased stability, but was still inferior to the high stability observed for the more sterically crowded complexes [^{67}Ga(**6EtO**)]$^+$ and [^{67}Ga(**6EtO·2MeO**)]$^+$. This trend could

be explained by the increased lipophilicity of complexes $[^{67}Ga(\mathbf{6MeO})]^+$, $[^{67}Ga(\mathbf{6EtO})]^+$ and $[^{67}Ga(\mathbf{6EtO{\cdot}2MeO})]^+$ compared to the other four. The binding site for Fe(III) and Ga(III) on transferrin lies in a shallow, polar pocket, which would experience more repulsion from an apolar, ball-like complex than from a more polar one.

7.3.5 Log $P_{o/w}$ Measurements

The increase in polarity was demonstrated by log $P_{o/w}$ measurements. While the octanol water partition coefficients for compounds $[^{67}Ga(\mathbf{0MeO})]^+$, $[^{67}Ga(\mathbf{2MeO})]^+$ $[^{67}Ga(\mathbf{4MeO})]^+$ and $[^{67}Ga(\mathbf{6MeO})]^+$ remain in the more polar, negative region, $[^{67}Ga(\mathbf{8MeO})]^+$, $[^{67}Ga(\mathbf{6EtO})]^+$ and $[^{67}Ga(\mathbf{6EtO{\cdot}2MeO})]^+$ exhibit positive log $P_{o/w}$ values from 0.66 to 1.16 (Table 7.2), corresponding to the retention times measured by HPLC. According to a comprehensive review,[171] one desirable property for ^{99m}Tc complexes to have optimal myocardial retention and low liver uptake is a log $P_{o/w}$ value within the range of 0.5 to 1.2. Since the latter 3 compounds fall within these margins, they were considered good candidates for the development of a potential cardiac imaging agent.

Table 7.2 Log $P_{o/w}$ values and corresponding HPLC retention times of the seven new compounds.

Complex	R_t [10 min]	Log $P_{o/w}$	Stability versus Tf [10 min/1 h/ 2 h; % complex intact]
$[^{67}Ga(\mathbf{0MeO})]^+$	9.9	-1.25	96/ 74/ 66
$[^{67}Ga(\mathbf{2MeO})]^+$	10.8	-0.83	95/ 66/ 55
$[^{67}Ga(\mathbf{4MeO})]^+$	11.6	-0.32	76/ 59/ 52
$[^{67}Ga(\mathbf{6MeO})]^+$	11.8	-0.03	86/ 85/ 82
$[^{67}Ga(\mathbf{8MeO})]^+$	12.4	0.66	97/ 96/ 96
$[^{67}Ga(\mathbf{6EtO})]^+$	14.6	1.10	95/ 92/ 91
$[^{67}Ga(\mathbf{6EtO{\cdot}2MeO})]^+$	15.4	1.16	94/ 93/ 93

7.3.6 Biodistribution

To evaluate the biodistribution profile of the synthesized H_2**dedpa** derivatives, each of the radiochemical complexes was prepared and subsequently diluted in phosphate buffered saline to a concentration of 100 μCi/mL. For each compound, 16 mice were injected intravenously and 4 animals were sacrificed at each time point after 2 minutes, 30 minutes, 1 h and 2 h. Activity is represented in % ID/g (Figure 7.6). The most hydrophilic complexes [^{67}**Ga(0MeO)]**$^+$, [^{67}**Ga(2MeO)]**$^+$ and [^{67}**Ga(4MeO)]**$^+$ have biodistribution profiles similar to those previously investigated in benzyl-nitro derivatives (Chapter 4). Predominantly renal excretion was observed, with bone uptake between 3 – 4 % ID/g (for complete tables see appendix B). This confirms the slightly decreased stability observed in the *in vitro* transferrin challenge for these 3 complexes. In the case of [^{67}**Ga(6MeO)]**$^+$ a distinct change in biodistribution behaviour was observed. Clearance was observed via both renal and hepatobilary excretion.

[^{67}**Ga(6MeO)]**$^+$ seems to clear rapidly from all organs except the liver within 2 h; this had not yet been observed for any H_2**dedpa** derivative. The rapid blood clearance was an important improvement. The very low bone uptake indicates high *in vivo* stability of this complex; however, due to the low lipophilicity, the compound showed no persistent retention in the myocardium. [^{67}**Ga(8MeO)]**$^+$ showed very similar behaviour. The fast clearance profile was maintained, still, no retention in the myocardium was observed. An increased uptake in the liver and the intestines was seen. [^{67}**Ga(6EtO)]**$^+$ was the first compound of the series to show a somewhat persistent heart uptake, above 1 % ID/g; however, blood and lung clearance were inferior to those of [^{67}**Ga(8MeO)]**$^+$. Due to increased lipophilicity, the uptake in the liver increased.

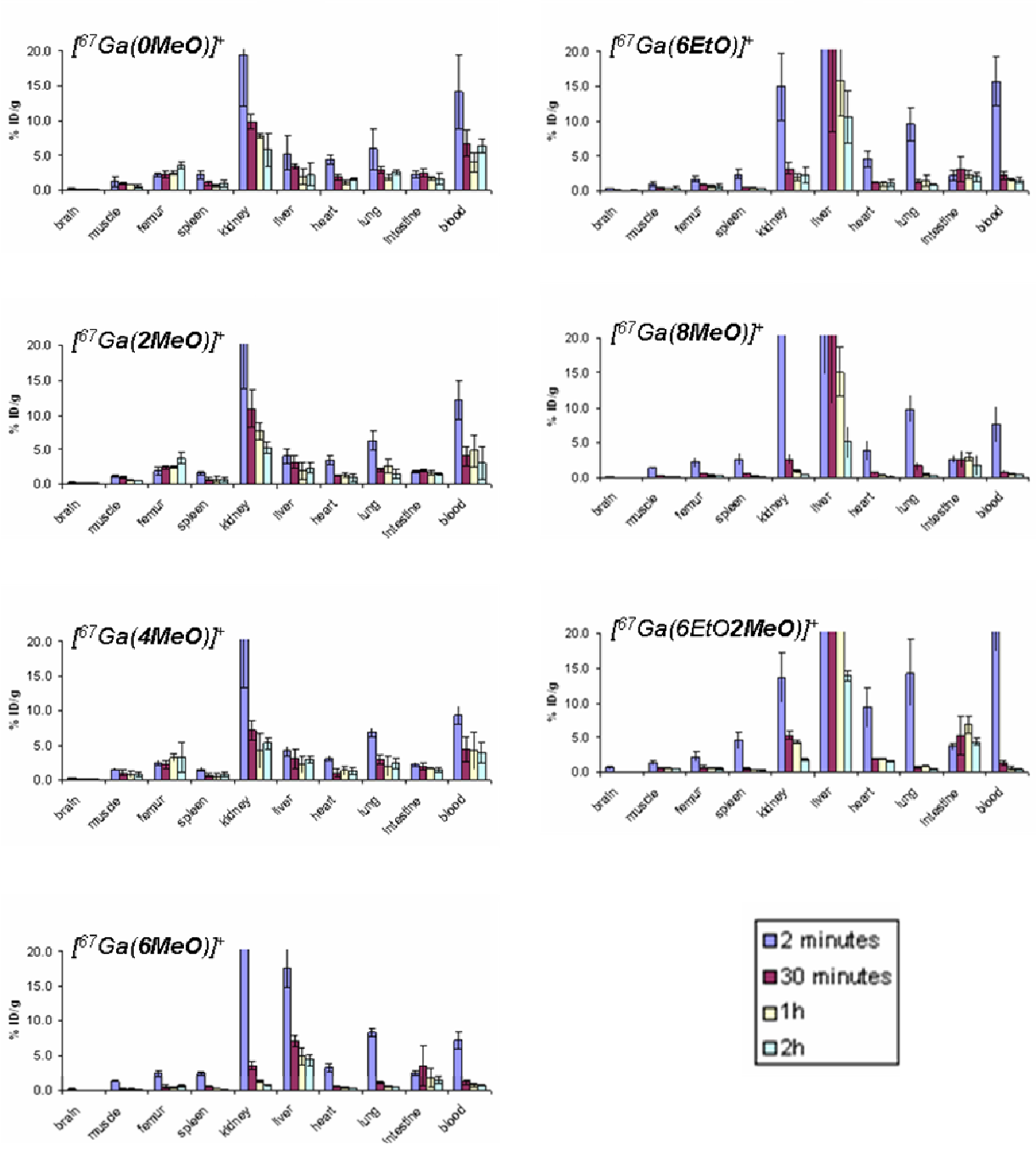

Figure 7.6 Biodistribution of [^{67}Ga(**0MeO**)]$^{+}$, [^{67}Ga(**2MeO**)]$^{+}$, [^{67}Ga(**4MeO**)]$^{+}$, [^{67}Ga(**6MeO**)]$^{+}$, [^{67}Ga(**8MeO**)]$^{+}$, [^{67}Ga(**6EtO**)]$^{+}$and [^{67}Ga(**6EtO·2MeO**)]$^{+}$ in female ICR mice over 2h.

As the most lipophilic of the complexes investigated, **[^{67}Ga(6EtO·2MeO)]$^{+}$** showed the best results in terms of biodistribution. The complex cleared well from both blood and lung after 30 minutes. Bone uptake was low, confirming the high stability observed in the transferrin challenge. After the initial, high uptake (above 9 % ID/g) the heart uptake dropped at the 30 minute time point, but it remained persistently above 1.5 % ID/g, resulting in heart/blood and heart/lung values greater then 3 (Table 7.3).

Table 7.3 Heart/blood, heart/lung and heart/liver ratios for compounds [^{67}Ga(**8MeO**)]$^{+}$, [^{67}Ga(**6EtO**)]$^{+}$, [^{67}Ga(**6EtO·2MeO**)]$^{+}$

Complex	2 min ± SD	30 min ± SD	1 h ± SD	2 h ± SD
[^{67}Ga(**8MeO**)]$^{+}$				
heart/blood	0.50 ± 0.07	0.73 ± 0.12	0.64 ± 0.07	0.53 ± 0.05
heart/liver	0.17 ± 0.03	0.03 ± 0.02	0.02 ± 0.00	0.04 ± 0.01
heart/lung	0.38 ± 0.09	0.41 ± 0.08	0.50 ± 0.32	0.45 ± 0.30
[^{67}Ga(**6EtO**)]$^{+}$				
heart/blood	0.29 ± 0.03	0.55 ± 0.13	0.65 ± 0.17	0.91 ± 0.70
heart/liver	0.16 ± 0.02	0.11 ± 0.13	0.07 ± 0.01	0.13 ± 0.08
heart/lung	0.51 ± 0.17	0.89 ± 0.15	0.84 ± 0.44	1.33 ± 0.59
[^{67}Ga(**6EtO·2MeO**)]$^{+}$				
heart/blood	0.33 ± 0.15	1.62 ± 0.43	3.37 ± 0.61	3.80 ± 0.81
heart/liver	0.31 ± 0.06	0.06 ± 0.00	0.07 ± 0.02	0.14 ± 0.60
heart/lung	0.66 ± 0.10	4.59 ± 5.19	2.29 ± 0.51	3.28 ± 0.60

The significant liver uptake (above 13 % ID/g) even after 2 hours renders this compound a poor candidate for cardiac imaging with PET. The cause for the high liver uptake may not lie solely with the increased lipophilicity. When compared with the compounds based on the bis(salycilaldimine) scaffold,[173] it becomes clear that an

increased number of benzylic groups could specifically target the liver, because this functional group is preferentially metabolized in liver microsomes to afford more water-soluble species, which are then subsequently excreted.[178]

7.4 Conclusion

The synthesis, labelling and biodistribution of seven new lipophilic derivatives of H_2**dedpa** for the purpose of cardiac perfusion imaging were described. The solid state structure obtained for [Ga(**6EtO·2MeO**)][ClO_4] showed that derivatization at the 4 position on the pyridyl ring is feasible and provides additional possibilities for functionalization without impacting metal coordination. While high initial uptake and slow clearance from liver remain issues, four of these novel complexes have shown improved blood, lung and kidney clearance compared to derivatives reported previously. The two complexes [^{67}**Ga(6EtO)]**$^+$ and [^{67}**Ga(6EtO·2MeO)]**$^+$ with log $P_{o/w}$ values > 1.1 have shown persistent heart uptake over the course of 2 h above 1 % ID/g, one of which shows a larger heart uptake value than the currently commercially used $^{82}Rb^+$.

Chapter 8: Conclusions and Future Work

8.1 Further Enhancing the H_2dedpa Technology

Significant intellectual property is associated with the work in this thesis and one full patent application has been filed; therefore, suggestions for future work are intentionally vague in order to not jeopardize this coverage and future filings.

As described within the experimental portion of this thesis, a variety of acyclic chelates were investigated for their capability to chelate the (radio-)metals ^{99m}Tc, $^{185/187}$Re, $^{63/64/65}$Cu and $^{67/68/69/71}$Ga. The most efficient, multifunctional chelate identified was H_2**dedpa**, which was subsequently functionalized to furnish a bioconjugate with the cyclic peptide RGD (Chapter 6) or to form small lipophilic cations upon coordination of Ga (Chapter 7). The techniques described within this work include a wide array of methods such as organic and inorganic synthesis, physico-chemical methods, radiochemistry and biological studies; typical for multidisciplinary fields like medicinal inorganic chemistry. In addition to the first applications of the scaffold described within this thesis, there is a large field of opportunities arising from this discovery. *In vivo* evaluations of the RGD conjugates are underway and will furnish information on how well bifunctionalized H_2dedpa derivatives localize in tumours and clear from non-target tissues. Some suggestions for further elaborations, as well as new ideas and perspectives are given in this chapter.

8.1.1 Extension of the Denticity for Other Metals of Interest

While the investigated metals Ga(III) and Cu(II) have a preference for hexadentate chelation scaffolds, a wide variety of metals of relevance in the field of imaging and therapy requires greater denticities and bite angles. The chelate library described in Chapter 4 includes two octadentate chelate systems and two hexadentate chelates with larger bite angle due to their propyl backbones. Investigation of these systems for coordination with metals In, Y, Lu, Gd is of great interest. A second screening involving radionuclides of In, Y and Lu could be used to find lead chelates for these metal ions. Among selection criteria, more emphasis could be put on *in vitro* stability and less on fast

labelling conditions because of the longer half-lives of these radiometals. Once a lead compound is established, the corresponding non-radioactive complex must be formed and investigated for its structure and thermodynamic stability. Functionalization through the backbone is already explored and could also be investigated with octadentate ligand systems. The corresponding model derivatives are shown in Figure 8.1.

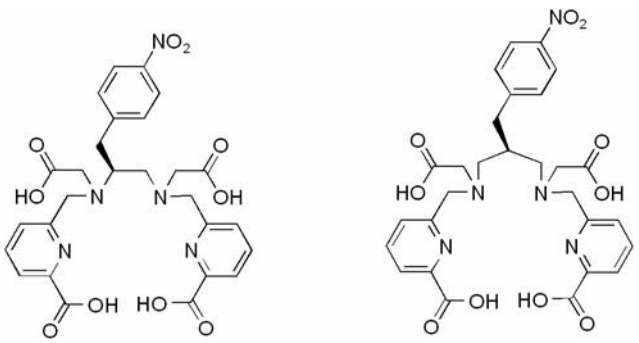

Figure 8.1 Proposed octadentate model compounds based on the H_2**dedpa** scaffold.

8.1.2 H_2dedpa Peptide Derivatives of Relevance for Clinical Applications

After successful conjugation to RGD, and subsequent *in vivo* imaging, it will become apparent if the clearance profile of the dedpa derivatives is satisfactory enough to consider other targeting moieties for H_2**dedpa**-linked targeting entities. After successful derivatization of the pyridine moiety (Chapter 7) this could be a point of attachment for prosthetic groups, which can facilitate clearance or enhance circulation.

In terms of application to other targeting moieties, the synthesized isothiocyanato derivatives can be easily conjugated to antibodies or other targeting moieties carrying a lysine that is not essential for the biological recognition of the target molecule. The minimum concentration necessary for quantitative labelling, especially with $^{67/68}$Ga, is so low that even kit formulations using any type of targeting moiety could be prepared easily. This could alleviate the current need for complicated automation and purification systems such as the ones currently used for the production of ^{68}Ga-DOTATOC.[166]

8.2 Small Molecule Imaging Agents

8.2.1 New Lipophilic Ligand Systems for Imaging of Myocardial Bloodflow

A first compound series for imaging of myocardiac bloodflow was synthesized and described in Chapter 7. It was found that aryl functionalization increased the liver uptake greatly with increased lipophilicity of the ligand system. In order to decrease uptake in the liver, but maintain the high persistent uptake in the myocardium, other ways of introducing lipophilicity must be investigated.

From investigations by others and those described in this thesis, it can be concluded that the optimal log $P_{o/w}$ window for Ga-based complexes might only partially overlap with the optimal window given for ^{99m}Tc-based complexes for the purpose of heart imaging ($P_{o/w}$ = 0.5 – 1.2). Ga-complexes with log $P_{o/w}$ < 1 were all found to clear the myocardium to a significant extent before 2 h. The optimal log $P_{o/w}$ window for persistent heart upake of Ga-based complexes was found to be 1- 2. This, together with a reduced number of aryl functionalities must be taken into consideration when a new series of lipophilic H_2**dedpa** derivatives for this purpose is designed and synthesized.

8.2.2 Alternative H_2dedpa Derivatives as Small Molecule Imaging Agents

Besides modulating the physical properties of H_2**dedpa** complexes in order to achieve accumulation in the myocardium, there are other functionalities, which can be attached to a chelate to subsequently direct localization and excretion. One of the currently most pursued and investigated small prosthetic groups is the nitroimidazole fragment, which is known to accumulate in hypoxic cells.[179] Imaging hypoxic tissues is difficult and desperately sought. It was found that among nitroimidazole derivatives 2-nitroimidazole can be reduced most efficiently to form a reactive chemical species, which can bind to cell components in the absence of sufficient oxygen. The PET tracer ^{18}F-

fluoromisonidazole (FMISO) is in clinical use for the imaging of hypoxia[180] however, its biodistribution profile is not optimal and the development of non-cyclotron but generator-based radiopharmaceuticals is a persistent, strong driving force.[181] Some NOTA nitroimidazole conjugates and their uptake for imaging hypoxic tissues have been reported. Low tumor and high kidney and liver uptake rendered these conjugates poor candidates for further development.[182] Since the more polar H_2**dedpa** derivatives exhibit low uptake in those organs, a nitroimidazole derivative of this chelate could be an interesting target compound. Below, examples of a previously reported conjugate and a hypothetical H_2dedpa nitroimidazole derivative are shown (Figure 8.2).

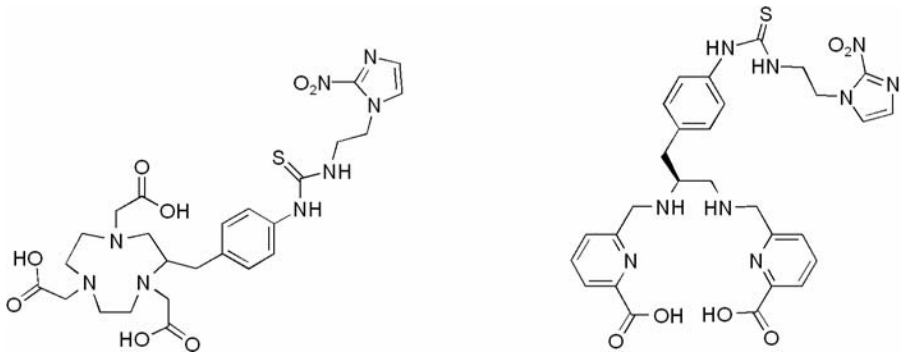

Figure 8.2 Nitroimidazole derivatives of NOTA (left) and H_2**dedpa** (right).

Finally, it can be concluded that while acyclic chelates are sometimes disregarded due to their perceived lack of thermodynamic stability for the purpose of radiometal chelation, fast coordination and kinetic inertness can be more valued qualities. In some cases, an acyclic ligand system can exhibit high thermodynamic stability along with the expected rapid kinetics, and can give rise to a chelate of surprisingly superior qualities compared to the often favoured macrocyclic systems.

References

(1) Lippard, S. J. *J. Am. Chem. Soc.* **2010**, *132*, 14689-14693.
(2) Ehrlich, P. *Deutsch. Med. Woch.* **1910**, 1893-1896.
(3) Maxwell, G.; Hollanger, S. *J. Med.* **1993**, *24*, 4-5.
(4) Sutton, B. M.; Hempel, J. C.; Hill, D. T. *Curr. Clin. Pract.* **1983**, *7*, 6-16.
(5) Holman, B. L.; Jones, A. G.; Lister-James, J.; Davison, A.; Abrams, M. J.; Kirshenbaum, J. M.; Tumeh, S. S.; English, R. J. *J. Nucl. Med.* **1984**, *25*, 1350-1355
(6) Orvig, C.; Thompson, K. H. *Science* **2003**, *300*, 936-939.
(7) Lauterbur, P. C. *Nature* **1973**, *242*, 190-191.
(8) Terreno, E.; Castelli, D. D.; Viale, A.; Aime, S. *Chem. Rev.* **2010**, *110*, 3019-3042.
(9) Merbach, A. E.; Toth, E. *The Chemistry of Contrast Agents in Medical Magnetic Resonance Imaging*; John Wiley & Sons Ltd: New York, 2001.
(10) Major, J. L.; Meade, T. J. *Acc. Chem. Res.* **2009**, *42*, 893-903.
(11) Caravan, P. *Chem. Soc. Rev.* **2006**, *35*, 512-523.
(12) Weinmann, H. J.; Laniado, M.; Muetzel, W. *Physiol. Chem. Phys. Med. NMR* **1984**, *16*, 167-172.
(13) Henriksen, T.; Maillie, D. *Radiation and Health*; English ed.: New York, 2003.
(14) Jurisson, S. S.; Lydon, J. D. *Chem. Rev.* **1999**, *99*, 2205-2218.
(15) *Handbook of Radiopharmaceuticals*; John Wiley and Sons Ltd.: West Sussex, 2003.
(16) ClinicalTrials.gov, NCI, accessed 22.04.2011, 2011.
(17) Brechbiel, M. W. *Dalton Trans.* **2007**, 4918-4928.
(18) Helisch, A.; Forster, G. J.; Reber, H. *Eur. J. Nucl. Med. Mol. Imaging* **2004**, *31*, 1386-1392.
(19) Miao, Y.; Owen, N. K.; Whitener, D.; Gallazzi, F.; Hoffman, T. J.; Quinn, T. P. *Int. J. Cancer* **2002**, *101*, 480-487.
(20) Dilworth, J. R.; Parrott, S. J. *Chem. Soc. Rev.* **1998**, *27*, 43-55.
(21) Lagunas-Solar, M. C.; Kiefer, P. M.; Carvacho, O. F.; Lagunas, C. A.; Cha, Y. P. *Int. J. Radiat. Appl. Instrum. Appl. Radiat. Isot.* **1991**, *42*, 643-657.
(22) Gleason, G. I. *Int. J. Appl. Radiat. Isot.* **1960**, *8*, 90-94.
(23) McElvaney, K. D.; Hopkins, K. T.; Welch, M. J. *Int. J. Labelled Compd. Radiopharm.* **1984**, *19*, 521-542.
(24) Breeman, W. A.; Verbruggen, A. M. *Eur. J. Nucl. Med. Mol. Imaging* **2007**, *34*, 978-981.
(25) Alberto, R. In *Compr. Coord. Chem. II*; Mc Cleverty, J. A., Meer, T. S., Eds.; Elsevier Science: Amsterdam, 2003; Vol. 5.
(26) Davison, A.; Orvig, C.; Trop, H. S.; Sohn, M.; Depamphilis, B. V.; Jones, A. G. *Inorg. Chem.* **1980**, *19*, 1988-1992.
(27) Liu, S. *Chem. Soc. Rev.* **2004**, *33*, 445-461.
(28) Shi, J.; Kim, Y.-S.; Chakraborty, S.; Jia, B.; Wang, F.; Liu, S. *Bioconjugate Chem.* **2009**, *20*, 1559-1568.
(29) Riddoch, R. W.; Schaffer, P.; Valliant, J. F. *Bioconjugate Chem.* **2006**, *17*, 226-235.
(30) Baidoo, K. E.; Lin, K.-S.; Zhan, Y.; Finley, P.; Scheffel, U.; Henry N. Wagner, J. *Bioconjugate Chem.* **1998**, *9*, 218-225.

(31) Francesconi, L. C.; Graczyk, G.; Wehrli, S.; Shaikh, S. N.; Mcclinton, D.; Liu, S.; Zubieta, J.; Kung, H. F. *Inorg. Chem.* **1993**, *32*, 3114-3124.
(32) Cantorias, M. V.; Howell, R. C.; Todaro, L.; J.E., C.; Berndorff, D.; Rogers, R. D.; Francesconi, L. C. *Inorg. Chem.* **2007**, *46*, 7326-7340.
(33) Bolzati, C.; Benini, E.; Cazzola, E.; Jung, C.; Tisato, F.; Refosco, F.; Pietzsch, H. J.; Spies, H.; Uccelli, L.; Duatti, A. *Bioconjugate Chem.* **2004**, *15*, 628-637.
(34) Schwartz, D. A.; Abrams, M. J.; Hauser, M. M.; Gaul, F. E.; Larsen, S. K.; Rauh, D.; Zubieta, J. A. *Bioconjugate Chem.* **1991**, *2*, 333-336.
(35) Alberto, R.; Schibli, R.; Egli, A.; Schubiger, A. P.; Abram, U.; Kaden, T. A. *J. Am. Chem. Soc.* **1998**, *120*, 7987-7988.
(36) Schibli, R.; La Bella, R.; Alberto, R.; Garcia-Garayoa, E.; Ortner, K.; Abram, U.; Schubiger, P. A. *Bioconjugate Chem.* **2000**, *11*, 345-351.
(37) Bernard, J.; Ortner, K.; Spingler, B.; Pietzsch, H. J.; Alberto, R. *Inorg. Chem.* **2003**, *42*, 1014-1022.
(38) Sogbein, O. O.; Merdy, P.; Morel, P.; Valliant, J. F. *Inorg. Chem.* **2004**, *43*, 3032-3034.
(39) Maria, L.; Fernandes, C.; Garcia, R.; Gano, L.; Paulo, A.; Cordeiro-Santos, I.; Santos, I. *Dalton Trans.* **2009**, 603-606.
(40) Storr, T.; Obata, M.; Fisher, C. L.; Bayly, S. R.; Green, D. E.; Brudzinska, I.; Mikata, Y.; Patrick, B. O.; Adam, M. J.; Yano, S.; Orvig, C. *Chem. Eur. J.* **2004**, *11*, 195-203.
(41) Palma, E.; Correia, J. D. G.; Oliveira, B. L.; Gano, L.; Santos, I. C.; Santos, I. *Dalton Trans.* **2011**, *40*, 2787-2796.
(42) James, S.; Maresca, K. P.; Allis, D. G.; Valliant, J. F.; Eckelman, W.; Babich, J. W.; Zubieta, J. *Bioconjugate Chem.* **2006**, *17*, 579-589.
(43) Müller, C.; Hohn, A.; Schubiger, P. A.; Schibli, R. *Eur. J. Nucl. Med. Mol. Imaging* **2006**, *33*, 1007-1016.
(44) Staveren, D. R. v.; Mundwiler, S.; Hoffmanns, U.; Pak, J. K.; Spingler, B.; Metzler-Nolte, N.; Alberto, R. *Org. Biomol. Chem.* **2004**, *2*, 2593-2603.
(45) Alves, S.; Correia, J. D. G.; Gano, L.; Rold, T. L.; Prasanphanich, A.; Haubner, R.; Rupprich, M.; Alberto, R.; Decristoforo, C.; Santos, I.; Smith, C. J. *Bioconjugate Chem.* **2007**, *18* 530-537.
(46) Stephenson, K. A.; Banerjee, S. R.; Besanger, T.; Sogbein, O. O.; Levadala, M. K.; McFarlane, N.; Lemon, J. A.; Boreham, D. R.; Maresca, K. P.; Brennan, J. D.; Babich, J. W.; Zubieta, J.; Valliant, J. F. *J. Am. Chem. Soc.* **2004**, *126*, 8598-8599.
(47) Stephenson, K. A.; Reid, L. C.; Zubieta, J.; Babich, J. W.; Kung, M.-P.; Kung, H. F.; Valliant, J. F. *Bioconjugate Chem.* **2008**, *19*, 1087-1094.
(48) Blower, P. J.; Lewis, J. S.; Zweit, J. *Nucl. Med. Biol.* **1996**, *23*, 957-980.
(49) Wadas, T. J.; Wong, E. H.; Weisman, G. R.; Anderson, C. J. *Curr. Pharm. Des.* **2007**, *13*, 3-16.
(50) Boswell, C. A.; Sun, X.; Niu, W.; Weisman, G. R.; Wong, E. H.; Rheingold, A. L.; Anderson, C. J. *J. Med. Chem.* **2004**, *47*, 1465-1474.
(51) Cutler, C. S.; Giron, M. C.; Reichert, D. E.; Snyder, A. Z.; Herrero, P.; Anderson, C. J.; Quarless, D. A.; Koch, S. A.; Welch, M. J. *Nucl. Med. Biol.* **1999**, *36*, 305-316.
(52) Plössl, K.; Chandra, R.; Qu, W.; Lieberman, B. P.; Kung, M.-P.; Zhou, R.; Huang, B.; Kung, H. F. *Nucl. Med. Biol.* **2008**, *35*, 83-90.
(53) Green, M. A.; Welch, M. J.; Huffman, J. C. *J. Am. Chem. Soc.* **1984**, *106*, 3689-3691.

(54) Velikyan, I.; Maecke, H.; Langstrom, B. *Bioconjugate Chem.* **2008**, *19*, 569-573.
(55) André, J. P.; Maecke, H. R.; Zehnder, M.; Macko, L.; Akyel, K. G. *Chem. Commun.* **1998**, 1301-1302.
(56) Hilfiker, K. A.; Brechbiel, M. W.; Rogers, R. D.; Planalp, R. P. *Inorg. Chem.* **1997**, *36*, 4600-4603.
(57) Harris, W. R.; Pecoraro, V. L. *Biochemistry* **1983**, *22*, 292-299.
(58) Ferreira, C. L.; Lamsa, E.; Woods, M.; Duan, Y.; Fernando, P.; Bensimon, C.; Kordos, M.; Guenther, K.; Jurek, P.; Kiefer, G. E. *Bioconjugate Chem.* **2010**, *21*, 531-536.
(59) Ambrosini, V.; Tomassetti, P.; Castellucci, P.; Campana, D.; Montini, G.; Rubello, D.; Nanni, C.; Rizzello, A.; Franchi, R.; Fanti, S. **2008**, *35*, 1431-1438.
(60) Bartholomä, M. D.; Louie, A. S.; Valliant, J. F.; Zubieta, J. *Chem. Rev.* **2010**, *110*, 2903-2920.
(61) Pellissier, A.; Bretonniere, Y.; Chatterton, N.; Pecaut, J.; Delangle, P.; Mazzanti, M. *Inorg. Chem.* **2007**, *46*, 3714-3725.
(62) Liu, S. *Adv. Drug. Deliv. Rev.* **2008**, *60*, 1347-1370.
(63) Steigman, J.; Eckelman, W. C. *The Chemistry of Technetium in Medicine*; Nuclear Science Publication NAS-NS-3204, National Academy Press: Washington, DC, 1992.
(64) Dilworth, J. R.; Parrott, S. J. *Chem. Soc. Rev.* **1998**, *27*, 43–55.
(65) Hom, R. K.; Katzenellenbogen, J. A. *Nucl. Med. Biol.* **1997**, *24*, 485-498.
(66) Rattat, D.; Eraets, K.; Cleynhens, B.; Knight, H.; Fonge, H.; Verbruggen, A. *Tetrahedron Lett.* **2004**, *45*, 2531-2534.
(67) Schibli, R.; Schwarzbach, R.; Alberto, R.; Ortner, K.; Schmalle, H.; Dumas, C.; Egli, A.; Schubiger, P. A. *Bioconjugate Chem.* **2002**, *13*, 750-756.
(68) Liu, Y.; Pak, J.-K.; Schmutz, P.; Bauwens, M.; Mertens, J.; Knight, H.; Alberto, R. *J. Am. Chem. Soc.* **2006**, *128*, 15996-15997.
(69) Ferreira, C. L.; Ewart, C. B.; Bayly, S. R.; Patrick, B. O.; Steele, J.; Adam, M. J.; Orvig, C. *Inorg. Chem.* **2006**, *45*, 6979-6987.
(70) Wust, F.; Spies, H.; Johannsen, B. *Bioorg. Med. Chem. Lett.* **1996**, *6*, 2729-2734.
(71) Hom, R. K.; Katzenellenbogen, J. A. *J. Org. Chem.* **1997**, *62*, 6290-6297.
(72) Bales, B. L.; Messina, L.; Vidal, A.; Peric, M.; Nascimento, O. R. *J. Phys. Chem. B* **1998**, *102*, 10347-10358.
(73) Simons, A.; Helenius, K. *Biochim. Biophys. Acta* **1975**, *415*, 29-79.
(74) Saw, M. M.; Kurz, P.; Agorastos, N.; Hor, T. S. A.; Sundram, F. X.; Yan, Y. K.; Alberto, R. *Inorg. Chim. Acta* **2006**, *259*, 4087 - 4094.
(75) Cazzola, E.; Benini, E.; Pasquali, M.; Mirtschink, P.; Walther, M.; Pietzsch, H.-J.; Uccelli, L.; Boschi, A.; Bolzati, C.; Duatti, A. *Bioconjugate Chem.* **2008**, *19*, 450-460.
(76) Uehara, T.; Uemura, T.; Hirabayashi, S.; Adachi, S.; Odaka, K.; Akizawa, H.; Magata, Y.; Irie, T.; Arano, Y. *J. Med. Chem.* **2007**, *50*, 543-549.
(77) Zhang, Z.; Lyster, D. M.; Webb, G. A.; Orvig, C. *Nucl. Med. Biol.* **1992**, *19*, 327-335.
(78) *SAINT, Bruker AXS Inc.: Madison, WI 1999*.
(79) *SADABS, Bruker AXS Inc.: Madison, WI 1999*.
(80) Altomare, A. B., M. C.; Camalli, M.; Cascarano, G. L.; Giocavazzo,; C.; Guagliardi, A. M., A. G. G.; Polidori, G.; Spagna,; R., H. W. *J. Appl. Crystallogr* **1999**, *32*, 115-119.

(81) Beurskens, P. T. A., G.; Beurskens, G.; Bosman, W. P.; Gleder,; R. d.; Israel, R. S., J. M. M. *University of Nijmegen: Nijmegen, The Netherlands* **1994**.
(82) *SHELXTL, Bruker AXS Inc.: Madison, WI 1999*.
(83) Troutner, D. E.; Volkert, W. A.; Hoffman, T. J.; Holmes, R. A. *Int. J. Appl. Radiat. Isot.* **1984**, *35*, 467-470.
(84) Houghten, R. A.; Beckman, A.; Ostresh, J. M. *Int. J. Pept. Protein Res.* **1986**, *27*, 653.
(85) Storr, T.; Fisher, C. L.; Mikata, Y.; Yano, S.; Adam, M. J.; Orvig, C. *Dalton Trans.* **2005**, 654-655.
(86) Ferreira, C. L.; Ewart, C. B.; Barta, C. A.; Little, S.; Yardley, V.; Martins, C.; Polishchuk, E.; Smith, P. J.; Moss, J. R.; Merkel, M.; Adam, M. J.; Orvig, C. *Inorg. Chem.* **2006**, *45*, 8414-8422.
(87) Banerjee, S. R.; Wei, L. H.; Levadala, M. K.; Lazarova, N.; Golub, V. O.; O'Connor, C. J.; Stephenson, K. A.; Valliant, J. F.; Babich, J. W.; Zubieta, J. *Inorg. Chem.* **2002**, *41*, 5795-5802.
(88) Schibli, R.; Bella, R. L.; Alberto, R.; Garcia-Garayoa, E.; Ortner, K.; Abram, U.; Schubiger, P. A. *Bioconjugate Chem.* **2000**, *3*, 345-351.
(89) He, H.; Lipowska, M.; Christoforou, A. M.; Marzilli, L. G.; Taylor, A. T. *Nucl. Med. Biol.* **2007**, *34*, 709-716.
(90) Wadas, T. J.; Wong, E. H.; Weisman, G. R.; Anderson, C. J. *Chem. Rev.* **2010**, *110*, 2858-2902.
(91) Green, M. A. *J. Nucl. Med.* **1990**, *31*, 1641-1645.
(92) Storr, T.; Thompson, K. H.; Orvig, C. *Chem. Soc. Rev.* **2006**, *35*, 534-544.
(93) Liu, S.; Pietryka, J.; Ellars, C. E.; Edwards, D. S. *Bioconjugate Chem.* **2002**, *13*, 902-913.
(94) Hueting, R.; Christlieb, M.; Dilworth, J. R.; Garoya, E. G.; Gouverneur, V.; Jones, M. W.; Maes, V.; Schibli, R.; Sun, X.; Tourvé, D. A. *Dalton Trans.* **2010**, *39*, 3620-3632.
(95) Bryan, J. N.; Jia, F.; Mohsin, H.; Sivaguru, G.; Miller, W. H.; Anderson, C. J. *Nucl. Med. Biol.* **2005**, *32*, 1473-1480.
(96) Alberto, R. A. In *PCT Int. Appl. 2001025243*; Mallinckrodt Inc., USA, 2001.
(97) Callahan, A. P.; Rice, D. E.; Knapp, F. F. *J. Nucl. Med.* **1987**, *28*, 656-657.
(98) Volkert, W. A.; Hoffman, T. J. *Chem. Rev.* **1999**, *99*, 2269-2292.
(99) Cole, W. C.; DeNardo, S. J.; Meares, C. F.; McCall, M. J.; DeNardo, G. L.; Epstein, A. L. *J. Nucl. Med.* **1987**, *28*, 83-90.
(100) Bayly, S. R.; King, R. C.; Honess, D. J.; Barnard, P. J.; Betts, H. M.; Holland, J. P.; Hueting, R.; Bonnitcha, P. D.; Dilworth, J. R.; Aigbirhio, F. I.; Christlieb, M. *J. Nucl. Med.* **2008**, *49*, 1862-1868.
(101) Paterson, B. M.; White, J. M.; Donnelly, P. S. *Dalton Trans.* **2010**, *39*, 2831-2837.
(102) Wilchek, M.; Bayer, E. A. *Anal. Biochem.* **1988**, *171*, 1.
(103) Wilchek, M.; Bayer, E. A. *Methods Enzymol.* **1990**, *184*, 123.
(104) Wilbur, D. S.; Hamlin, D. K.; Vesella, R. L.; Stray, J. E.; Buhler, K. R.; Stayton, P. S.; Klumb, L. A.; Pathare, P. M.; Weerawarna, S. A. *Bioconjugate Chem.* **1996**, *7*, 689-702.
(105) Goodwin, D. A.; Meares, C. F.; Osen, M. *J. Nucl. Med.* **1998**, *39*, 1813-1818.
(106) Perron, V.; Abbot, S.; Moreau, N.; Lee, D.; Penney, C.; Zacharie, B. *Synthesis* **2009**, *41*, 283-289.

(107) Boros, E.; Lin, Y.-H. S.; Ferreira, C. L.; Patrick, B. O.; Hafeli, U. O.; Adam, M. J.; Orvig, C. *Dalton Trans.* **2011**, *40*, 6253-6259.
(108) Platas-Iglesias, C.; Mato-Iglesias, M.; Djanashvili, K.; Muller, R. N.; Elst, L. V.; Peters, J. A.; Blas, A. d.; Rodríguez-Blas, T. *Chem. Eur. J.* **2004**, *10*, 3579-3590.
(109) Mato-Iglesias, M.; Roca-Sabio, A.; Palikas, Z.; Esteban-Gomez, D.; Platas-Igesias, C.; Toth, E.; de Blas, A.; Rodrigues-Blas, T. *Inorg. Chem.* **2008**, *47*, 7840-7851.
(110) Alberto, R.; Egli, A.; Abram, U.; Hegetschweiler, K.; Gramlich, V.; Schubiger, P. A. *J. Chem. Soc., Dalton Trans.* **1994**, 2815-20.
(111) Alberto, R.; Schibli, R.; Schubiger, A. P.; Abram, U.; Pietzsch, H. J.; Johannsen, B. *J. Am. Chem. Soc.* **1999**, *121*, 6076-6077.
(112) Banerjee, S. R.; Levadala, M. K.; Lazarova, N.; Wei, L. H.; Valliant, J. F.; Stephenson, K. A.; Babich, J. W.; Maresca, K. P.; Zubieta, J. *Inorg. Chem.* **2002**, *41*, 6417-6425.
(113) Antunes, P.; Delgado, R.; Drew, M. G. B.; Félix, V.; Maecke, H. *Inorg. Chem.* **2007**, *46*, 3144-3153.
(114) Maresca, K. P.; Marquis, J. C.; Hillier, S. M.; Lu, G.; Femia, F. J.; Zimmerman, C. N.; Eckelman, W. C.; Joyal, J. L.; Babich, J. W. *Bioconjugate Chem.* **2010**, *21*, 1032-1042.
(115) Rufini, V.; Calcagni, M. L.; Baum, R. P. *Semin. Nucl. Med.* **2006**, *36*, 228-247.
(116) Harris, W. R.; Martell, A. E. *Inorg. Chem.* **1976**, *15*, 713-720.
(117) Bandoli, G.; Dolmella, A.; Porchia, M.; Refosco, F.; Tisato, F. *Coord. Chem. Rev.* **2001**, *214*, 43-90.
(118) Wadas, T. J.; Wong, E. H.; Weisman, G. R.; Anderson, C. J. *Chem. Rev.* **2010**, *110*, 2858-2902.
(119) Bandoli, G.; Dolmella, A.; Tisato, F.; Porchia, M.; Refosco, F. *Coord. Chem. Rev.* **2009**, *253*, 56-77.
(120) Sun, Y.; Anderson, C. J.; Pajeau, T. S.; Reichert, D. E.; Hancock, R. D.; Motekaitis, R. J.; Martell, A. E.; M. J. Welch *J. Med. Chem.* **1996**, *39*, 458-470.
(121) Clarke, E. T.; Martell, A. E. *Inorg. Chim. Acta* **1991**, *190*, 37-46.
(122) Clarke, E. T.; Martell, A. E. *Inorg. Chim. Acta* **1991**, *181*, 273-280.
(123) Delgado, R.; Quitino, S.; Teixeira, M.; Zhang, A. *J. Chem. Soc., Dalton Trans.* **1997**, 55-63.
(124) Maecke, H. R.; André, J. P. Ernst Schering Research Foundation Workshop, 2007; p 215-242.
(125) Anger, H. O.; Gottschalk, A. *J. Nucl. Med.* **1963**, *4*, 326.
(126) Jones-Wilson, T. M.; Motekaitis, R. J.; Sun, Y.; Anderson, C. J.; Martell, A. E.; Welch, M. J. *Nucl. Med. Biol.* **1995**, *22*, 859-68.
(127) Bollinger, J. E.; Mague, J. T.; O'Connor, C. J.; Banks, W. A.; Roundhill, D. M. *Dalton Trans.* **1995**, 1677-1688.
(128) Mathias, C. J.; Lewis, M. R.; Reichert, D. E.; Laforest, R.; Sharp, T. L.; Lewis, J. S.; Yang, Z.-F.; Waters, D. J.; Snyder, P. W.; Low, P. S.; Welch, M. J.; Green, M. A. *Nucl. Med. Biol.* **2003**, *30*, 725-731.
(129) Wong, E.; Caravan, P.; Liu, S.; Rettig, S. J.; Orvig, C. *Inorg. Chem.* **1996**, *35*, 715.
(130) Caravan, P.; Rettig, S. J.; Orvig, C. *Inorg. Chem.* **1997**, *36*, 1306-1315.
(131) Ferreiros-Martinez, R.; Esteban-Gomez, D.; Platas-Igesias, C.; de Blas, A.; Rodriguez-Blas, T. *Dalton Trans.* **2008**, 5754-5758.

(132) Malyshev, K. V.; Smirnov, V. V. *Radiokhimiya* **1975**, *17*, 137-140.
(133) Ali, M. S.; Quadri, S. Y. *Bioconjugate Chem.* **1996**, *7*, 576-583.
(134) Altomare, A.; Burla, M. C.; Camalli, M.; Cascarano, G. L.; Giacovazzo, C.; Guagliardi, A.; Moliterni, A. G. G.; Polidori, G.; Spagna, R. *J. Appl. Crystallogr.* **1999**, *32*, 115-119.
(135) Sheldrick, G. M. SHELXS 97, Program for the Refinement of Crystal Structures, University Göttingen, 1997.
(136) Sluis, P. v. d.; Spek, A. L. *Acta Crystallogr., Sect A* **1990**, *A46*, 194-201.
(137) Velikyan, I.; Beyer, G. J.; Langstrom, B. *Bioconjugate Chem.* **2004**, *15*, 554-560.
(138) Heppeler, A.; Froidevaux, S.; Maecke, H. R.; Jermann, E.; Béhé, M.; Powell, P.; Hennig, M. *Chem. Eur. J.* **1999**, *5*, 1974–1981.
(139) Boros, E.; Ferreira, C. L.; Cawthray, J. F.; Price, E. W.; Patrick, B. O.; Wester, D. W.; Adam, M. J.; Orvig, C. *J. Am. Chem. Soc.* **2010**, *132*, 15726–15733.
(140) Bottari, E.; Anderegg, G. *Helv. Chim. Acta* **1967**, *50*, 2349-2356.
(141) McMurry, T. J.; Brechbiel, M.; Kumar, K.; Gansow, O. A. *Bioconjugate Chem.* **1992**, *3*, 108-117.
(142) Wei, L.; Ye, Y.; Wadas, T. J.; Lewis, J. S.; Welch, M. J.; Achilefu, S.; Anderson, C. J. *Nucl. Med. Biol.* **2009**, *36*, 277–285.
(143) Sephton, R. G.; Hodgson, G. S.; De Abrew, S.; Harris, A. W. *J. Nucl. Med.* **1978**, *19*, 930-935.
(144) Wong, E. H.; Weisman, G. R.; Hill, D. C.; Reed, D. P.; Rogers, M. E.; Condon, J. P.; Fagan, M. A.; Calabrese, J. C.; Lam, K.-C.; Guzei, I. A.; Rheingold, A. L. *J. Am. Chem. Soc.* **2000**, *112*, 10561.
(145) Bevilacqua, A.; Gelb, R. I.; Hebard, W. B.; Zompa, L. J. *Inorg. Chem.* **1987**, *26*, 2699-2706.
(146) Martell, A. E.; Motekaitis, R. J.; Clarke, E. T.; Delgado, R.; Sun, Y.; Ma, R. *Supramol. Chem.* **1996**, *6*, 353.
(147) Smith, R. M.; Martell, A. E. *Critical Stability Constants Vols. 1-6*; Plenum Press: New York, 1989.
(148) Bernhardt, P. V.; Bramley, R.; Engelhardt, L. M.; Harrowfield, J. M.; Hockless, D. C.; Korybut-Daszkiewiecz, B. R.; Krausz, E. R.; Morgan, T.; Sargeson, A. M. *Inorg. Chem.* **1995**, *34*, 3589.
(149) Woodin, K. S.; Heroux, K. J.; Boswell, C. A.; Wong, E. H.; Weisman, G. R.; Niu, W.; Tomellini, S. A.; Anderson, C. J.; Zakharov, L. N.; Rheingold, A. L. *Eur. J. Inorg. Chem.* **2005**, *25*, 4829–4833.
(150) Macrae, C. F.; Edgington, P. R.; McCabe, P.; Pidcock, E.; Shields, G. P.; Taylor, R.; Towler, M.; Streek, J. v. d. *J. Appl. Cryst.* **2006**, *39*, 453-457.
(151) Boros, E.; Ferreira, C. L.; Cawthray, J. F.; Price, E. W.; Patrick, B. O.; Wester, D. W.; Adam, M. J.; Orvig, C. *manuscript in preparation*.
(152) Versari, A.; Camellini, L.; Carlinfante, G.; Frasoldati, A.; Nicoli, F.; Grassi, E.; Gallo, C.; Giunta, F. P.; Fraternali, A.; Salvo, D.; Asti, M.; Azzolini, F.; Iori, V.; Sassatelli, R. *Clin.Nucl. Med.* **2010**, *35*, 321-328.
(153) Fritzberg, A. R.; Abrams, P. G.; Beaumier, P. L.; Kasina, S.; Morgan, A. C.; Rao, T. N.; Reno, J. M.; Sanderson, J. A.; Srinivasan, A.; Wilbur, D. S. *Proc. Natl. Acad. Sci. U.S.A.* **1988**, *85*, 4025-4029.

(154) Chen, Q.; Strand, S. E.; Tennvall, J.; Lindrgren, L.; Hindorf, C.; Sjögren, H. O. *J. Nucl. Med.* **1997**, *38*, 1934-1939.
(155) Eisenwiener, K. P.; Prata, M. I.; Buschmann, I.; Zhang, H. W.; Santos, A. C.; S.Wenger; Reubi, J. C.; Maecke, H. R. *Bioconjugate Chem.* **2002**, *13*, 530–541.
(156) Dearling, J. L. J.; Voss, S. D.; Dunning, P.; Snay, E.; Fahey, F.; Smith, S. V.; Huston, J. S.; Meares, C. F.; Treves, S. T.; Packard, A. B. *Nucl. Med. Biol.* **2011** *38*, 29-38.
(157) Struthers, H.; Mindt, T. L.; Schibli, R. *Dalton Trans.* **2010**, *39*, 675-696.
(158) Corson, D. T.; Meares, C. F. *Bioconjugate Chem.* **2000**, *11*, 292-299.
(159) Brechbiel, M. W.; Gansow, O. A.; Atcher, R. W.; Schlom, J.; Simpson, D. E.; Esteban, J.; Colcher, D. *Inorg. Chem.* **1986**, *25*, 2772-2781.
(160) McCall, M. J.; Diril, H.; Meares, C. F. *Bioconjugate Chem.* **1990**, 222-226.
(161) DeNardo, S. J.; Liu, R.; Albrecht, H.; Natarajan, A.; Sutcliffe, J. L.; Anderson, C.; Li Peng; Ferdani, R.; Cherry, S. R.; Lam, K. S. *J. Nucl. Med.* **2009**, *50*, 625-634.
(162) Jeong, J. M.; Hong, M. K.; Chang, Y. S.; Lee, Y.-S.; Kim, Y. J.; Cheon, G. J.; Lee, D. S.; Chung, J.-K.; Lee, M. C. *J. Nucl. Med.* **2008** *49*, 830-836.
(163) Lewis, E. A.; Boyle, R. W.; Archibald, S. J. *Chem. Commun.* **2004**, 2212-2213.
(164) Prasanphanich, A. F.; Nanda, P. K.; Rold, T. L.; Ma, L.; Lewis, M. R.; Garrison, J. C.; Hoffman, T. J.; Sieckman, G. L.; Figueroa, S. D.; Smith, C. J. *Proc. Natl. Acad. Sci. U.S.A.* **2007**, *104* 12462-12467.
(165) Mindt, T. L.; Struthers, H.; Brans, L.; Anguelov, T.; Schweinsberg, C.; Maes, V.; Tourwé, D.; Schibli, R. *J. Am. Chem. Soc.* **2006**, *128*, 15096–15097.
(166) deJong, M.; Breeman, W. A. P.; Bernard, B. F.; Gameren, A. v.; Bruin, E. d.; Bakker, W. H.; Pluijm, M. E. v. d.; Visser, T. J.; Mäcke, H. R.; Krenning, E. P. *Eur. J. Nucl. Med.* **1999**, *26*, 693-698.
(167) Milenic, D. E.; Brady, E. D.; Brechbiel, M. W. *Nat. Rev. Drug Discovery* **2004**, *3*, 488-499.
(168) Reilly, R. M.; Kiarash, R.; Sandhu, J.; Lee, Y. W.; Cameron, R. G.; Hendler, A.; Vallis, K.; Gariépy, J. *J. Nucl. Med.* **2000**, *41*, 903-911.
(169) Orlova, A.; Tolmachev, V.; Pehrson, R.; Lindborg, M.; Tran, T.; Sandström, M.; Nilsson, F. Y.; Wennborg, A.; Abrahmsén, L.; Feldwisch, J. *Cancer Res.* **2007**, *67*, 2178-2186.
(170) Zeng, X.; Coquiere, D.; Alenda, A.; Garrier, E.; Prange, T.; Li, Y.; Reinaud, O.; Jabin, I. *Chem. Eur. J.* **2006**, *12*, 6393-6402.
(171) Liu, S. *Dalton Trans.* **2007**, 1183-1193.
(172) Fujino, T.; Ishii, Y.; Takeuchi, T.; Hirasawa, K.; Tateda, K.; Kikuchi, K.; Hasebe, N. *Circ. J.* **2003**, *67*, 757-762.
(173) Hsiao, Y.-M.; Mathias, C. J.; Wey, S.-P.; Fanwick, P. E.; Green, M. A. *Nucl. Med. Biol.* **2009**, *36*, 39-45.
(174) Tsang, B. W.; Mathias, C. J.; Green, M. A. *J. Nucl. Med.* **1993**, *34*, 1127-1131.
(175) Andrianina-Ralambomanana, D.; Dorothee, R.-R.; Clement, R. A.; Maugein, J.; Pelinski, L. *Bioorg. Med. Chem.* **2008**, *16*, 9546-9553.
(176) Ménage, S.; Galey, J.-B.; Dumats, J.; Hussler, G.; Seité, M.; Luneau, I. G.; Chottard, G.; Fontecave, M. *J. Am. Chem. Soc.* **1998**, *120*.
(177) Plössl, K.; Zhuang, Z. P.; Meegalla, S. K.; Bradshaw, J.; Frederick, D.; Stevenson, D. A.; Kung, M. P.; Kung, H. F. *J. Labelled Compd. Radiopharm.* **1995**, *37*, 306-308.
(178) Harper, C.; Drew, R. T.; Fouts, J. R. *Drug. Metab. Dispos.* **1975**, *3*, 381-388.

(179) Nunn, A.; Linder, K.; Strauss, H. *Eur. J. Nucl. Med. Mol. Imaging* **1995**, *22*, 265-280.
(180) Barthel, H.; Wilson, H.; Collingridge, D. R.; Brown, G.; Osman, S.; Luthra, S. K.; Brady, F.; Workman, P.; Price, P. M.; Aboagye, E. O. *Br. J. Cancer* **2004**, *90*, 2232-2242.
(181) Melo, T.; Duncan, J.; Ballinger, J. R.; Rauth, A. M. *J. Nucl. Med.* **2000**, *41*, 169-176.
(182) Hoigebazar, L.; Jeong, J. M.; Choi, S. Y.; Choi, J. Y.; Shetty, D.; Lee, Y.-S.; Lee, D. S.; Chung, J.-K.; Lee, M. C.; Chung, Y. K. *J. Med. Chem.* **2010**, *53*, 6378–6385.

Appendices

Appendix A Crystallographic Data

Complex	**[Re(L1)(CO)$_3$]**	**[Cu(dipin-NO$_2$)(OH$_2$)]**	**[Re(Me$_2$dipin-NO$_2$)(CO)$_3$] [Re(Br$_3$(CO)$_3$]**	**[Ga(dedpa)][ClO$_4$]**
Formula	C21 H27 N2 O7 Re	C21 H18 Cu N4 O7	C27.50 H22 Br1.50 N4 O10.50 Re1.50	C16 H16 Cl Ga N4 O8
Fw	605.65	501.93	975.66	497.50
Description	colorless plate	green plate	colorless blade	colorless prism
Space group	*P* - 1	*P* - 1	*P* 2$_1$/c	*P* – 1
a [Å]	6.8109(11)	7.143(2)	12.3723(10)	7.8880(12)
b [Å]	10.4134(19)	8.335(2)	17.5236(14)	8.9681(12)
c [Å]	17.057(4)	18.901(5)	14.8402(12)	13.264(2)
α [°]	102.114(8)	77.781(4)	90.00	87.389(7)
β [°]	94.058(13)	79.755(5)	112.128(2)	77.692(8)
γ [°]	102.511(9)	65.266(4)	90.00	85.503(7)
V [Å^3]	1146.1(4)	993.9(5)	2980.5(4)	913.5(2)
Z	2	2	4	2
ρ_{calc} [g/cm^3]	1.755	1.677	2.174	1.809
T [K]	173	90	90	103
μ [mm^{-1}]	5.344	1.155	8.173	1.710
F $_{000}$	596	514	1856	504
reflns collcd/ unique	9144/ 3421	6190/ 2560	50217/ 8033	15309/ 4391
	(R_{int} = 0.053)	(R_{int} = 0.072)	(R_{int} = 0.048)	(R_{int} = 0.020)
residuals (F^2, all data)	wR_2 = 0.142	wR_2 = 0.254	wR_2 = 0.074	wR_2 = 0.087
residuals (F, I > 2σ(I))	R_1 = 0.063	R_1 = 0.130	R_1 = 0.035	R_1 = 0.026
goodness of fit indicator	1.013	1.162	1.017	1.300

Complex	**[Ga(dp-N-NO_2)][ClO_4]**	**[Cu(dedpa)]**	**[Ga(6EtO2MeO)][ClO_4]**
Formula	C31 H30 Cl Ga N6 O13	C16 H22 Cu N4 O7	C45.28 H63.14 Cl Ga N4 O18.47
Fw	799.78	445.92	1064.25
Description	colorless plate	blue prism	colorless tablet
Space group	$P\,2_1/c$	P nn2	$P\,2_1/c$
a [Å]	20.317(2)	11.352(2)	15.8043(13)
b [Å]	14.0298(17)	15.584(3)	15.1916(13)
c [Å]	24.060(3)	10.6461	20.8101(17)
α [°]	90.00	90.00	90.00
β [°]	98.966(2)	90.00	92.183(2)
γ [°]	90.00	90.00	90.00
V [$Å^3$]	6774.4(14)	1883.4(6)	4992.7(7)
Z	8	4	4
ρ_{calc} [g/cm^3]	1.568	1.573	1.416
T [K]	90	90.0	90
μ [mm^{-1}]	0.968	1.207	0.682
F_{000}	3280	924	2234
Reflns collcd/ unique	29750/ 9225	40349/ 5484	57970/ 9817
	(R_{int} = 0.085)	(R_{int} = 0.033)	(R_{int} = 0.043)
Residuals (F^2, all data)	wR_2 = 0.167	wR_2 = 0.053	wR_2 = 0.192
Residuals (F, I > 2σ(I))	R_1 = 0.107	R_1 = 0.023	R_1 = 0.089
Goodness of fit indicator	0.958	1.068	1.067

Appendix B Biodistribution Data

B.1 Biodistribution of Compounds $[^{67}Ga(dedpa)]^+$, $[^{67}Ga(dp\text{-}N\text{-}NO_2)]^+$, $[^{67}Ga(dp\text{-}bb\text{-}NO_2)]$

Biodistribution data of $[^{67}Ga(\mathbf{dedpa})]^+$ in female ICR mice (% ID/g , n = 4).

Organ/Tissue	30 min ± SD	1 h ± SD	2 h ± SD	4 h ± SD
Brain	0.26 ± 0.13	0.24 ± 0.12	0.21 ± 0.10	0.13 ± 0.06
Femur	2.18 ± 1.09	2.13 ± 1.06	1.89 ± 0.94	2.21 ± 1.10
Muscle	1.21 ± 0.60	1.15 ± 0.57	1.09 ± 0.54	1.12 ± 0.56
Spleen	1.36 ± 0.68	1.35 ± 0.67	1.27 ± 0.63	0.98 ± 0.49
Kidney	8.08 ± 4.00	7.82 ± 3.91	9.14 ± 4.57	8.30 ± 4.15
Liver	3.70 ± 1.85	3.69 ± 1.84	3.17 ± 1.58	2.73 ± 1.36
Intestine	2.09 ± 1.05	2.12 ± 1.06	1.99 ± 0.99	1.99 ± 0.99
Heart	2.64 ± 1.32	2.49 ± 1.24	2.41 ± 1.20	2.00 ± 1.00
Lung	4.87 ± 2.43	4.89 ± 2.44	4.84 ± 2.42	3.26 ± 1.63
Serum	16.06 ± 8.03	9.04 ± 4.52	12.04 ± 6.02	12.23 ± 6.11

Biodistribution data of $[^{67}Ga(\mathbf{dp\text{-}N\text{-}NO_2})]^+$ in female ICR mice (% ID/g , n = 4).

Organ/Tissue	30 min ± SD	1 h ± SD	2 h ± SD	4 h ± SD
Brain	0.16 ± 0.02	0.15 ± 0.01	0.16 ± 0.01	0.12 ± 0.01
Femur	1.54 ± 0.20	1.66 ± 0.09	1.97 ± 0.06	2.71 ± 0.88
Muscle	0.80 ± 0.07	0.60 ± 0.02	0.61 ± 0.02	0.57 ± 0.05
Spleen	2.32 ± 0.15	3.25 ± 0.27	3.20 ± 0.28	4.23 ± 0.79
Kidney	5.29 ± 0.14	4.19 ± 0.04	3.59 ± 0.40	4.45 ± 0.36
Liver	3.35 ± 0.57	3.42 ± 0.60	4.43 ± 0.42	4.51 ± 0.67
Intestine	1.70 ± 0.05	1.45 ± 0.12	1.89 ± 0.14	1.54 ± 0.12
Heart	1.80 ± 0.35	2.06 ± 0.07	1.88 ± 0.19	1.65 ± 0.22
Lung	11.18 ± 0.79	10.65 ± 0.56	8.52 ± 0.33	5.65 ± 0.54
Blood	5.77 ± 1.21	6.54 ± 0.05	5.90 ± 0.42	4.52 ± 0.46
Urine	411.14 ± 45.93	166.83 ± 48.91	47.17 ± 14.64	16.98 ± 3.51

Biodistribution data of $[^{67}Ga(\mathbf{dp\text{-}bb\text{-}NO_2})]^+$ in female ICR mice (% ID/g , n = 4).

Organ/Tissue	30 min ± SD	1 h ± SD	2 h ± SD	4 h ± SD
Brain	0.16 ± 0.02	0.18 ± 0.02	0.19 ± 0.01	0.13 ± 0.01
Femur	1.56 ± 0.12	2.29 ± 0.28	2.61 ± 0.21	3.44 ± 0.08
Muscle	0.91 ± 0.05	1.01 ± 0.24	0.72 ± 0.07	0.70 ± 0.05
Spleen	1.22 ± 0.12	1.13 ± 0.10	1.45 ± 0.92	1.17 ± 0.08
Kidney	12.98 ± 0.80	11.04 ± 0.92	9.40 ± 0.13	10.10 ± 0.23
Liver	4.40 ± 0.25	3.89 ± 0.50	3.24 ± 0.59	3.63 ± 0.15
Intestine	2.04 ± 0.08	2.07 ± 0.27	1.78 ± 0.26	1.87 ± 0.12
Heart	2.22 ± 0.20	2.19 ± 0.23	1.91 ± 0.16	1.74 ± 0.15
Lung	4.30 ± 0.45	3.79 ± 0.29	3.76 ± 0.43	3.09 ± 0.23
Blood	7.40 ± 0.65	7.36 ± 0.42	7.43 ± 0.61	5.40 ± 0.41
Urine	94.71 ± 22.67	55.80 ± 25.63	33.64 ± 18.18	13.60 ± 3.06

B.2 Biodistribution of Compounds $[^{67}Ga(0MeO)]^+$, $[^{67}Ga(2MeO)]^+$, $[^{67}Ga(4MeO)]^+$, $[^{67}Ga(6MeO)]^+$, $[^{67}Ga(8MeO)]^+$, $[^{67}Ga(6EtO)]^+$, $[^{67}Ga(6EtO{\cdot}2MeO)]^+$.

Biodistribution data of $[^{67}Ga(\mathbf{0MeO})]^+$, (% ID/g , n = 4).

Organ	2 min ± SD	30 min ± SD	1h ± SD	2h ± SD
Brain	0.22 ± 0.13	0.16 ± 0.03	0.10 ± 0.04	0.13 ± 0.02
Muscle	1.25 ± 0.67	0.93 ± 0.14	0.81 ± 0.04	0.60 ± 0.24
Femur	2.24 ± 0.26	2.33 ± 0.50	2.55 ± 0.28	3.65 ± 0.57
Spleen	2.21 ± 0.53	1.08 ± 0.34	0.67 ± 0.12	1.02 ± 0.45
Kidney	19.40 ± 7.38	9.86 ± 1.11	7.87 ± 0.36	5.78 ± 2.34
Liver	5.31 ± 2.46	3.41 ± 0.27	2.01 ± 1.14	2.26 ± 1.56
Heart	4.39 ± 0.65	1.88 ± 0.42	1.14 ± 0.33	1.69 ± 0.12
Lung	5.90 ± 2.95	2.95 ± 0.48	1.87 ± 0.38	2.60 ± 0.33
Intestine	2.32 ± 0.49	2.48 ± 0.51	1.77 ± 0.22	1.63 ± 0.81
Blood	14.16 ± 5.22	6.70 ± 1.89	4.05 ± 1.36	6.33 ± 0.96
Heart/blood	0.34 ± 0.12	0.28 ± 0.02	0.28 ± 0.03	0.27 ± 0.04
Heart/liver	1.16 ± 1.01	0.55 ± 0.12	0.76 ± 0.56	1.86 ± 2.48
Heart/lung	1.06 ± 0.94	0.63 ± 0.04	0.60 ± 0.06	0.65 ± 0.09

Biodistribution data of $[^{67}Ga(\mathbf{2MeO})]^{+}$, (% ID/g , n = 4).

Organ	2 min ± SD	30 min ± SD	1h ± SD	2h ± SD
Brain	0.24 ± 0.05	0.11 ± 0.01	0.11 ± 0.04	0.09 ± 0.06
Muscle	1.18 ± 0.21	1.00 ± 0.11	0.58 ± 0.05	0.56 ± 0.06
Femur	1.93 ± 0.51	2.47 ± 0.17	2.52 ± 0.15	3.77 ± 0.79
Spleen	1.61 ± 0.27	0.71 ± 0.20	0.75 ± 0.30	0.64 ± 0.40
Kidney	31.68 ± 17.82	10.90 ± 2.68	7.71 ± 1.27	5.34 ± 0.82
Liver	4.00 ± 1.03	3.24 ± 0.80	1.92 ± 1.25	2.37 ± 0.66
Heart	3.46 ± 0.71	1.20 ± 0.14	1.33 ± 0.40	0.97 ± 0.57
Lung	6.27 ± 1.39	2.13 ± 0.27	2.65 ± 1.01	1.55 ± 0.70
Intestine	1.79 ± 0.10	2.01 ± 0.25	1.72 ± 0.27	1.52 ± 0.13
Blood	12.11 ± 2.79	4.05 ± 1.34	4.85 ± 2.28	3.07 ± 2.36
Heart/blood	0.28 ± 0.01	0.31 ± 0.07	0.32 ± 0.12	0.34 ± 0.05
Heart/liver	0.88 ± 0.13	0.38 ± 0.05	1.28 ± 1.51	0.39 ± 0.14
Heart/lung	0.55 ± 0.05	0.56 ± 0.04	0.51 ± 0.09	0.60 ± 0.08

Biodistribution data of [^{67}Ga(**4MeO**)]$^{+}$, (% ID/g , n = 4).

Organ	2 min ± SD	30 min ± SD	1h ± SD	2h ± SD
Brain	0.26 ± 0.14	0.14 ± 0.05	0.11 ± 0.05	0.11 ± 0.04
Muscle	1.55 ± 0.06	1.04 ± 0.31	0.83 ± 0.49	0.80 ± 0.26
Femur	2.51 ± 0.40	2.26 ± 0.56	3.21 ± 0.52	3.27 ± 2.11
Spleen	1.60 ± 0.29	0.73 ± 0.19	0.52 ± 0.41	0.81 ± 0.29
Kidney	23.71 ± 10.31	7.19 ± 1.43	4.17 ± 2.55	5.30 ± 0.80
Liver	4.15 ± 0.83	3.07 ± 1.34	2.20 ± 1.19	3.02 ± 0.43
Heart	3.16 ± 0.28	1.05 ± 0.63	1.34 ± 0.62	1.31 ± 0.47
Lung	6.87 ± 0.63	2.94 ± 0.70	2.01 ± 1.47	2.35 ± 0.68
Intestine	2.21 ± 0.25	2.01 ± 0.49	1.63 ± 0.15	1.48 ± 0.40
Blood	9.30 ± 1.34	4.44 ± 1.78	4.21 ± 2.63	3.97 ± 1.54
Heart/blood	0.34 ± 0.05	0.27 ± 0.17	0.35 ± 0.09	0.33 ± 0.05
Heart/liver	0.78 ± 0.14	0.49 ± 0.49	1.15 ± 1.52	0.43 ± 0.14
Heart/lung	0.46 ± 0.08	0.38 ± 0.23	1.29 ± 1.64	0.55 ± 0.09

Biodistribution data of $[^{67}Ga(\mathbf{6MeO})]^{+}$, (% ID/g , n = 4).

Organ	2 min ± SD	30 min ± SD	1h ± SD	2h ± SD
Brain	0.20 ± 0.04	0.04 ± 0.01	0.02 ± 0.01	0.02 ± 0.01
Muscle	1.33 ± 0.11	0.23 ± 0.05	0.17 ± 0.04	0.16 ± 0.04
Femur	2.40 ± 0.43	0.52 ± 0.27	0.46 ± 0.11	0.75 ± 0.14
Spleen	2.42 ± 0.31	0.53 ± 0.11	0.27 ± 0.02	0.16 ± 0.04
Kidney	35.85 ± 8.19	3.52 ± 0.54	1.32 ± 0.15	0.81 ± 0.09
Liver	17.64 ± 2.84	7.07 ± 0.82	4.86 ± 1.14	4.32 ± 0.80
Heart	3.21 ± 0.52	0.59 ± 0.06	0.37 ± 0.05	0.29 ± 0.04
Lung	8.26 ± 0.53	1.17 ± 0.14	0.65 ± 0.07	0.41 ± 0.01
Intestine	2.44 ± 0.32	3.46 ± 2.80	1.78 ± 1.28	1.48 ± 0.44
Blood	7.16 ± 1.28	1.21 ± 0.32	0.80 ± 0.20	0.74 ± 0.11
Heart/blood	0.45 ± 0.05	0.50 ± 0.09	0.48 ± 0.10	0.40 ± 0.10
Heart/liver	0.18 ± 0.02	0.08 ± 0.01	0.08 ± 0.03	0.07 ± 0.02
Heart/lung	0.38 ± 0.06	0.50 ± 0.04	0.57 ± 0.09	0.71 ± 0.12

Biodistribution data of [^{67}Ga(**8MeO**)]$^{+}$, (% ID/g , n = 4).

Organ	2 min ± SD	30 min ± SD	1h ± SD	2h ± SD
Brain	0.19 ± 0.06	0.04 ± 0.01	0.02 ± 0.01	0.02 ± 0.02
Muscle	1.34 ± 0.23	0.21 ± 0.07	0.12 ± 0.06	0.07 ± 0.02
Femur	2.15 ± 0.67	0.52 ± 0.09	0.29 ± 0.12	0.28 ± 0.04
Spleen	2.62 ± 0.86	0.49 ± 0.18	0.23 ± 0.03	0.10 ± 0.03
Kidney	33.12 ± 9.34	2.63 ± 0.66	0.92 ± 0.19	0.44 ± 0.05
Liver	21.91 ± 6.96	23.45 ± 12.82	15.09 ± 3.57	5.04 ± 2.24
Heart	3.82 ± 1.55	0.62 ± 0.14	0.33 ± 0.02	0.18 ± 0.04
Lung	9.85 ± 1.91	1.59 ± 0.65	0.43 ± 0.17	0.30 ± 0.10
Intestine	2.65 ± 0.51	2.58 ± 1.21	2.88 ± 0.54	1.83 ± 1.36
Blood	7.54 ± 2.47	0.84 ± 0.15	0.52 ± 0.06	0.35 ± 0.07
Heart/blood	0.50 ± 0.07	0.73 ± 0.12	0.63 ± 0.07	0.52 ± 0.05
Heart/liver	0.17 ± 0.03	0.03 ± 0.02	0.02 ± 0.00	0.04 ± 0.01
Heart/lung	0.37 ± 0.08	0.41 ± 0.08	0.50 ± 0.32	0.45 ± 0.30

Biodistribution data of $[^{67}Ga(\mathbf{6EtO})]^{+}$, (% ID/g , n = 4).

Organ	2 min ± SD	30 min ± SD	1h ± SD	2h ± SD
Brain	0.38 ± 0.07	0.07 ± 0.02	0.06 ± 0.01	0.06 ± 0.03
Muscle	0.99 ± 0.24	0.49 ± 0.06	0.37 ± 0.06	0.43 ± 0.21
Femur	1.66 ± 0.42	0.90 ± 0.12	0.66 ± 0.14	0.65 ± 0.36
Spleen	2.43 ± 0.59	0.55 ± 0.04	0.42 ± 0.10	0.35 ± 0.03
Kidney	14.94 ± 4.75	3.26 ± 0.74	2.00 ± 0.47	2.30 ± 1.19
Liver	29.54 ± 8.83	23.36 ± 14.98	15.78 ± 4.88	10.52 ± 3.72
Heart	4.60 ± 1.10	1.19 ± 0.12	1.06 ± 0.30	1.17 ± 0.46
Lung	9.60 ± 2.40	1.36 ± 0.25	1.46 ± 0.74	0.89 ± 0.06
Intestine	2.24 ± 0.72	3.04 ± 1.80	2.36 ± 0.58	2.03 ± 0.58
Blood	15.71 ± 3.51	2.28 ± 0.55	1.64 ± 0.15	1.50 ± 0.40
Heart/blood	0.29 ± 0.03	0.55 ± 0.13	0.65 ± 0.17	0.91 ± 0.70
Heart/liver	0.16 ± 0.02	0.11 ± 0.13	0.07 ± 0.01	0.13 ± 0.08
Heart/lung	0.51 ± 0.16	0.89 ± 0.15	0.84 ± 0.44	1.33 ± 0.59

Biodistribution data of $[^{67}Ga(\mathbf{6EtO{\cdot}2MeO})]^{+}$, (% ID/g , n = 4).

Organ	2 min ± SD	30 min ± SD	1h ± SD	2h ± SD
Brain	0.66 ± 0.17	0.05 ± 0.01	0.04 ± 0.01	0.03 ± 0.01
Muscle	1.34 ± 0.39	0.66 ± 0.18	0.61 ± 0.21	0.56 ± 0.16
Femur	2.25 ± 0.66	0.77 ± 0.16	0.65 ± 0.17	0.59 ± 0.09
Spleen	4.56 ± 1.23	0.56 ±0.15	0.43 ± 0.18	0.24 ± 0.07
Kidney	13.66 ± 3.60	5.31 ± 1.32	4.40 ± 3.93	1.82 ± 0.50
Liver	30.16 ± 3.95	32.28 ± 7.98	28.86 ± 9.24	13.94 ± 6.10
Heart	9.31 ± 2.87	1.94 ± 0.42	1.91 ± 0.41	1.63 ± 0.36
Lung	14.34 ± 4.83	0.74* ± 0.45	0.85 ± 0.18	0.50 ± 0.06
Intestine	3.71 ± 0.51	5.35 ± 2.15	6.83 ± 3.48	4.39 ± 1.89
Blood	32.50 ± 14.98	1.29 ± 0.53	0.57 ± 0.11	0.44 ± 0.13
Heart/blood	0.33 ± 0.15	1.62 ± 0.43	3.37 ± 0.61	3.80 ± 0.81
Heart/liver	0.31 ± 0.06	0.06 ± 0.00	0.07 ± 0.02	0.14 ± 0.60
Heart/lung	0.66 ± 0.10	4.59 ± 5.19	2.29 ± 0.51	3.28 ± 0.60

***Animal 5 of 16 showed abnormal lung uptake not in accordance with the other 3 sacrificed animals at this time point. Q-test confirmed this data to be an outlier with 99% confidence.*